AD

USAAVLABS TECHNICAL REPORT 68-66

FABRICATION AND TESTING OF THE COMPOSITE MATERIALS AIRCRAFT WING SECTION

By

Fred E. Bauch

Robert W. Nordlie

Robert C. Lair

September 1968

U. S. ARMY AVIATION MATERIEL LABORATORIES
FORT EUSTIS, VIRGINIA

CONTRACT DA 44-177-AMC-407(T)
GOODYEAR AEROSPACE CORPORATION
AKRON, OHIO

211

DEPARTMENT OF THE ARMY
U S ARMY AVIATION MATERIEL LABORATORIES
FORT EUSTIS, VIRGINIA 23604

This program was carried out under Contract DA 44-177-AMC-407(T) with Goodyear Aerospace Corporation.

The data contained in this report are the result of research conducted in design, fabrication, and test of a fiber glass reinforced plastic wing section for evaluation of structural characteristics, fabrication techniques, and joining techniques. Comparison is made of test results and analytical effort based on tests of small specimens.

The report has been reviewed by the U.S. Army Aviation Materiel Laboratories and is considered to be technically sound. It is published for the exchange of information and the stimulation of future research.

Task 1F162204A17003
Contract DA 44-177-AMC-407(T)
USAAVLABS Technical Report 68-66

September 1968

FABRICATION AND TESTING OF THE COMPOSITE MATERIALS AIRCRAFT WING SECTION

Final Report

GER 13857

By

Fred E. Bauch
Robert W. Nordlie
Robert C. Lair

Prepared by

Goodyear Aerospace Corporation
Akron, Ohio

for

U. S. ARMY AVIATION MATERIEL LABORATORIES
FORT EUSTIS, VIRGINIA

ABSTRACT

A 7-foot-long aircraft wing test section was fabricated with fiber glass reinforced plastic materials and subjected to static and dynamic tests. Good correlation between predicted and actual test values was obtained. The structure failed in compression buckling of the aft cell, top panel. A design modification was incorporated in the fabrication of a second test structure.

BLANK PAGE

TABLE OF CONTENTS

LIST OF ILLUSTRATIONS

LIST OF TABLES

LIST OF SYMBOLS

A	area, $in.^2$
A_1	skin area, $in.^2$ - Equation (131)
A_2	cap area, $in.^2$ - Equation (131)
$\mathcal{A}$	forward cell of torque box
a	unloaded side of compression panel, in.
$\mathcal{B}$	aft cell of torque box
BL	butt line
b	loaded side of compression panel, in.
C	distance from neutral axis, in.
C_1	constant defined by Equation (54)
C_2	constant defined by Equation (55)
C_3	constant defined by Equation (56)
c/c_{cr}	ratio of damping coefficient to critical damping coefficient
D	dimension (see Figure 25); also, skin bending stiffness, per inch
DUL	design ultimate load
d	sandwich skin thickness, in.
E	modulus of elasticity, psi
E'	modulus of elasticity of equivalent solid plate, psi
e	distance to shear center, in.
F	ultimate strength, psi
F'	strength of equivalent solid plate, psi

F_s	ultimate shear strength, psi
FRP	fiber glass reinforced plastic
f	calculated stress, psi
f	resonant frequency, Hz
G	shear modulus, psi
g	acceleration
H	dimension (Figure 25); also, constant defined by Equation (134)
Hz	cycles per second
h	panel thickness, in.
I	moment of inertia, $in.^4$
J	dimension (Figure 25)
K	constant; also, dimension (Figure 25)
k	constant
L	length, in.
LAA	low angle of attack
ℓ_n	natural logarithms
M	bending moment, in.-lb
MS	margin of safety
P	concentrated load, lb
Q	static moment (first moment of area) $in.^3$
q	shear flow, lb/in.
q'	shear flow prior to balancing, lb/in.

R	dimension (Figure 25); also, constant, defined by Equation (141)
R_W	weight ratio
R_I	weight ratio as affected by compression modulus
R_{III}	weight ratio with a load factor of 2.0
S	constant defined by Equation (140)
S_n	beam peak displacement during the nth cycle of vibration
S_{n+1}	beam peak displacement during the (n + 1) cycle of vibration
sc	shear center
T	torque, in.-lb
t	thickness, in.
t'	thickness of equivalent solid plate, in.
V	shear load, lb
V'	parameter relating shear and bending stiffness, Equation (129)
W	weight
WL	water line
X	horizontal distance, in.; also, horizontal and chordwise axis
x	distance to Y-Y axis, in.
Y	vertical axis
y	distance to X-X axis, in.; also, deflection (with subscript), in.
Z	horizontal and spanwise axis
α	phase angle, deg
Δ	incremental change

Δs	element length, in.
δ	deflection, in.
ϵ	strain, in./in.
μ	Poisson's ratio
ρ	radius of gyration of cross section; also, density (with subscript)
σ	stress level, psi
σ_{cr}	buckling stress of panel, psi
ϕ	angular deflection, rad or deg

SUBSCRIPTS

a	cell $\mathcal{A}$
b	cell $\mathcal{B}$
b	bending
br	bearing
c	compression
c	core
cr	critical
F	reinforced plastic material
m	miscellaneous
N	new configuration
n	number of cycles
O	original configuration
s	shear

sc	shear center
st	skin
T	torque
t	tension
V	shear load
X	spanwise
Y	chordwise
x	related to horizontal axis of wing section
y	related to vertical axis of wing section
vert	vertical
horiz	horizontal
1, 2, 3, . . .	identifying numbers
0. 25 c	25 percent line of chord

INTRODUCTION

GENERAL

Goodyear Aerospace Corporation fabricated two 7-foot-long fiber glass reinforced plastic aircraft wing test sections to verify that conventional methods of analysis will accurately predict the load-carrying capability of a composite structure. The program has been funded by the U.S. Army Aviation Materiel Laboratories; the U.S. Naval Air Development Center, Aero Structures Department; and Goodyear Aerospace Corporation (GAC).

PROGRAM OBJECTIVE

The objective of this program was to apply data generated from small specimen tests to the design of a large test structure to determine the stress distributions within the structure due to moment, shear, and torque, and to predict the structure's deflections and rotations under various loading conditions.

PROGRAM BACKGROUND

In the initial phase of the program, a design configuration was established and construction materials were screened and tested. Also, a stress analysis was made, material allowables were established (from laminate and sandwich specimens), and wing section tools were fabricated.

The design of the test sections was selected primarily to provide an established aerodynamic section (NACA23015) for which the actual moment-torque and moment-shear ratios were known. The skin and core construction was established on the basis of 3-ply minimum practical outer skin thickness.

Materials were chosen on the bases of availability, ease of processing, and cost. Since there were no designated design requirements with respect to magnitudes of moments, shears, and torques, the materials were not oriented to optimize for any particular loading condition but were arranged to minimize the variables in construction which would affect correlation of test data with analytical data.

PROGRAM PLAN

This program was conducted in the four phases outlined in this section.

Phase I - Preparation for Test

1. Design

   a. Joint specimens Types I through IV

   b. Joint specimens Type V (torque boxes)

   c. Test fixtures for joint specimens

   d. Test fixtures for wing section

2. Fabrication

   a. Joint specimens Types I through IV

   b. Joint specimens Type V

   c. Tool tryout part

   d. Test article, 7-foot long

Phase II - Testing (Performed at the U.S. Naval Air Development Center, Aero Structures Department)

1. Fabrication of test fixtures

2. Testing

   a. Joint specimens (static to destruction)

   b. Test article

      (1) Shear center determination
      (2) Vibration scan
      (3) Free vibration (nondestructive)
      (4) Forced vibration (nondestructive)
      (5) Load deflection - bending, torsion, bending plus torsion (nondestructive)
      (6) Destructive load - bending

Phase III - Analysis and Refinement

1. Design study - Theoretical evaluation of variations in material properties on configuration weight (Refer to Appendix I)

2. Test data analysis

3. Wing section design modification

Phase IV - Fabrication for Retesting

1. Tool rework

2. Test article No. 2

TEST PLAN

The program test plan was developed by the U.S. Naval Air Development Center, Aero Structures Department, and the Goodyear Aerospace Corporation. The test plan and description, as reported in Appendix II, are a part of the Aero Structures Department Report No. P14[1].

GAC DEVELOPMENT SUPPORT

DISCUSSION OF STRUCTURE AND ANALYSIS

Prior to the execution of this contract, a stress analysis for the initial evaluation of a fiber-glass-reinforced-plastic (FRP) aircraft wing test section was made. This analysis included section properties, bending stresses, shear flow patterns from VQ/I shears, shear center, and torsional shear flow. Estimates of the maximum bending stresses to be reacted by the structure and maximum expected shear stresses were included. Bending and torsional deflections for the maximum loads were also calculated.

The analysis was based on standard unsymmetrical bending methods for bending stresses and VQ/I shear distribution, while the shear flow distribution analysis was based on successive approximation.

The structure, as designed, was a two-cell box beam of integral cap section and sandwich construction (see Figure 1). A multicell beam provides more shear webs and is considered to be more efficient than a pure monocoque section. The airfoil section chords were 70.6 inches, of which the structural two-cell box was approximately 48 inches. The maximum depth of the section was 9.4 inches. Sandwich construction was used to achieve greater buckling resistance in both compression and shear, and also to minimize the need for transverse ribs. The test section was 84 inches

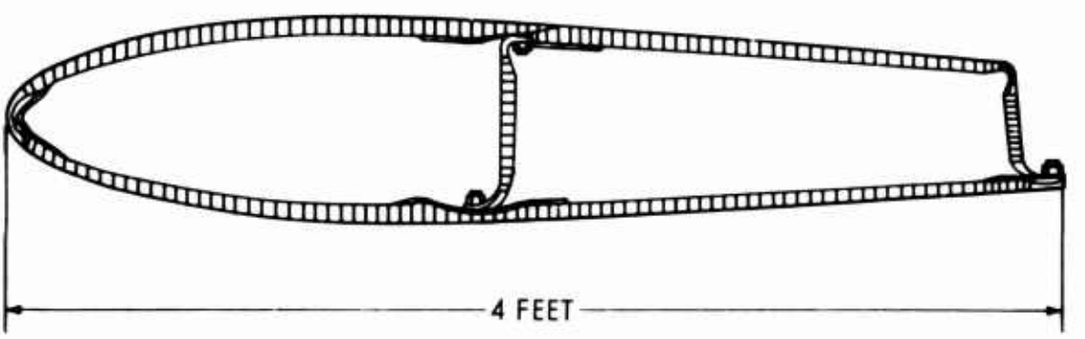

SANDWICH SKINS: 3-PLY EPOXY FIBER GLASS
CORE: 1/8-INCH CELL, 1/2-INCH-THICK ALUMINUM HONEYCOMB

Figure 1. Fiber Glass Reinforced Plastic Wing Test Section.

long. The sandwich had a 0.50-inch core thickness with 0.030-inch-thick skins. The integral cap sections were made of the same laminate as the skins and varied in thickness from 0.25 inch to 0.375 inch. The two-cell box consisted of two moldings. The first began at the center spar and progressed to form the leading edge and lower surface of the total section; the second molding, formed as a hat section, began at the lower edge of the center spar and became the center spar, upper aft surface, and aft spar. The two sections were joined by three spanwise rows of bolts along the lower and upper center spar caps and the lower cap of the aft spar.

The skins and spar caps utilized a controlled-flow epoxy (E-293) resin, preimpregnated into 481 glass fabric (I-550 finish). The core material was 1/8-inch cell (0.001-5052), aluminum honeycomb with a density of 4.5 pcf. These materials were tested in solid laminate and sandwich specimen forms and were evaluated for mechanical properties. To obtain representative values, the panels from which the specimens were obtained were manufactured and processed in the same manner as the full-size parts. The accumulated test data included tension, compression, flexure and the associated moduli, as well as flatwise tension and compression for both the foam-filled and unfilled sandwiches. The laminates were tested in both the warp and fill directions, with the sandwich specimens having the core-ribbon direction appropriately oriented. The first four design allowables listed in Table I were derived from these small specimen tests while the last two were taken from MIL-HDBK-17[2]. These values were used in the structural analysis of the wing test section.

The initial wing test section was designed to have the fabric warp direction for the skins, spar webs, and spar caps in a spanwise direction, maintaining

TABLE I. DESIGN ALLOWABLES

Property	Design Allowables (psi)
Ultimate Tensile Strength (F_t)	50,000
Tensile Modulus (E_t)	3.5×10^6
Ultimate Compressive Strength (F_c)	40,000
Compressive Modulus (E_c)	3.5×10^6
Ultimate Shear Strength (F_s)	14,000
Shear Modulus (G)	0.81×10^6

the plies in a 0- to 90-degree orientation. The airfoil contour used for the test section was also used in the design of the GA-22A aircraft wing at station 85.0. The wing airfoil at the root section was an NACA-23015, tapering to NACA-23009 at the tip section. The test section thickness was approximately 13.3 percent of chord length.

STRESS ANALYSIS

General

The analysis assesses the distribution of stresses that were encountered by the cantilever, two-cell, sandwich box beam of airfoil configuration during static tests involving bending and torsion.

Figure 2 is a cross-sectional layout of the test article. The cross section is divided into 57 elements, for which the areas and element centers of gravity are indicated. Also shown are the quarter-chord locations, the overall center of gravity, and the shear center. The indicated elements are treated as concentrated areas in a manner similar to that used for conventional sheet-stringer construction. All areas (material) are considered to be fully effective in this analysis.

Initially, it was decided that the test section should be loaded by representative shears, moments, and torques that would be encountered by an aircraft wing. Therefore, the loads used in this analysis were taken from loads at wing station 85.0 of the GA-22A aircraft for a low angle-of-attack condition. Because the stress level that results from these loads is quite low for this configuration, the loads are considered to be of representative proportions; they are used as a basis for ratioing, estimating the maximum load-carrying capacity of the test section, and preserving the proportionality of bending moments, shear, and torque that might be applied to an actual wing section. The loads used are as follows:

$$M_x = 30,000 \text{ in.-lb}$$

$$M_y = -34,000 \text{ in.-lb}$$

$$V_y = 4,420 \text{ lb}$$

$$V_x = -520 \text{ lb}$$

$$T_{0.25c} = -10,500 \text{ in.-lb (wing pitching moment about 25 percent line of chord)}$$

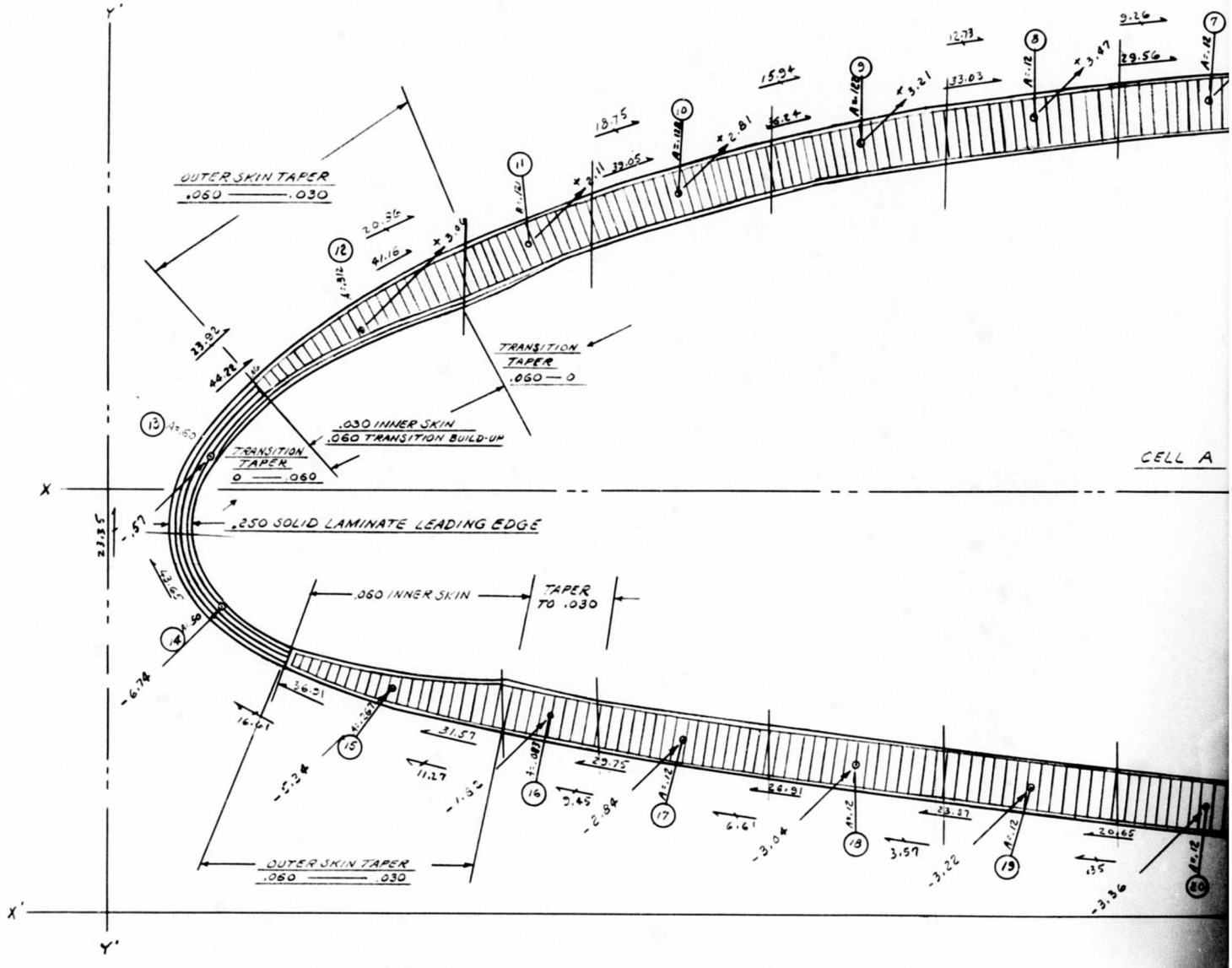

Figure 2. Test Section Layout for the Stress Analysis of the No. 1 Wing.

A

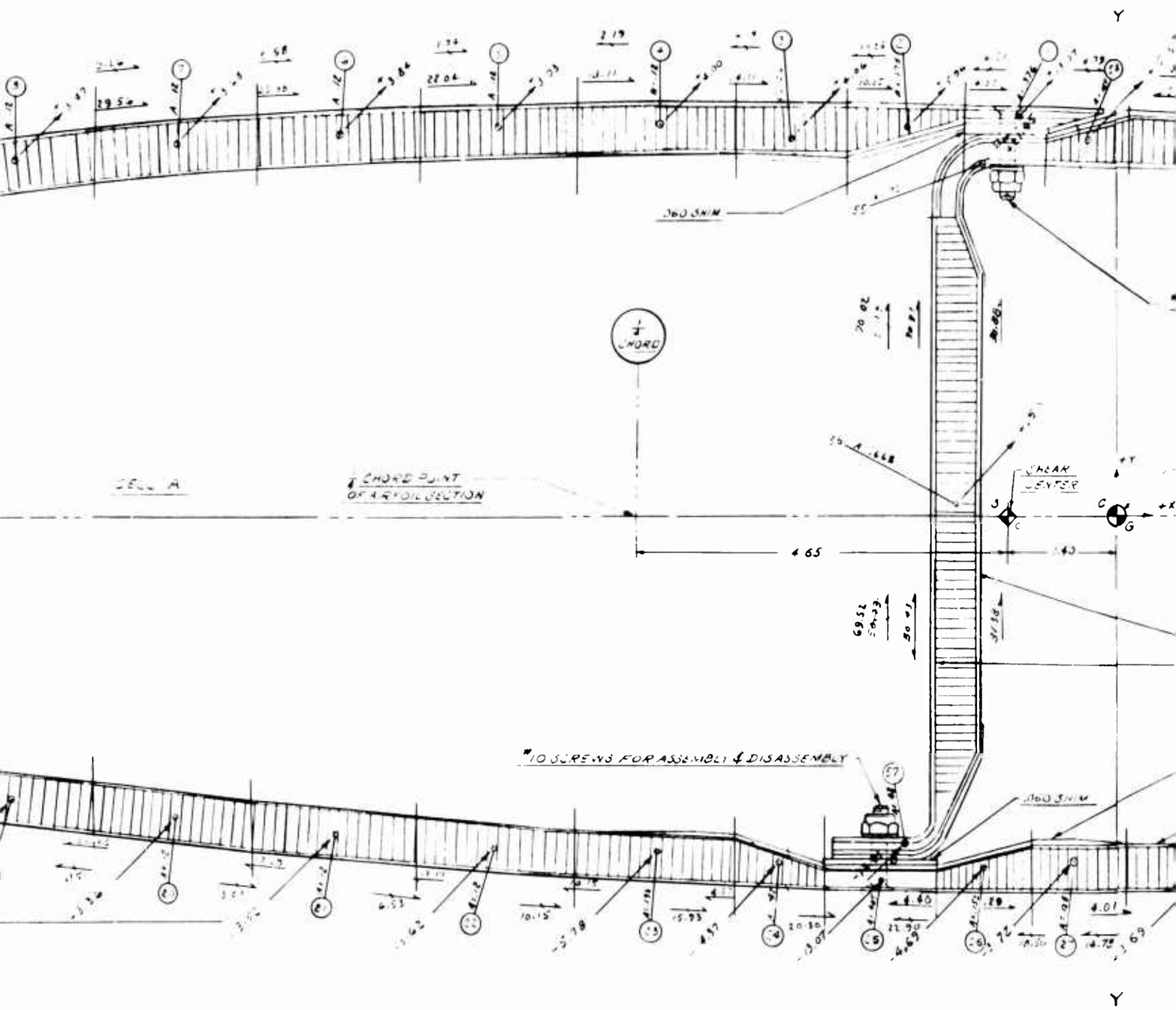
Y
300 SHIM
1/4 CHORD
SECT A
1/4 CHORD POINT OF AIRFOIL SECTION
SHEAR CENTER
C
G
4.65
10 SCREWS FOR ASSEMBLY & DISASSEMBLY
300 SHIM
Y

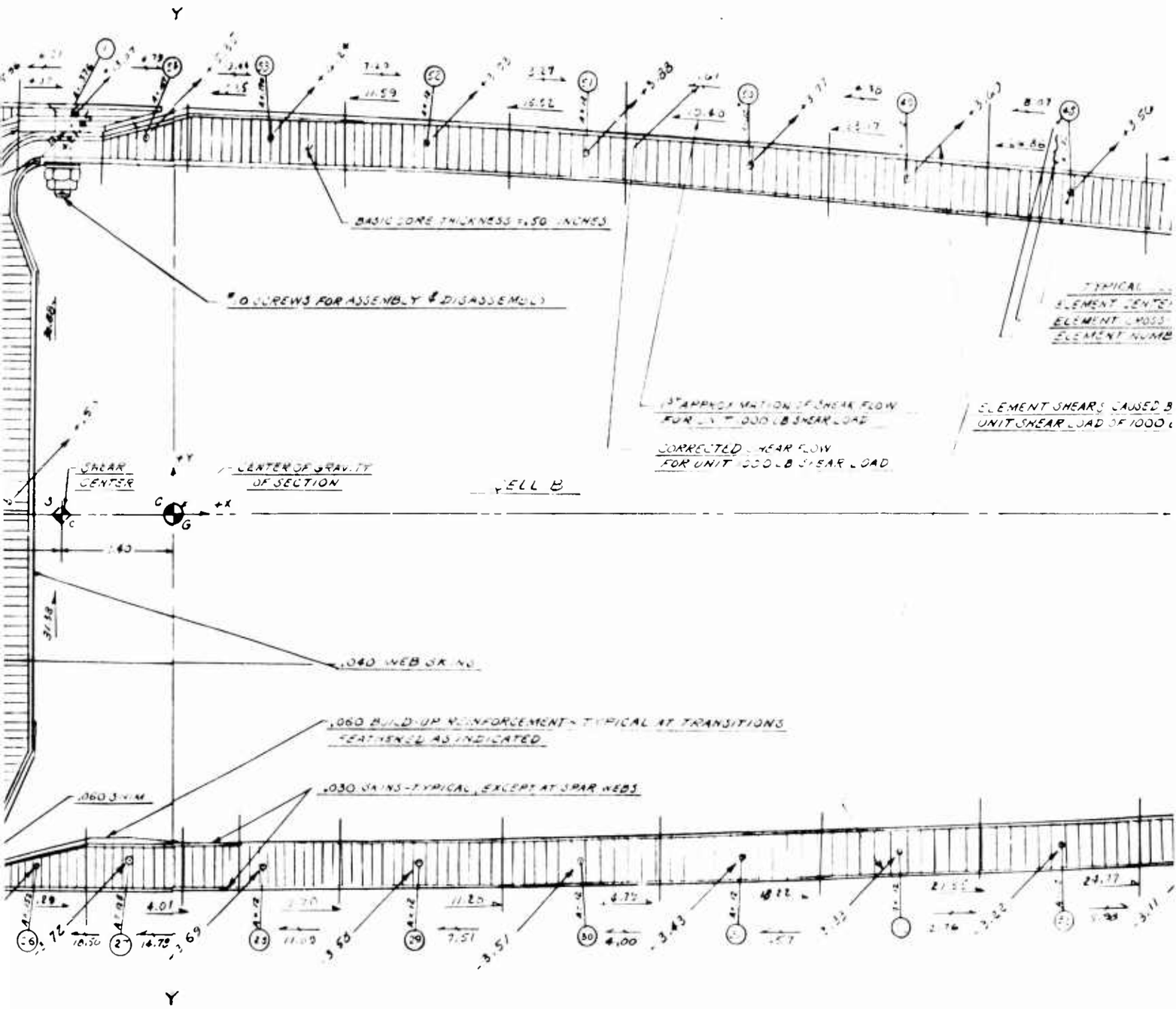
Y
BASIC CORE THICKNESS = .50 INCHES
"O SCREWS FOR ASSEMBLY & DISASSEMBLY
APPROXIMATION OF SHEAR FLOW FOR UNIT 1000 LB SHEAR LOAD
CORRECTED SHEAR FLOW FOR UNIT 1000 LB SHEAR LOAD
ELEMENT SHEARS CAUSED B
UNIT SHEAR LOAD OF 1000
SHEAR CENTER
CENTER OF GRAV. IT OF SECTION
CELL B
.040 WEB SKIN
.060 BUILD-UP REINFORCEMENT - TYPICAL AT TRANSITIONS FEATHERED AS INDICATED
.060 SKIN
.030 SKINS - TYPICAL EXCEPT AT SPAR WEBS
Y

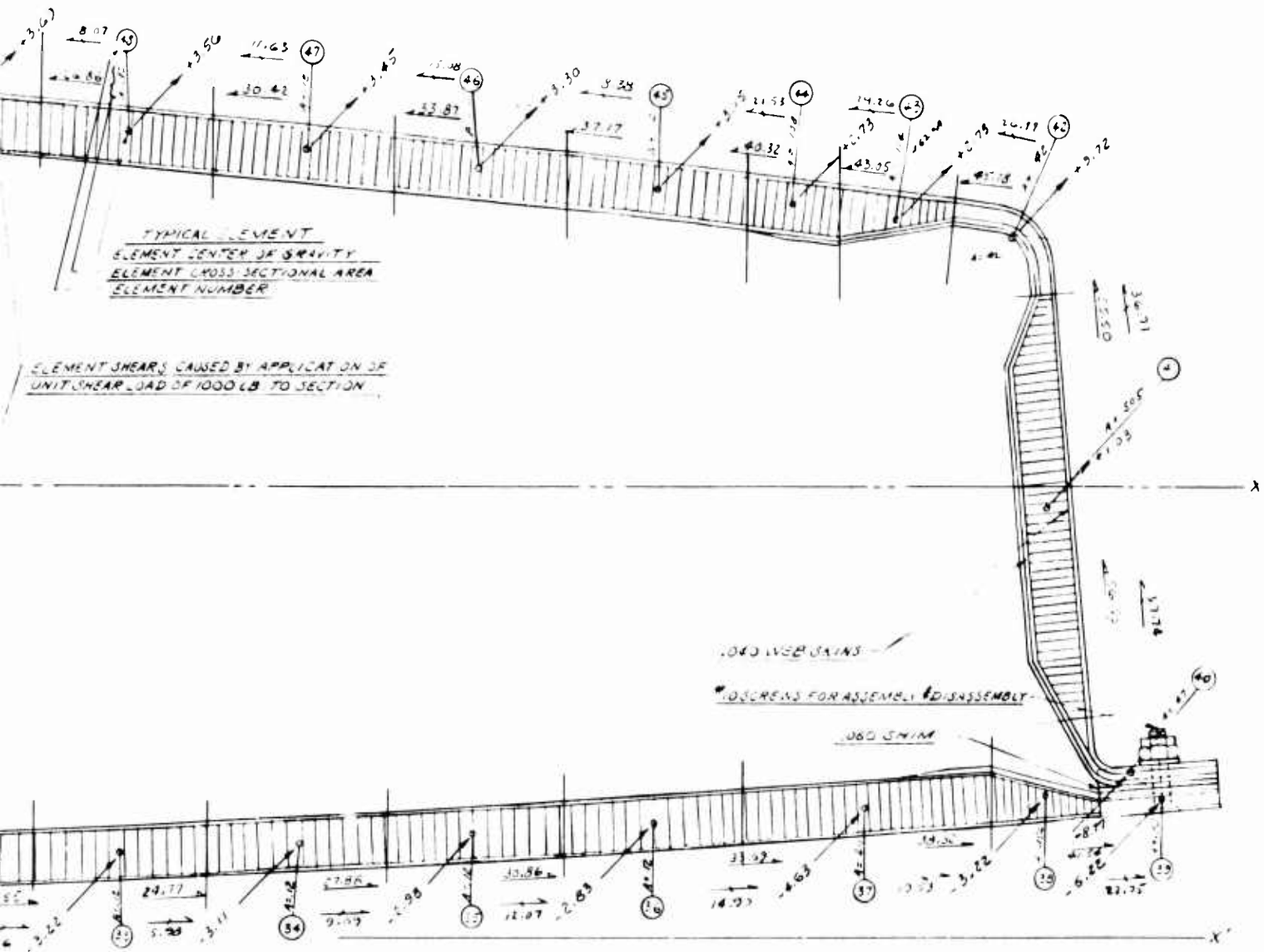
TYPICAL ELEMENT
ELEMENT CENTER OF GRAVITY
ELEMENT CROSS-SECTIONAL AREA
ELEMENT NUMBER
ELEMENT SHEARS CAUSED BY APPLICATION OF
UNIT SHEAR LOAD OF 1000 LB TO SECTION
.060 WEB SKINS
#10 SCREWS FOR ASSEMBLY & DISASSEMBLY
.060 SKIN

The torque loading about the shear center was computed as follows:

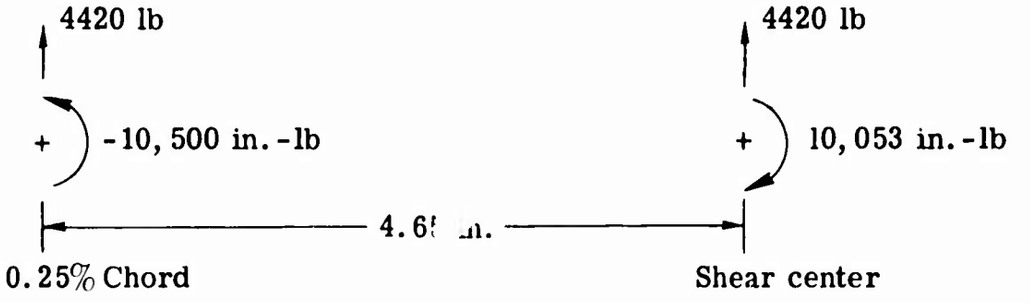

$$T_{sc} = -10,500 + (4.65 \times 4420)$$
$$= -10,500 + 20,553 \qquad (1)$$
$$= 10,053 \text{ in.-lb}$$

The planned static test loading called for the shear load to be applied as a concentrated load at the tip. Since shear loads on the GA-22A wing were distributed airloads, an exact load simulation was not practical. It was, however, practical to obtain the correct shear-bending relationship at one wing butt line (BL) by dividing the maximum moment by the maximum shear.

$$\frac{M_x}{V_y} = \frac{300,000}{4,420} = 67.8 \text{ inches} \qquad (2)$$

Therefore, the test loading of 4420 pounds shear produces a bending moment of 300,000 inch-pounds at BL 67.8. For the bending tests, this BL will be the critical section for bending. Shear and torsional shear will be constant at all stations.

Because the GA-22A airplane was not a highly loaded aircraft, and because it was considered desirable to use a fairly representative test section, it was desirable to increase the GA-22A load factor to achieve the intent of this program. This was accomplished by using the following criteria. The maximum calculated bending stress for the GA-22A loads applied to the test section was 10,440 psi at BL 67.8. It was considered desirable to obtain a maximum stress of 40,000 psi. Therefore, the load factor to be applied to the test loads was 40,000/10,440 = 3.83. This load factor was applied to obtain the design ultimate loads for the static tests.

The bending and shear loads about the Y-Y axis produce only minor stresses and are not considered to be test loadings. These loads were considered in the bending stress analysis, but they were not considered for the shear analysis.

Torsion loading for the low angle-of-attack (LAA) condition produced rather low torsional shear stresses in the test wing. Therefore, when the bending and torsion were combined, rather insignificant torsional effects resulted. A fictitious condition was therefore arbitrarily assumed as a pure torsion test. The applied torque for this condition was set at 186,000 inch-pounds, which was 4.83 times as large as the torque used in the combined bending and torque condition. Table II indicates the bending stress in the section elements.

TABLE II. BENDING STRESSES, LOW ANGLE OF ATTACK x 3.83

Element	f_b (LAA) (psi)	f_b (LAA x 3.83) (psi)	Element	f_b (LAA) (psi)	f_b (LAA x 3.83) (psi)
1	-10,434	-40,000	30	+8,820	+33,750
2	-10,042	-39,900	31	+8,649	+33,150
3	-9,712	-37,200	32	+8,428	+32,300
4	-10,034	-39,600	33	+8,320	+31,850
5	-9,923	-38,000	34	+7,951	+30,450
6	-9,683	-37,000	35	+7,642	+29,250
7	-9,332	-35,700	36	+7,288	+27,900
8	-8,840	-33,840	37	+6,855	+26,250
9	-8,060	-30,850	38	+6,511	+24,950
10	-6,788	-26,000	39	+6,515	+24,960
11	-5,457	-20,900	40	+5,902	+22,600
12	-3,239	-12,400	41	-303	-1,160
13	-28	-107	42	-6,615	-25,300
14	+3,717	+14,230	43	-6,920	-26,500
15	+5,697	+21,800	44	-7,290	-27,950
16	+6,314	+24,200	45	-7,607	-29,100
17	+6,850	+26,200	46	-7,998	-30,600
18	+7,370	+28,200	47	-8,411	-32,200
19	+7,840	+30,000	48	-8,712	-33,350
20	+8,218	+31,450	49	-9,072	-34,750
21	+8,628	+33,050	50	-9,102	-34,850
22	+8,938	+34,200	51	-9,600	-36,750
23	+8,932	+34,200	52	-9,759	-37,400
24	+9,152	+35,050	53	-9,818	-37,600
25	+9,597	+36,700	54	-9,754	-37,400
26	+9,211	+35,250	55	-9,138	-35,000
27	+9,019	+34,500	56	-255	-977
28	+9,183	+35,150	57	+8,619	+33,000
29	+8,991	+34,400			

Shear Stress Analysis

Table III indicates average shear stresses for the elements contained in the cross section of the test beam. The largest calculated spar web shear stress for the combined bending and torque condition in Table III is 14,846 psi. From Reference 2, the shear allowable for the spar web skins is 14,000 psi. Therefore, the shear margin of safety (MS) is

$$MS = \frac{14,000}{14,846} - 1 = -0.05 \qquad (3)$$

For the basic purposes of the program, the negative margin of safety is considered to be satisfactory.

TABLE III. SUMMARY OF SHEAR STRESS CALCULATIONS

(1) Item	(2) t	(3) q_V V 16,929	(4) q_T T 36,503	(5) $q_V + q_T$ (3) + (4)	(6) q_{T1} T_1 186,000	(7) f_{sV} (3) / (2)	(8) f_{sT} (4) / (2)	(9) $f_{sV} + f_{sT}$ (5) / (2)	(10) f_{sT1} (6) / (2)
1-2	.100	274.5	-53.9	220.6	-260.4	2745	-539	2206	-2604
2-3	.080	173.4	-53.9	119.5	-260.4	2168	-674	1494	-3255
3-4	.060	105.0	-53.9	51.1	-260.4	1750	-898	852	-4340
4-5	.060	37.1	-53.9	-16.8	-260.4	618	-898	280	-4340
5-6	.060	-29.5	-53.9	-83.4	-260.4	-492	-898	-1390	-4340
6-7	.060	-94.6	-53.9	-148.5	-260.4	-1577	-898	-2475	-4340
7-8	.060	-156.7	-52.9	-210.6	-260.4	-2612	-898	-3510	-4340
8-9	.060	-215.5	-53.9	-269.4	-260.4	-3592	-898	-4490	-4340
9-10	.060	-270.0	-53.9	-323.9	-260.4	-4500	-898	-5398	-4340
10-11	.060	-317.5	-53.9	-371.4	-260.4	-5292	-898	-6190	-4340
11-12	.060	-353.0	-53.9	-406.9	-260.4	-5883	-898	-6782	-4340
12-13	.100	-405.6	-53.9	-459.5	-260.4	-4056	-539	-4595	-2604
13-14	.250	-396.0	-53.9	-449.9	-260.4	-1584	-216	-1800	-1040
14-15	.100	-281.5	-53.9	-335.4	-260.4	-2815	-539	-4499	-2604
15-16	.060	-191.5	-53.9	-245.4	-260.4	-3192	-898	-4090	-4340
16-17	.060	-160.0	-53.9	-213.9	-260.4	-2667	-898	-3565	-4340
17-18	.060	-111.8	-53.9	-165.7	-260.4	-1863	-898	-2762	-4340
18-19	.060	-60.5	-53.9	-114.4	-260.4	-1008	-898	-1940	-4340
19-20	.060	-6.1	-53.9	-60.0	-260.4	-102	-898	-1000	-4340
20-21	.060	51.0	-53.9	-2.9	-260.4	850	-898	-48	-4340
21-22	.060	110.3	-53.9	56.4	-260.4	1838	-898	940	-4340

TABLE III - Continued

(1) Item	(2) t	(3) q_V V = 16,929	(4) q_T T = 38,503	(5) $q_V + q_T$ (3) + (4)	(6) q_{T1} T_1 186,000	(7) f_{sV} (3) (2)	(8) f_{sT} (4) (2)	(9) $f_{sV} + f_{sT}$ (5) (2)	(10) f_{sT_1} (6) (2)
22-23	.060	175.4	-53.9	121.5	-260.4	2923	-898	2025	-4340
23-24	.080	269.5	-53.9	215.6	-260.4	4492	-674	3593	-3255
24-25, 57	.100	344.0	-53.9	290.1	-260.4	5733	-539	4835	-2604
25, 57-26	.100	-393.0	-55.8	-448.8	-269.6	-3930	-558	-4488	2696
26-27	.080	-313.4	-55.8	-369.2	-269.6	-3917	-697	-4615	-3370
27-28	.060	-253.8	-55.8	-309.6	-269.6	-4230	-930	-5160	-4495
28-29	.060	-187.5	-55.8	-243.3	-269.6	-3125	-930	-4055	-4493
29-30	.060	-127.0	-55.8	-182.8	-269.6	-2117	-930	-3047	-4493
30-31	.060	-67.8	-55.8	-123.6	-269.6	-1130	-930	-2060	-4493
31-32	.060	-9.6	-55.8	-65.4	-269.6	-160	-930	-1090	-4493
32-33	.060	46.8	-55.8	-9.0	-269.6	780	-930	-150	-4493
33-34	.060	101.0	-55.8	45.2	-269.6	1683	-930	753	-4493
34-35	.060	153.9	-55.8	98.1	-269.6	2565	-930	1635	-4493
35-36	.060	204.5	-55.8	148.7	-269.6	3408	-930	2478	-4493
36-37	.060	252.0	-55.8	196.2	-269.6	4200	-930	3270	-4493
37-38	.060	330.0	-55.8	274.2	-269.6	5500	-930	4570	-4493
38-39, 40	.100	385.6	-55.8	329.8	-269.6	3856	-558	3298	-2696
39, 40-41	.080	639.0	-55.8	583.2	-269.6	7987	-697	7290	-3370
41-42	.080	622.0	-55.8	566.2	-269.6	7775	-697	7077	-3370
42-43	.100	457.0	-55.8	401.2	-269.6	4570	-558	4012	-2696
43-44	.080	411.5	-55.8	355.7	-269.6	5144	-697	4446	-3370
44-45	.060	364.0	-55.8	308.2	-269.6	6067	-930	5137	-4493
45-46	.060	311.4	-55.8	255.6	-269.6	5190	-930	4260	-4493
46-47	.060	267.0	-55.8	211.2	-269.6	4450	-930	3520	-4493
47-48	.060	197.4	-55.8	141.6	-269.6	3290	-930	2360	-4493
48-49	.060	136.7	-55.8	80.9	-269.6	2278	-930	1348	-4493
49-50	.060	74.3	-55.8	18.5	-269.6	1238	-930	308	-4493
50-51	.060	10.3	-55.8	-45.5	-269.6	172	-930	758	-4493
51-52	.060	-55.5	-55.8	-111.3	-269.6	-925	-930	1855	-4493
52-53	.060	-121.9	-55.8	-177.7	-269.6	-2032	-930	2962	-4493
53-54	.080	-228.0	-55.8	-283.8	-269.6	-2850	-697	-3545	-3370
54-55, 1	.100	-318.0	-55.8	-373.8	-269.6	-3180	-558	-3738	-2696
55, 1-56	.080	-1185.8	-1.9	-1187.7	-9.2	-14822	-24	-14846	-115
56-57, 25	.080	-1177.3	-1.9	-1179.2	-9.2	-14716	-24	-14740	-115

Compression Buckling

Compression buckling calculations for the subject sandwich material are based on a equivalent solid plate material, using an equivalent thickness and an effective modulus, where the bending stiffness and the extensional stiffness are considered. The plate is considered to be simply supported along the spanwise edges and clamped along the short edges.

Equation (4) is used to find bending stiffness (EI).

$$E(2)(d)\left(\frac{t_c + d}{2}\right)^2 = \frac{E't'^3}{12} \tag{4}$$

Equation (5) is used to find extensional stiffness (EA).

$$2Ed = E't'$$

$$E' = \frac{2Ed}{t'} \tag{5}$$

By substituting Equation (5) into Equation (4), we find that

$$\frac{2Ed}{t'}\,\frac{t'^3}{12} = E\,\frac{d(t_c + d)^2}{2}$$

$$t'^2 = 3\,(t_c + d)^2$$

$$t' = \sqrt{3}\,(t_c + d) \tag{6}$$

E' and t' are used in the buckling equations for the equivalent solid.

Equation (6) is used to find t' in the equivalent-thickness sandwich:

$$t' = \sqrt{3}\ (t_c + d)$$
$$= 1.732\ (0.50 + 0.03)$$
$$= 0.918 \text{ in.}$$

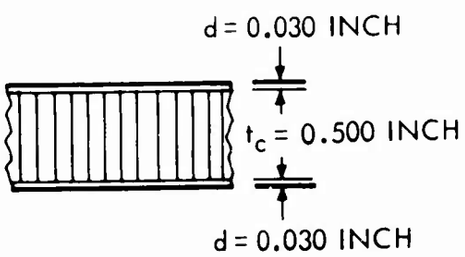

Equation (5) is used to determine the effective modulus in the equivalent-thickness sandwich:

$$E' = \frac{2Ed}{t'} = \frac{2 \times 3,000,000 \times 0.030}{0.918} = 196,000 \text{ psi}$$

The following equation is used to determine the panel buckling (assumed as flat plate) in the equivalent-thickness sandwich:

$$\frac{a}{b} = \frac{84}{23} = 3.66 \tag{7}$$

$$F'_{c_{cr}} = KE'\left(\frac{t'}{b}\right)^2 \tag{8}$$

K = 3.62 (u = 0.30) for simply supported edges[2]

Substitution into Equation (8) gives a buckling stress for the equivalent plate,

$$F'_{cr} = 3.62 \times 196,000\left(\frac{0.918}{23}\right)^2 = 1135 \text{ psi}$$

The buckling stress for the sandwich is found from equation (9).

$$F_{c_{cr}} = F'_{c_{cr}}\ (t'/2d) \tag{9}$$

Substitution into (9) gives,

$$F_{c_{cr}} = 1135 \times 0.918/0.060 = 17,350 \text{ psi}$$

K = 6.3 for clamped sides and simply supported ends so that

$$F_{c_{cr}} = 6.3/3.62 \times 17,350 = 30,300 \text{ psi}$$

The aft panel, which is considered to be critical for buckling, has an average calculated compression stress of 33,625 psi across the panel width. Assuming K = 6.3 for the clamped edges, the buckling MS is

$$MS = 30,300/33,625 - 1 = -0.10 \quad (10)$$

For the basic purposes of this program, the negative margin of safety is considered to be satisfactory. Also, since the calculated buckling stress does not consider any curvature in the panel or the variation in stress along the length of the panel, the negative margin of 10 percent is considered to be satisfactory in establishing a design ultimate load for the test specimen.

Vertical Deflection

The vertical deflection calculations are based on the maximum compressive stress of 40,000 psi.

For the 100 percent DUL deflection calculations that follow, assume the test section to be a cantilever beam with a concentrated load.

BENDING DEFLECTION

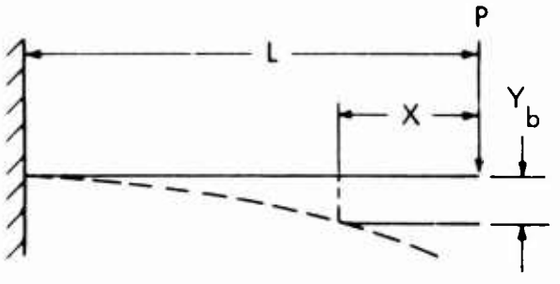

$$y_b = \frac{P}{6EI}(X^3 - 3L^2X + 2L^3) \quad (11)$$

P = 3.83 x 4,420 lb
= 16,929 lb
I = 138.59 in.^{4}
E = 3,500,000 psi
L = 84 in.
X = 0

SHEAR DEFLECTION

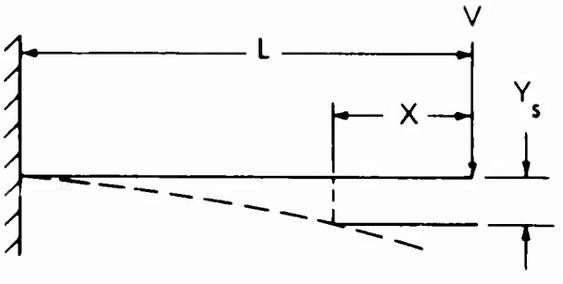

$$y_s = \frac{V(L - X)}{AG} \quad (12)$$

V = 16,929 lb = P
A = 11.71 in.^{2}
G = 810,000 psi
L = 84 in.
X = 0

BENDING DEFLECTION

Substitution into Equation (11) yields

$$y_b = \frac{16,929 \times 1,185,408}{6 \times 3,500,000 \times 138.59}$$

$$= 6.90 \text{ in.}$$

SHEAR DEFLECTION

Substitution into Equation (12) yields

$$y_s = \frac{16,929 \times 84}{11.71 \times 810,000}$$

$$= 0.15 \text{ in.}$$

The total deflection at the tip is $y_b + y_s$.

$$y_b + y_s = 6.90 + 0.15$$

$$= 7.05 \text{ in.} \qquad (13)$$

Table IV gives vertical deflections for 70 percent design ultimate load (DUL).

TABLE IV. VERTICAL DEFLECTION CALCULATIONS FOR 70 PERCENT DUL WITH P = 11,850 LB

x	x^3	$-3L^2x$	$2L^3$	$x^3-3L^2x+2L^3$	$\frac{P}{6EI}$	y_b	L-x	$\frac{V}{AG}$	y_s	y_b+y_s	Wing BL
0	0	0	1,185,408	1,185,408	0.0000040716	4.826	84	0.001249	0.105	4.93	0
6	216	-127,008	1,185,408	1,058,616	0.0000040716	4.310	78	0.001249	0.097	4.41	6
20	8,000	-423,360	1,185,408	770,048	0.0000040716	3.135	64	0.001249	0.067	3.20	20
34	39,304	-719,712	1,185,408	505,000	0.0000040716	2.056	50	0.001249	0.062	2.12	34
42.5	76,766	899,640	1,185,408	362,534	0.0000040716	1.476	41.5	0.001249	0.052	1.53	42.5
51	132,651	-1,079,568	1,185,408	238,491	0.0000040716	0.971	33	0.001249	0.041	1.01	51
68	314,432	-1,439,424	1,185,408	60,416	0.0000040716	0.246	16	0.001249	0.020	0.27	68
80.75	526,535	-1,709,316	1,185,408	2,627	0.0000040716	0.011	3.25	0.001249	0.004	0.015	80.75
84	592,704	-1,778,112	1,185,408	0	0.0000040716	0	0	0.001249	0	0	84

Torque Distribution

The schematic in this section represents a cross section of the test specimen. The shear flow q in pounds per inch for the specimen is indicated by the arrows, and the cell sections are labeled α and β. The parameters needed for the torque distribution calculations for T = 1000 in.-lb are given in Equations (14) through (18), and the calculation follows.

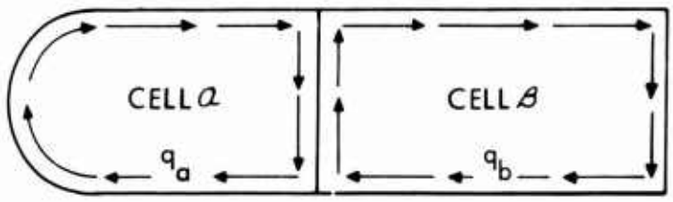

$$A_a = 157 \tag{14}$$

$$\sum \left(\frac{\Delta s}{t}\right)_a = 636.6 \tag{15}$$

$$A_b = 193 \tag{16}$$

$$\sum \left(\frac{\Delta s}{t}\right)_b = 750 \tag{17}$$

$$\sum \left(\frac{\Delta s}{t}\right)_{ab} = 20.8 \tag{18}$$

For these calculations, the angle of deflection ϕ_a for cell α is equal to the angle of deflection ϕ_b for cell β. Then,

$$\frac{q_a \sum \left(\frac{\Delta s}{t}\right)_a - q_b \sum \left(\frac{\Delta s}{t}\right)_{ab}}{2A_a} = \frac{q_b \sum \left(\frac{\Delta s}{t}\right)_b - q_a \sum \left(\frac{\Delta s}{t}\right)_{ab}}{2A_b} \tag{19}$$

By substituting the appropriate parameters in Equations (14) through (18) into Equation (19), Equation (20) results:

$$\frac{636.6q_a - 20.8q_b}{314} = \frac{750q_b - 20.8q_a}{386} \tag{20}$$

By solving Equation (20) for q_a in terms of q_b, Equation (21) results

$$2.081q_a = 2.009\, q_b \tag{21}$$

Then

$$q_a = 0.9654\, q_b \tag{22}$$

To solve for q_a or q_b when T = 1000 in.-lb,

$$2A_aq_a + 2A_bq_b = 1000 \tag{23}$$

By substituting Equations (14) and (16) into Equation (23), Equation (24) is derived:

$$314q_a + q_b = 1000 \tag{24}$$

By substituting Equation (22) into Equation (24), the value of q_b and of q_a is found to be

$$q_a = 1.40 \tag{25}$$

$$q_b = 1.45 \tag{26}$$

By substituting Equations (25) and (26) into Equation (20), the value of ϕ_a and/or ϕ_b can be determined.

$$\phi_a = \phi_b = \frac{636.6 \times 1.40 - 20.8 \times 1.45}{314} \times \frac{L}{G} \tag{27}$$

$$= 2.74\ L/G \text{ (radians per 1000 in.-lb torque)} \tag{28}$$

where L = length, inches

G = shear modulus, psi

Twist Angle Estimate

The symbol ϕ is used to denote angular deflection which is, in this case, the angle of the estimated twist for a 64-inch test specimen at DUL and at 70 percent DUL. The calculations for the twist angles are given below.

$$\phi = \frac{2.74\ T_{sc}\ L}{G} \tag{29}$$

where G = 810,000 psi

L = 64 inches

T_{sc} = 10,053 x 3.83 = 38,500 in.-lb

By substituting the values of the unknowns in Equation (29), we arrive at Equation (30).

$$\phi = \frac{2.74 \times 57.3 \times 38,500 \times 64}{810,000} \qquad (30)$$

$$= 0.477 \text{ degree at 100 percent DUL}$$

$$= 0.334 \text{ degree at 70 percent DUL}$$

PROCESSING

TORQUE BOXES AND NO. 1 WING TEST SECTION

General

The basic fabrication procedure used in the manufacture of parts for this contract is a multistage positive pressure molding process. The process specification is presented in Appendix III. In this process, controlled-flow epoxy glass prepreg reinforcements are combined with an aluminum honeycomb core to form a structural sandwich. The positioning of reinforcements, core materials, release films, bleeder material, and the vacuum bag in the mold is a hand-layup procedure.

Fabrication Problems

While the materials and processes used to manufacture test articles for this program worked out quite well, a number of fabrication problems were encountered. Several of the difficulties were attributed to properties of the controlled-flow epoxy prepreg used in the parts. Other problems were functions of test article design and the bag molding process. These problems with their solutions are given in the following paragraphs.

Flow Control

A loss of flow control of the prepreg was encountered at the beginning of the program. Upon application of heat and pressure, resin flowed from the edge band and cap strip areas into the honeycomb core cells, filling them with resin. The flow control was regained by re-establishing the correct degree of advancement of the prepreg (refer to the process specification, Appendix III) and by lowering the resin content of the edge band prepreg.

Moisture Sensitivity

It was found that the E293 prepreg system was extremely moisture sensitive. Moisture pickup increases resin gel time and causes the resin to foam during cure. A number of steps were taken to minimize the moisture contamination of this material. The vendor was instructed to wrap and seal the prepreg rolls in a protective cover of laminated polyethylene, aluminum foil, and Kraft paper prior to shipment from his plant. A handling procedure was established which made it mandatory that prepreg be brought to room temperature before

its protective covering could be removed after removal from refrigeration. Gel time checks were run on the prepreg periodically to monitor moisture pickup. All layups were made in a temperature and humidity controlled environment (for limits, refer to the process specification in Appendix III). The above precautionary measures were successful in reducing the moisture problem.

Venting

In the layup procedure, the outer skin of a part is laid up, the core is placed on the skin, the cap strips are partially laid up, and the part is vacuum bagged and autoclave cured. The second layup stage includes completion of the cap strip layups, inner skin and edge reinforcement layups, vacuum bagging, and autoclave curing.

During fabrication of the torque box specimens, a problem arose which appeared to involve volitalization of the resin mix in the prepreg used for the inner skins. Mold-side skins cured out with high quality, but the bag-side skins had a white, cloudy appearance. It was found that by venting the core material into the layup edge bleeder, this apparent volatile problem could be eliminated. Panels vented in this manner have bag-side skins which are as clear as mold-side skins. This procedure has been incorporated into the process specification.

Bridging and Wrinkling of Reinforcing Material

The design of the test parts calls for a large number of plies of prepreg to be formed into closed right-angle corners with small radii (i.e., upper forward and rear spar caps of the aft cell). Both of these areas contribute to the complexity of the layup and bagging procedure. There is a tendency of the reinforcement to bridge in the upper spar caps of the aft cell and to wrinkle on the lower spar caps of the aft cell. To prevent the occurrence of these faults, the layup procedure is staged over several days. The outer skins are laid up, bagged, and debulked overnight under vacuum. The core and cap strip material are added and again debulked under vacuum prior to cure. This staging allows the prepreg material to seat out a few plies at a time without bridging or wrinkling. The debulking, care in placement of bleeder material, and pleating techniques developed for the bagging operation have produced high-quality laminates in areas which are prone to produce laminates of inferior quality.

NO. 2 WING TEST SECTION

General

In general, the fabrication process for the second wing test section was the same as that for the first section except that stiffener layups and bonding procedures were added.

Stiffener Layup Procedure

The balsa blocks are shaped to drawing dimensions and oven-dried for 1 hour at 150°F, 1 hour at 180°F, and 8 hours at 250°F. They are then sealed with a one-ply Style 116 cloth epoxy resin wet layup. The areas of the inner skins of the test sections which are to receive the stiffeners are then prepared for bonding. An epoxy adhesive is applied to the balsa blocks, which are then bonded in place. After the adhesive is cured, the sealer ply on the balsa is abraded. A seven-ply E293-481-I-550 epoxy prepreg layup is made over the balsa forms. This layup is vacuum bagged and autoclave-cured for 3 hours at 290°F and 30 psi.

JOINT SPECIMEN TESTS

GENERAL

Four different types of joint specimens representing different panel edge designs were evaluated. The objective of this investigation was to evaluate the transfer of load from the sandwich skin panels to attachment fittings and from sandwich skin panels to spar caps. A total of 33 tests were performed (30 tension tests and 3 compression tests). Twenty tests were performed at Goodyear Aerospace Corporation and thirteen at the U.S. Naval Air Development Center, Aero Structures Department.

SPECIMEN DESCRIPTIONS

Figure 3 shows the test specimen configuration for the specimens described in this subsection.

Specimen Type I

This specimen represented the sandwich panel edge configuration which was used in the design of the torque boxes and the wing test articles. The honeycomb core was filled with syntactic foam in the reinforced areas. The vacuum bag side of the specimen had a laminate reinforcement in the attachment area which was integrally molded with the sandwich skin. The mold side of the specimen had the same reinforcement laminated to the facing after the primary cure of the sandwich.

Specimen Type II

The attachment area of these specimens was made of solid laminate equal in thickness to the honeycomb. Sandwich skin thickness was gradually increased as it approached the solid laminate area. The honeycomb cells which were adjacent to the solid laminate were filled with syntactic foam. It was originally intended that the edge attachment represen' d by this specimen configuration would be used on the wing test section. After fabrication and test of the tensile type joint specimens, the Type II design was discarded in favor of the Type I design.

Specimen Type III

The attachment area of these specimens was made of solid laminate approximately 1/4 inch thick. This simulated a wing section lower panel spar cap. The honeycomb was tapered in thickness and foam filled where it approached the attachment area. Doubler plies were added to the bag side skin as it transitioned from sandwich to solid laminate.

Specimen Type IV

These specimens are similar to Type I specimens with the exception of steel inserts that were used to replace the laminate buildup in the attachment areas.

TEST RESULTS

Goodyear Tests

Results of all Goodyear Aerospace Corporation joint specimen tests are tabulated in Table V. The first 12 of the GAC tests were performed using Type I specimens with varying numbers of ply buildups at the ends. Two different material systems were evaluated and compared. In addition, two specimens without core foam were tested. Results of this comparison are shown in Figure 4. The remaining tests are, in general, duplicates of the Navy tests.

The apparent bolt bearing stress in the skins of the foam-filled sandwich specimens without reinforcing doublers is approximately twice the bolt bearing strength of similar specimens without the foam-filled core. Based on approximate EA values for the syntactic foam and the basic laminate, the ratio of load distribution is approximately one to one. Then as the laminate thickness is increased, the contribution of the syntactic foam becomes less significant. The joint strength increases to that required to fail the basic sandwich skins with the full buildup of 12 plies of 181 laminate on each skin. This buildup thickness and bolt pattern is designed to withstand proportional limit bearing stresses and the concentration factor associated with loading through the bolt holes. The syntactic foam is intended to provide a stabilizing influence at the edge of the laminate when the full reinforcement is used.

Aero Structures Department Tests

Joint specimen types I through IV were tested at the Aero Structures Department of the Naval Air Development Center to supplement the program at GAC for evaluating various methods of fabricating glass-fiber-reinforced plastic wing section joints and transition areas. The results of the tests are presented in Table VI. Three replicates of each type were tested in tension, and one Type I specimen was also tested in compression. The expected tension failing load for Types I, II, and IV was 7950 pounds; for Type III it was 4250 pounds. Photographs of specimen failures of each type are shown in Figures 5 through 8.

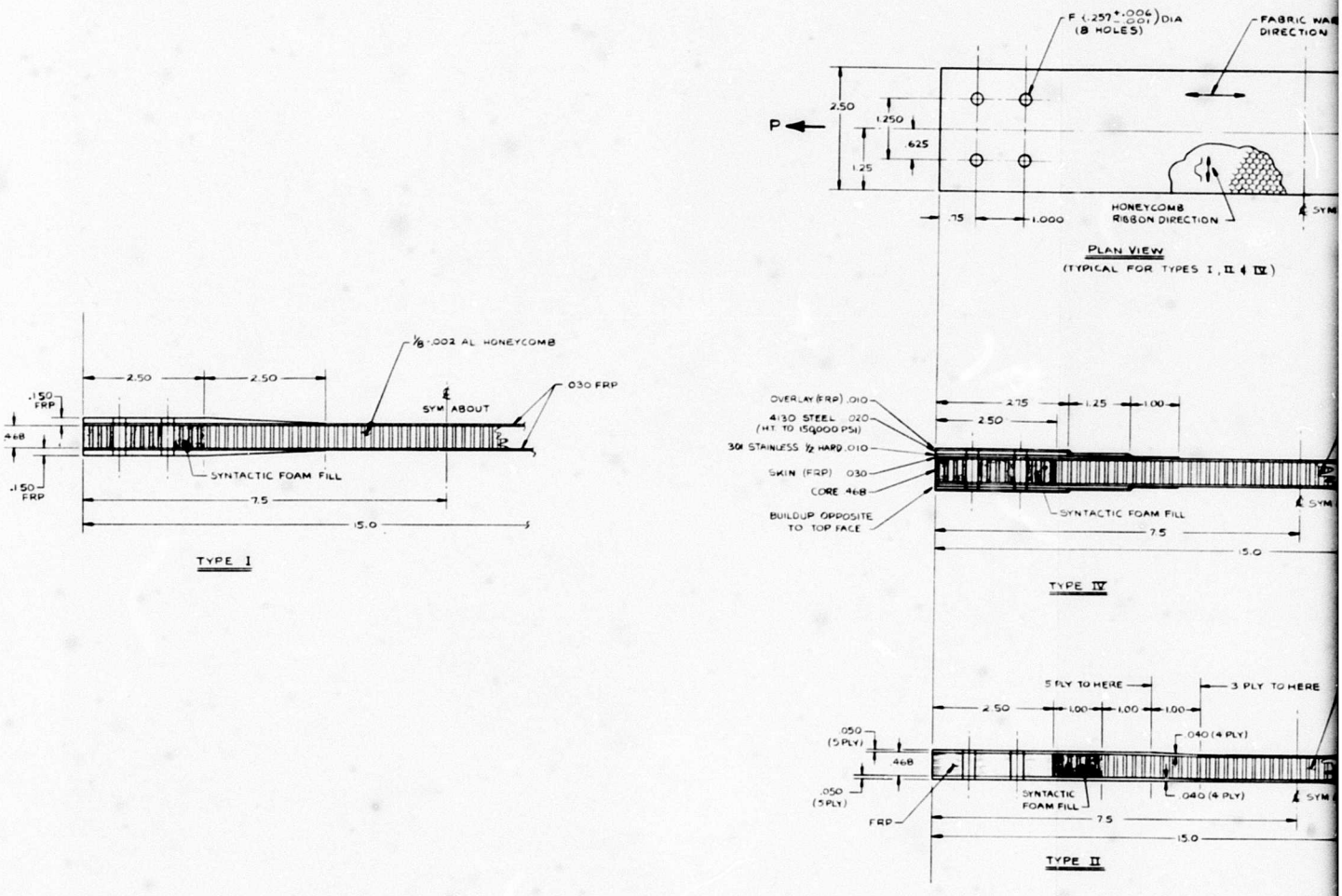

Figure 3. Joint Specimen Configuration.

A

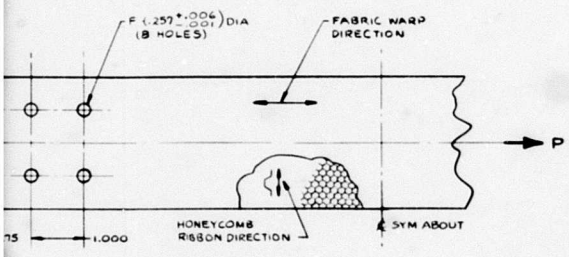

PLAN VIEW
(TYPICAL FOR TYPES I, II & IV)

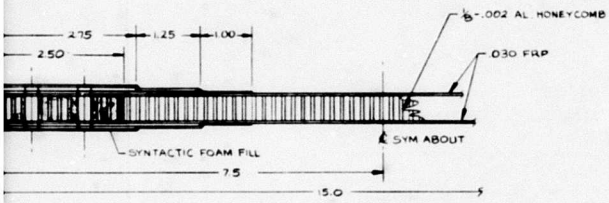

TYPE IV

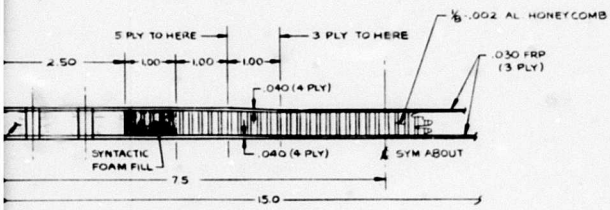

TYPE II

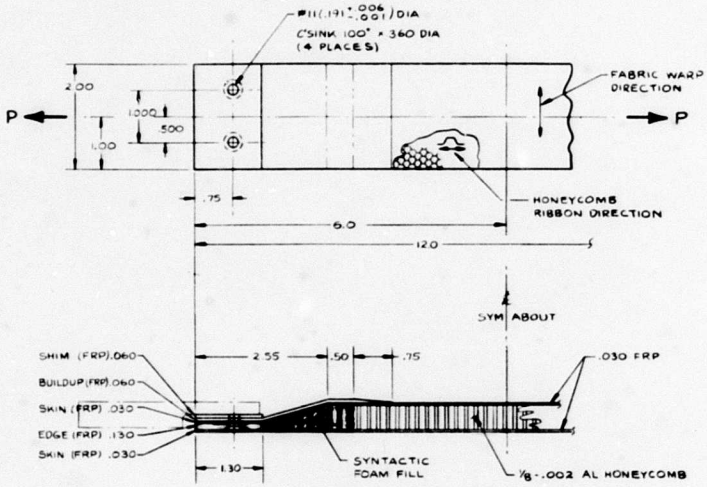

TYPE III

B

TABLE V. JOINT SPECIMEN TEST RESULTS
(GOODYEAR AEROSPACE CORP)

Specimen	Width of Specimen (in.)	No. of Plies		Failing Load (lb)	Skin Stress* (F_t)	Bearing Stress** (F_{br} - Avg)	Type of Failure
		Skin	Buildup				
T-I-0-1-P	2.498	3	0	4760	31,700	79,300	1
T-I-0-2-U	2.505	3	0	4170	27,600	69,500	1
T-I-3-1-P	2.490	3	3	6640	44,400	55,300	2
T-I-3-2-U	2.498	3	3	7970	53,200	66,300	1
T-I-6-1-P	2.493	3	6	7350	49,200	40,800	2
T-I-6-2-U	2.504	3	6	8540	56,800	47,400	3
T-I-9-1-P	2.501	3	9	8250	54,900	34,400	2
T-I-9-2-U	2.489	3	9	8570	57,300	35,700	3
T-I-12-1-U	2.520	3	12	8885	58,750	29,600	3
T-I-12-2-U	2.539	3	12	8745	57,500	29,200	3
T-I-0-1-P-N	2.442	3	0	2070	14,100	34,600	8
T-I-0-2-P-N	2.498	3	0	2030	13,550	33,800	8
C-II-2-1-U***	2.487	3	51	4460	29,900	14,850	5
C-I-12-2-U	2.536	3	12	8250	54,300	27,500	6
T-II-2-1-U	2.487	3	51	8765	58,600	17,100	3
T-II-2-2-U	2.493	3	51	8850	59,250	17,130	3
T-III-6-	2.0	3	6 - 1 side	4600	38,300	37,800	7
T-III-6-2	2.0	3	6 - 1 side	4490	37,500	36,000	7
T-IV-ST-1-P	2.5	3	STL	8710	58,000	-	3
T-IV-ST-2-P	2.5	3	STL	8100	54,000	-	3

*Tensile stress in basic sandwich skins.

**Apparent bearing stress, if laminate in bolt area is considered to react loads (disregarding syntactic foam).

***Doubler plies placed between core and skin on bag side, resulting in lower failing load.

TABLE V - Continued

SPECIMEN NUMBERING SYSTEM

X-X-X-X-X-N

- N — No syntactic foam used. Where this symbol is omitted, syntactic foam is used in joint area.
- X — Type of core-bond and material
  - P - Primed core (E-293 + 481 glass fabric, I-550 finish)
  - U - Unprimed core (E-293 + 7581 glass fabric, S-920 finish)
- X — Specimen Number
- X — Number of buildup plies per face, in addition to basic 3-ply sandwich skins. STL - steel; all others FRP.
- X — Type of Specimen (Refer to Figure 3)
- X — Type of Test
  - T - Tension
  - C - Compression

TYPES OF FAILURE

1	Tension - through first line of bolts.
2	Delamination between buildup plies on mold side and basic skin (secondary bond failure).
3	Tension failure of skin on mold side due to stress concentration at end of buildup (possibly from sanding).
4	Tension failure - both sandwich skins.
5	Compression failure at end of buildup on bag side of skin from eccentricity and foamed resin in prepreg skin.
6	Compression failure in sandwich skins at center of specimen.
7	Interlaminar shear between basic skin on mold side and edge band and pull-through of countersunk head in outer skin. Screws partially sheared.
8	Bearing failures under bolts.

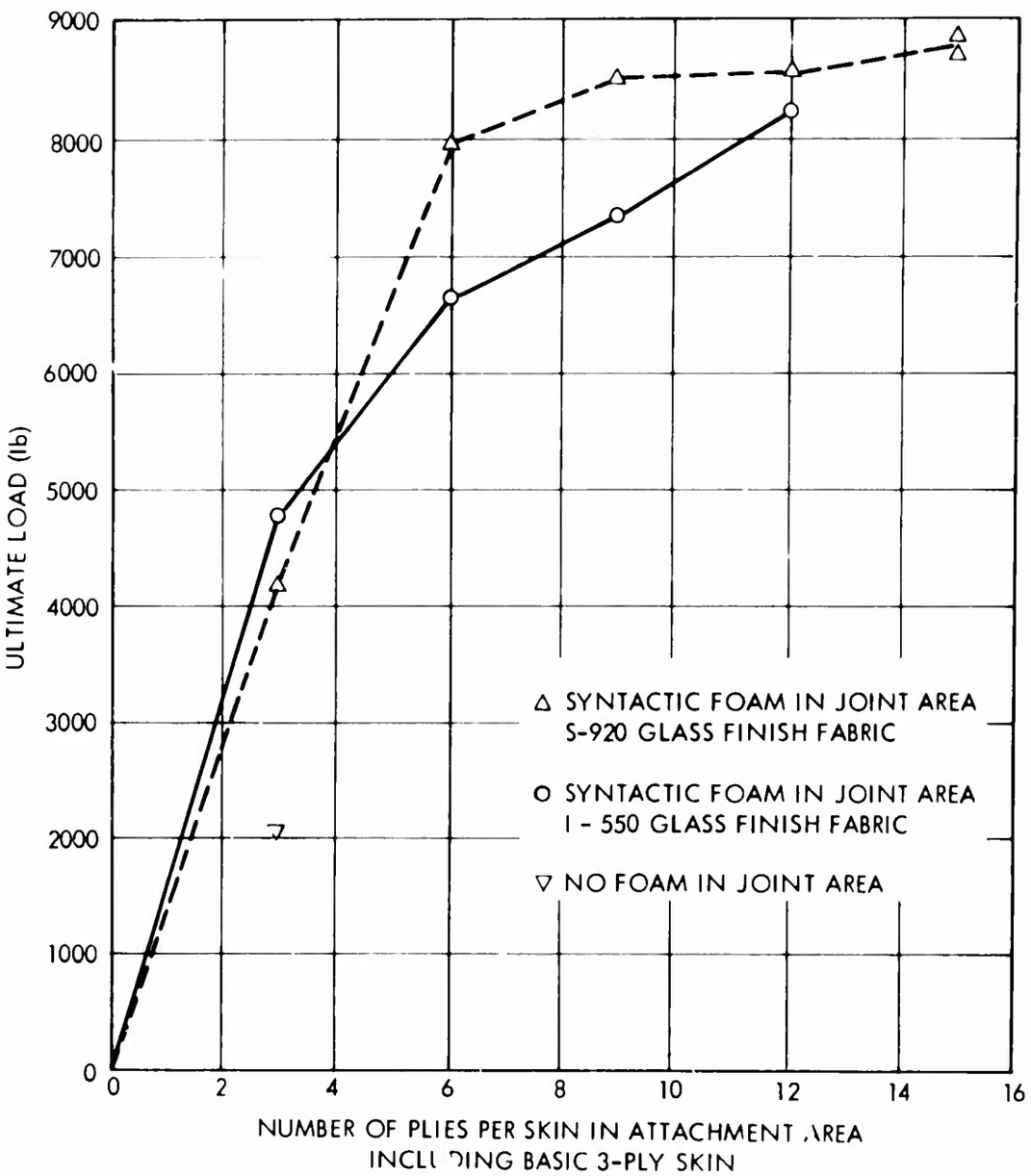

Figure 4. Comparison of the Two Material Systems in Tension.

TABLE VI. JOINT SPECIMEN TEST RESULTS
(NAVAL AIR DEVELOPMENT CENTER)

Specimen	Expected Failing Load (lb)	Failing Load (lb)	Skin Stress at Failure (psi)	Failure Mode Expected *	Actual Failure Mode*
I-1	7950	8060	53,700	1	3
I-2	7950	7340	48,900	1	4
I-3	7950	7655	51,000	1	5
I-4	6000	6990	46,600	8	8
II-1	7950	8175	54,500	1	1
II-2	7950	8940	59,600	1	5
II-3	7950	8600	57,300	1	4
III-1	4250	4175	34,800	2	6
III-2	4250	3930	32,700	2	7
III-3	4250	3995	33,300	2	6
IV-1	7950	8455	56,200	1	4
IV-2	7950	8075	53,800	1	4
IV-3	7950	8625	57,500	1	4

*Types of failure:

1 Tension failure in both facings (central sandwich)

2 Bolt shear

3 Tension failure of both facings

4 Tension failure of facing on mold side and subsequent failure and unbonding of other facing from core

5 Tension failure of facing on bag side and subsequent failure and unbonding of other facing from core

6 Interlaminar shear between the facing on mold side and the edgeband; pull-through of countersunk head in the outer facing and unbonding of other facing

7 Tension through line of bolts in facing of mold side

8 Compression failure of both facings (central sandwich)

NOTE: All failures occurred at or near the edge of the reinforced area unless otherwise specified.

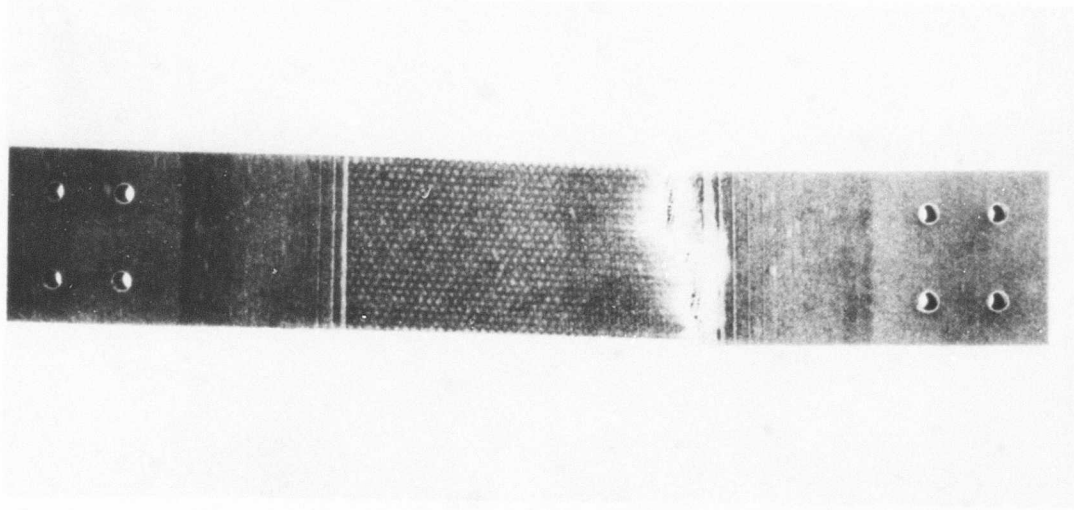

Figure 5. Specimen No. 3, Type I - Failure of Facing on Bag Side at Edge of Reinforcement.

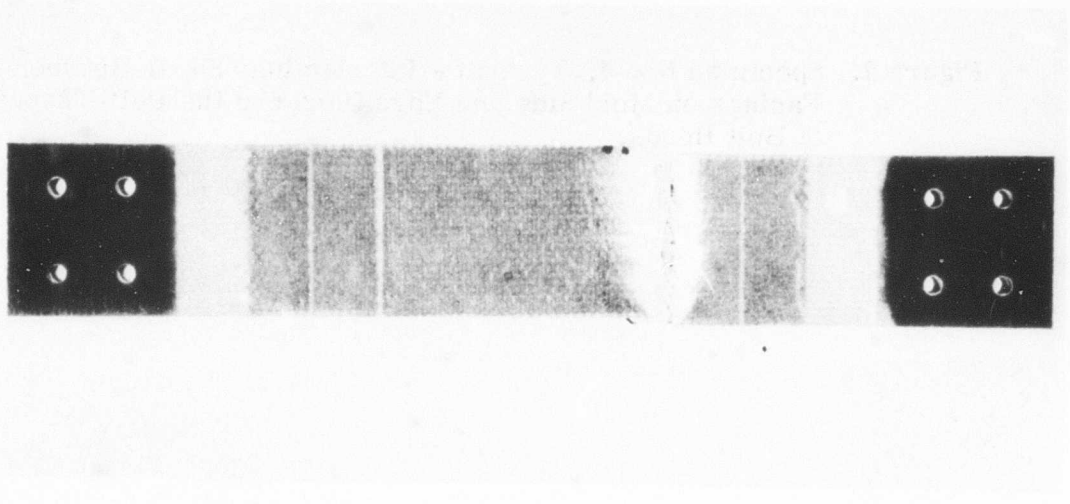

Figure 6. Specimen No. 3, Type II - Failure of Facing on Mold Side at Edge of Reinforcement.

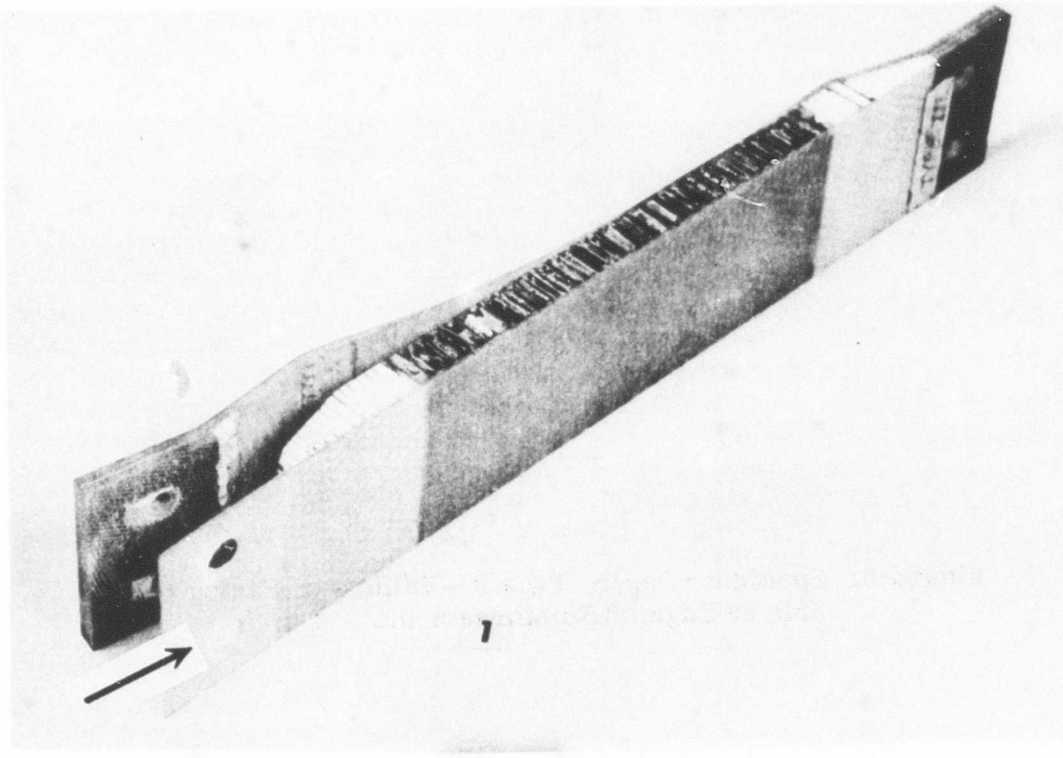

Figure 7. Specimen No. 1, Type III - Interlaminar Shear Between Facings on Mold Side and Edge Band and the Pull-Through of Bolt Heads.

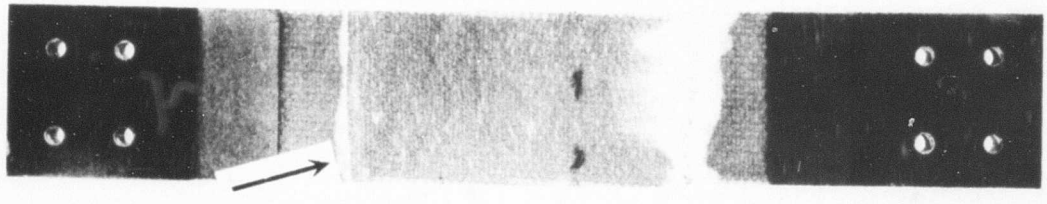

Figure 8. Specimen No. 1, Type IV - Failure of Facing on Mold Side at Edge of Reinforcement.

Test results, as described below and in Table VI, were reported in the Aero Structures Department Summary Report on Static Tests of GAC Joint Specimens Types I through IV.

For specimens of Types III and IV, areas of delamination were noted before failure. For Type III, delamination was evident around the countersink holes for all three specimens, indicating bearing failure. The area of delamination is shown in Figure 7 and indicated by the arrow. The loads at which delamination initiated were 4000, 3600, and 3750 pounds for specimens 1, 2, and 3 respectively. For Type IV, delamination occurred at the edge of the reinforced area as shown in Figure 8. Delamination was noted only for specimens 1 and 3 and occurred at 6000 and 6200 pounds respectively. The completion of these tests concluded the test program of small joint specimens at the Aero Structures Department.

TORQUE BOX TESTS

GENERAL

Two torque box sections (joint test specimens Type V) specified in the program plan were fabricated for test. The following is a discussion involving the design and testing of these specimens and an analysis of the test results.

The torque box specimens were representative of the aft cell of the two-cell wing section. Specimen V-A was fabricated with the lower cover bolted to the flanges of the hat section, while specimen V-B contained completely bonded joints. The objectives of this subprogram were as follows:

1. To compare bolted and bonded joints for strength and stiffness
2. To determine torsional strength of the structure
3. To determine torsional stiffness of the structure

The two specimens were delivered to the U.S. Naval Air Development Center, Aero Structures Department for testing. Each box section was 30 inches long. Eighteen inches of the center portion was the test section. Specimen configurations are shown in Figures 9 and 10.

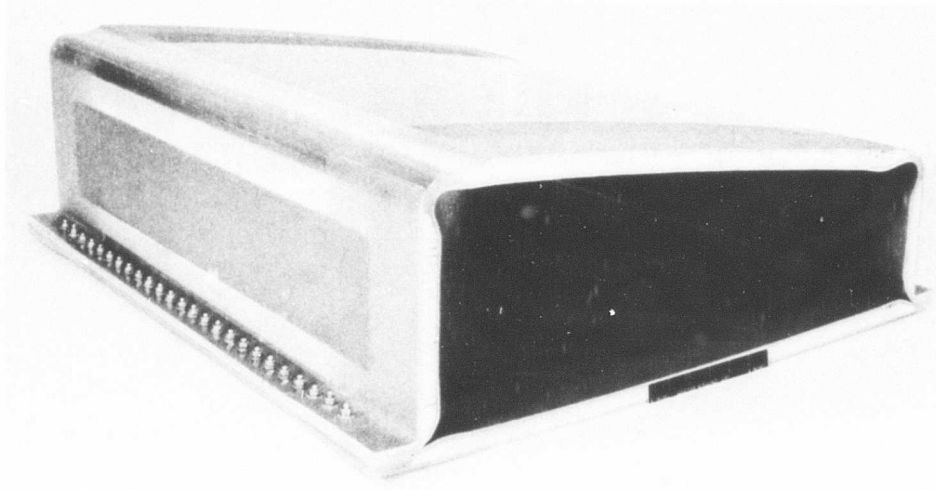

Figure 9. Torque Box Configuration.

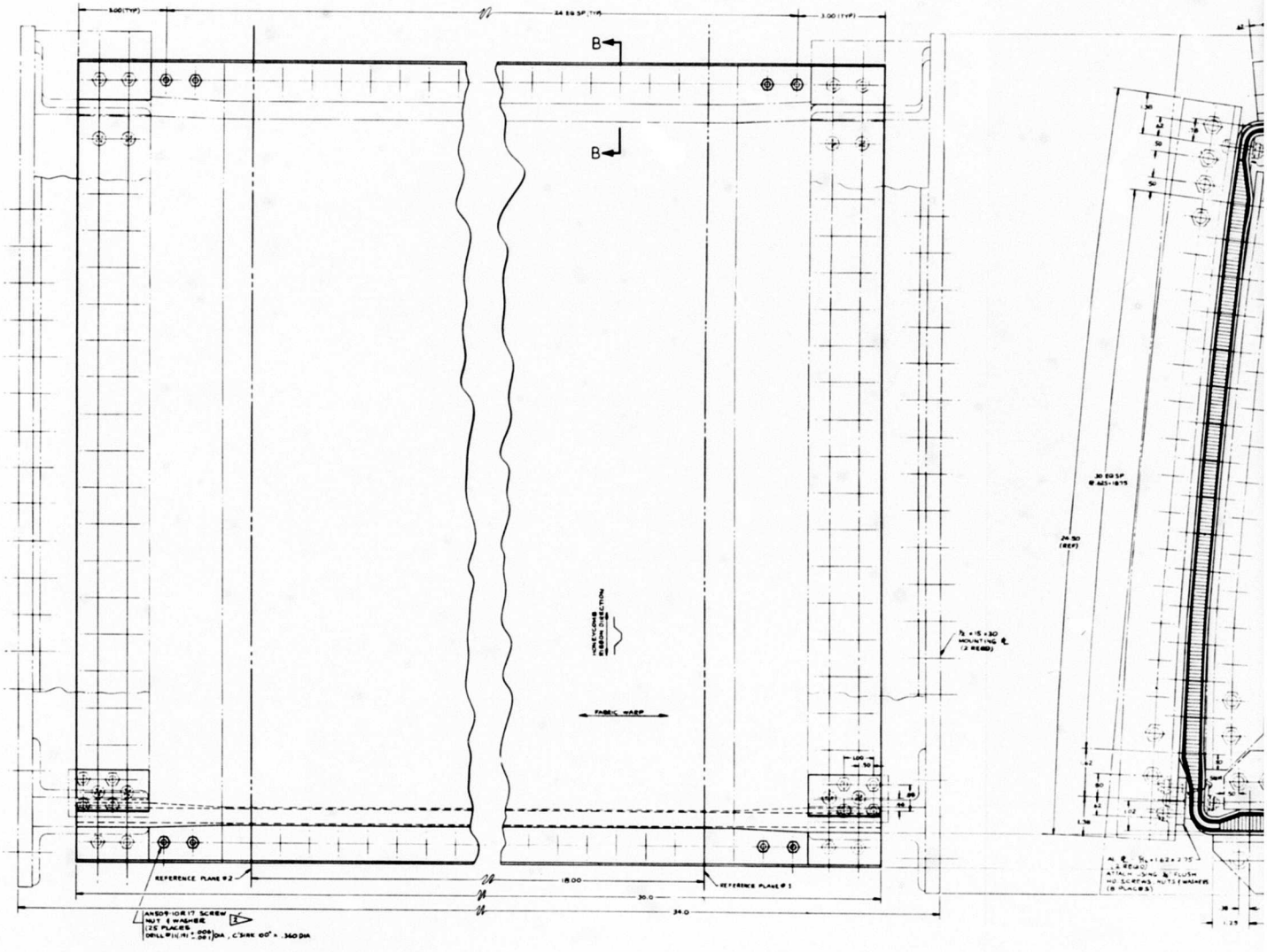

Figure 10. Type V Joint Test Specimen.

A

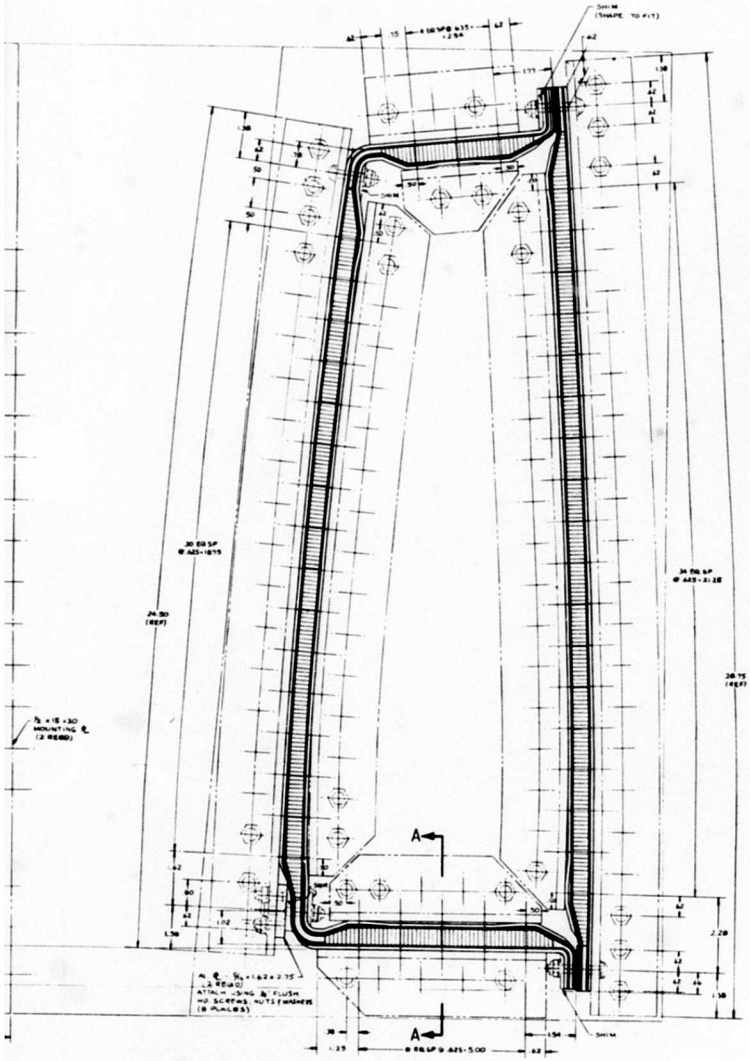

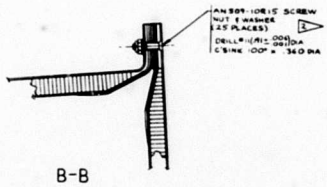

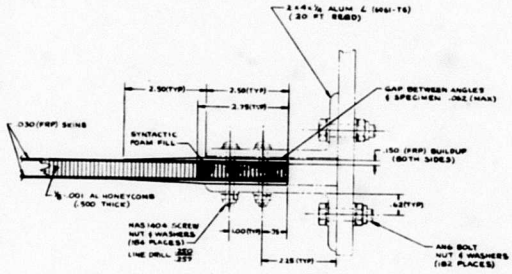

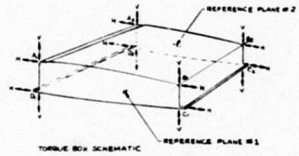

1. MAXIMUM TORQUE EXPECTED = 326,000 in-LB TORSIONAL DEFLECTION @ MAX TORQUE = 2.0° (APPROX) FOR 15' TEST LENGTH
2. LOAD INCREMENTALLY AS FOLLOWS: 2,4,6,8,10,15,20,25,----100%. DEFLECTION READINGS AT LOWER PERCENTAGES MOST USEFUL FOR WING TEST SECTION EVALUATION. READ DEFLECTIONS OF SECTION AT REFERENCE PLANE #1 RELATIVE TO PLANE #2 (USE .001 DIAL INDICATORS OR EQUIV.) @ EACH LOAD INCREMENT AS SHOWN ABOVE.
3. DURING TEST, PARTICULARLY OBSERVE TRANSITION AREAS OF REDUCED SECTIONS ADJACENT TO LAPSTRIPS AT CORNERS FOR DELAMINATION.

NOTES: UNLESS OTHERWISE SPECIFIED

1. FOR AIRFOIL SECTION DIMENSIONS SEE DRAWING 66B3330.
2. SPECIMEN "A" AS SHOWN. SPECIMEN "B" SAME AS "A" EXCEPT BONDED JOINT IN LIEU OF AN509 SCREWS.

B

In the construction of the specimens, 481 weave cloth was used. Since no published shear data were available for this material, design data from MIL-HDBK-17[2] for 181 cloth were used to estimate the ultimate strength of the specimens. MIL-HDBK-17 gives an ultimate shear strength of 181 cloth, epoxy resin, as 14,000 psi. Then the failing torque T was calculated from

$$T = F_S (4t A) \tag{31}$$

where t, the sandwich skin thickness, = 0.030 in.

A, the area enclosed by the box median boundary, = 193 in.^{2}

Therefore,

$$T = 14,000 (4) (0.030) 193 = 324,000 \text{ in.-lb.}$$

On this basis, the design ultimate torque was established as 324,000 in.-lb.

Figure 11 shows the test setup in which the torque boxes were loaded. The beams were simply supported in bending at both ends. As viewed in Figure 11, the left-hand support had two load points to resist the torque. The loading plate was supported at the section centroid and was free to twist. Test loads were applied directly to load points on the loading plate in the form of a couple.

The test procedure was similar for each specimen and is outlined below. All torque was applied as shown in Figure 12.

1. Torque was applied to 20 percent DUL.
2. Torque was applied in same direction to 70 percent DUL.
3. Torque was applied in reversed direction to 60 percent DUL on the bolted specimen and 55 percent DUL on the bonded specimen.
4. Torque was applied to specimen failure.

Both specimens were instrumented with dial gages as shown in Figure 13, and readings were taken at the load increments defined as follows:

1. 20 percent DUL Test - 2 percent DUL increments (6480 in.-lb).
2. 70 percent DUL Test - 5 percent DUL increments (16,200 in.-lb).
3. Reversed Torque Test - 5 percent DUL increments (16,200 in.-lb).
4. Failure Test - 5 percent DUL increments (16,200 in.-lb).

In the first three tests, readings were also taken as the load was removed incrementally.

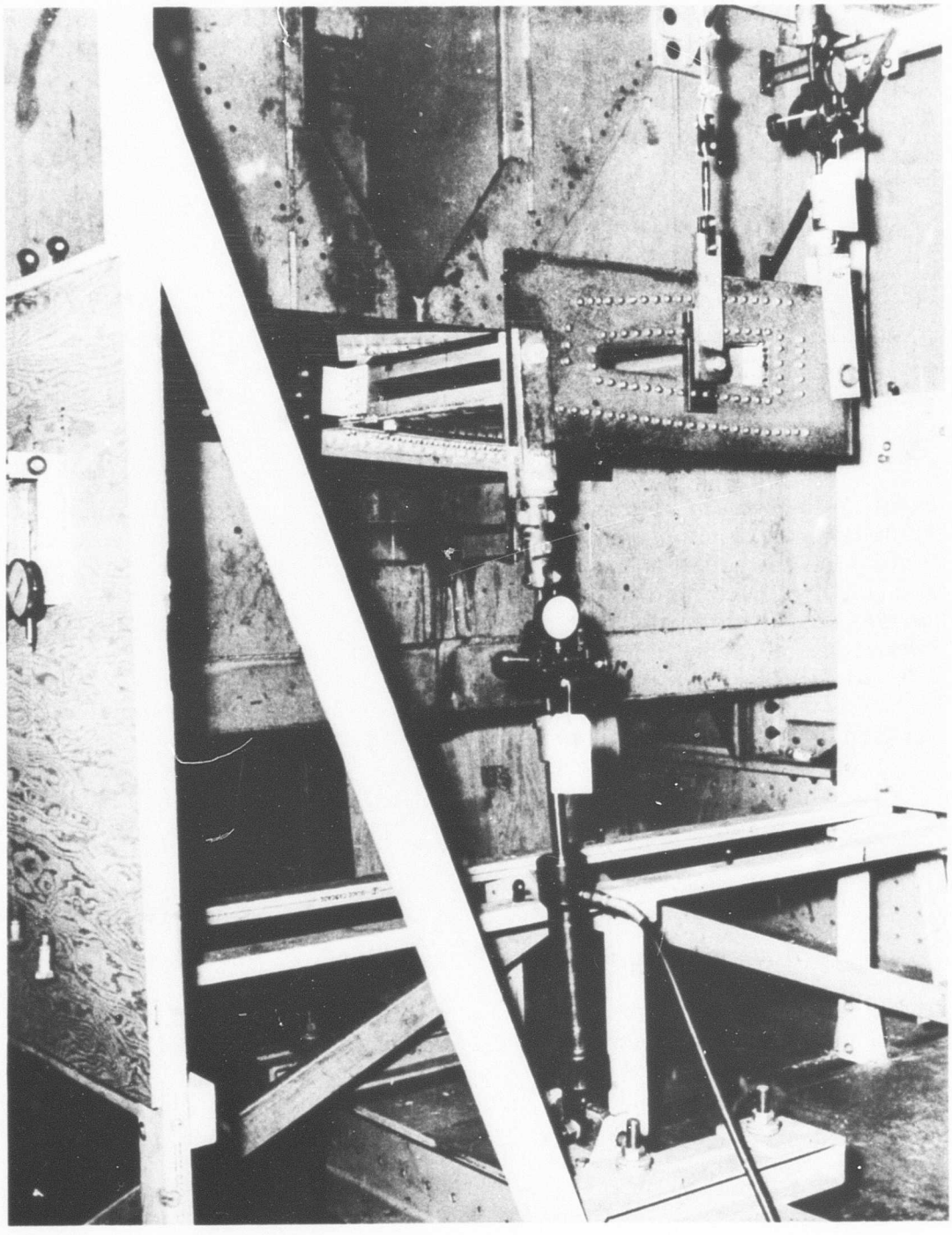

Figure 11. FRP Torque Box Test Setup.

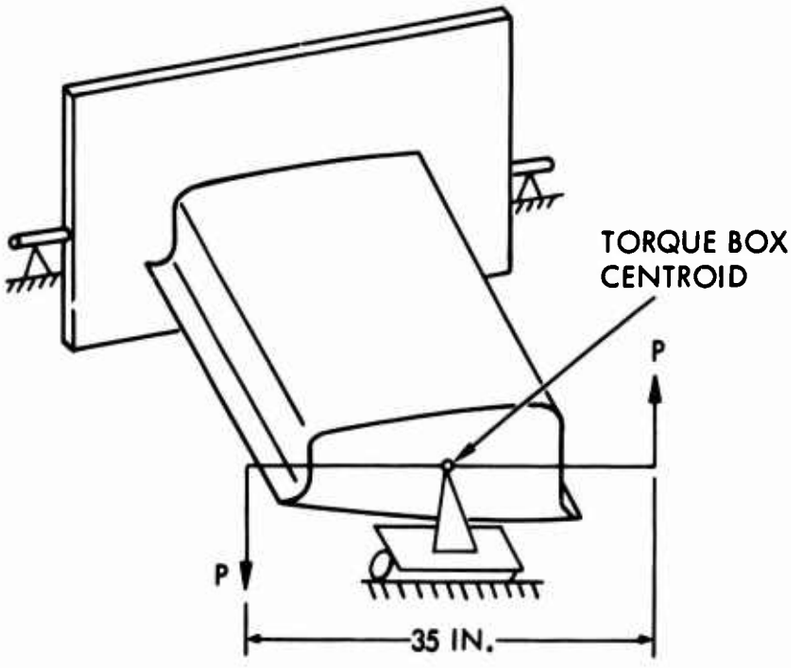

Figure 12. Torque Box Torsion Setup.

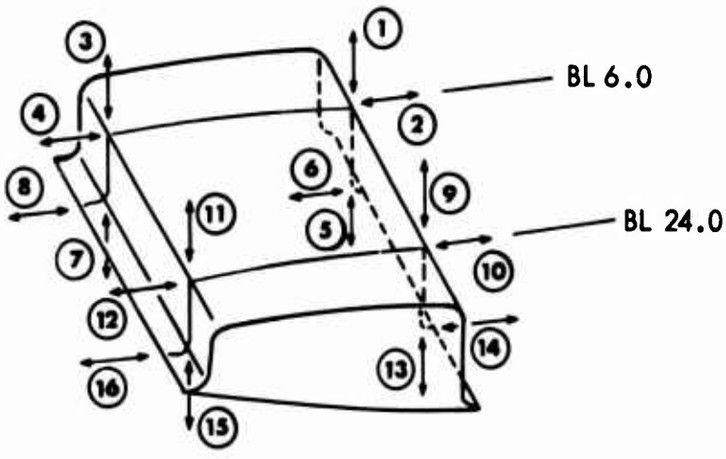

Figure 13. Location of Torque Box Deflection Points.

TORQUE BOX TEST SUMMARIES

Summary of Tests for Torque Box A

Loads were applied for the positive torsion condition (forward spar up) to 70 percent DUL. Slight cracking sounds were first heard while loading from 40 to 45 percent DUL. Continuous cracking sounds were heard while the load was being increased,with sharp cracking sounds heard at 45, 60, and 65 percent DUL. At 70 percent DUL, the load tended to drop off while deflection data were being recorded. A visual inspection was made after the load was removed. White striations were observed running spanwise along the upper and lower surface panels,with the majority near the rear spar and along the lower surface panel. The sandwich panel forming the rear spar had striations running along the span of the test section. Figure 14 shows the torque box after failure, with the striations indicated by the arrows. The striations indicated in Figure 14 are more numerous than those observed after the first run of the torsion test,due to additional striations forming during subsequent runs.

Loads were applied for the negative torsion condition (forward spar down). Slight cracking sounds were first heard while loading from 40 to 45 percent DUL. Continuous cracking sounds were heard as the load was increased further. While loading to 60 percent DUL, continuous sharp cracking sounds were heard. Although the load was to be increased to 70 percent DUL, loading was discontinued at 60 percent because of the sharp

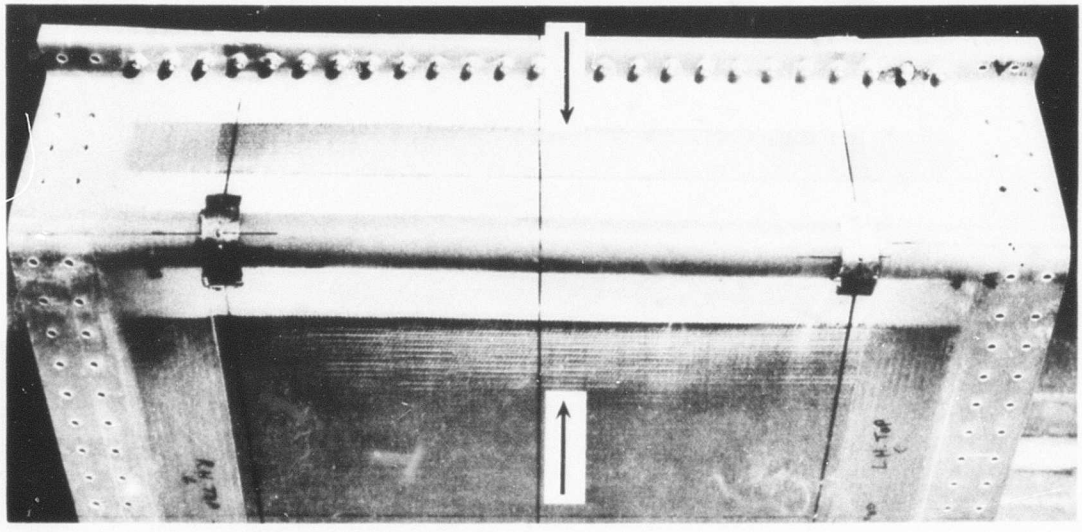

Figure 14. FRP Torque Box A - Striations Along the Upper Surface Panel and Rear Spar.

cracking sounds and the tendency of the loads to drop at each load increment above 50 percent DUL. A visual inspection revealed white areas along the edges of the inboard and outboard reinforcements of the lower surface panel. The white areas appeared to be delamination of the reinforcing material from the facing of the surface panel.

Loads were applied for the positive torsion condition to failing load. No cracking sounds were heard prior to loading from 65 to 70 percent DUL. Continuous cracking sounds were heard as the load was increased. Striations appeared at 75 percent DUL along the lower surface panel near the forward spar. While loading from 75 to 80 percent DUL, the number of striations along the lower surface panel and along the rear spar increased. From 80 to 85 percent DUL, striations appeared along the upper surface near the rear spar. Failure occurred at 85 percent DUL (275,400 in.-lb) while an attempt was being made to increase the load to 90 percent. Just before failure, the striations along the lower surface panel formed into a wide band around the test section, where failure finally occurred. Figures 15 and 16 show the failure of the lower surface panel. Failure occurred in shear of both facings of the lower surface panel along the edges of the spanwise and chordwise reinforced areas of the panel.

Summary of Tests for Torque Box B

For the positive torsion condition to 70 percent DUL, slight cracking was first heard at 40 percent DUL. Continuous sharp cracking sounds were heard as the load was increased from 55 to 70 percent DUL. White striations appeared spanwise along the rear spar at about 65 percent DUL. Striations also appeared along the span of the lower surface panel near the rear spar. Striations were also observed along the span of the inner facing of the lower surface panel near the rear spar and in the center of the panel.

For the negative torsion condition, cracking sounds were first heard at 35 percent DUL and continued as the load was increased. At 55 percent DUL, continuous sharp cracking sounds were heard. The loading was discontinued rather than risk failure in the negative torsion condition.

The beam was again loaded for the positive torsion condition to failing load. Cracking sounds were first heard while loading to 60 percent DUL. Sharp cracking sounds were heard as the load was increased above 70 percent DUL. The loads tended to drop at each increment above 70 percent DUL. As with beam A, the number of striations increased to form a wide band around the test section of the lower surface panel. Failure occurred very gradually while loading from 80 percent to 85 percent DUL. Final failure occurred at 84 percent DUL (272,160 in.-lb) in shear of the facings of the lower surface panel along the edges of the reinforced areas. The failure is shown in Figures 17 and 18.

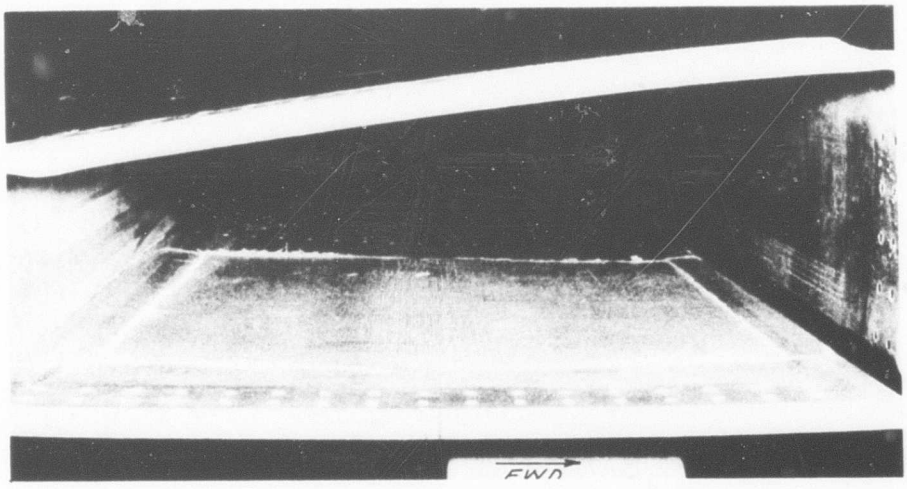

Figure 15. FRP Torque Box A - Shear Failure of Inner Facing of the Lower Surface Panel Along the Edges of the Reinforced Areas.

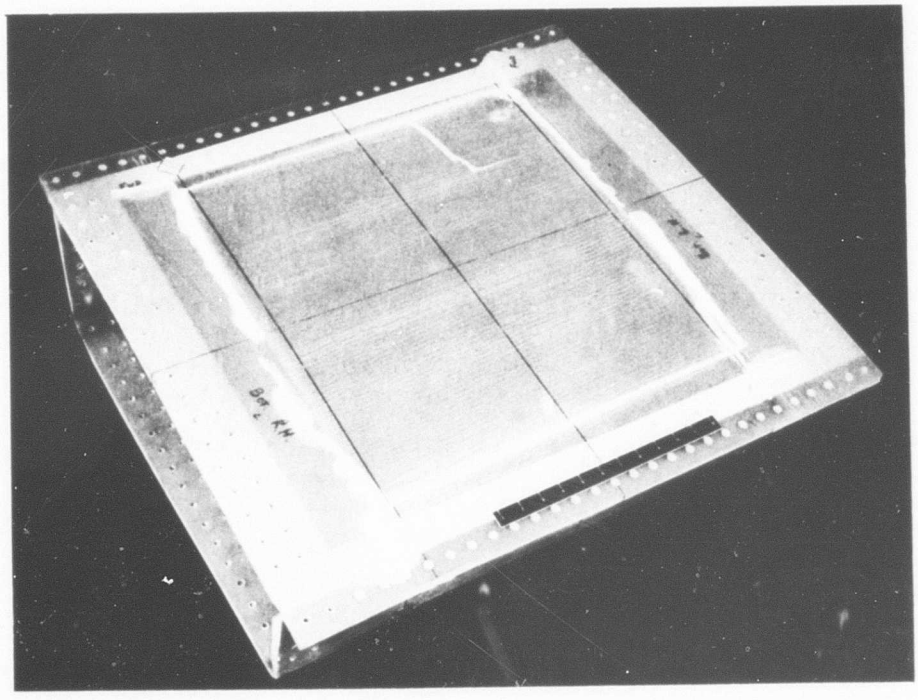

Figure 16. Failed Outside Lower Panel of the Bolted Torque Box.

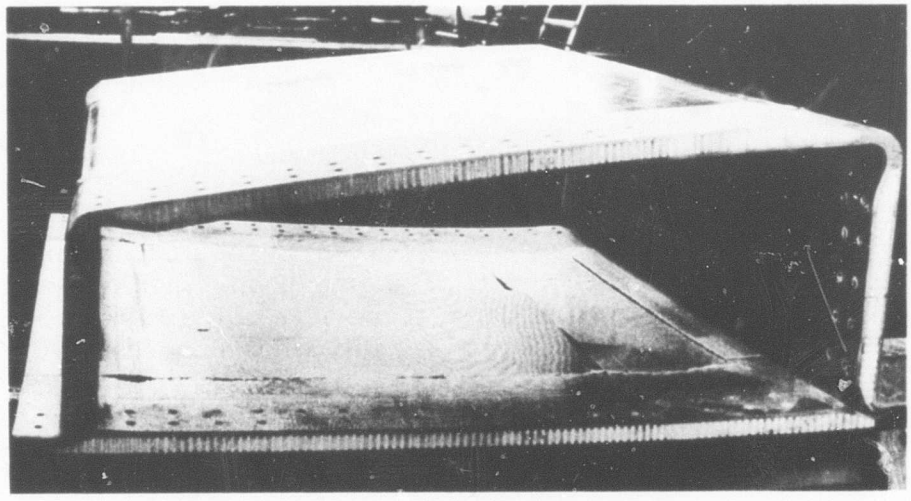

Figure 17. FRP Torque Box B - Shear Failure of Inner Facing of the Lower Surface Panel Along the Edges of the Reinforced Areas.

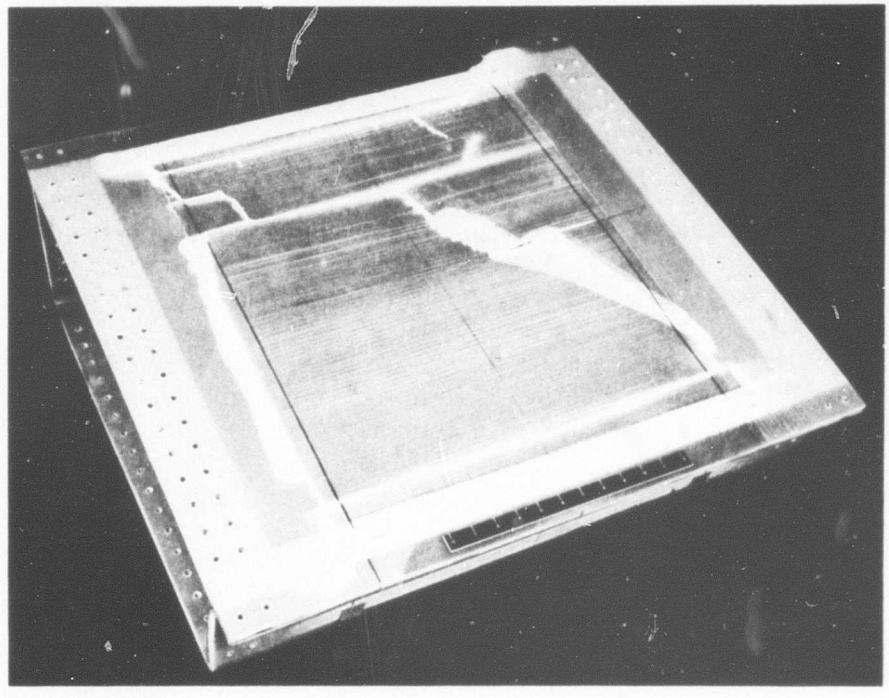

Figure 18. Failed Outside Lower Panel of the Bonded Torque Box.

TEST ANALYSIS - STRENGTH

The predicted design ultimate load of 324,000 in.-lb was derived in the preceding part of the report and was based on an ultimate shear strength of 14,000 psi, skin thickness of 0.030 inch, and a section box area of 193 square inches. By substituting these values into the formula $T = 4AtF_s$, the value for the ultimate torsional load T is found to be 324,000 in.-lb. Both test specimens failed at about 85 percent of the DUL, where the calculated shear stress is 12,000 psi. From an examination of the specimen, it appears that failure initiated at the edge of the reinforcement. The following reasons are presented for failure at 85 percent DUL:

1. The shear ultimate strength of the material is less than 14,000 psi.

2. Stress concentrations may occur at the edges.

3. Repeated and/or reversed loadings may reduce the strength allowables.

Subsequent GAC shear tests have indicated that 12,000 psi is a more realistic strength for the material. In general, test results were in the 12,000- to 13,000-psi range. These tests were performed on solid laminates. It is believed that for sandwich skins, where the skin ply next to the core may be dimpled, the allowables may be slightly less than for a solid laminate. The added, but not computed, core stiffness may make up for this difference. Thus, it is concluded that the design shear allowable should not exceed 12,000 psi.

Criteria for the stress concentration at the edge can be substantiated since failure initiated at the edges. Apparently this concentration factor is relatively low, or failure would have occurred earlier in the test.

Criteria for the repeated and/or reversed loading failure cannot be fully evaluated from the above tests. It is noted, however, that the reversed loading tests were stopped at lower than the intended 70 percent DUL because of cracking sounds. Inspection of the load deflection curve indicates considerably more deflection during the reversed loading test than in the normal loading test. Whether this was caused by the repeated loading or by the reversed loading cannot be determined from the test procedure that was followed.

TEST ANALYSIS - DEFLECTION

The 30-inch-long test specimen was reinforced over 6 inches at each end.

This provided an 18-inch test section. Deflection data were obtained at BL 6 and at BL 24, and calculations were made based on the difference in deflection between these two stations. Deflection gages reading only vertical displacement were used in determining the angle of twist because the motions are greatest in this direction (see Figure 13).

The basic deflection quantity $\Delta\phi/\Delta L$ was obtained from the test data, where $\Delta\phi$ is rotation at BL 24 minus the rotation at BL 6, and ΔL is distance between BL 24 and BL 6, equalling 18 inches. Thus, $\Delta\phi/\Delta L$ is rotation in radians per inch of length.

The basic torsional deflection is

$$\Delta\phi/\Delta L = T/KG \qquad (32)$$

where T is torque in in.-lb

K is a constant geometric factor depending on the cross-section configuration

For the cross section of the test specimen, K was calculated to be 198.5 inches^4. G is the shear modulus of the material. If the shear modulus is constant over the entire stress range, then $\Delta\phi/\Delta L$ would always be proportional to the shear stress, and plots of $\Delta\phi/\Delta L$ versus torque would result in a straight line.

The original predicted rotation of the test specimen over the 18-inch test length was 2 degrees at DUL. This was based on using a G value of 810,000 psi, as given by MIL-HDBK-17[2], over the entire range in the calculation. It was known that this G value would decrease at higher stress levels. However, the magnitude of change was not known. Thus, the original prediction was realistically a minimum rotation prediction.

The G value of 810,000 psi[2] was specified to have a proportional limit of 1800 psi. However, no value of G for higher stress levels is given. A torsion test conducted at GAC on a circular tube constructed of 481 cloth epoxy resin laminate indicated a shear modulus of approximately 700,000 psi at stress levels below 2000 psi. Other tests performed at GAC on similar laminate materials using the Rail shear test method showed primary G values in the 550,000- to 720,000-psi range, with secondary G values ranging from 360,000 to 450,000 psi. These experimental values are all tangent moduli.

Calculations of $\Delta\phi/\Delta L$ for the various tests are presented in Table VII. In Figure 19, these values are plotted as a function of the stress level for

TABLE VII. TORQUE BOX TORSION TEST RESULTS - CALCULATIONS OF $\Delta\theta/\Delta L$

Tests		Positive Torsion (rad/in. x 10^6)				Negative Torsion (rad/in. x 10^6)		Positive Torsion (rad/in. x 10^6)	
%	Actual Load	20% DUL		70% DUL		60% DUL	55% DUL	Failure	
DUL	(in.-lb)	Bolted	Bonded	Bolted	Bonded	Bolted	Bonded	Bolted	Bonded
2	6,480	-	13.06	-	-	-	-	-	-
4	12,960	20.56	29.44	-	-	-	-	-	-
5	16,200	-	-	-	76.94	58.33	64.17	50.83	178.33
6	19,440	53.89	52.22	-	-	-	-	-	-
8	25,920	89,17	73.61	-	-	-	-	-	-
10	32,400	121.39	108.06	-	153.33	134.44	158.33	128.33	142.50
12	38,880	152.22	133.33	-	-	-	-	-	-
14	45,360	186.67	160.28	-	-	-	-	-	-
15	48,600	-	-	96.67	221.11	219.72	223.33	232.78	232.78
16	51,840	229.72	192.22	-	-	-	-	-	-
18	58,320	261.67	227.22	-	-	-	-	-	-
20	64,800	299.44	261.39	203.06	312.50	330.28	325.00	357.50	348.33
25	81,000	-	-	297.22	401.67	519.17	511.94	538.33	478.89
30	97,200	-	-	417.22	509.44	735.56	667.78	800.83	661.11
35	113,400	-	-	532.50	613.06	919.72	843.61	1000.28	851.67
40	129,600	-	-	675.56	731.94	1125.28	1019.44	1170.28	1047.78
45	145,800	-	-	825.28	872.22	1295.00	1190.56	1348.61	1203.33
50	162,000	-	-	987.50	1025.28	1601.67	1310.56	1540.83	1396.39
55	178,200	-	-	1214.44	1203.33	1695.28	1552.78	1735.83	1564.44
60	194,400	-	-	1420.00	1418.61	1845.00	1545.56	1950.83	1738.06
65	210,600	-	-	1668.06	1686.11	-	-	2156.39	1900.00
70	226,800	-	-	1997.22	1935.00	-	-	2362.22	2152 78
75	243,000	-	-	-	-	-	-	2644.72	2571.11
80	259,200	-	-	-	-	-	-	2989.17	2881.39
85	275,400	-	-	-	-	-	-	3481.11	-
60	194,400	-	-	-	1830.83	-	-	-	-
50	162,000	-	-	1663.33	1643.06	-	-	-	-
40	129,600	-	-	-	1445.56	1631.39	1368.89	-	-
30	97,200	-	-	1226.94	1244.72	-	1200.00	-	-
20	64,800	-	-	-	967.22	1180.83	993.33	-	-
10	32,400	-	-	620.00	718.89	909.17	758.33	-	-
0	0	-	16.67	-	419.44	-	544.17	-	-

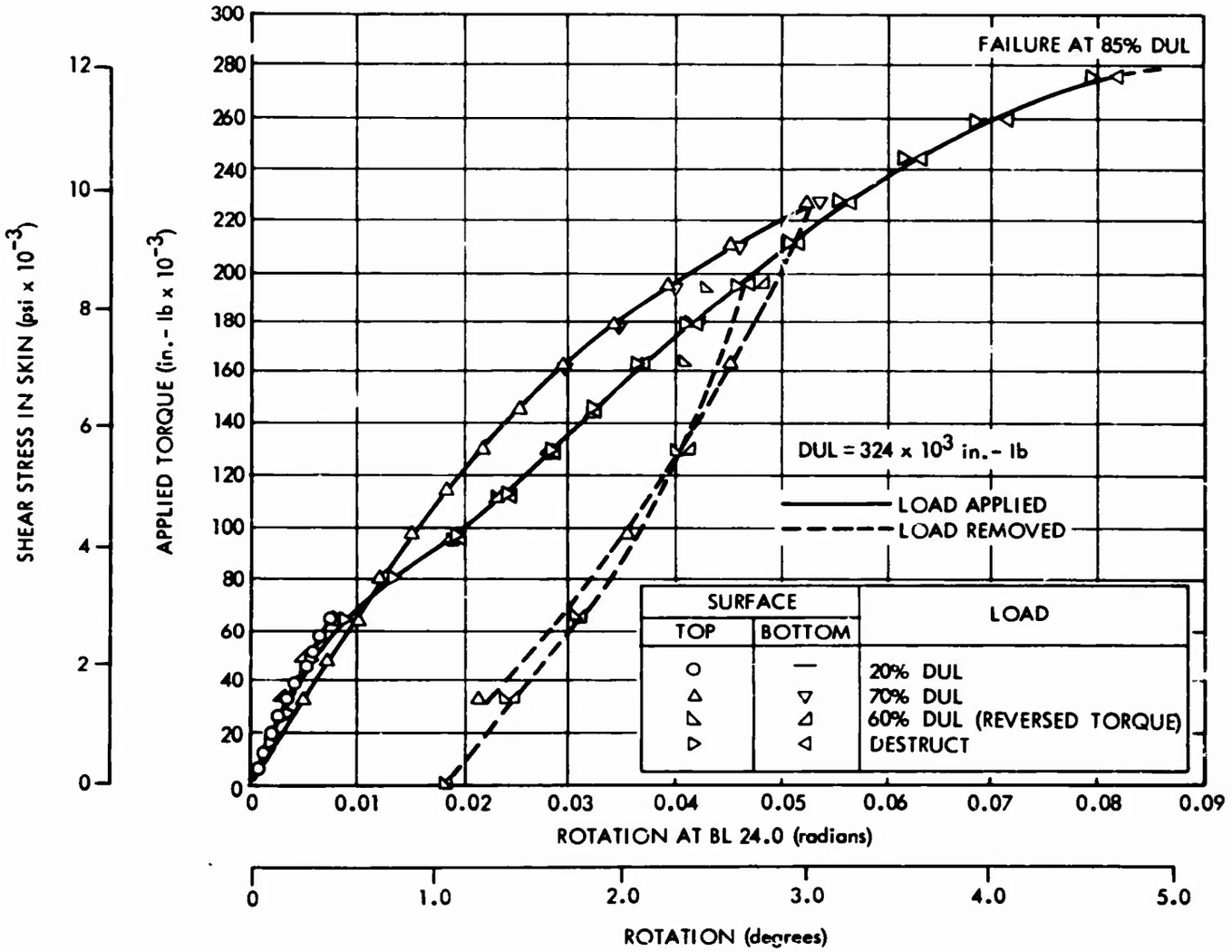

Figure 19. Bolted Torque Box Torsion Test With Total Rotation at BL 24.0.

the bolted torque box; in Figure 20, for the bonded torque box. It is noted that the slope of the plotted line, which represents G, decreases as the load increases. It is also noted that the shapes of the reversed torque test curve and the destruction test curve are considerably different from the 70 percent curve. Whether this resulted from previous preloading to 70 percent DUL or from the stress reversal cannot be determined, because of the nature of the test programming.

Figures 21 and 22 compare the torsional deflections of the bolted torque box and the bonded torque box for the 70 percent test and for the destruction test. Although the differential was not significant, it is evident that the bonded specimen was stiffer than the bolted specimen.

Figures 21 and 22 also show the relationship of the slope for the deflection-stress curve to G modulus. Figure 21 is plotted for both test specimens for the 70 percent test. Figure 22 repeats the plot for the destruction test. Included is a derived scale for which the secant modulus at any point on the curve may be read directly by extending the line from the origin to the point on the scale.

Inspection of the curves in Figures 21 and 22 shows that the basic G value of 810,000 psi was exceeded during the low stress levels but that the shear stiffness dropped off rapidly at the higher stress levels. This sharply increased the amount of torsional deflection.

Prediction of the torsional deflection of a torque box is dependent upon the secant shear modulus of the material, which varies with the stress level. Thus, a complete shear stress-strain curve is required. These data are generally not available because of the difficulty involved in obtaining good shear stress-strain data. As an example, from Figure 22 at 70 percent DUL, the secant G is 500,000 psi for the bonded specimen and 460,000 psi for the bolted specimen. Secant G at very low stress levels is approximately 1,000,000 psi.

TEST SECTION WEIGHTS

1. Total weights of the 30-inch-long torque boxes were as follows:

Bolted Specimen	31.71 pounds
Bonded Specimen	31.24 pounds

2. Weights of the 18-inch-long gage sections of the boxes were:

Bolted Specimen	13.08 pounds
Bonded Specimen	12.89 pounds

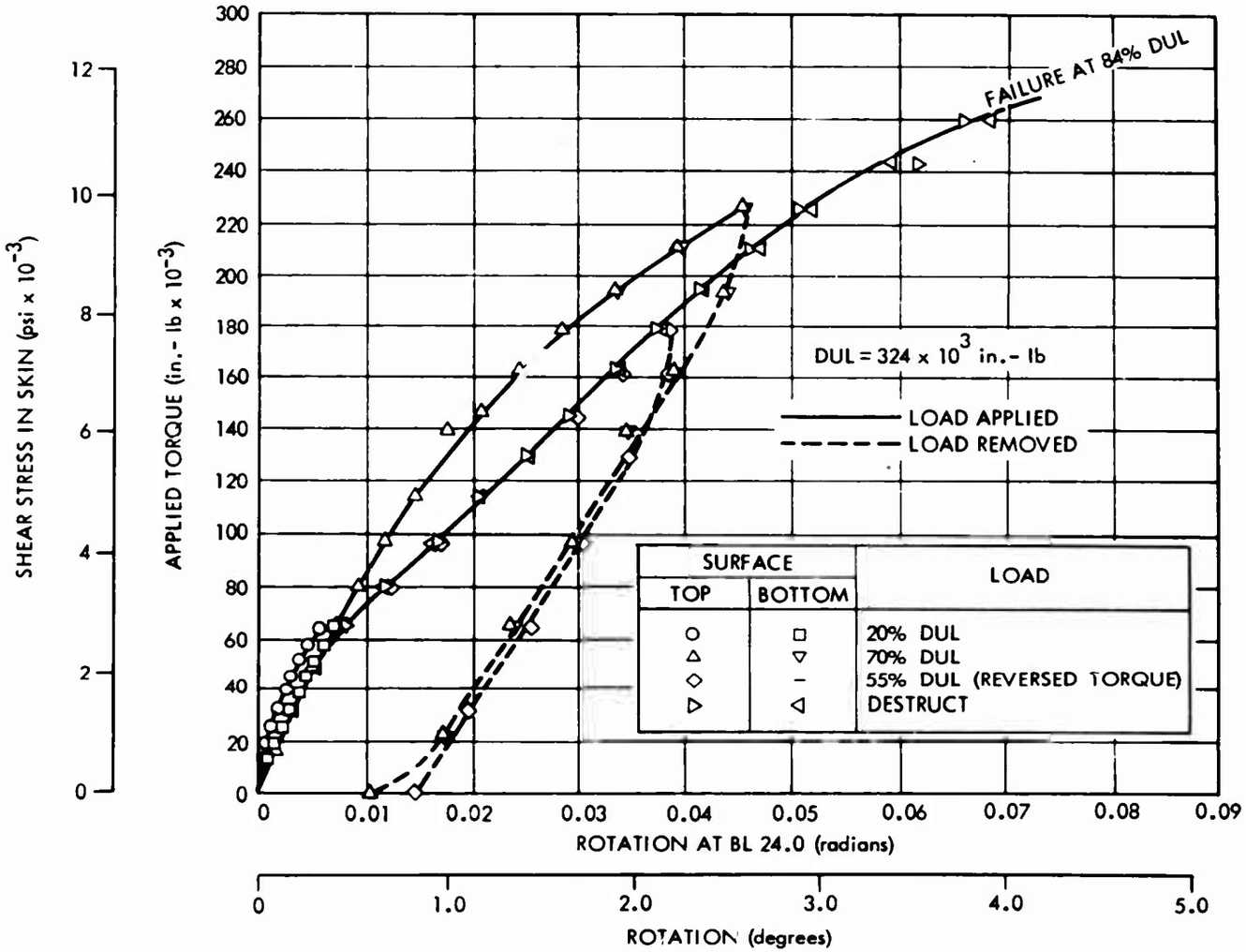

Figure 20. Bonded Torque Box Torsion Test With Total Rotation at BL 24.0.

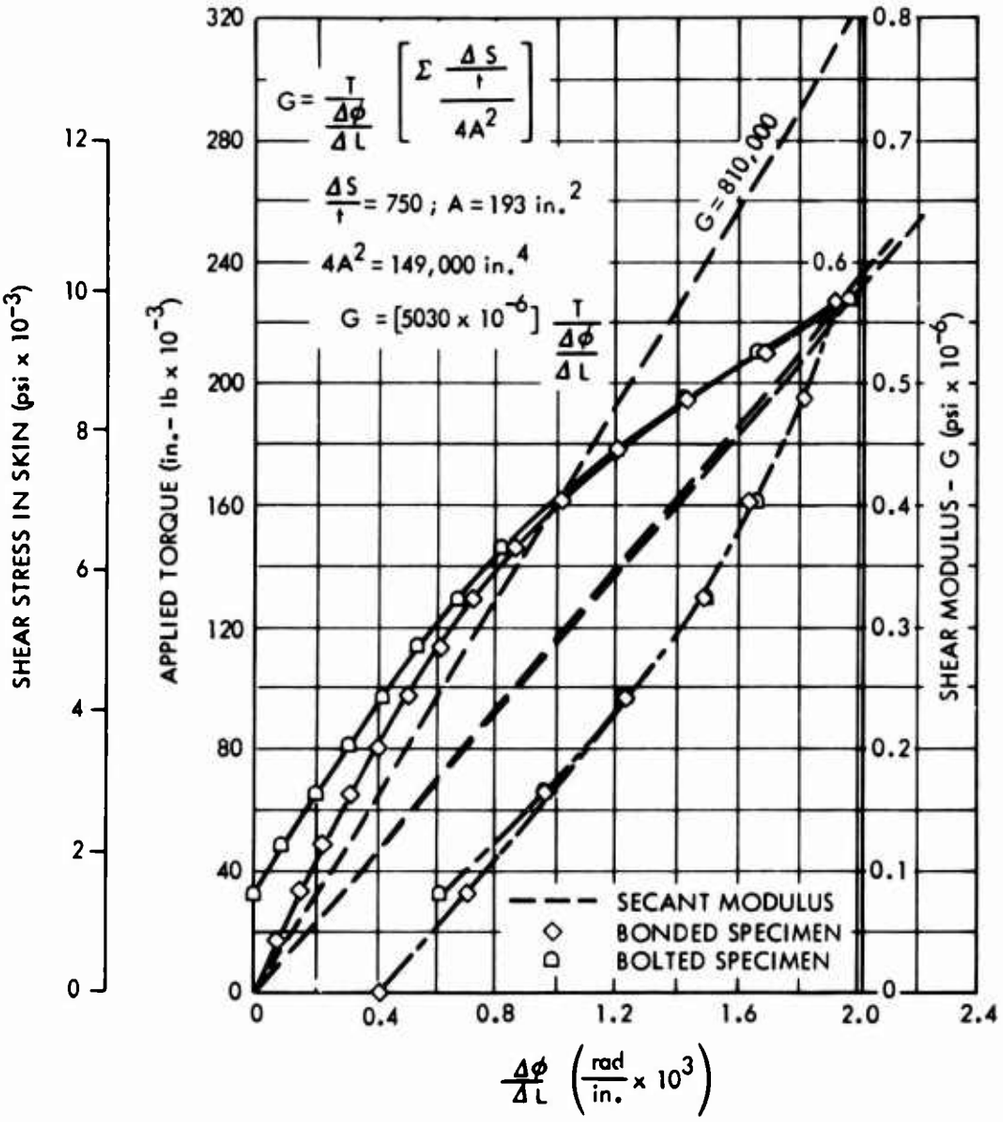

Figure 21. Comparison of Torsional Stiffness in the Bonded and Bolted Torque Boxes at 70 Percent DUL.

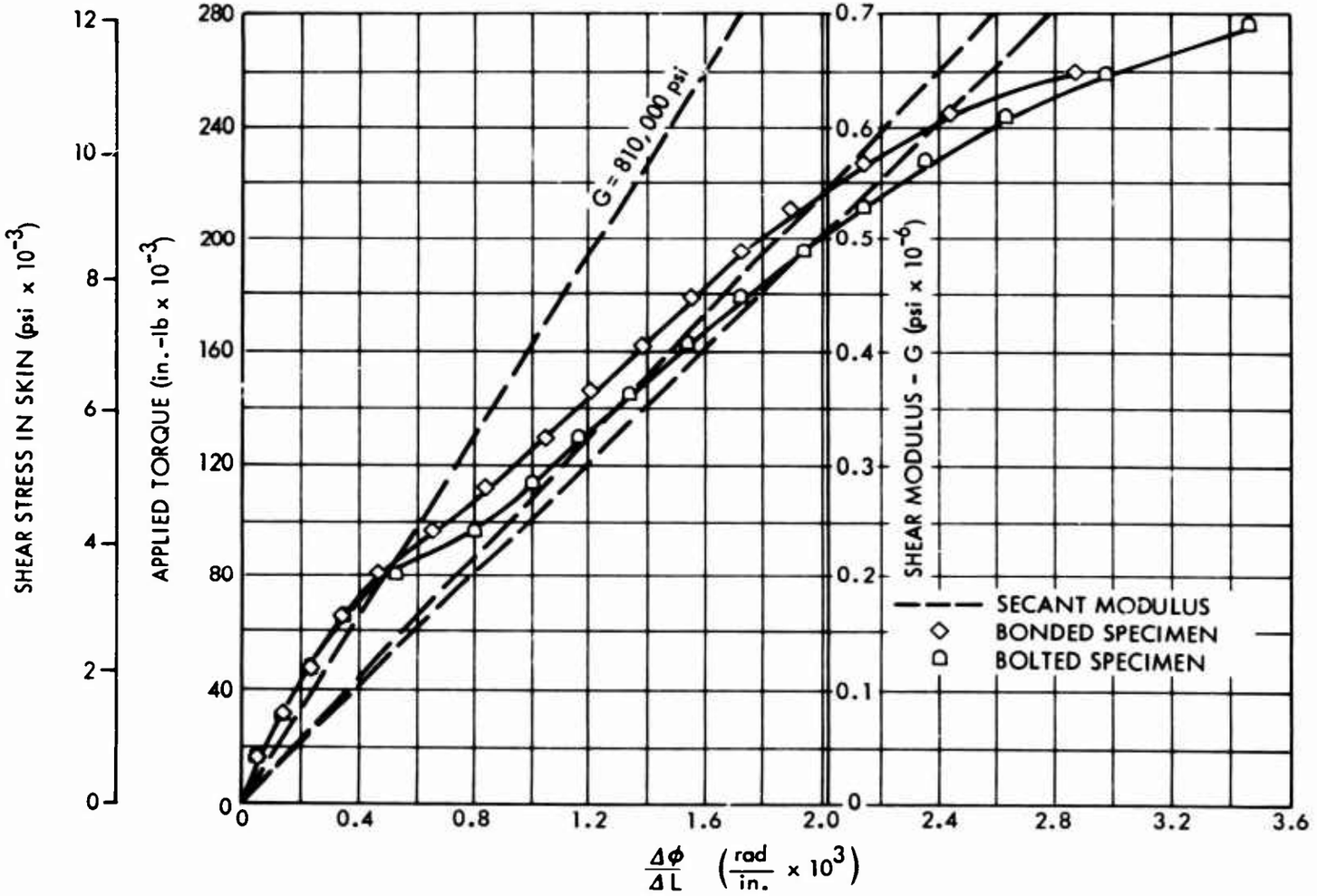

Figure 22. Comparison of Torsional Stiffness in the Bonded and Bolted Torque Box Specimens During Destruct Testing.

NO. 1 WING SECTION
TEST RESULTS AND DATA REDUCTION

GENERAL

During January 1967, the No. 1 wing test section was fabricated and delivered to the Naval Air Development Center for test. The completed wing section is shown in Figures 23 and 24. The total weight of the test article was 138 pounds. After testing was completed, the reinforced ends of the beam were removed and a 64-inch wing section was weighed. The weight of this section was 72.5 pounds. Therefore, the test section weight was 1.13 pounds per inch.

According to the Naval Air Development Center, Aero Structures Department summary report,[5] the workmanship of the wing section was generally very good. The only defects detected were dimensional deviations of the structure from the drawing and a slight angle deviation from the Y-axis for the center spar. This deviation was probably caused by springback of the spar after removal from the mold. Allowing for springback in the design of tooling should correct this defect.

The wing section was tested by the Aero Structures Department. The test data for shear center determination, dynamic testing, and static testing are reduced in this subsection. The dynamic testing included a vibration survey, free vibration (pluck tests), and forced vibration; static testing included cantilever bending to 70 percent DUL, cantilever bending plus torsion to 70 percent DUL, torsion, and cantilever bending to failure. The instrumentation and test results for these tests are discussed in the following paragraphs.

SHEAR CENTER DETERMINATION

It was necessary to establish the shear center of the section for cantilever and shear loading to minimize torsion in the specimen during cantilever bending tests. This was done in the following manner.

An end plate, with loading points 1 and 2, was attached to the free end of the specimen (see Figure 25). Dial indicators were positioned as shown in Figure 13. The end plate was scribed with the indicated axes and with the points representing the section centroid and calculated shear center. The section centroid and calculated shear center were determined before specimen fabrication.[1]

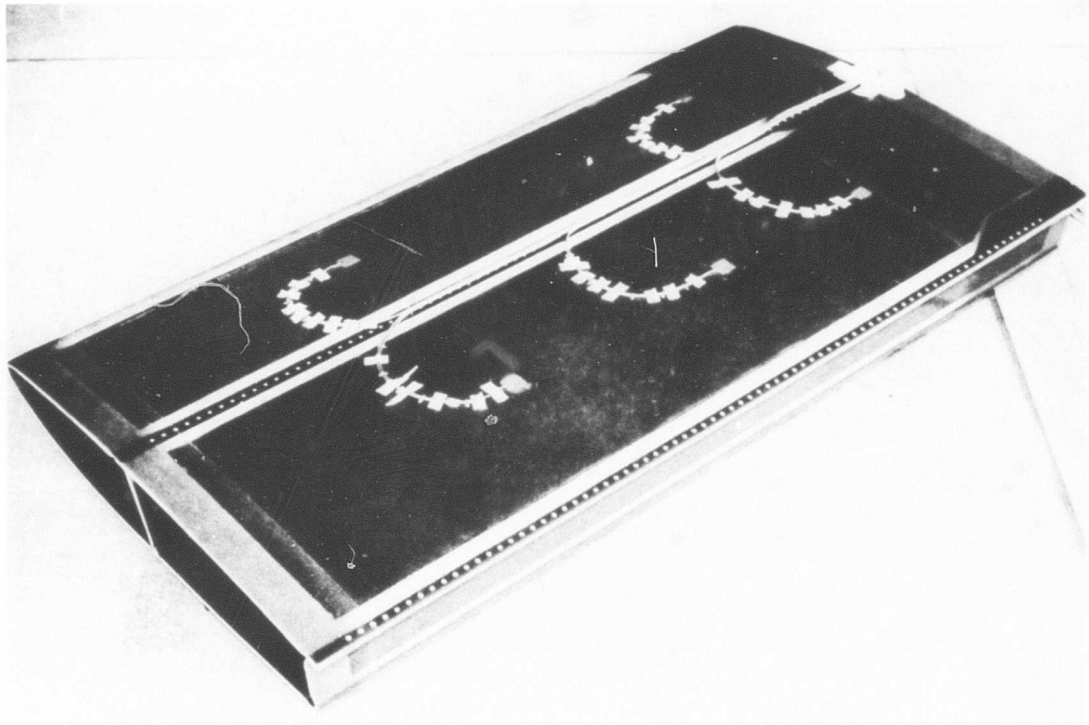

Figure 23. Lower Surface of the No. 1 FRP Wing Section.

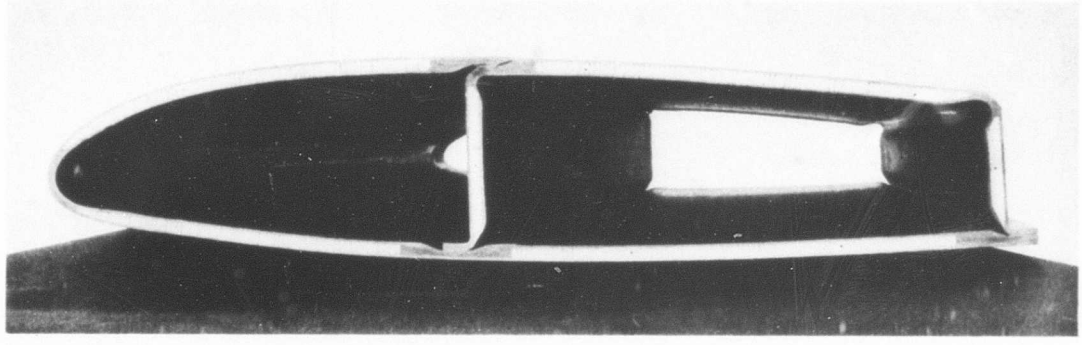

Figure 24. End View of the No. 1 FRP Wing Section.

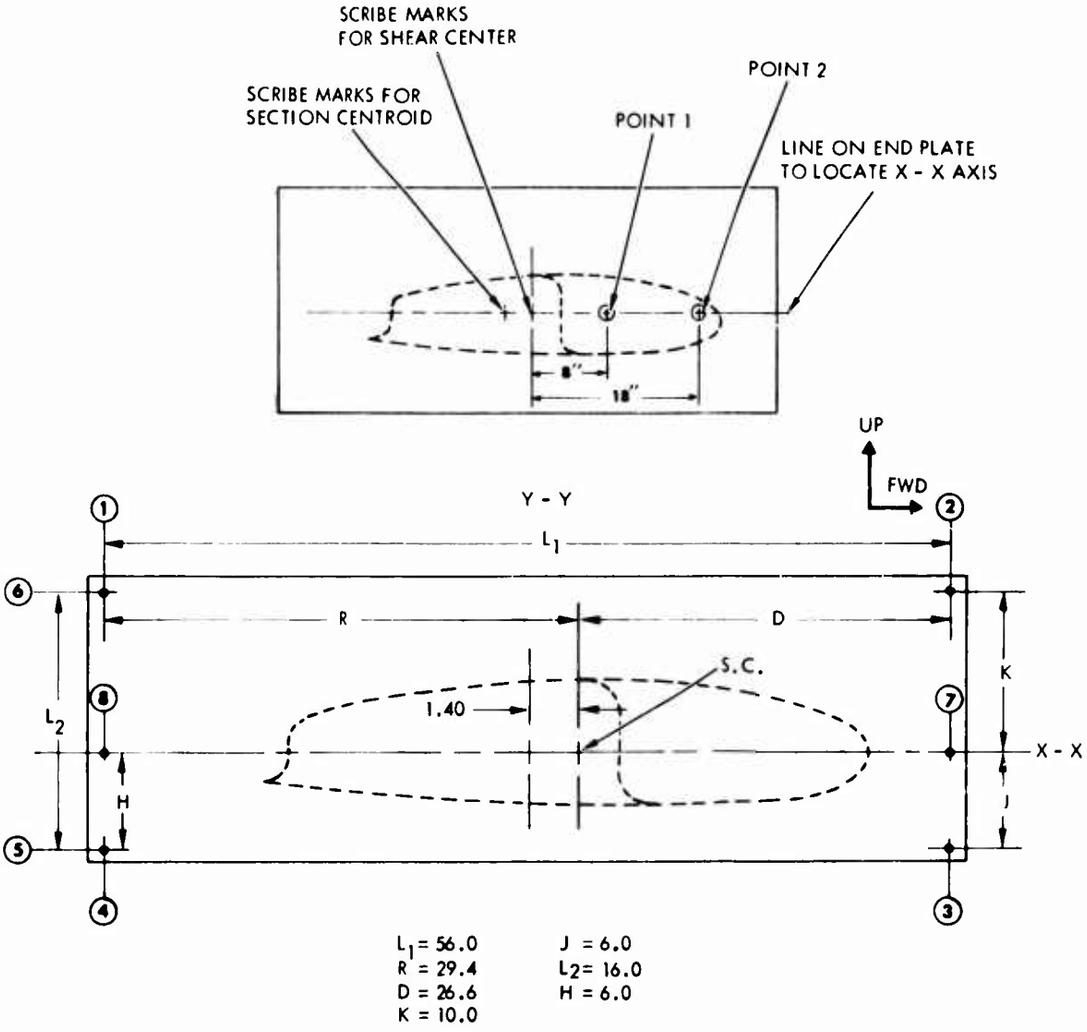

Figure 25. End Plate Configuration for Shear Center Establishment.

With a 1000-pound shear load applied at point 1, torque was applied to the specimen by an amount equal to

$$T_1 = e \times 1000 \tag{33}$$

The dial indicators at test points 7 and 8 measured the deflection dependent on the angle of twist.

$$\delta_{71} = s_7\phi_1 + \delta_{b1} \tag{34}$$

$$\delta_{81} = -s_8\phi_1 + \delta_{b1} \tag{35}$$

The same shear load was then applied at test point 2, and the resultant torque can be calculated from Equation (36).

$$T_2 = (e + 10) \times 1000 \tag{36}$$

The dial indicator deflections can then be represented by Equations (37) and (38).

$$\delta_{72} = s_7\phi_2 + \delta_{b2} \tag{37}$$

$$\delta_{81} = -s_8\phi_2 + \delta_{b2} \tag{38}$$

Then, by eliminating bending deflections from the dial indicators, the deflection readings can be represented by Equations (37) through (42).

$$\delta_{71} - \delta_{81} = (s_7 + s_8)\,\phi_1 \tag{39}$$

$$\text{or} \quad \phi_1 = \frac{\delta_{71} - \delta_{81}}{s_7 + s_8} \tag{40}$$

$$\delta_{72} - \delta_{82} = (s_7 + s_8)\,\phi_2 \tag{41}$$

$$\text{or} \quad \phi_2 = \frac{\delta_{72} - \delta_{82}}{s_7 + s_8} \tag{42}$$

Since

$$\phi_1 = T_1/K = 1000\,e/K \tag{43}$$

and

$$\phi_2 = T_2/K = 1000\,(e + 10)/K \tag{44}$$

then,

$$\frac{\phi_1}{\phi_2} = \frac{e}{e + 10} = \frac{\delta_{71} - \delta_{81}}{\delta_{72} - \delta_{82}} \tag{45}$$

and solving Equation (45) for e, we get

$$e = 10\left[\frac{\delta_{71} - \delta_{81}}{(\delta_{72} - \delta_{71}) - (\delta_{82} - \delta_{81})}\right] \tag{46}$$

The test results used in determining the shear center are tabulated in Table VIII.

TABLE VIII. RESULTS OF SHEAR CENTER DETERMINATION TEST

V Shear Load (lb)	Load Point	δ_7 Deflection Point 7 (in.)	δ_8 Deflection Point 8 (in.)	$\delta_7 - \delta_8$ (in.)
200	1	0.075	0.059	0.016
1000	1	0.406	0.302	0.104
200	1	0.087	0.069	0.018
200	1	0.080	0.061	0.019
1000	1	0.400	0.299	0.101
200	1	0.081	0.063	0.018
200	2	0.092	0.048	0.044
1000	2	0.459	0.239	0.220
200	2	0.096	0.051	0.045
200	2	0.092	0.048	0.044
1000	2	0.456	0.238	0.218
200	2	0.095	0.051	0.044

By substituting values from Table VIII into Equation (46), the value for e is determined in Equations (47) through (49).

$$e_1 = \left(\frac{0.104}{0.220 - 0.104}\right) \times 10 = 8.97 \quad (47)$$

$$e_2 = \left(\frac{0.101}{0.218 - 0.101}\right) \times 10 = 8.63 \quad (48)$$

$$e_{avg} = 8.80 \quad (49)$$

Therefore, the shear center is 0.8 inch aft of the calculated position.

DYNAMIC TESTING

The dynamic test phase of this program consisted of a vibration scan from 0 to 500 Hz, free vibration as a cantilever, and forced vibration. Figure 26 shows the test setup for the vibration scan. The quick-disconnect fitting, indicated by the arrow, was used for the free vibration. This figure also shows the shaker used in the forced vibration survey. Accelerometer and strain gage locations are shown in Figure 27.

The first vibration scan was performed with a speaker located at mid-span, mid-chord. For a second survey, the speaker was moved to the outboard leading edge. The purpose of these tests was to determine those frequencies at which resonance of the structure occurred.

The original test plan called for torsion free bending and pure torsion loading for the free vibration tests. Bending with no torque loading was achieved by applying the shear load at the shear center. Since pure torsion loading was not feasible, the shear load was applied eccentrically to the shear center at point 2 (see Figure 25). Thus, both bending and torque loading were applied. During the bending vibration tests, the specimen was deflected to three different root section stress levels and released. A single loading of 1000 pounds was used for the torsion plus bending vibration tests. Tests were performed with a bungee cord attached to the end of the specimen with a preload of 200 pounds, and then with no bungee preload. These tests were conducted to determine the fundamental frequencies in bending and torsion and to determine the damping characteristics of the construction.

The forced vibration tests were performed to determine natural frequencies, mode shapes, and damping characteristics of the wing due to forced

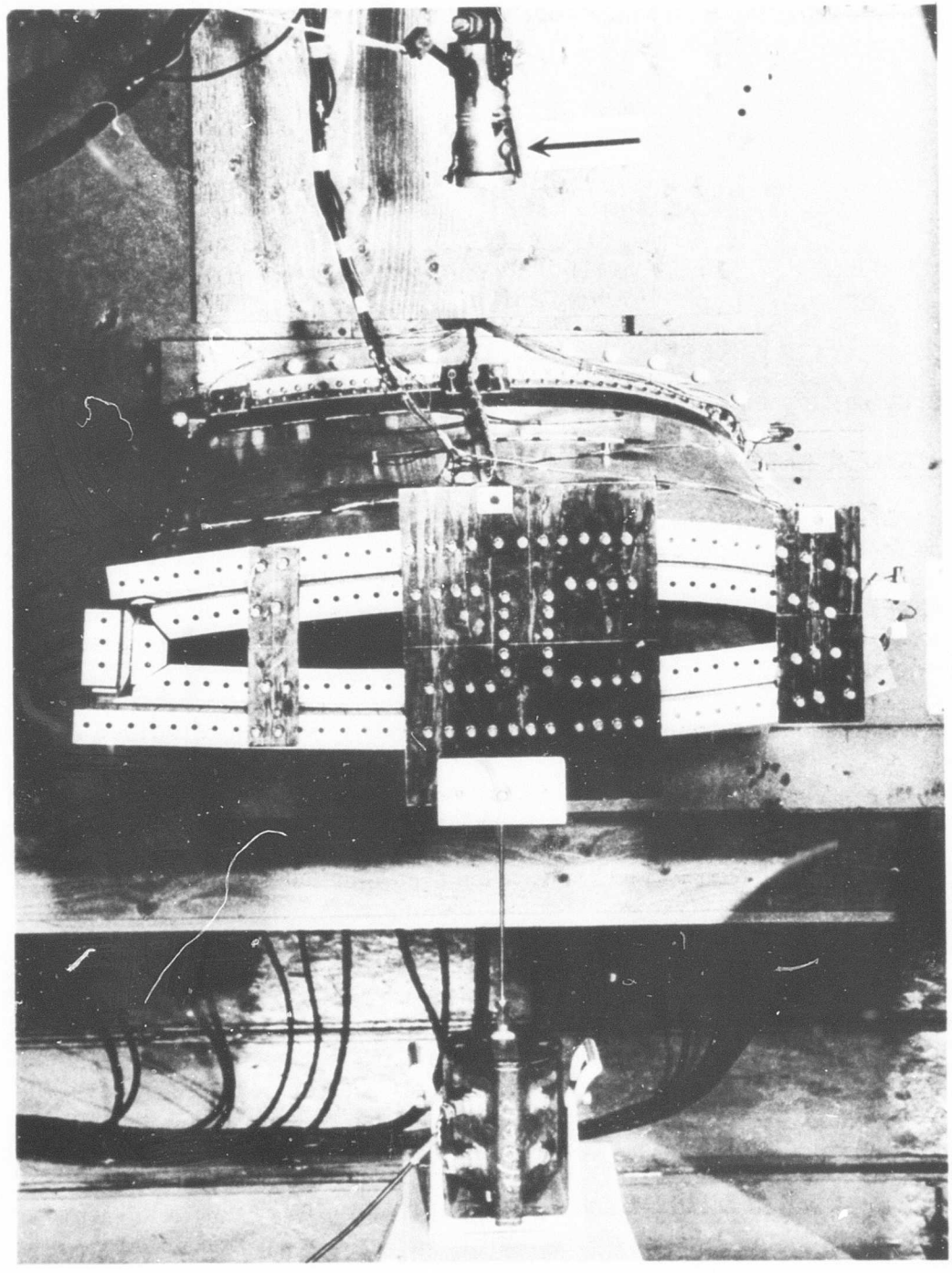

Figure 26. Vibration Survey Test Setup.

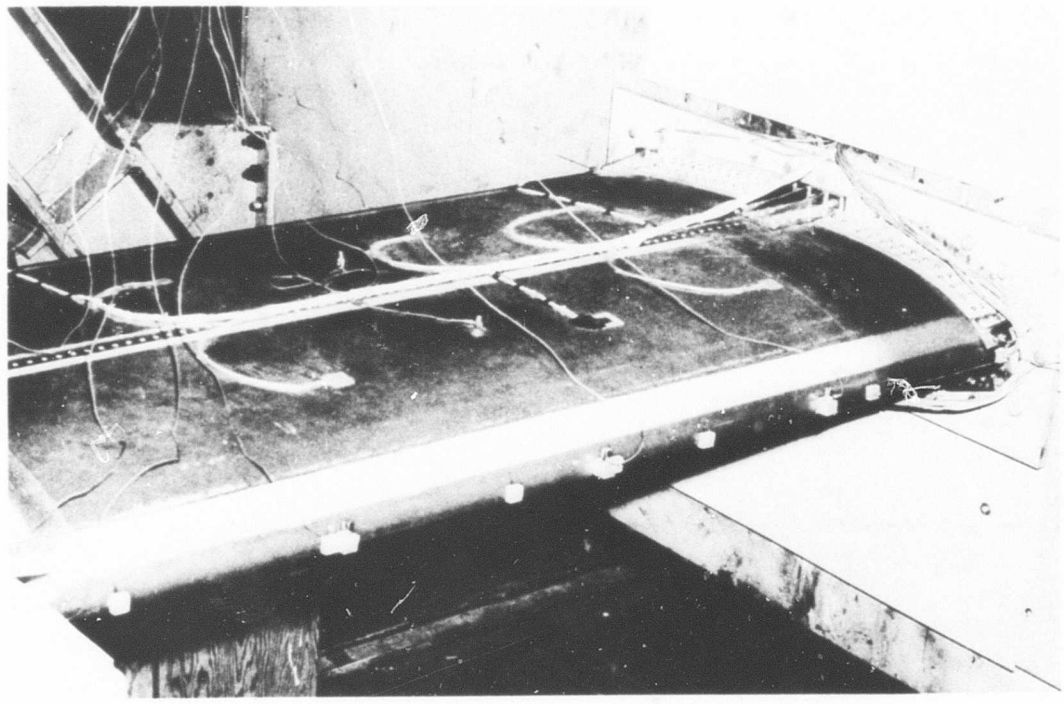

Figure 27. Vibration Survey Instrumentation.

vibration. A voice coil exciter and a portable shaker were used to apply the vibration inputs at the free end of the wing. Vibration loads were applied at both the wing cross-section shear center and at a point near the leading edge of the wing. Accelerometer instrumentation readings were obtained at all of the natural frequencies. Instrumentation and details of each test and the results are described below.

Vibration Scan

For the vibration scan, 13 accelerometers were mounted to the specimen as shown in Figure 28. Response of the accelerometers to the speaker survey indicated resonances at the frequencies shown in Table IX.

For the free vibration tests, the specimen was instrumented with 16 strain rosettes as shown in Figure 29. During the free vibration tests, 12 of the 48 gages were active and continuously recording. Although 12 axial strain gages were active, only 6 were used in obtaining the ratio

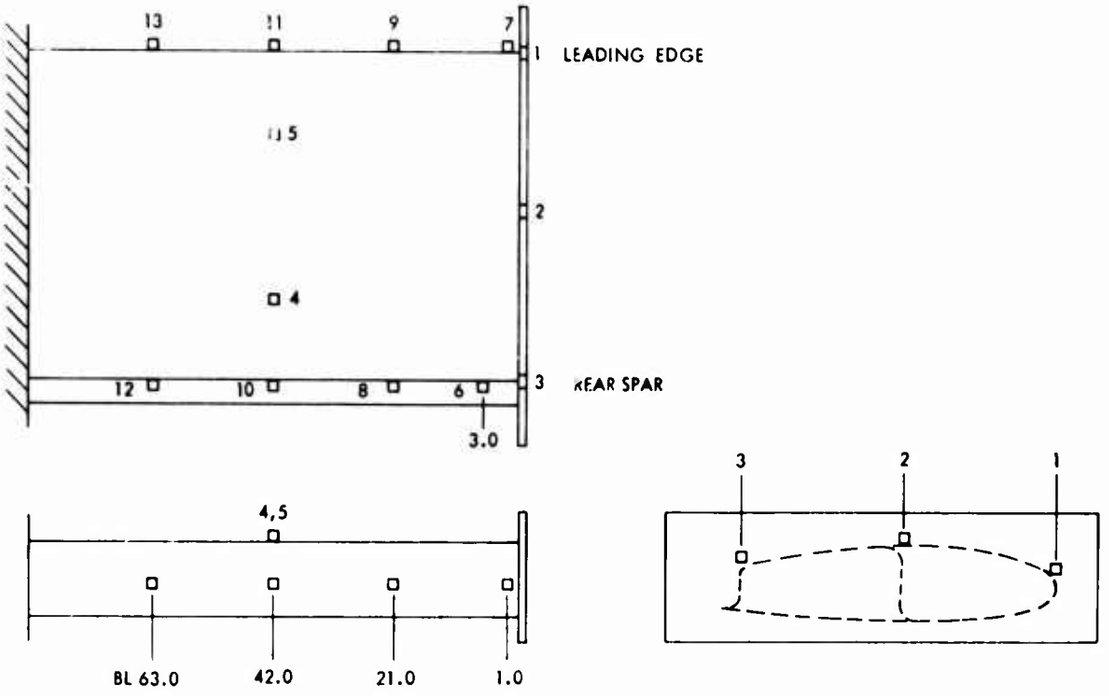

Figure 28. Vibration Survey Accelerometer Locations.

TABLE IX. RESULTS OF VIBRATION SURVEY		
Resonant Frequency	Speaker Location	
	Mid-span, Mid-chord	Outboard Leading Edge
f_1	18.2	18.2
f_2	48.6	48.6
f_3	101.6	101.4
f_4	106.5	107.4
f_5	141.9	159.0
f_6	195.0	187.0
f_7	260.0	240.0
f_8	-	291.0

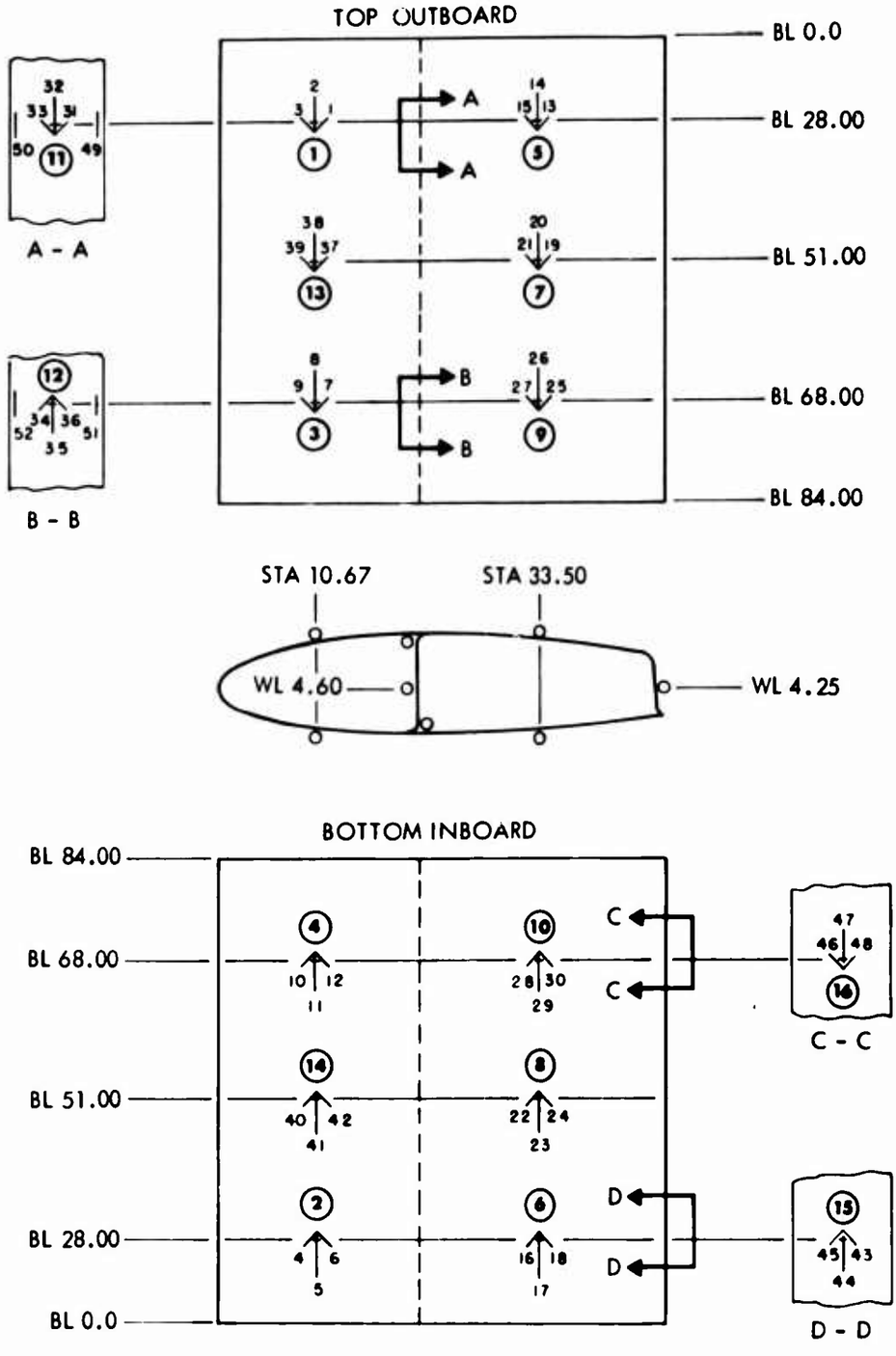

Figure 29. Strain Gage Numbers and Locations.

of the damping coefficient to the critical damping coefficient (c/c_{cr}) values given in Table X. Strain traces from the outboard gages were too small for obtaining reliable data. The accelerometers shown in Figure 28 were also active. However, noise generated by the quick-release mechanism prevented use of the accelerometer recordings for data reduction.

During the bending free vibration tests, the specimen was deflected to three different positions, corresponding to approximate stress levels of 2000, 6000, and 12,000 psi. The highest strain gage reading was at the root section. The specimen was then released, and free vibration was allowed to damp to zero. These tests were repeated with a bungee cord attached at the free end and preloaded to 200 pounds.

For torsional plus bending free vibration, a 1000-pound shear load was applied at point 2 (see Figure 25). The load was then released, and vibration was allowed to damp to zero. This test was also repeated with a bungee cord preload of 200 pounds at the free end. The actual stress levels at the root section during the torsion-free bending tests are shown in Table X.

The c/c_{cr} ratio values given in the table were obtained by logarithmic decrements determined from the traces of the strain gages. The ratio, c/c_{cr}, is given by

$$c/c_{cr} = \frac{1}{2\pi} \ell n \left(\frac{S_n}{S_{n+1}} \right) \tag{50}$$

where S_n is the beam peak displacement during the nth cycle of vibration

S_{n+1} is the peak displacement during the following cycle

Since tip deflection bears a linear relationship to the normal stress or strain level at any point on the cross section, Equation (50) can be replaced by

$$c/c_{cr} = \frac{1}{2\pi} \ell n \left(\frac{\epsilon_n}{\epsilon_{n+1}} \right) \tag{51}$$

This expression was used in reducing the data from the free vibration strain gage traces.

The fundamental frequency in cantilever bending of the wing section was also determined during these tests. Regardless of the initial tip deflection or presence of the bungee preload, the strain gage traces indicated a natural frequency at approximately 17.1 Hz.

TABLE X. PERCENT CRITICAL DAMPING AT FUNDAMENTAL FREQUENCY

Gage No.	2000 psi		6000 psi		12,000 psi	
	σ_{max}	c/c_{cr}	σ_{max}	c/c_{cr}	σ_{max}	c/c_{cr}
	NO BUNGEE PRELOAD					
20	-1170	0.027	-3500	0.035	-7350	0.012
23	1080	0.031	3400	0.041	7000	0.014
8	-1850	0.023	-5740	0.035	-11400	0.010
11	1420	0.023	4800	0.036	9310	0.015
26	-1600	0.030	-4950	0.036	-9930	0.012
29	1490	0.017	4800	0.036	9700	0.013
Avg	-	0.025	-	0.036	-	0.013
	200-LB BUNGEE PRELOAD					
20	-1170	0.029	-3580	0.042	-7250	0.027
23	960	0.045	3220	0.038	10200	0.020
8	-1750	0.027	-5590	0.018	-11300	0.023
11	952	0.025	4350	0.032	9200	0.021
26	-1440	0.040	-3810	0.030	-9650	0.031
29	1370	0.047	4510	0.040	9450	0.024
Avg	-	0.036	-	0.033	-	0.024

Because the accelerometers did not provide useful data for the free vibration test, it was not possible to determine natural frequency in torsion. The 12 active strain gages recorded axial strains only. These resulted from bending caused by the 1000-pound shear load. However, it was possible to evaluate the pure bending strain from the readings of the gages. Prior to the failure in obtaining useful accelerometer data, a strain gage analysis was not intended. Results of the data reduction for the bending load analysis are presented in Table X.

A graphic presentation of the strain decay from the 12,000- and 6000-psi stress levels is given in Figures 30 and 31. In tests where the bungee preload was not used, the damping coefficient was higher at the

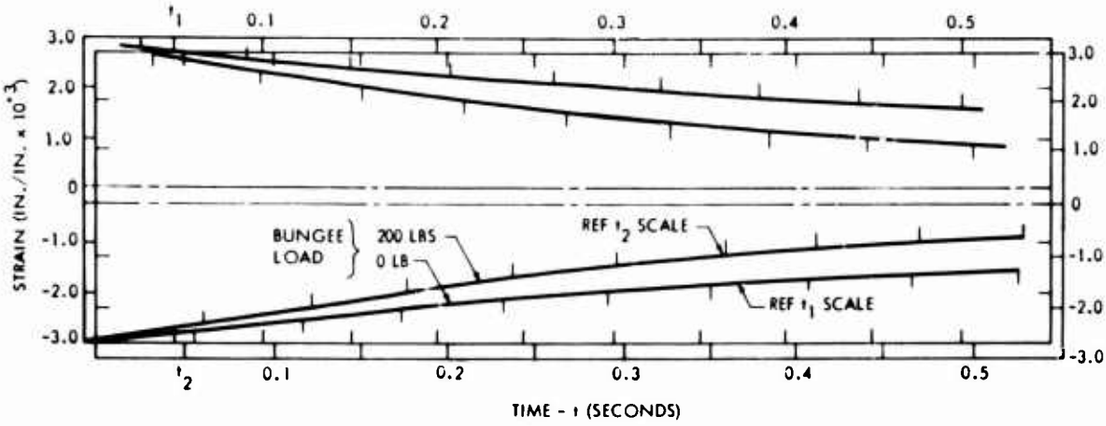

Figure 30. Strain Decay During the Free Vibration Test for σ_{max} = 12,000 psi as Determined From Strain Gage No. 8.

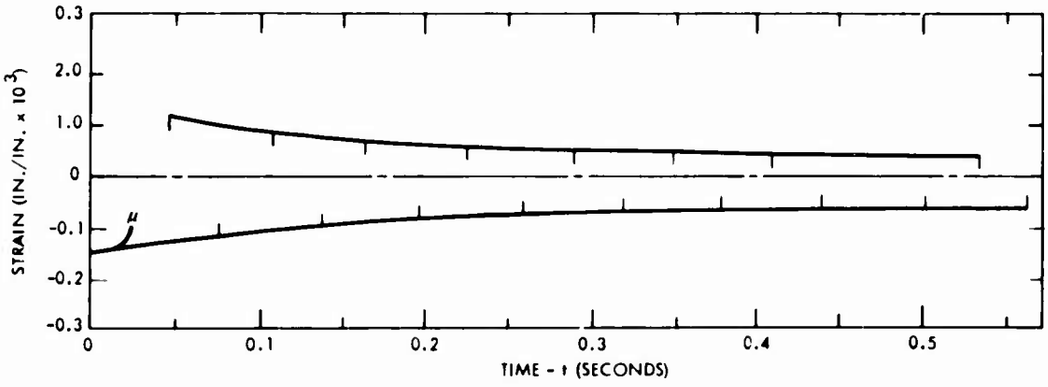

Figure 31. Strain Decay During the Free Vibration Test for σ_{max} = 6000 psi as Determined From Strain Gage No. 8.

6000-psi load than at the 2000-psi load. However, at the 12,000-psi load, the coefficient was much lower.

When the bungee preload of 200 pounds is considered, the coefficient values at 2000 psi and 6000 psi are essentially equal to the values obtained when the preload was not used. However, at the 12,000-psi load, the percent of critical damping did not drop off nearly as much.

Because of the uncertainties involved in obtaining the damping coefficients, a Goodyear Aerospace Corporation development program was initiated to investigate damping properties on a specimen scale rather than on a complete wing. Results of this investigation are intended to supplement the wing test data.

In this investigation, both laminate and sandwich specimens were subjected to low-stress-level free vibration tests in air and in a vacuum. Specimen configurations, test setups, and test procedures are presented in the following paragraphs.

The reinforcing material of the specimens was 481-I-550 fiber glass fabric impregnated with E293 epoxy resin. The laminate specimen was 3/32 inch thick, 1 inch wide, and 13 inches long. One end of the beam was potted into a 6-inch cube of U.S. Gypsum No. 30 Ultracal Plaster. The cantilevered free length of the specimen was 7-15/16 inches. Dimensions of the sandwich specimen were 1/2 inch thick, 2-1/4 inches wide, and 39 inches long. It was made up of 3-ply (0.030-inch) skins and 1/8-0.001-5052-H39 aluminum honeycomb core. After potting, the free length of the sandwich beam was 33-3/16 inches.

The laminate beam plaster end support was secured to the test chamber with weights and clamps, while the sandwich beam end support was bonded to a 420-pound steel block, which in turn was bonded to the chamber floor. This mounting arrangement established a rigid beam support. A 12-gram accelerometer was attached to the free end of each beam. Laminate tests were run at atmospheric pressure and at a pressure of 40 microns of Hg. The free end of the laminate specimen was deflected 0.066 inch and released. The decaying amplitude was recorded by the accelerometer. Sandwich tests were run at atmospheric pressure and at a pressure of 20 microns of Hg. The free end of the sandwich specimen was deflected 0.045 inch prior to release of the beam. It was found that upon release of the sandwich beam, the first two modes of vibration were excited. Since the amplitude of only the first mode was required to determine the c/c_{cr} damping ratio, the accelerometer was removed from the tip of the specimen and placed at the nodal point of the second mode. The test was rerun. The recorded amplitude was then that of the first mode of vibration only.

For the sandwich specimens used in these tests, the maximum stress level was less than 200 psi. At the maximum displacement, c/c_{cr} was 0.008 in air and 0.005 in a vacuum. The solid laminate specimens were deflected to a maximum stress level of approximately 620 psi. At this maximum displacement, the measured c/c_{cr} was 0.003 in air and in a vacuum.

Data reduction on the full wing section specimen indicated c/c_{cr} values ranging from 0.013 to 0.027 at maximum stress levels up to 12,000 psi. The large difference in c/c_{cr} between the full wing specimen and the small cantilever beam specimens is apparently due to air effects and possible friction in the bolted connections of the wing test configuration. The small-specimen tests indicate very little material damping capability in either the solid laminate or the sandwich construction.

Forced vibration tests of the wing section were performed using a portable shaker and a speaker, with excitation applied at the outboard end. Both shaker and speaker were located at the center of the cross section and at the leading edge, employing the frequencies shown in Table XI. Accelerometer data were recorded on oscillographs with a high paper speed in order to display phase relationships between pickups. The outputs of 12 accelerometers were recorded during the tests. A comparison of accelerometer traces for speakers and portable shaker excitation indicated no significant difference in response of the specimen. For this reason, data were evaluated only for the load condition where the shaker load was applied at the shear center.

Acceleration traces from the 12 active accelerometers were recorded during each vibration test. Calibration constants for the accelerometers are tabulated in Table XII, where k is the acceleration of 1 inch of height on the recording paper. Traces of the input were also recorded. However, the calibration for this curve was unknown. The relation of the input phase angle to the accelerometer phase angle was utilized.

Tabulation of data involved measuring the trace height for each accelerometer trace and relating the data to the input phase angle. Four phase angles were considered to be 0^{o}, 90^{o}, 180^{o}, and 270^{o}. A tabulation of the acceleration and phase angle data for all eight frequencies is presented in Table XIII. These data are sufficient to evaluate the g loads at the different phase angles.

To amplify the data, a series of plots is presented in Figure 32, sheets 1 through 8. This figure represents a plan view of the wing test section on which the 12 accelerometers were located. Acceleration values for each accelerometer are shown for the appropriate frequency and phase angle.

TABLE XI. RESONANT FREQUENCIES (Hz) APPLIED DURING FORCED VIBRATION TESTS

Resonant Frequencies	Speaker Location		Shaker Location	
	Outboard Shear Center	Outboard Leading Edge	Outboard Shear Center	Outboard Leading Edge
f_1	18.2	18.2	18.1	17.9
f_2	48.6	48.6	48.6	47.8
f_3	101.6	101.4	101.2	100.8
f_4	106.5	107.4	106.2	140
f_5	141.9	159	140.5	249
f_6	195	187	195	289
f_7	260	240	252	-
f_8	-	291	260	-

TABLE XII. ACCELEROMETER CALIBRATION VALUES

Accelerometer	Wing BL	k(g/in.)
1	0	46.5
2	0	46.5
3	0	46.5
4	42	6.5
5	42	6.5
6	3	46.5
7	3	46.5
8	21	18.8
9	21	18.8
10	42	6.5
12	63	4.9
13	63	4.9

TABLE XIII. FORCED VIBRATION SUMMARY

Accel. No.	18.1 Hz		48.2 Hz		101.2 Hz		106.2 Hz		140.5 Hz		195 Hz		252 Hz		260 Hz	
	g*	α**	g	α	g	α	g	α	g	α	g	α	g	α	g	α
1	11.90	90	7.90	270	3.25	0	0.70	270	0.64	0	0.82	180	2.73	180	2.44	180
2	11.60	90	0	0	1.74	0	1.16	0	0.47	0	0.35	0	1.62	0	1.40	0
3	11.80	90	10.20	90	1.39	270	2.54	0	1.08	270	1.05	0	3.14	180	4.30	180
4	0.86	90	0.57	90	0.76	270	1.80	270	1.14	90	2.28	270	1.12	180	0.42	180
5	0.97	90	0.45	270	2.10	270	0.32	0	0.27	270	1.04	270	0.42	0	0.47	0
6	10.70	90	9.85	90	1.16	270	2.32	0	0.93	270	0.75	90	4.30	180	4.30	180
Input***	3.80	0	5.60	0	8.00	0	7.50	0	8.00	0	5.95	0	3.70	0	7.60	0
7	11.00	90	7.55	270	2.32	90	1.39	270	0.46	270	0.50	90	1.75	180	1.63	180
8	3.76	90	4.23	90	0.70	270	1.64	270	1.32	270	1.41	180	1.95	180	2.05	180
9	3.29	90	3.05	270	2.82	270	0.37	270	0.61	270	0.19	0	0.75	180	1.36	180
10	1.10	90	1.42	90	0.32	0	1.70	270	0.99	180	0.95	180	1.04	0	0.97	0
11	-	-	-	-	-	-	-	-	-	-	-	-	-	-	-	-
12	0.37	90	0.67	90	0.20	0	1.15	270	0.57	180	0.84	180	2.00	0	1.67	0
13	0.35	90	0.49	270	1.60	270	0.21	90	0.30	180	0.32	0	0.39	0	0.72	0

*g - acceleration

**α - phase angle

***Input acceleration was not defined in the test. The input value shown is not considered to be a g value and is included for relative information only.

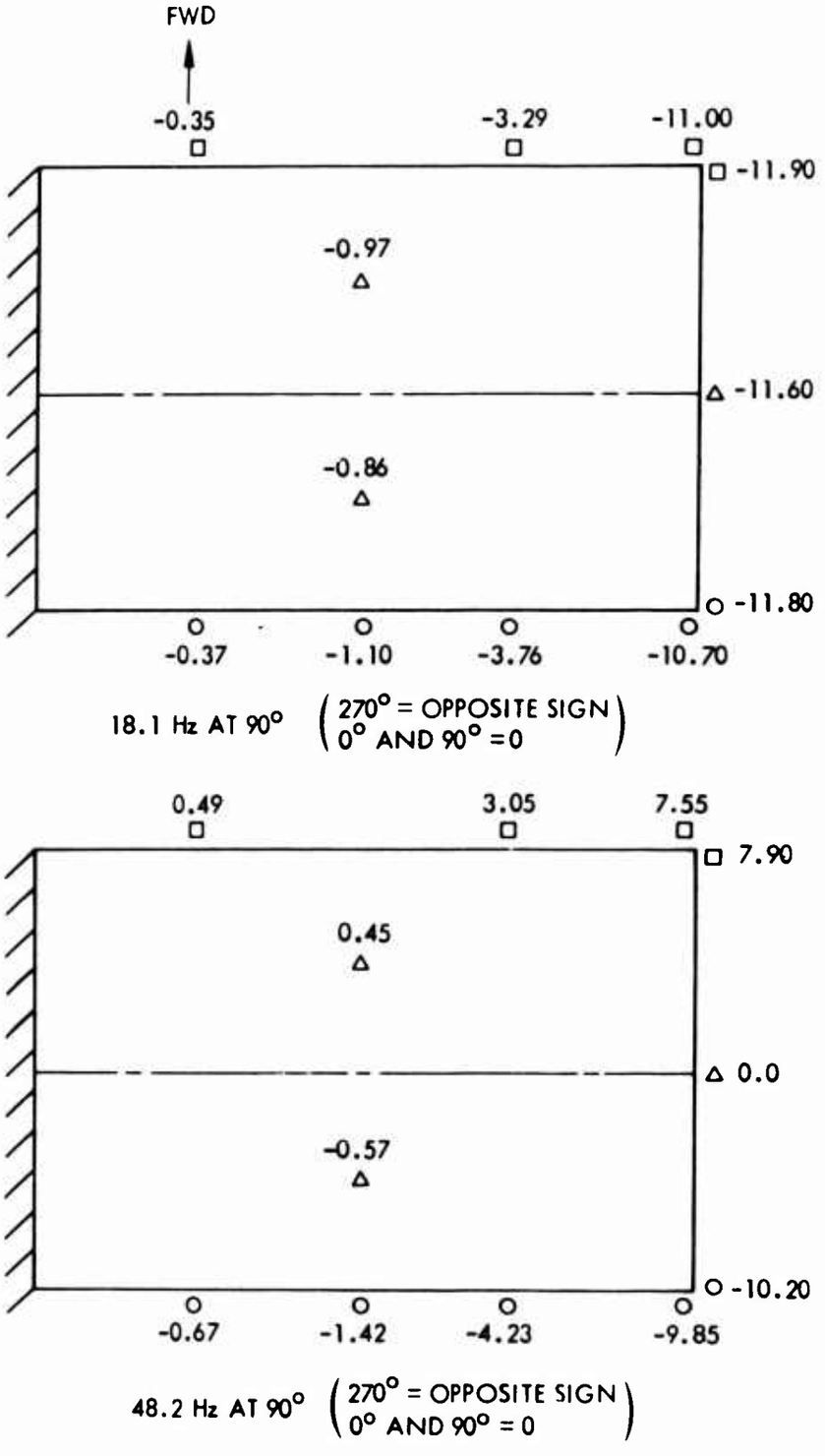

Figure 32. Acceleration at Wing Test Points During the Vibration Survey (Sheet 1 of 8).

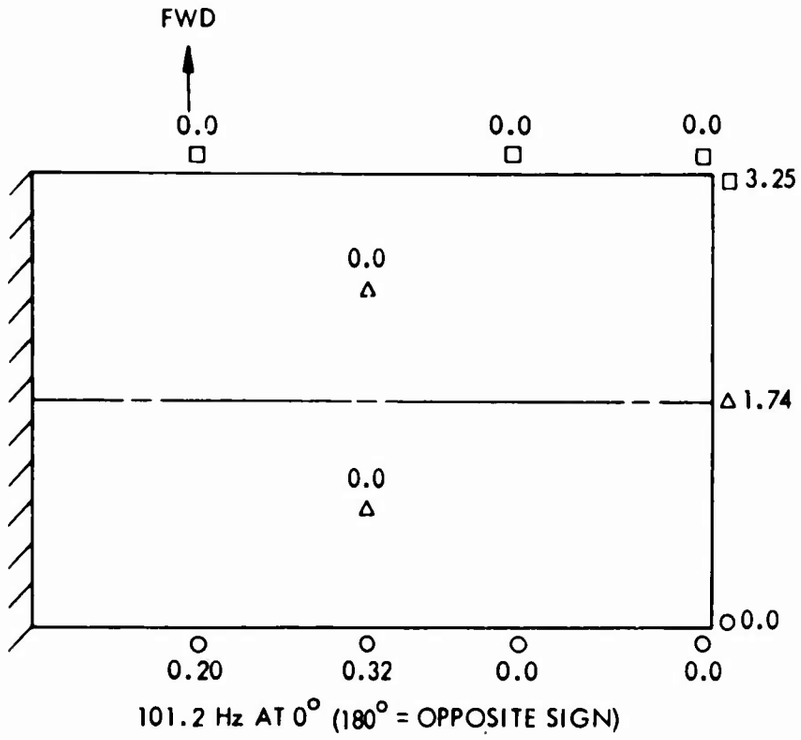

Figure 32. Continued (Sheet 2 of 8).

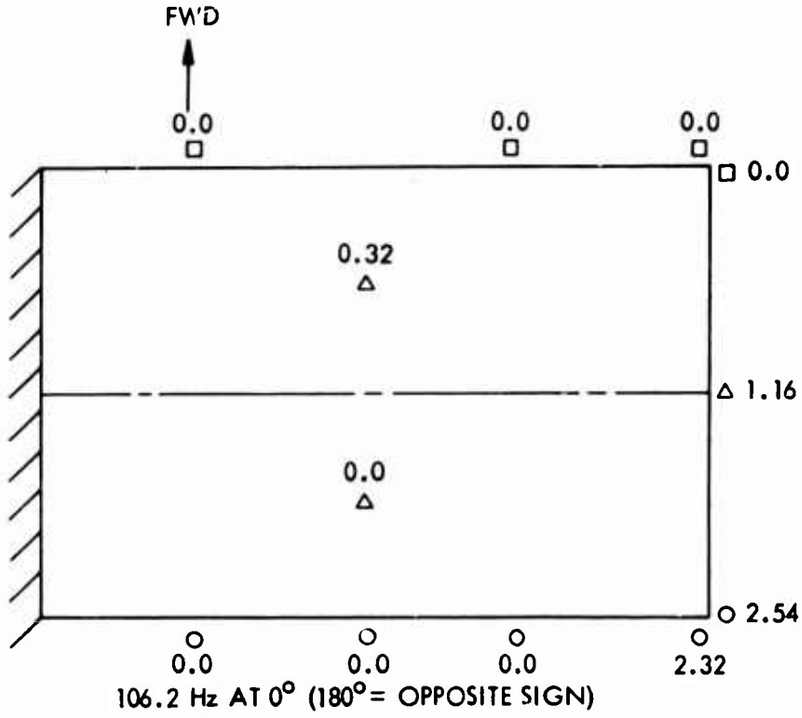

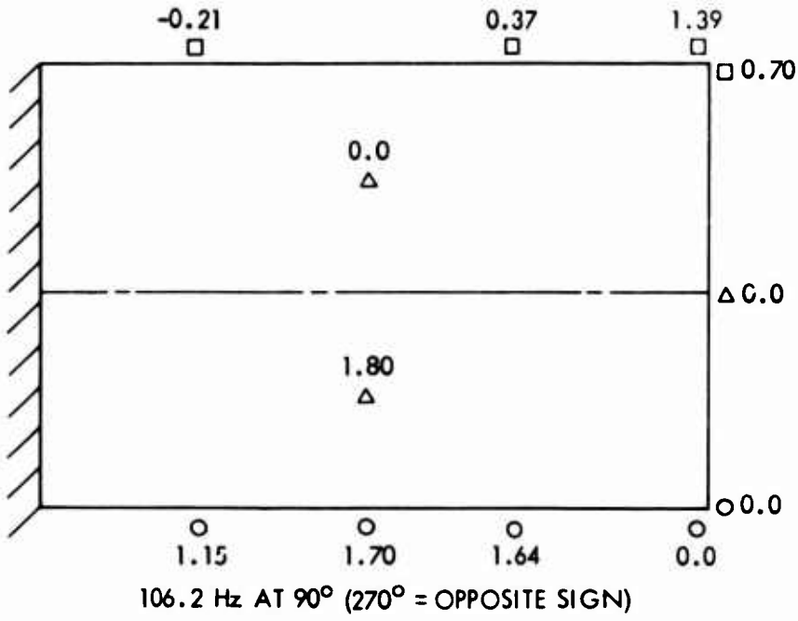

Figure 32. Continued (Sheet 3 of 8).

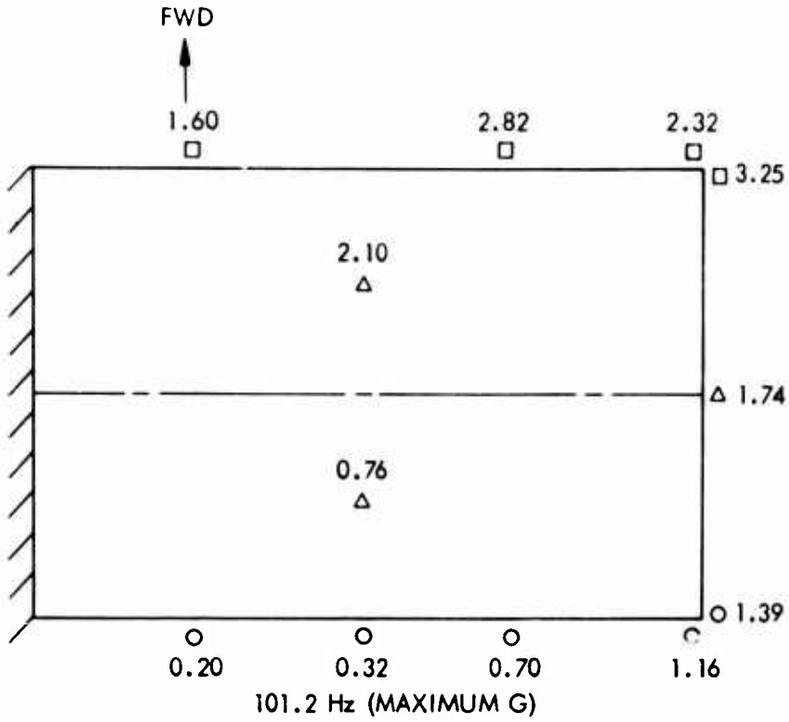

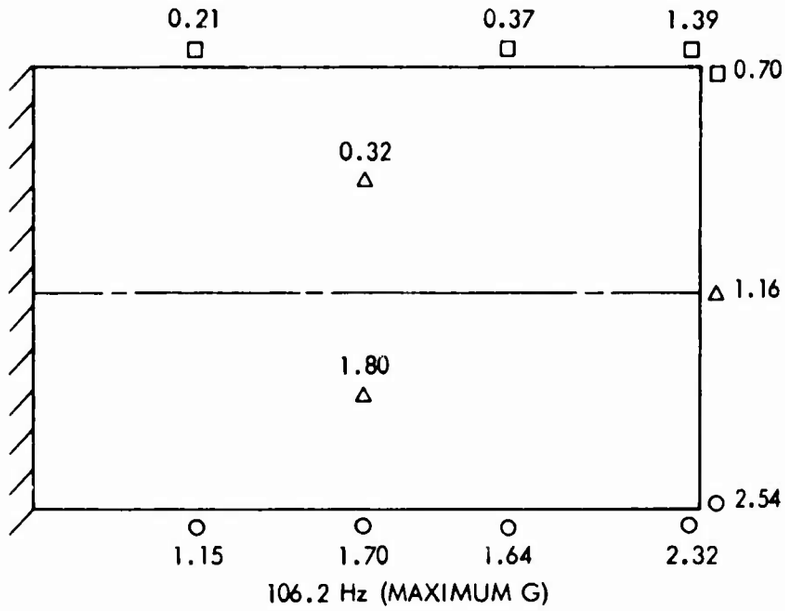

Figure 32. Continued (Sheet 4 of 8).

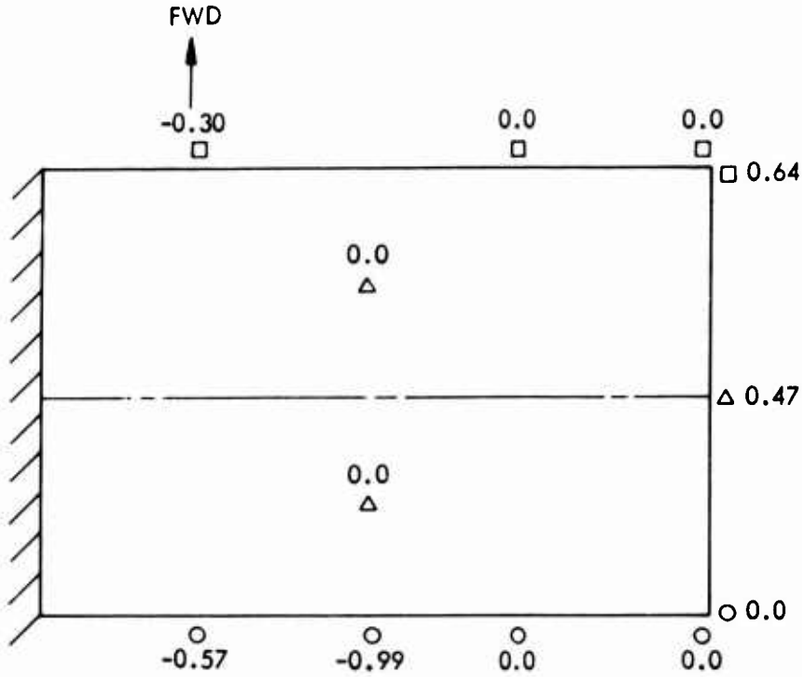

140.5 Hz AT 0° (180° = OPPOSITE SIGN)

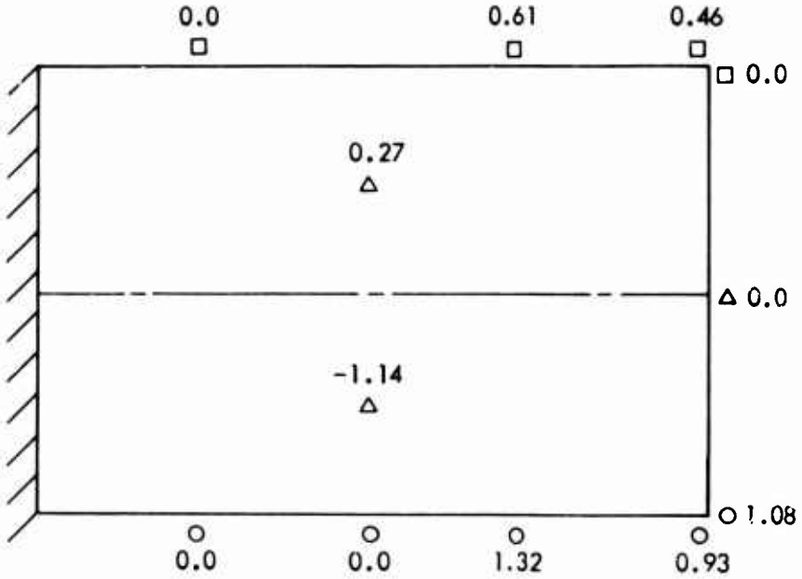

140.5 Hz AT 90° (270° = OPPOSITE SIGN)

Figure 32. Continued (Sheet 5 of 8).

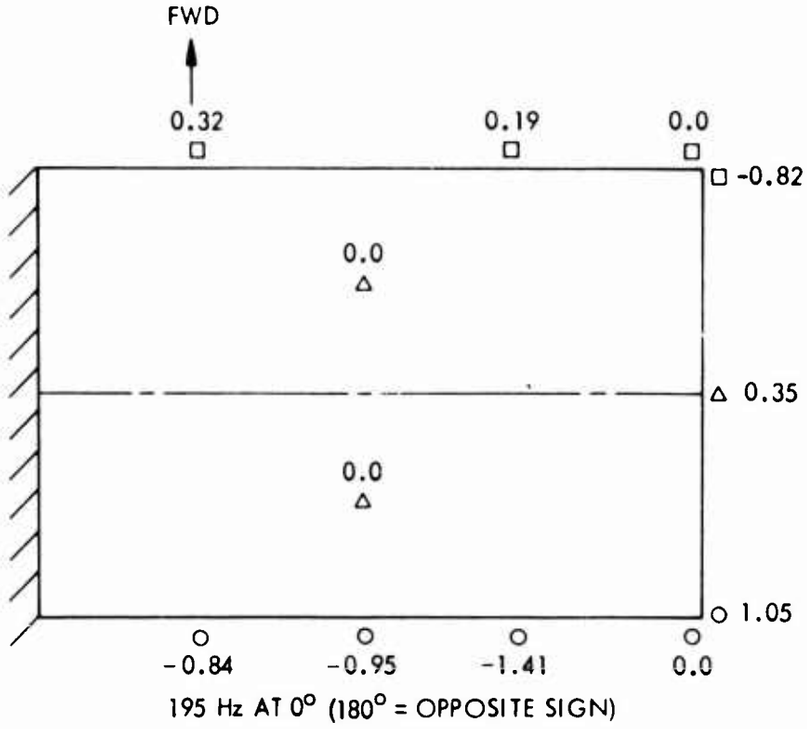

195 Hz AT 0° (180° = OPOSITE SIGN)

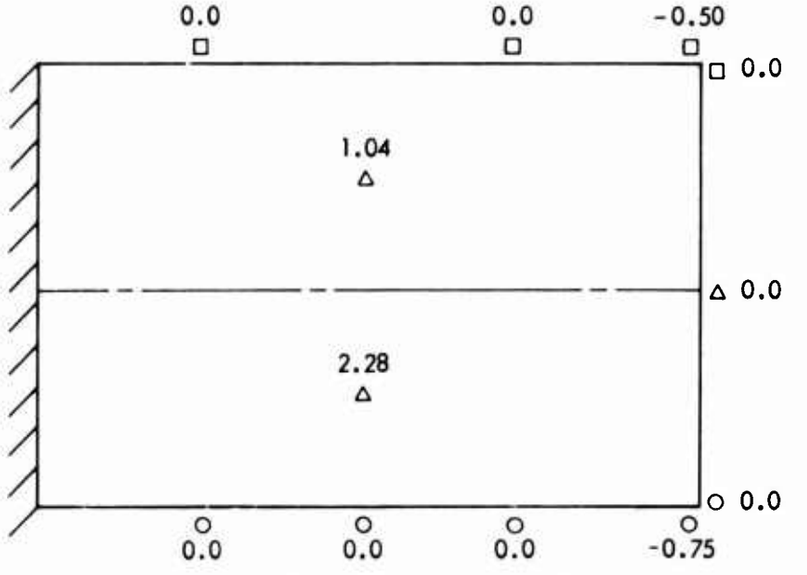

195 Hz AT 90° (270° = OPPOSITE SIGN)

Figure 32. Continued (Sheet 6 of 8).

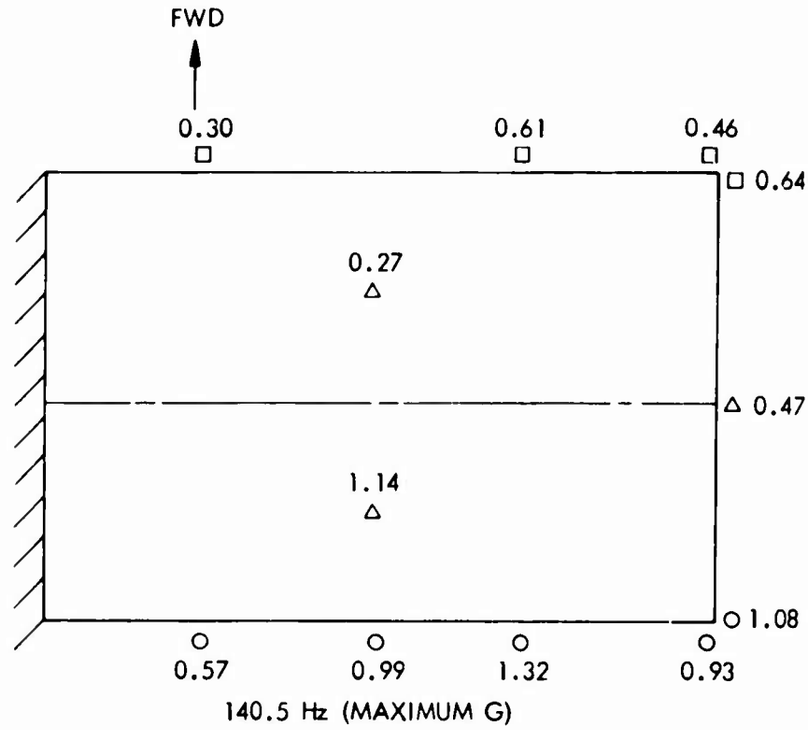

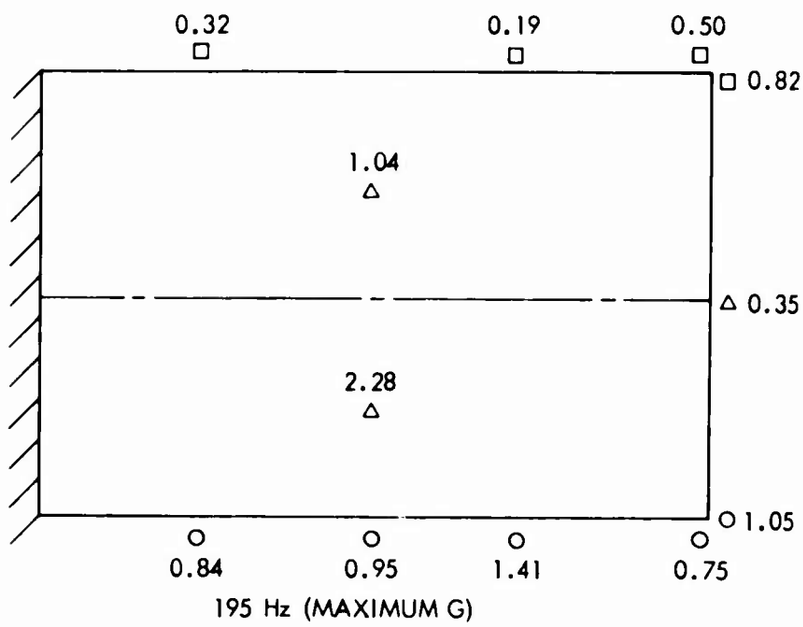

Figure 32. Continued (Sheet 7 of 8).

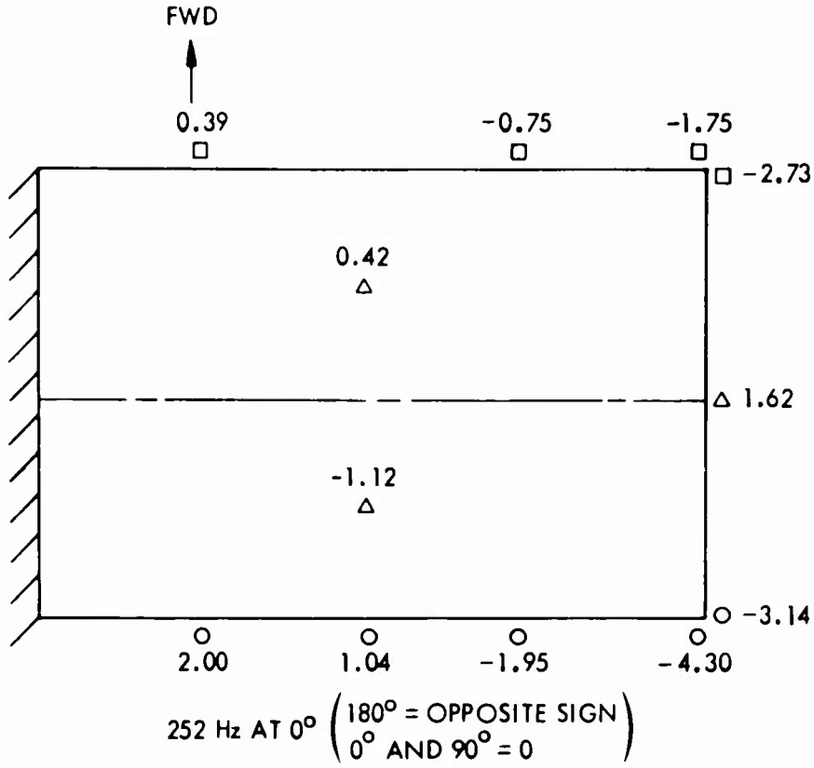

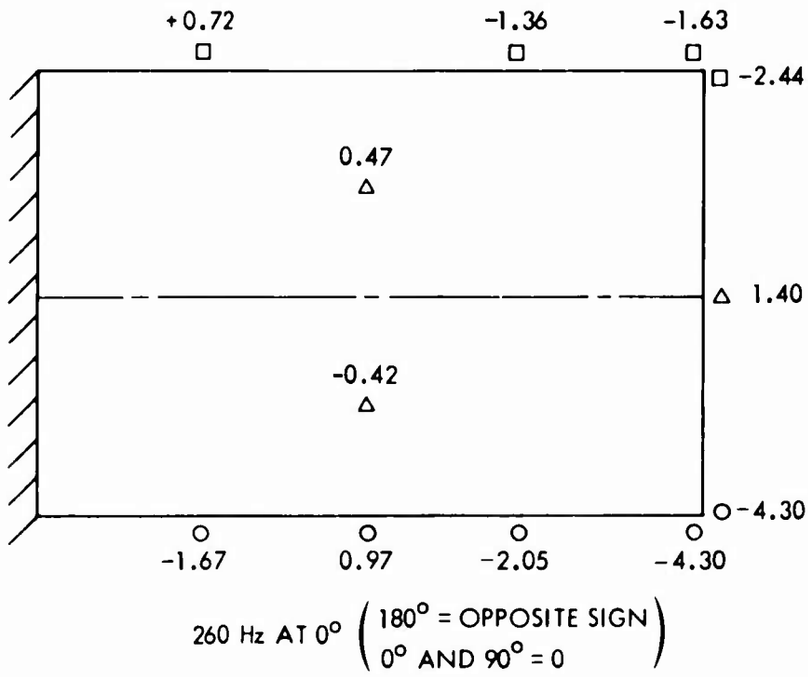

Figure 32. Continued (Sheet 8 of 8).

Analysis of the data, particularly at the higher frequencies, is difficult, and the number of acceleration pickups is marginal for a thorough vibration survey. Also, since the input acceleration is not known, the relationship of the g values at the various frequencies is indeterminate. The data at the lower frequencies, 18.1 and 48.2 Hz, show that accelerations are approximately proportional to the bending deflection of the test specimen. This proportion holds true at both the leading and trailing edges of the wing. When the 48.2 Hz frequency was applied, the accelerations held the same pattern. However, the leading and trailing edges were 180° out of phase, indicating a torsional mode of vibration. At the higher frequencies, considerable variations resulted in the pattern of accelerometer readings. Phase angles of the various accelerometers also became variable. Thus, the data analysis is inconclusive. It is recommended that mode lines be determined by other methods in future vibration testing. It is also suggested that input acceleration be recorded.

STATIC TESTS

The following order was used for the four different static tests performed on the No. 1 wing test section:

1. 70% DUL in bending
2. 70% DUL in bending plus torsion
3. Torsion test
4. 100 percent DUL in bending

The loadings specified in the test plan are outlined in Appendix I and are as follows:

1. The DUL for the bending condition is 1,151,000 in.-lb at BL 68.
2. The DUL for the torsion condition is 38,500 in.-lb.
3. The DUL for the bending plus torsion condition is 1,151,000 in.-lb at BL 68 bending and 38,500 in-lb in torsion.

Originally, the scheduled torsion test loading was to 70 percent of 38,500 in.-lb. In order to obtain measurable levels of strain, the loading was changed to 186,000 in.-lb prior to the actual test. However, torsion loading applied in the combined bending and torsion test was 70 percent of the 38,500 in.-lb loading.

Loads were applied at the free end of the cantelever beam test wing. For the bending tests, the load was applied at the shear center of the wing section. For the combined bending and torsion condition, the load was offset from the shear center a distance calculated to produce the desired load combination. A couple loading was applied for the torsion test.

The instrumentation included strain gages distributed as shown in Figure 29 and deflection gages (potentiometers) distributed as shown in Figure 33. Figures 34 and 35 are photographs of the test setup.

The general test results and applicable photographs included in this subsection were taken from the Aero Structures Department test summary report.[5]

For the 70 percent DUL cantilever bending tests, the load was applied through the shear center for the positive bending condition to 30 percent DUL, returned to zero load, and then taken to a maximum of 70 percent DUL. Slight cracking sounds were first heard as the load was increased above 30 percent DUL. The load also dropped off slightly while data were being recorded at each increment. As the load was increased above 60 percent DUL, continuous cracking sounds were heard. The load tended to drop off appreciably at 70 percent DUL while data were being recorded. While the load was maintained at 70 percent DUL, the deflection of

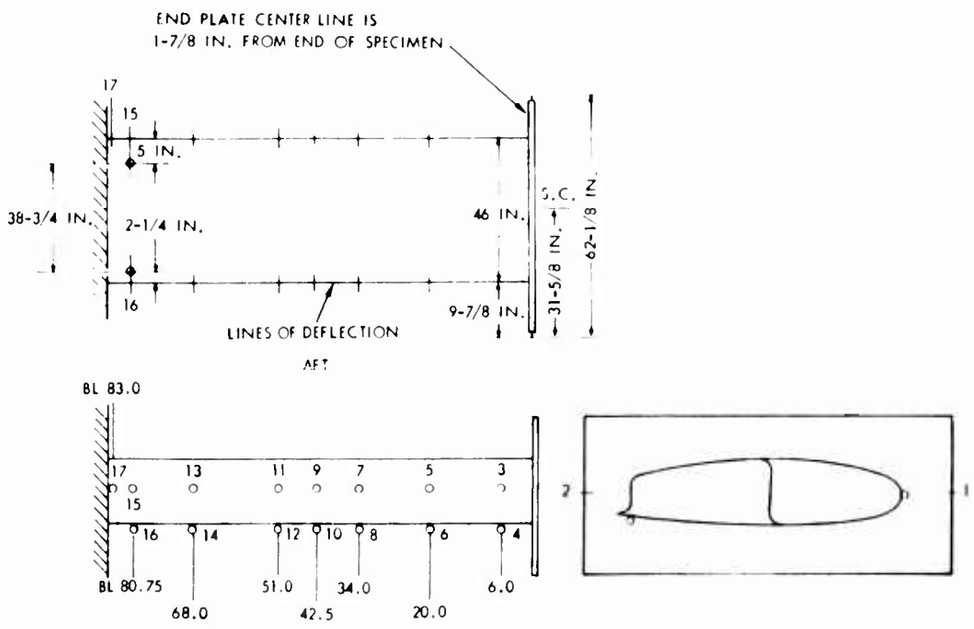

Figure 33. Location of Wing Section Deflection Points.

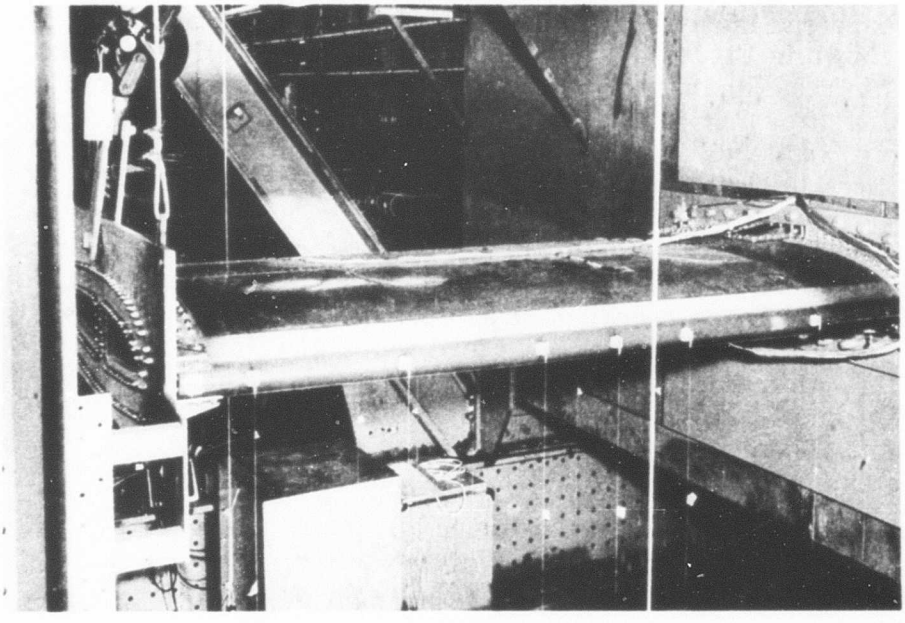

Figure 34. Static Test Setup for the Bending Condition of the FRP Wing Section.

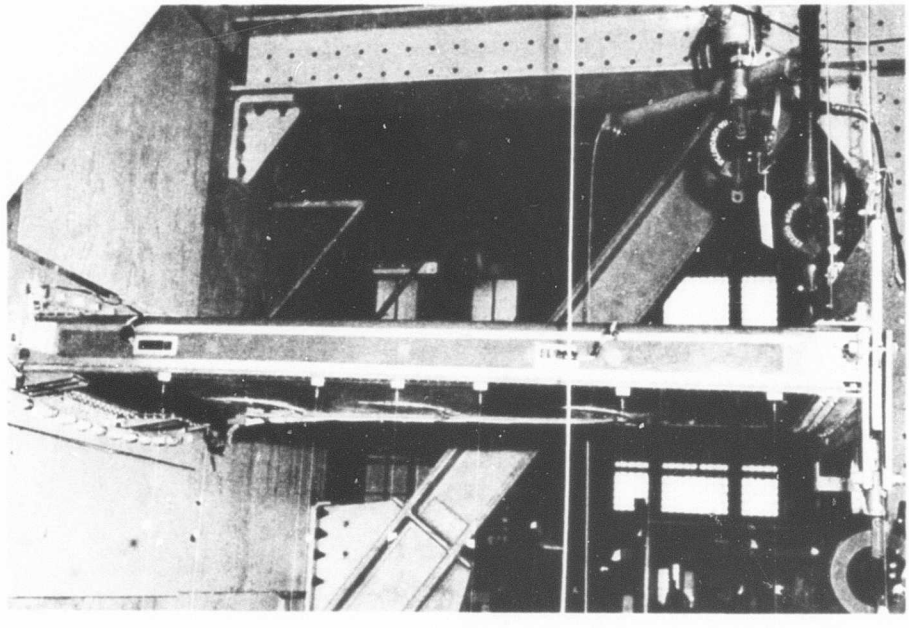

Figure 35. Static Test Setup for the Torsion Condition of the FRP Wing Section.

the outboard end increased. Deflection of the wing section at 70 percent DUL is shown in Figure 36. The load was incrementally decreased to zero. After the load was removed, the set at the outboard end of the wing section was 0.3 inch. Approximately 30 minutes later, the set decreased to 0.25 inch. The wing section was examined visually for damage, but no damage was evident.

The load was applied for the combined bending and torsion condition to 70 percent DUL and then returned to zero. The load dropped off slightly while data were being recorded at 50, 60, and 70 percent DUL. Slight cracking sounds were heard as the load was maintained at 60 and 70 percent DUL. After the load was removed, the leading edge of the wing section had a set of 0.35 inch. Five minutes later, the set decreased to 0.30 inch. The next day, the set returned to 0.25 inch. The wing section was examined visually for damage, but no damage was evident.

The loads were applied for the positive torsion condition to 186,000 in.-lb.

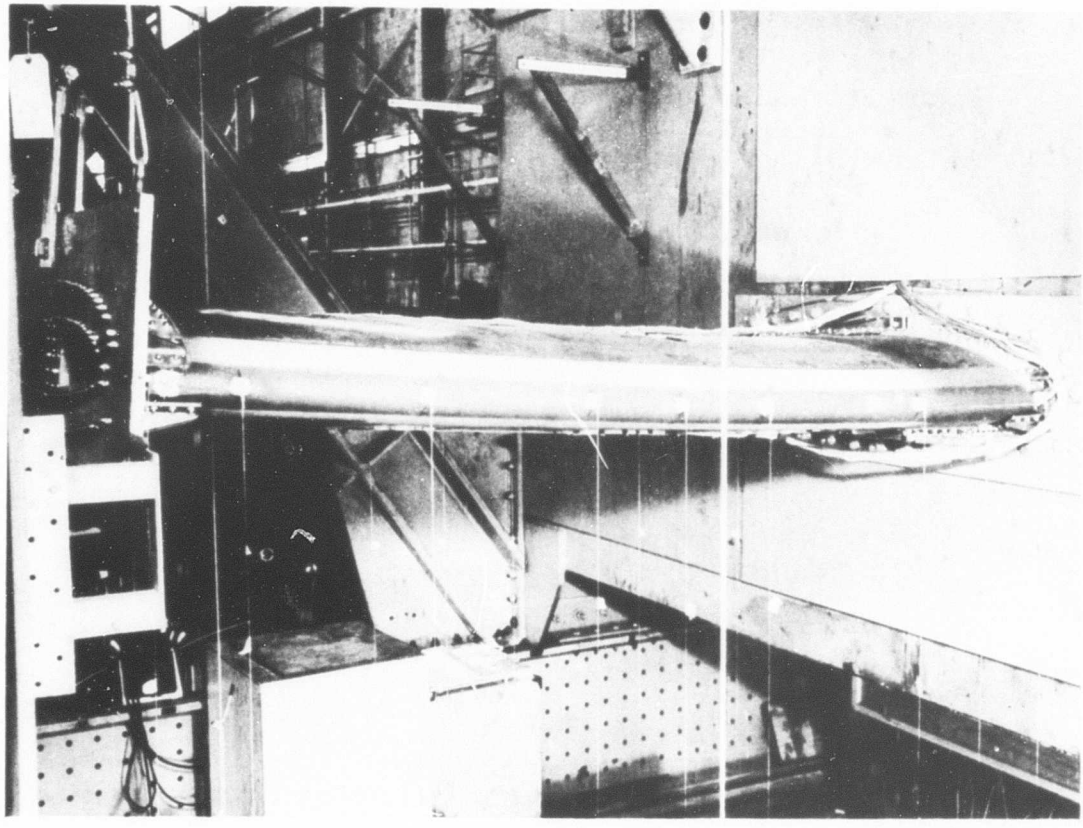

Figure 36. No. 1 FRP Wing Section - Bending Condition Deflection at 70 Percent DUL.

No cracking sounds were heard during the test. The load dropped off slightly while data were being recorded at 90 percent of the maximum load (167,400 in.-lb). The load was returned to zero and the wing section was visually examined. No damage was evident.

Load was applied for the positive bending condition to 100 percent DUL. No cracking sounds were heard below 60 percent DUL. Slight cracking sounds were heard as the load was increased to 70 percent DUL. The load dropped off slightly as data were recorded at 70 percent DUL. At 70 percent DUL, the upper surface panel of the aft cell buckled just outboard of the reinforced area at the inboard end. The failure mode was overall instability, and it appeared that the panel flattened out (buckling down) in that area. Loading was continued to 80 percent DUL. Continuous cracking sounds were heard as the load increased. The deflection of the wing section at 80 percent DUL is shown in Figure 37. Failure

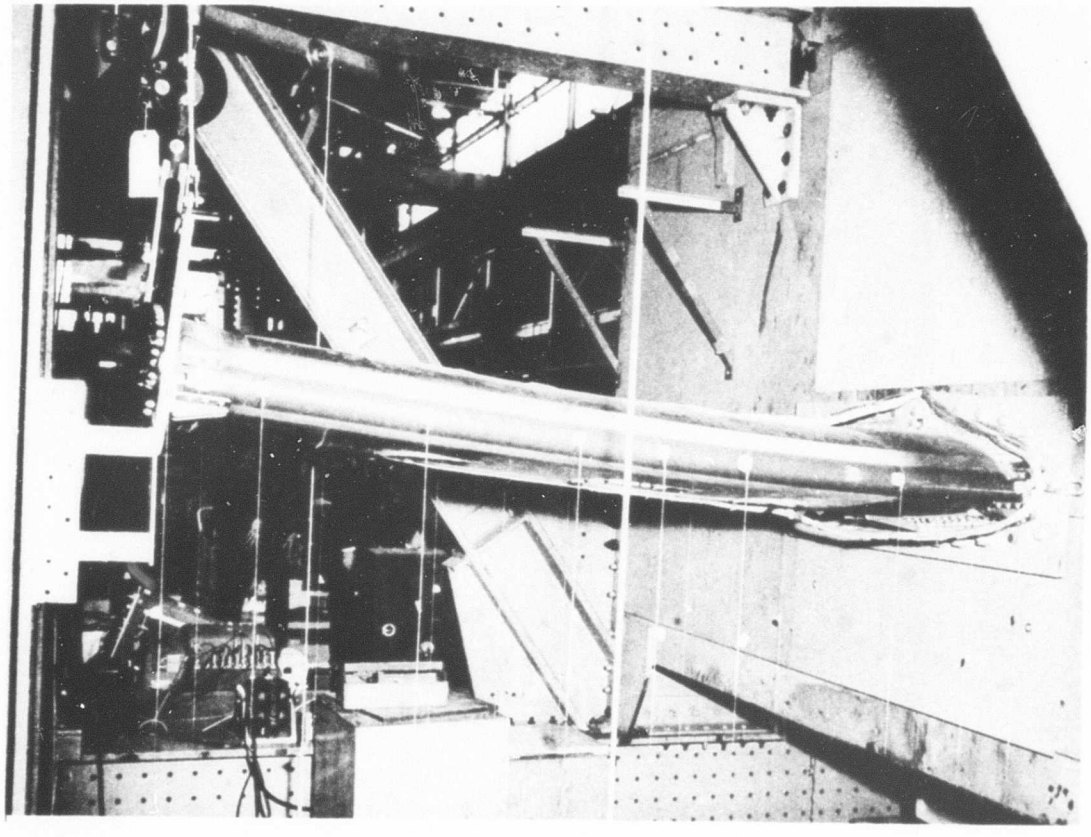

Figure 37. No. 1 FRP Wing Section - Bending Condition Deflection at 80 Percent DUL.

occurred at 80 percent DUL while data were being recorded. Two distinct sharp sounds were heard as the structures failed catastrophically. The failed wing section is shown in Figure 38. Failure occurred in several areas. Figure 39 shows the local buckling type failure of the upper surface panels. The failure was at BL 68.0 on the forward cell, which was about 1 inch outboard of the reinforced area. In the aft cell, the failure was at BL 64.0, which was about 5 inches outboard of the reinforced area. (The reference for butt-line stations is the outboard tip.) A closeup view of the failure in the area of the joint between the two sections is shown in Figure 40. Two bolts were sheared through the shank (one on each side of upper arrow); the head of another bolt was partially sheared off and the shank was bent (lower arrow). Several other bolts in the area were bent. Both the center and rear spars failed in shear. The failure of the center spar is shown in Figures 41 and 42. Failure of the

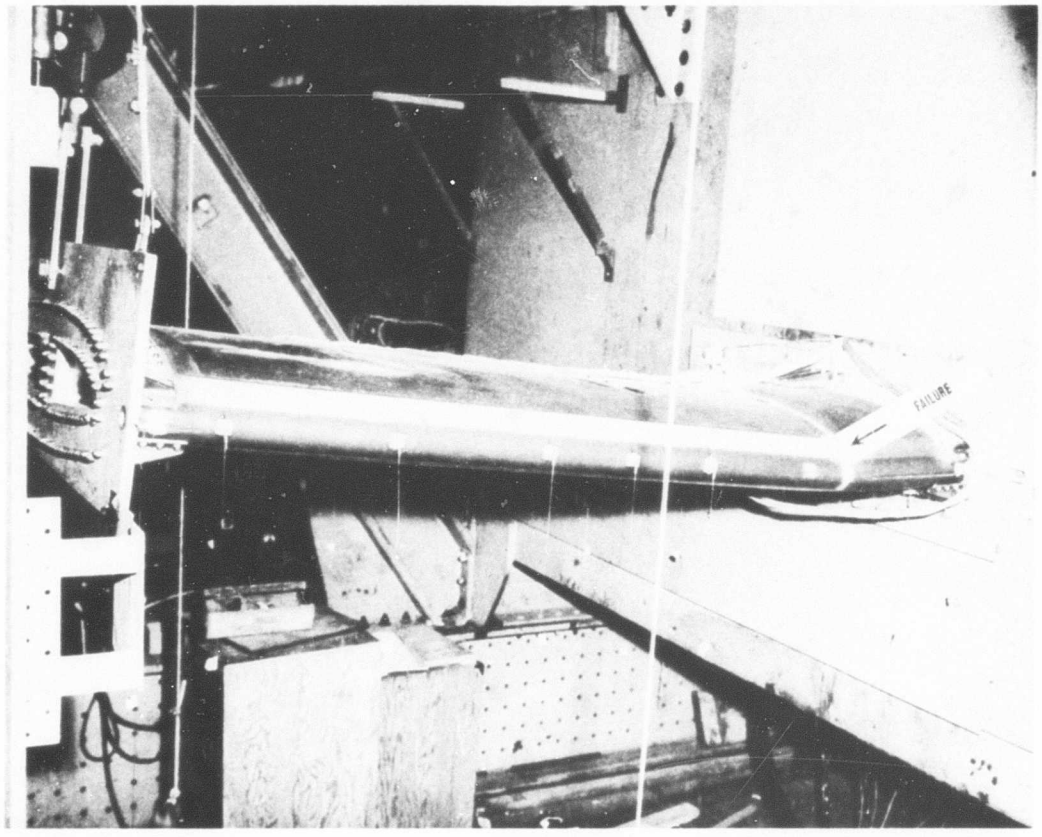

Figure 38. No. 1 FRP Wing Section - Overall View of the Failed Wing Section.

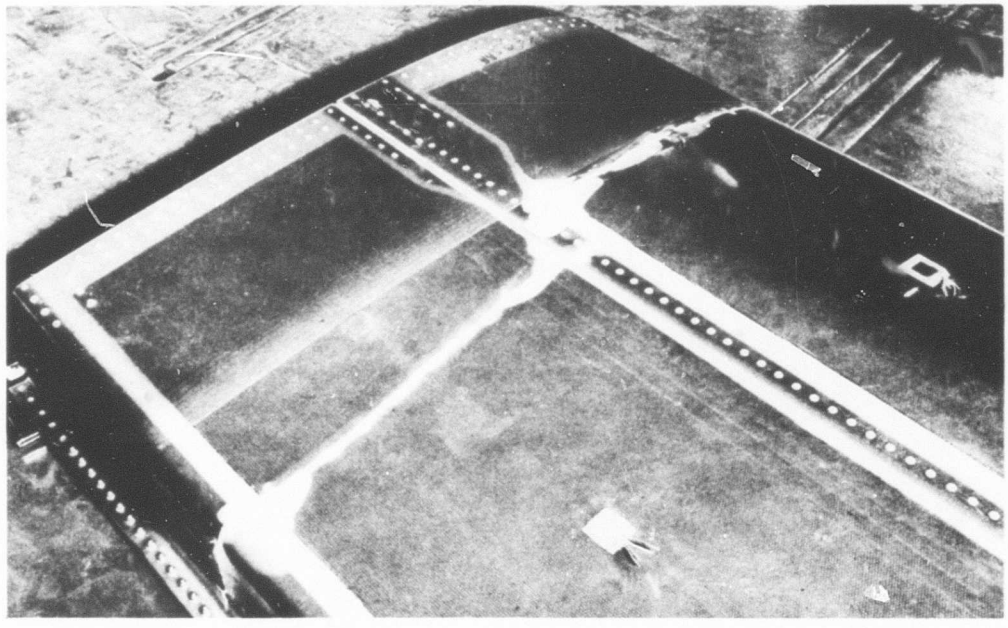

Figure 39. No. 1 FRP Wing Section - Failure of the Upper Surface Panels.

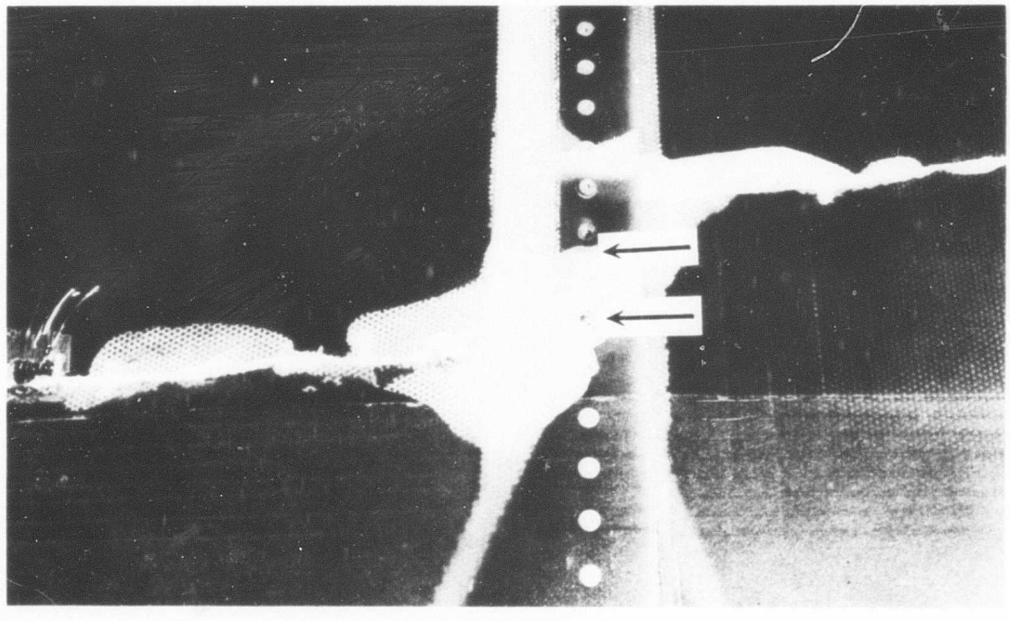

Figure 40. No. 1 FRP Wing Section - Failure of the Upper Surface Panel in the Joint Area.

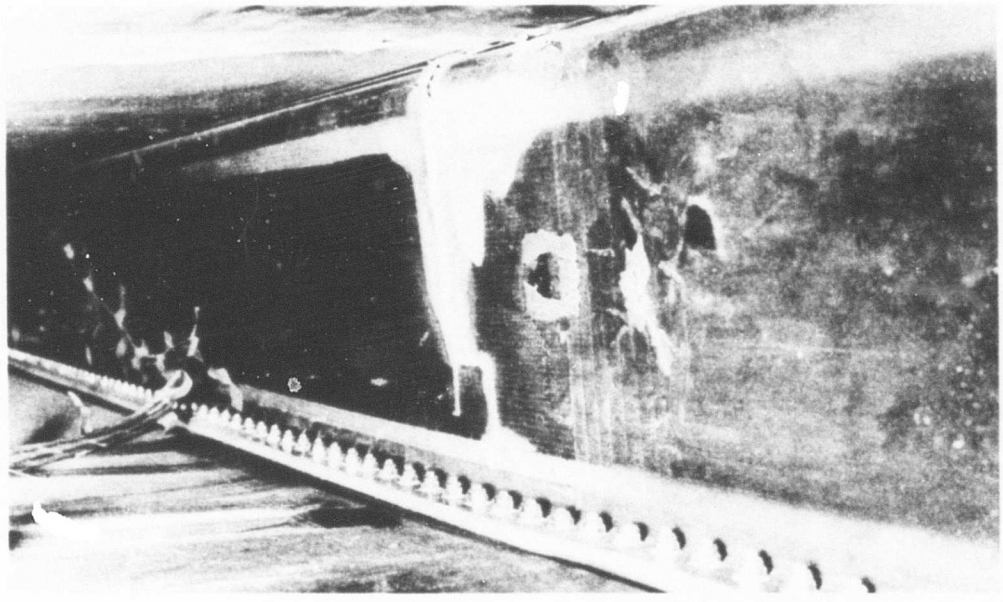

Figure 41. No. 1 FRP Wing Section - Shear Failure of the Center Spar Viewed Through the Forward Cell.

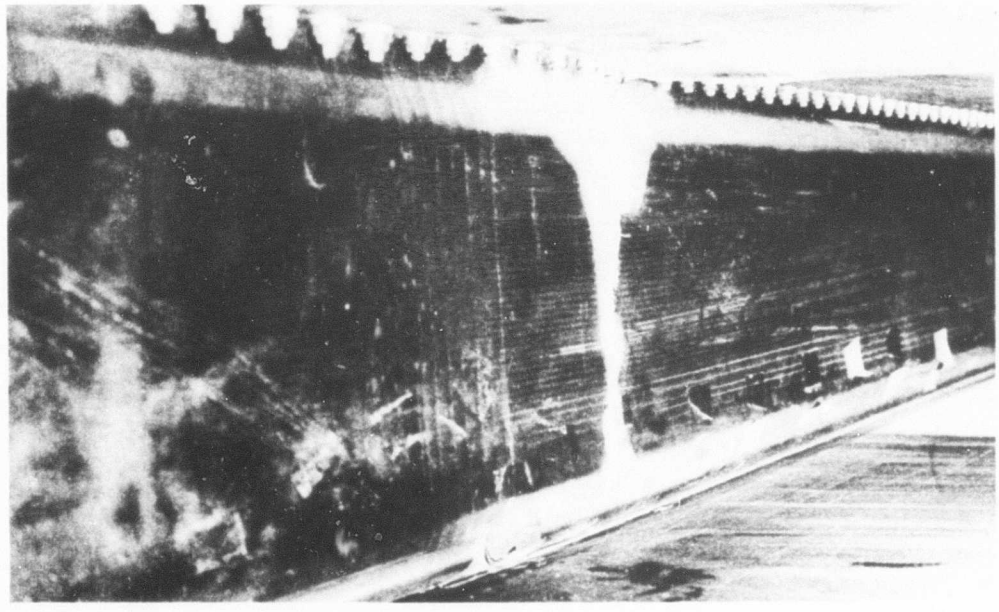

Figure 42. No. 1 FRP Wing Section - Shear Failure of the Center Spar Viewed Through the Aft Cell.

center spar occurred about 3.5 inches outboard of the reinforced area (BL 65.5). Failure of the rear spar is shown in Figure 43. Failure occurred about 6.0 inches outboard of the reinforced area (BL 63.0).

As stated in the Navy report[5] and in the section discussing the torque box tests, cracking noises emanated from the structures as loads were increased during the wing tests and the torque box tests. Occurrences of this nature are not unusual in a composite structure as stress levels become high. However, with the structures tested in this program, the cracking sounds initiated when skin stresses were relatively low and the cracking was more pronounced than had been anticipated.

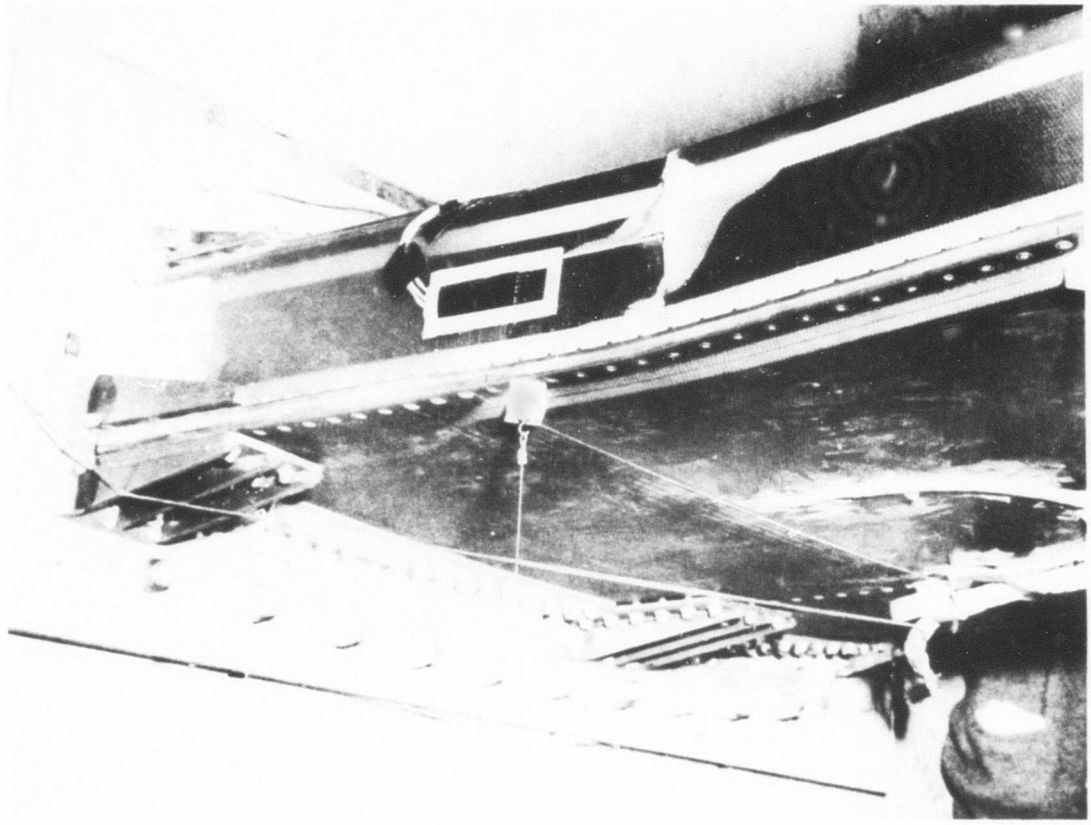

Figure 43. No. 1 FRP Wing Section - Shear Failure of the Rear Spar.

Two sets of sandwich tensile test specimens were fabricated and tested at GAC in an effort to verify a theory regarding the possible cause for the more pronounced cracking noises. One set of sandwich specimens was designed to simulate a section of the field of the wing's lower surface panel. A second, similar set was designed to simulate the syntactic foam-filled sandwich construction used at the panel edges. Test results for these specimens are shown as load deformation curves in Figures 44 and 45. The cracking noises made by the foam-filled specimens were first

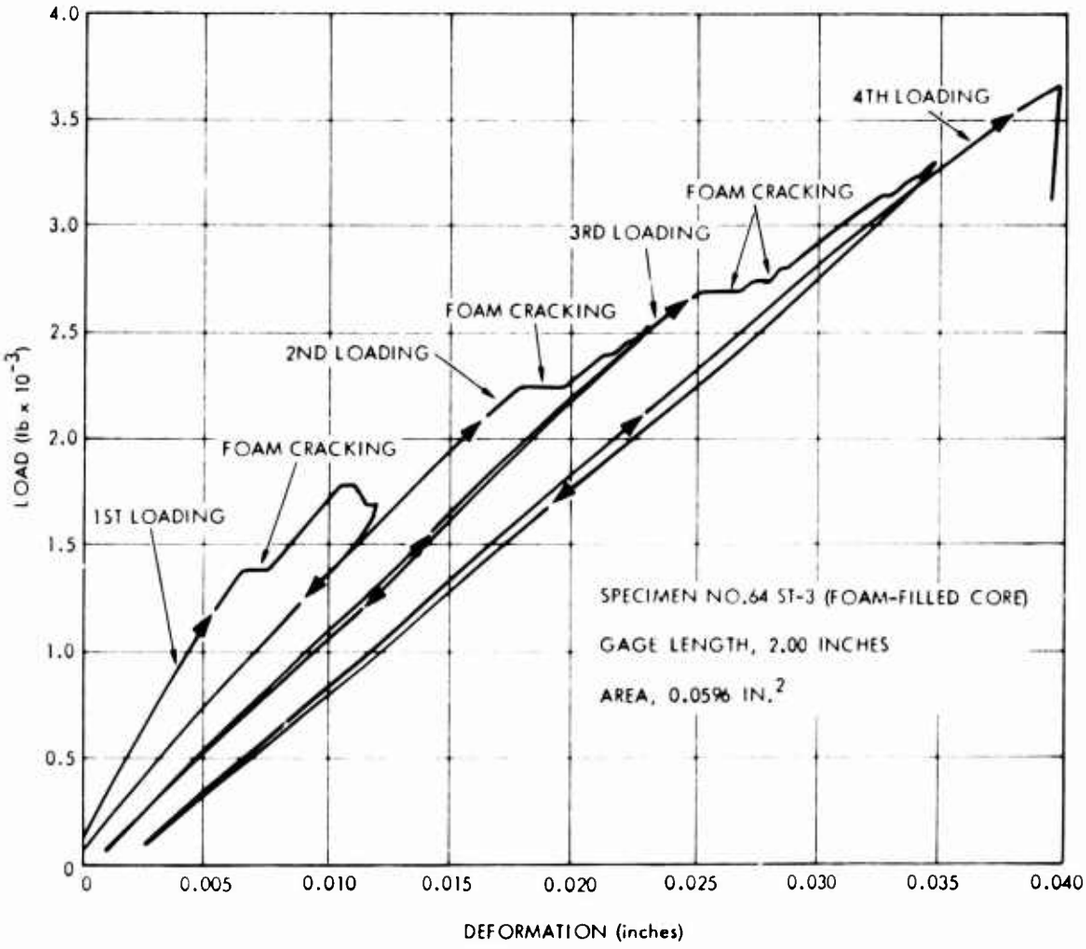

Figure 44. Load Deformation Curve for a Sandwich Tensile Specimen With a Foam-Filled Core.

heard at approximately 40 percent of the failing load. Abrupt elongations were traced on the extensometer curves coincident with the cracking noises (see Figure 44). On subsequent loading cycles, the cracking did not occur again until the maximum load of the previous cycle had been exceeded. The specimen without foam core filler emitted only slight cracking noises just prior to reaching tensile ultimate load. A strong similarity exists between the behavior of the foam-filled specimens and the wing test section. It is concluded that the majority of cracking sounds heard during the torque box and wing section tests emanated from the failing syntactic foam.

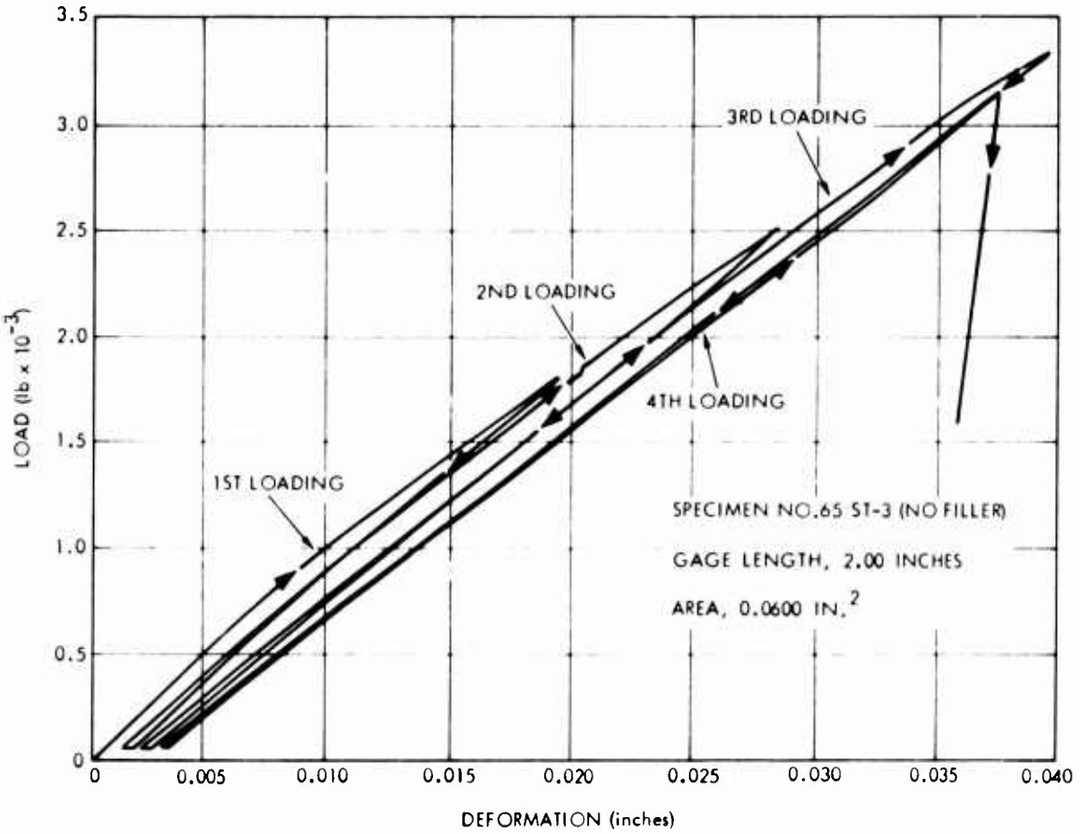

Figure 45. Load Deformation Curve for a Sandwich Tensile Specimen Without a Foam-Filled Core.

Static Test Data Reduction

The GAC computer program for interpretation of three strain gage rosettes was used to reduce the data obtained in all the static load tests from the 16 rosettes located as shown in Figure 29. The elastic properties used in obtaining stressed areas follow:

1. A shear modulus of 0.7×10^6 psi.
2. A major Poisson's ratio of 0.12.
3. A spanwise proportional limit tensile stress of 13,800 psi.
4. A spanwise primary tensile modulus of elasticity of 3.65×10^6 psi.
5. A spanwise secondary tensile modulus of elasticity of 2.68×10^6 psi.
6. A chordwise modulus of elasticity in tension of 3.47×10^6 psi.
7. A spanwise modulus of elasticity in compression of 3.72×10^6 psi.
8. A chordwise modulus of elasticity in compression of 3.58×10^6 psi.

The values of items 4 through 8 were determined from small-specimen tests performed at GAC.

Outputs from the program include stresses and strains related to the wing major axes, principal stresses, principal strains, and directions of the principal stresses and strains with respect to the wing axes. Typical data sheets developed in the program are shown in Figures 46 and 47. Data of particular interest were also plotted by the Calcomp Plotter. A typical graph is shown in Figure 48. A greater use of this facility will be made to reduce time in data reduction and presentation after the static tests for the second wing specimen.

EASIC REDUCTION OF STRAIN ROSETTE READINGS ON NON-ISOTROPIC MATERIALS

ROSETTE NO. 3

BENDING TEST 30% ULTIMATE LOAD LOAD INCREMENTS 1 (1) TO 30 (7)

BENDING TEST 70% ULTIMATE LOAD LOAD INCREMENTS 31 (7) TO 36 (13)

%LOAD	0	10	20	30	20	10	0	10	20	30
EPS1	-5018.	-1142.	-2164.	-3307.	-2274.	-1182.	0.	-1182.	-2164.	-3207.
EPS2	-40.	-481.	-942.	-1423.	-942.	-481.	-0.	-481.	-942.	-1463.
EPS3	-80.	-561.	-1082.	-1603.	-1142.	-521.	-0.	-541.	-1082.	-1643.
EPSX	-5018.	-1142.	-2164.	-3307.	-2274.	-1182.	0.	-1182.	-2164.	-3207.
EPSY	4858.	80.	140.	221.	120.	60.	-14.	100.	120.	161.
GAMXY	-40.	-100.	-140.	-240.	-200.	-140.	-20.	-80.	-120.	-180.
SIGX	-16854.	-4274.	-8103.	-12379.	-8262.	-4357.	-61.	-4159.	-8111.	-12254.
SIGY	15110.	-267.	-434.	-638.	-525.	-288.	-506.	-126.	-507.	-839.
TAUXY	-28.	-70.	-98.	-168.	-140.	-98.	-14.	-42.	-84.	-126.
EPSMAX	4898.	82.	142.	225.	124.	64.	1.	101.	122.	163.
EPSMIN	-5018.	-1144.	-2166.	-3311.	-2268.	-1166.	-141.	-1123.	-2166.	-3269.
GAMMAX	4958.	615.	1154.	1768.	1166.	615.	71.	612.	1144.	1716.
SIGMAX	15110.	-266.	-433.	-636.	-522.	-286.	-61.	-125.	-506.	-837.
SIGMIN	-16854.	-4274.	-8103.	-12381.	-8264.	-4360.	-509.	-4189.	-8112.	-12255.
TAUMAX	15982.	2034.	3835.	5873.	3871.	2037.	224.	2332.	3813.	5709.
THETP	90.12	92.34	91.74	91.95	92.46	93.27	179.53	91.41	91.53	91.53
THETPF	90.05	90.99	90.73	90.82	91.04	91.38	179.21	90.59	90.63	90.63

Figure 46. Typical Data Sheet for Reduction of Strain Rosette Readings for 30 and 70 Percent DUL.

BASIC REDUCTION OF STRAIN ROSETTE READINGS ON NON-ISOTROPIC MATERIALS

ROSETTE NO. 3

BENDING TEST — 70% ULTIMATE LOAD — LOAD INCREMENT 40 (1) 10 ( )

XLCAL	40	50	60	70	50	30	20	10	0
EPS1	-4329.	-5411.	-6593.	-7686.	-5711.	-3527.	-2384.	-1442.	-80.
EPS2	-1884.	-2345.	-2826.	-3347.	-2365.	-1403.	-902.	-421.	40.
EPS3	-2204.	-2826.	-3527.	-4349.	-3206.	-1984.	-1403.	-782.	-200.
EPSX	-4329.	-5411.	-6593.	-7886.	-5711.	-3527.	-2365.	-1442.	-80.
EPSY	241.	240.	240.	160.	140.	140.	60.	39.	-80.
GAMXY	-320.	-481.	-701.	-1002.	-841.	-581.	-501.	-361.	-240.
SIGX	-16225.	-20307.	-24765.	-29569.	-21484.	-13244.	-6895.	-4668.	-317.
SIGY	-1011.	-1486.	-2001.	-2942.	-1980.	-1028.	-612.	-399.	-325.
TAUXY	-224.	-337.	-491.	-701.	-589.	-407.	-351.	-253.	-168.
EPSMAX	247.	250.	258.	191.	177.	163.	86.	64.	40.
EPSMIN	-4333.	-5421.	-6611.	-7887.	-5741.	-3550.	-2391.	-1267.	-200.
GAMMAX	2291.	2836.	3434.	4078.	2956.	1856.	1293.	665.	160.
SIGMAX	-1008.	-1480.	-1990.	-2823.	-1902.	-1015.	-791.	-385.	-133.
SIGMIN	-16228.	-20313.	-24777.	-29584.	-21500.	-13257.	-8910.	-4693.	-449.
TAUMAX	7610.	9417.	11393.	13380.	9709.	6121.	4057.	2149.	168.
THETP	92.00	92.43	92.93	93.76	94.09	94.70	95.94	97.81	135.00
THETPP	90.84	91.02	91.2	91.50	91.73	91.90	92.48	93.35	134.53

Figure 47. Typical Data Sheet for Reduction of Strain Rosette Readings for 70 Percent DUL.

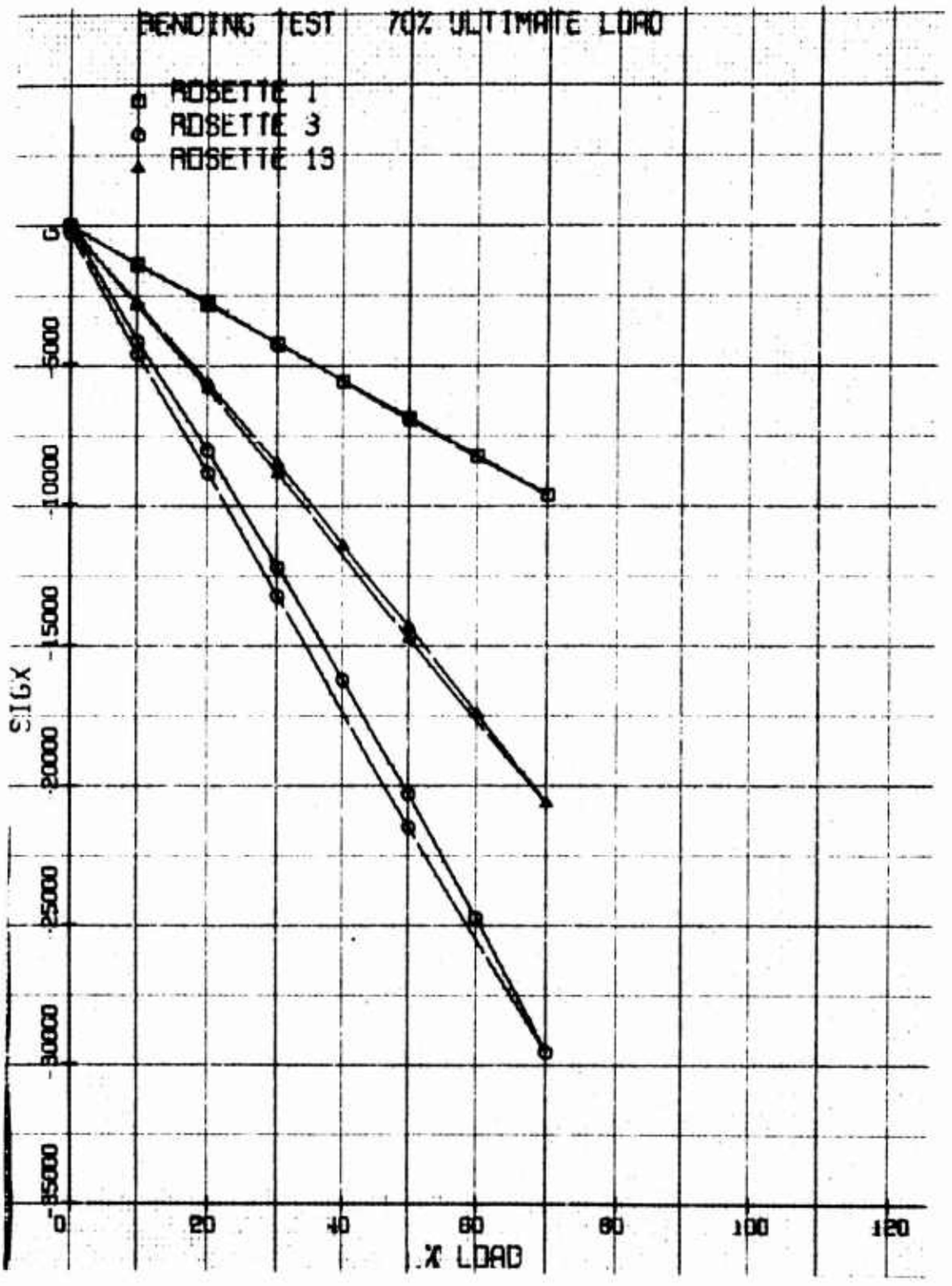

Figure 48. Typical Calcomp Plotter Graph.

For the bending stresses, strain rosettes were located at BL 28, BL 51, and BL 68, at the midpoint of each skin panel (lower aft, lower forward, upper aft, and upper forward). Standard strain gages, reading strain in the span direction, were located on the upper and lower spar caps of the center spar at BL 28 and BL 68. Using the computer data, actual stresses were plotted as a function of the percent DUL. The calculated stress curves are also plotted to show the relation of calculated to actual stresses. The basic bending stress data are plotted in Figures 49 through 57. Figures 49 through 52 are for skin bending stresses, Figures 53 through 56 are for spar cap axial stresses, and Figure 57 shows the relation of spanwise bending stress to chordwise bending stress at one point of the wing.

A comparison of the calculated stresses and actual stresses obtained from strain gage test data can also be obtained by inspection of Figures 49 through 57. Visual inspection during test indicated that the aft upper skin panel became unstable at approximately 40 percent DUL. Figure 50 supports this analysis, as the slope of the stress curve begins decreasing at approximately 40 percent DUL. This decrease becomes larger as the load is increased. This is most evident at BL 68 and is also evident at BL 51. Figure 49 shows a corresponding increase in the slope of the stress curve for the upper, forward skin panel. However, this increase in slope is not as great as the decrease in slope for the upper aft panel.

The upper skin stress plots show that, in general, the forward box skin was somewhat more highly stressed than the calculations indicated, while the aft box skin had somewhat lower stresses than calculated. This appears to be practical because of the unstable tendency of the aft box upper skin.

Inspection of the stress curves in Figures 51 and 52 for the lower skin panels shows that the measured stresses at BL 28 and BL 51 were lower than calculated, whereas good agreement was obtained between calculated and experimental stress levels at the root section, BL 68. Inspection of the stress curves in Figures 53 and 55 of the upper center spar cap shows that the measured stresses were considerably less than the calculated stresses at BL 68. The same comparison results for the lower center spar cap, although in this case the slope of the measured stress increased with the loading (see Figures 54 and 56).

Inspection of Figure 57 reveals that considerable transverse skin stress was measured in the aft panel, upper skin. This was the unstable panel. A transverse stress of 5000 psi was measured, while the longitudinal stress was 20,000 psi at 70 percent DUL.

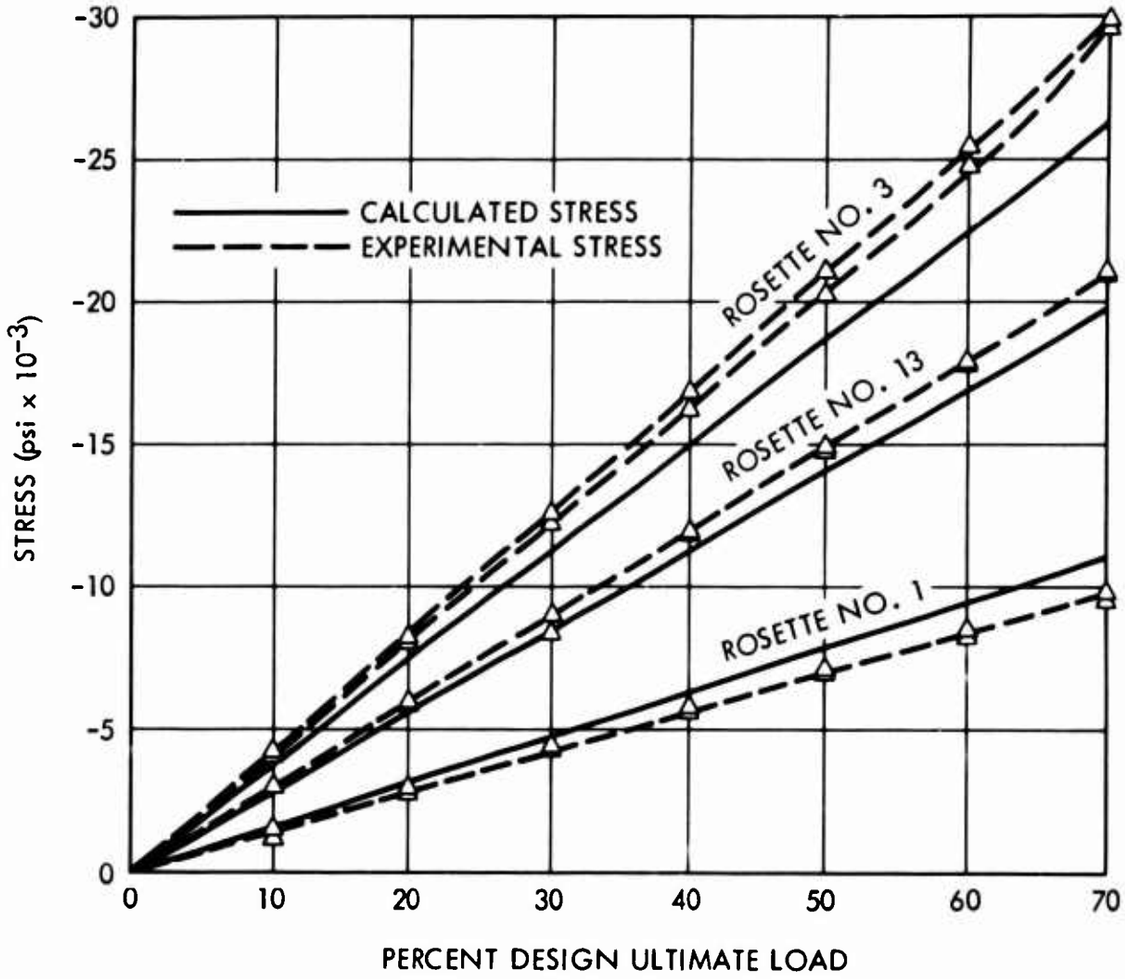

Figure 49. Comparison of Calculated and Experimental Stresses in the Top Skin of the Forward Panel for 70 Percent DUL in Bending, 70 Percent in Bending Plus Torsion, and Failing Load Tests.

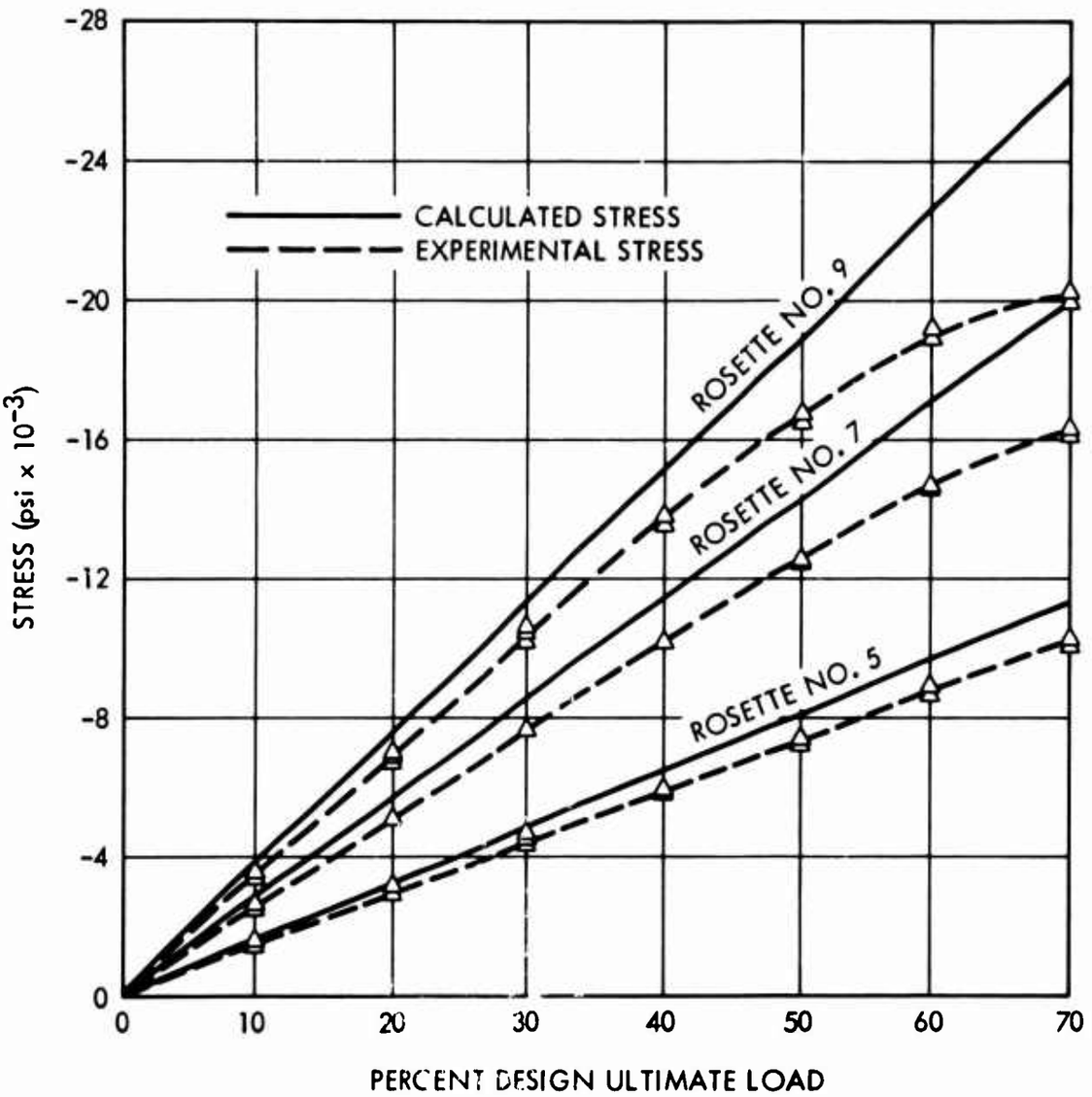

Figure 50. Comparison of Calculated and Experimental Stresses in the Top Skin of the Aft Panel for 70 Percent DUL in Bending, 70 Percent in Bending Plus Torsion, and Failing Load Tests.

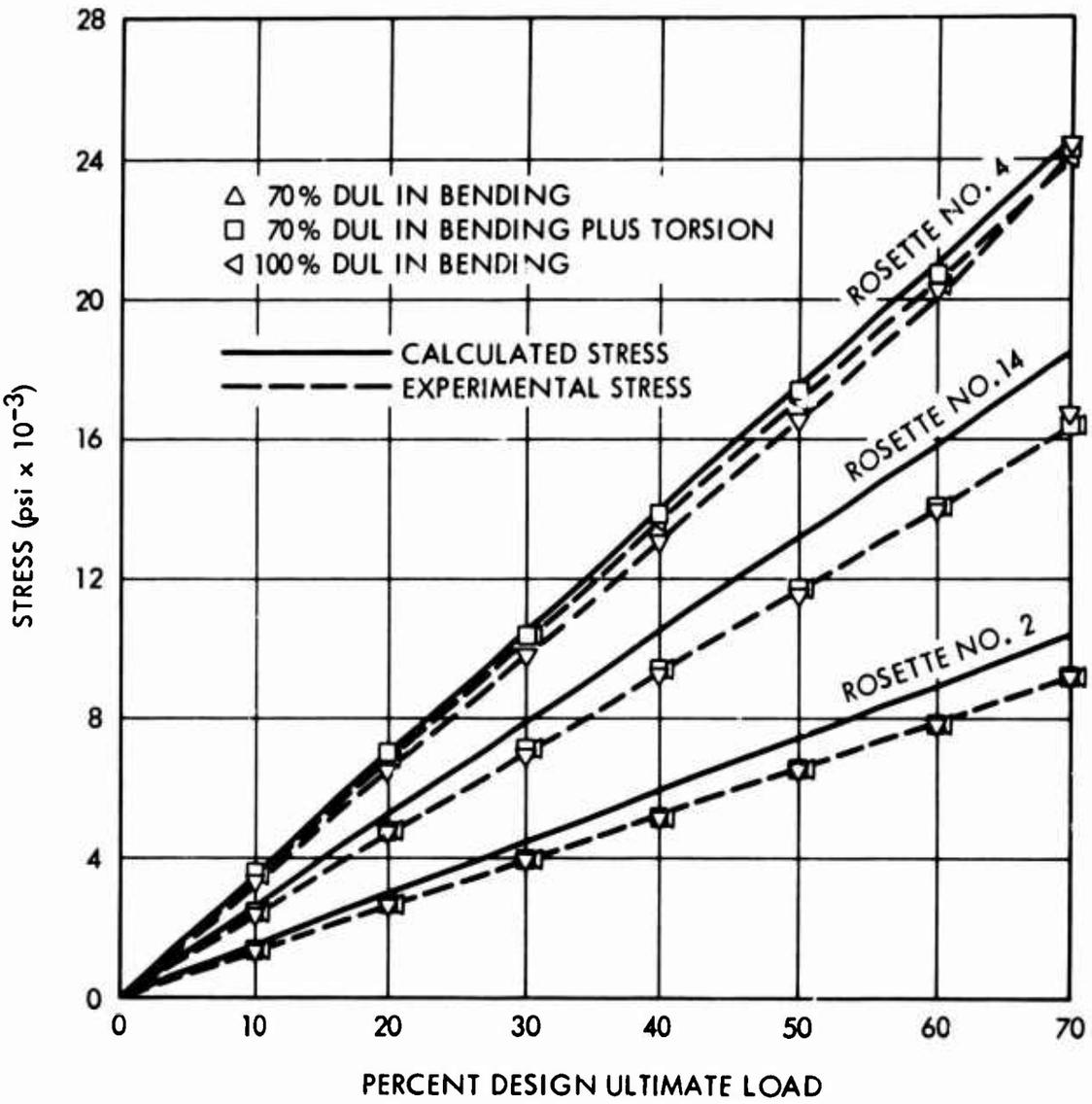

Figure 51. Comparison of Calculated and Experimental Stresses in the Lower Skin of the Forward Panel.

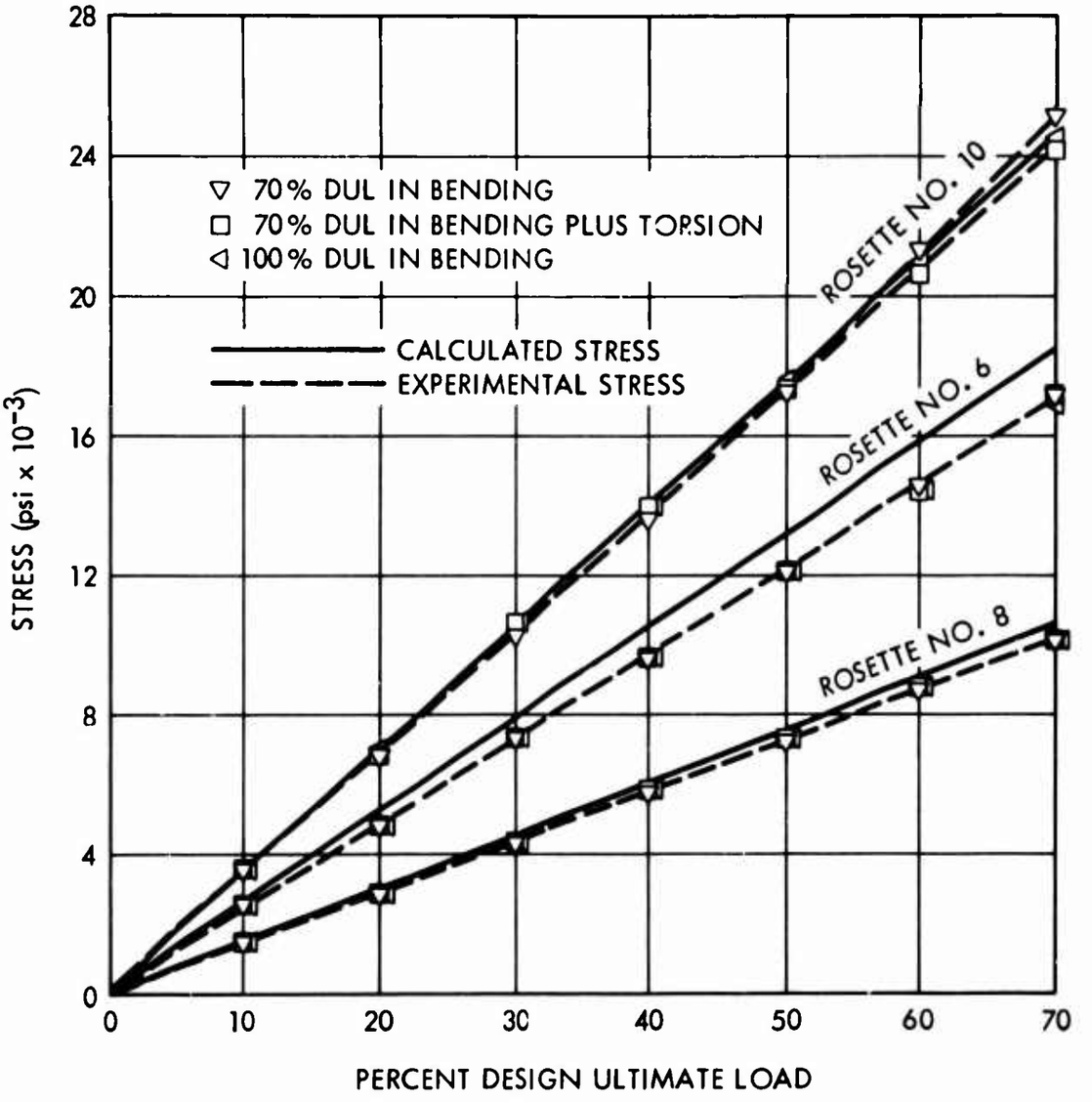

Figure 52. Comparison of Calculated and Experimental Stresses in the Lower Skin of the Aft Panel.

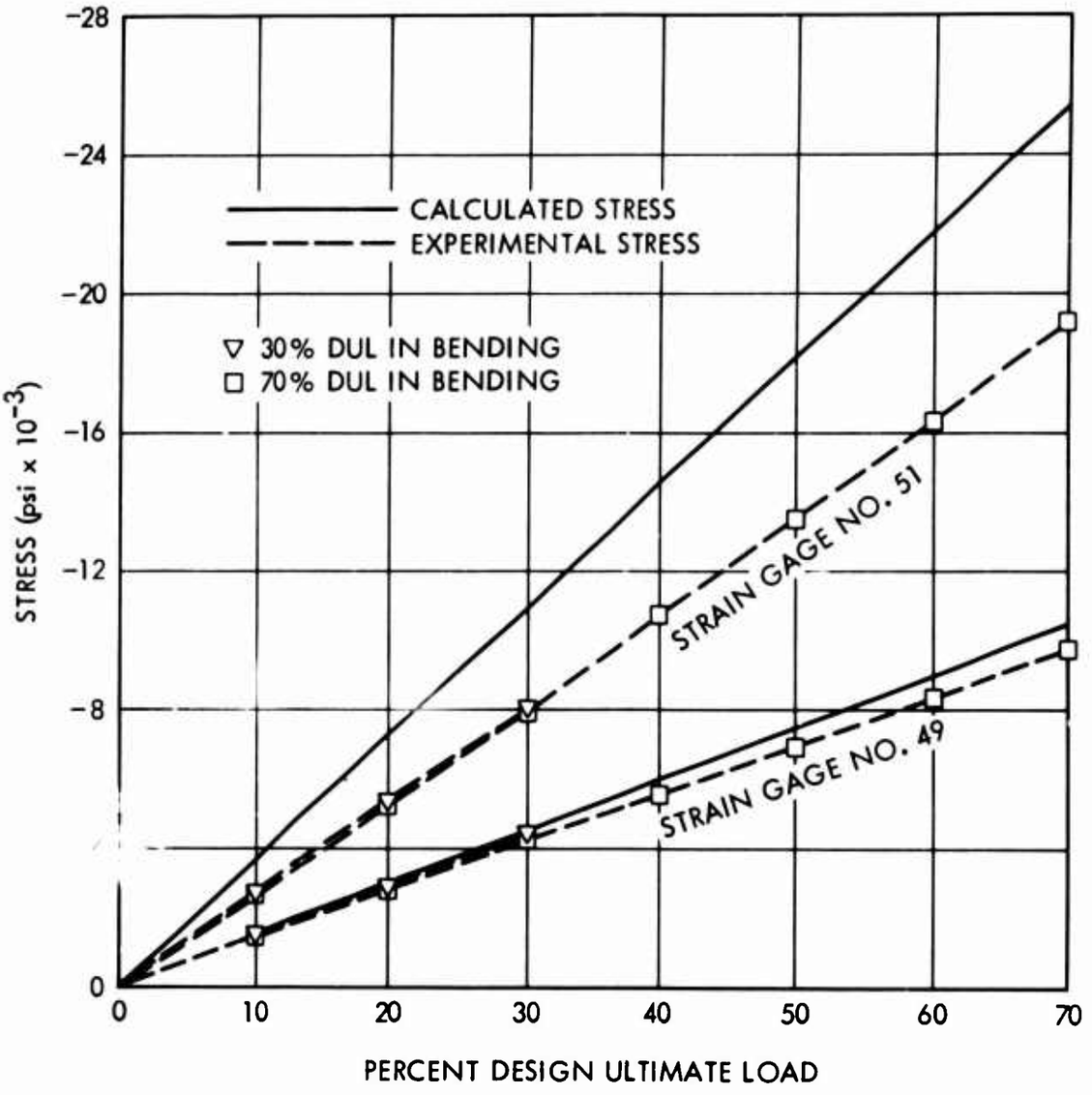

Figure 53. Spar Cap Stresses for Strain Gages 49 and 51.

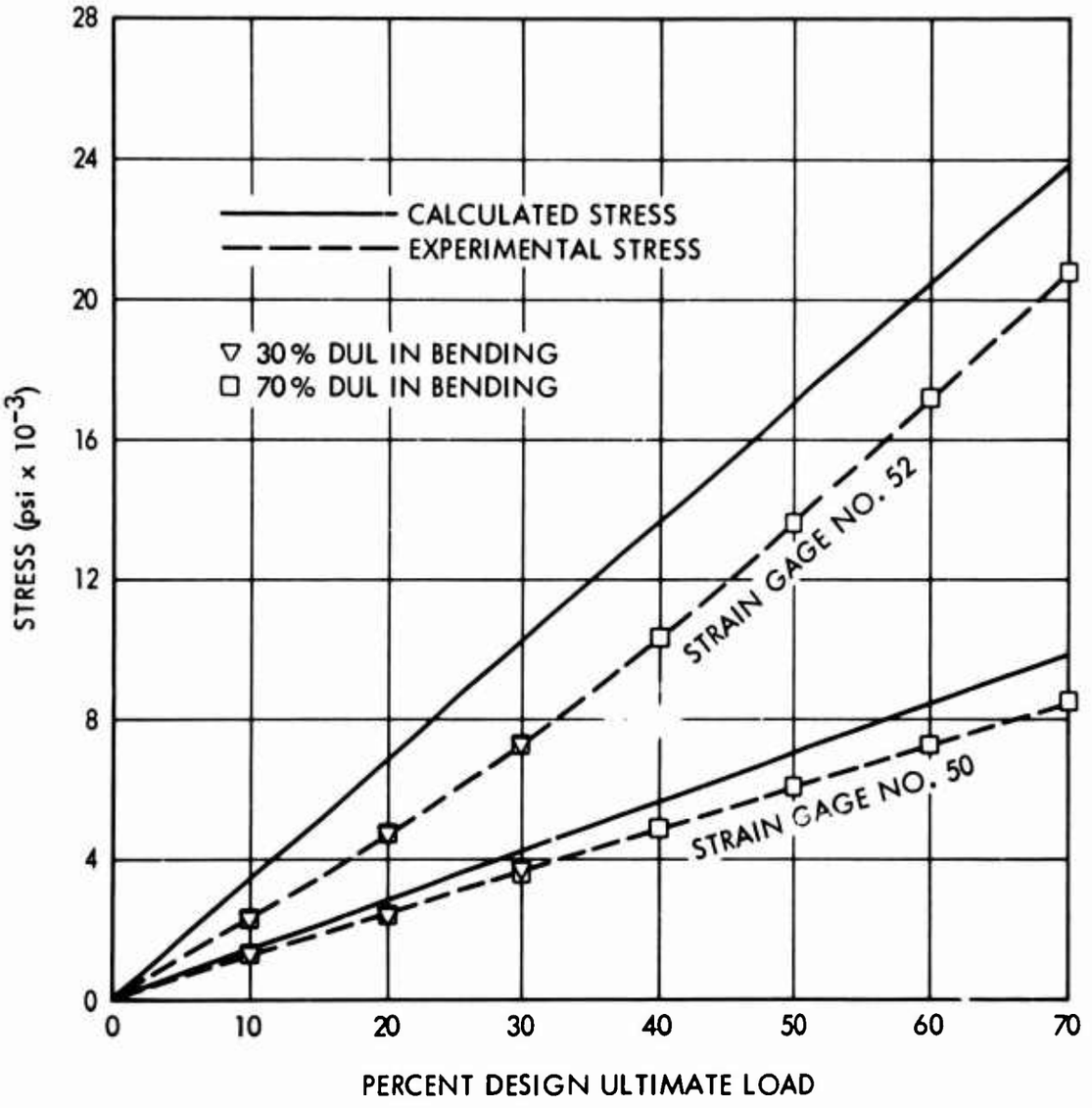

Figure 54. Spar Cap Stresses for Strain Gages 50 and 52.

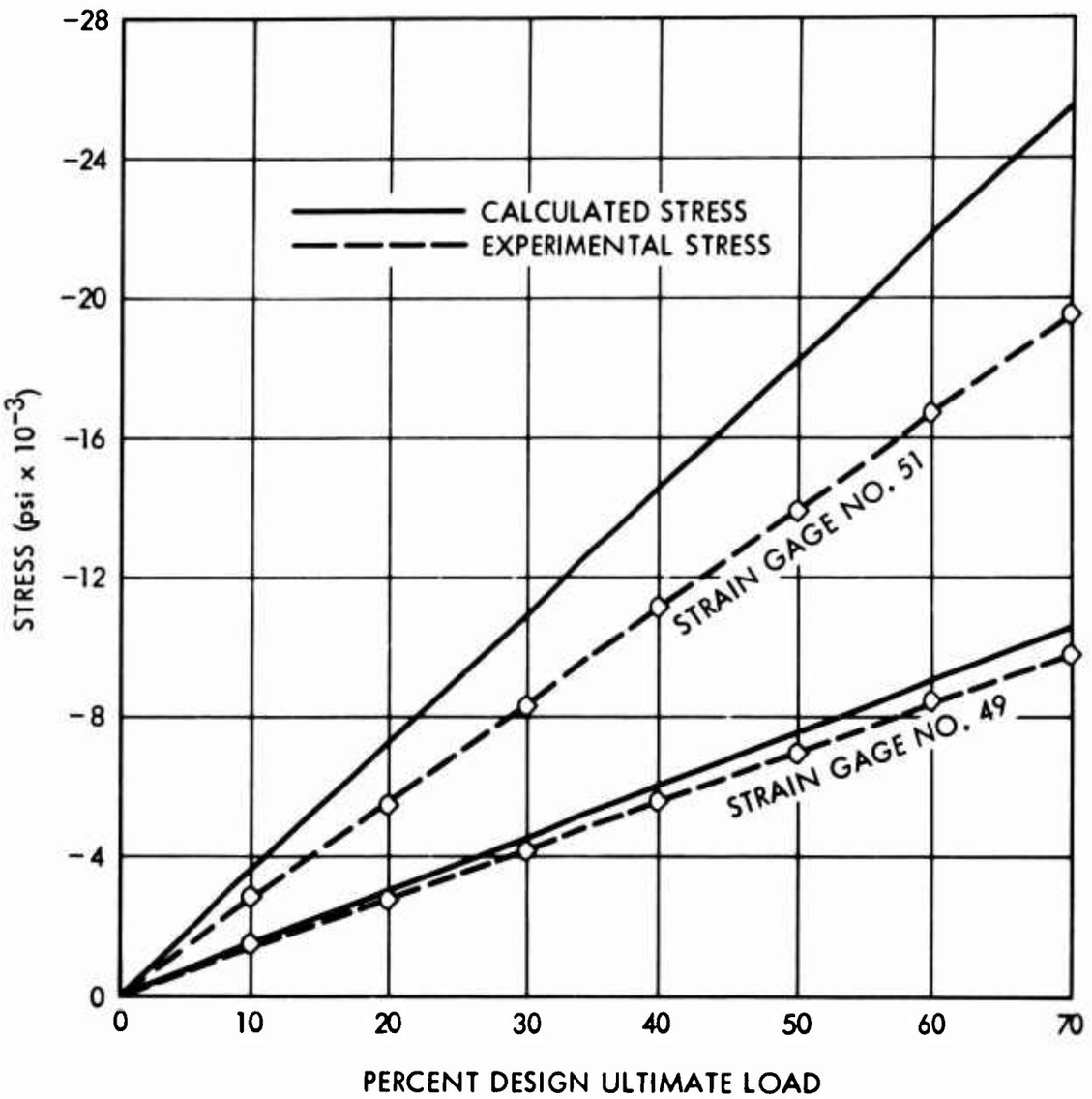

Figure 55. Spar Cap Bending Stresses During Failing Load Testing for Strain Gages 49 and 51.

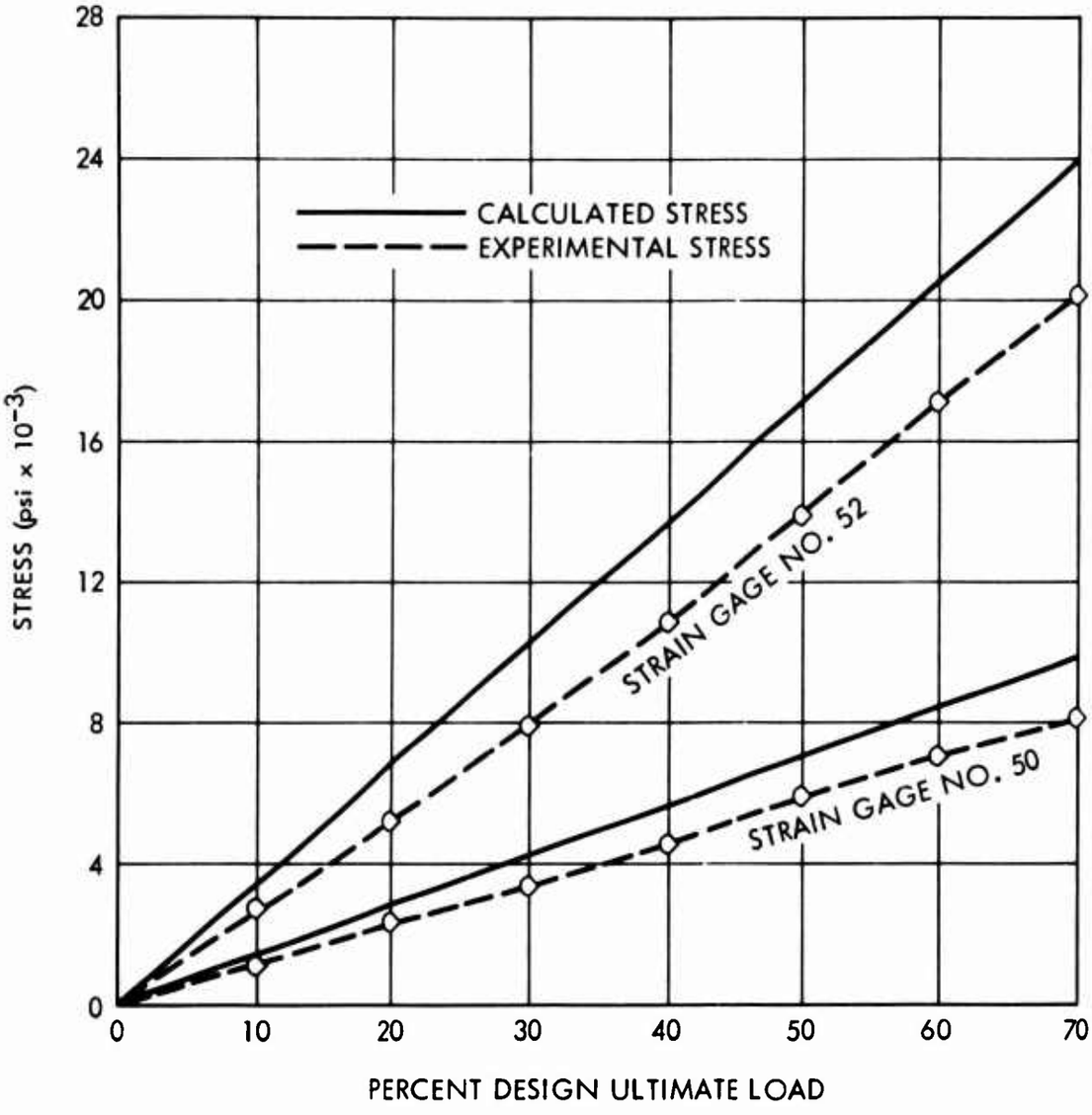

Figure 56. Spar Cap Stresses During Failing Load Testing for Strain Gages 50 and 52.

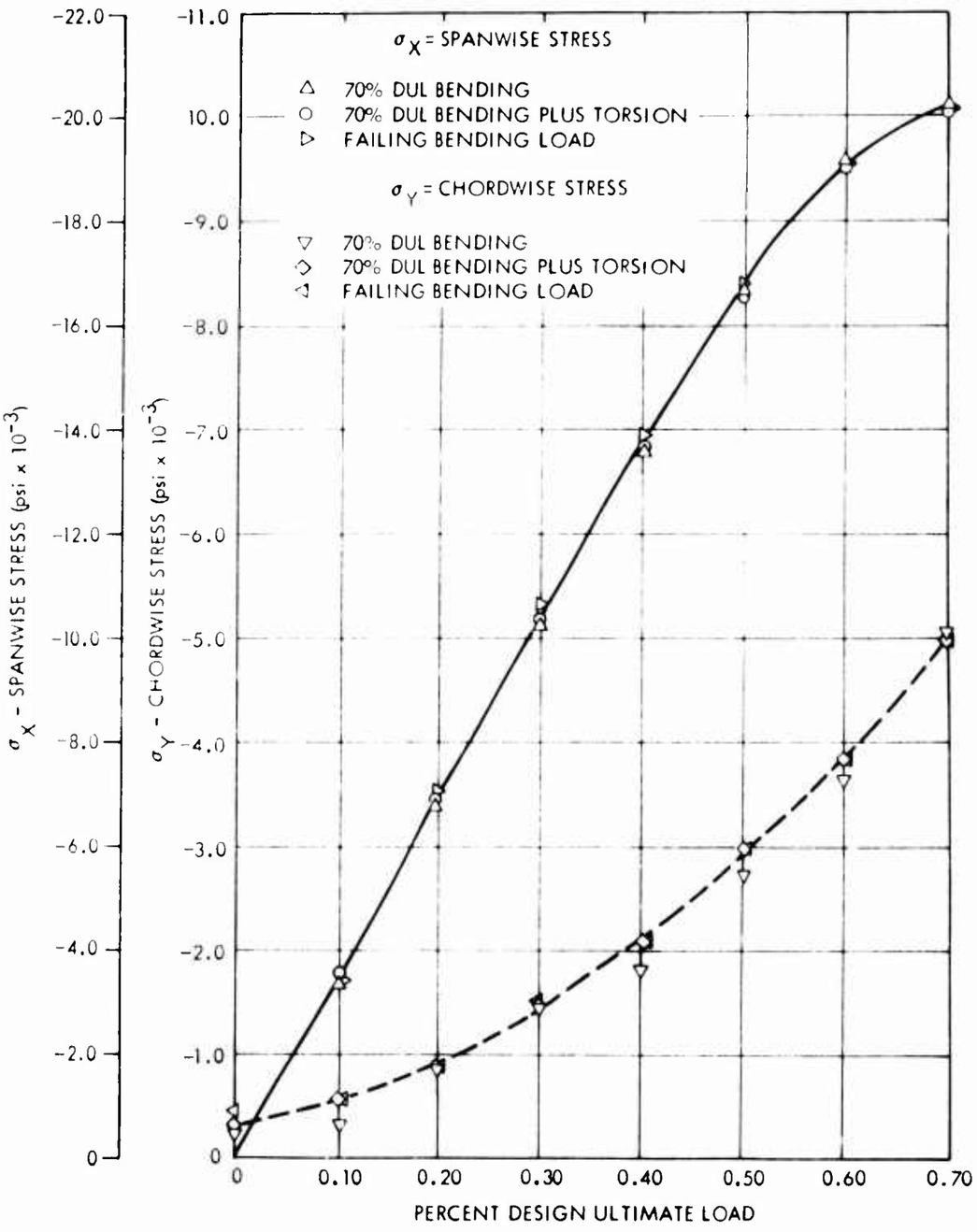

Figure 57. Stresses at Midpoint of Aft Upper Panel and 1.0 Inch Outboard of Reinforcing Plies at Root.

It has been concluded that the comparison of the calculated and measured strain was fairly reasonable considering the problem with instability, which undoubtedly affected the stress distribution. In general, the measured stresses were somewhat less than the calculated stresses, particularly for the spar caps. This may be partly explained by the additional bending section provided by foam-filled areas of the honeycomb core, but this cannot account for the large discrepancy between calculated and measured strains in the spar caps.

For the torsional stresses, the calculated and measured torsion shear stresses are plotted in Figures 58, 59, and 60 as a function of percent of DUL. The calculated stresses were obtained from the subsection pertaining to GAC development support in this report. The measured stresses were obtained from the computer analysis of the rosette strain gage readings. Single rosette gages were located in the upper forward, upper aft, lower forward, and lower aft skin panels at BL 28, BL 51, and BL 68. In addition, rosettes were located at the center and aft spar centerlines at BL 28 and BL 68.

The mechanics of transforming the strain gage readings into shear stress values involve the input of strain data and shear modulus into the computer analysis. Although shear strain data from the torque box tests described in this report indicated nonlinear stress-strain behavior at relatively low stress levels, an average G value of 700,000 psi was used in the computer analysis.

Figure 58 presents the shear comparison of calculated and measured stresses for the skins at the tip section BL 28. Figure 59 presents the shear comparison at the root section BL 68. Curves for the intermediate section BL 51 are not presented, since the measured stresses are equivalent to those measured at the tip section. Included on the two curves is a comparison of measured stresses using a G value of 810,000 psi instead of 700,000 psi. These values were computed only for the 100 percent load points.

An inspection of Figure 58 shows the measured stresses to be generally less than the calculated stresses, with a decreasing differential at the higher stress levels. If the higher G value were used at all stress levels, the measured curve would generally be higher than the calculated curve. It is believed that use of the actual shear stress-strain curve in the computer data reduction program would result in a test curve which would more closely follow the calculated straight-line curve.

Inspection of the skin torsional shear stresses at the root section BL 68 indicates the same basic results except that the differential between the

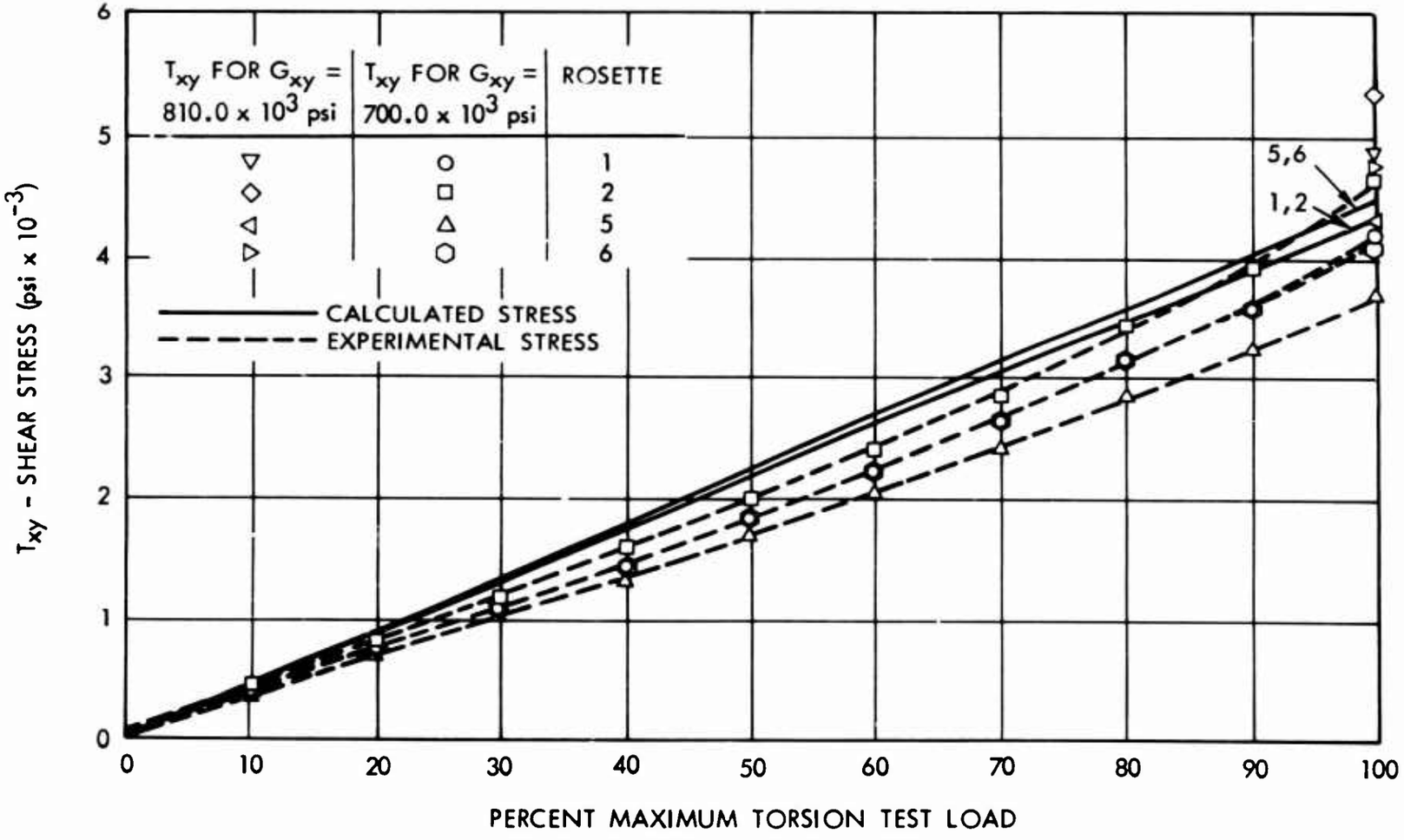

Figure 58. Shear Stresses at the Tip Section for the Pure Torque Test.

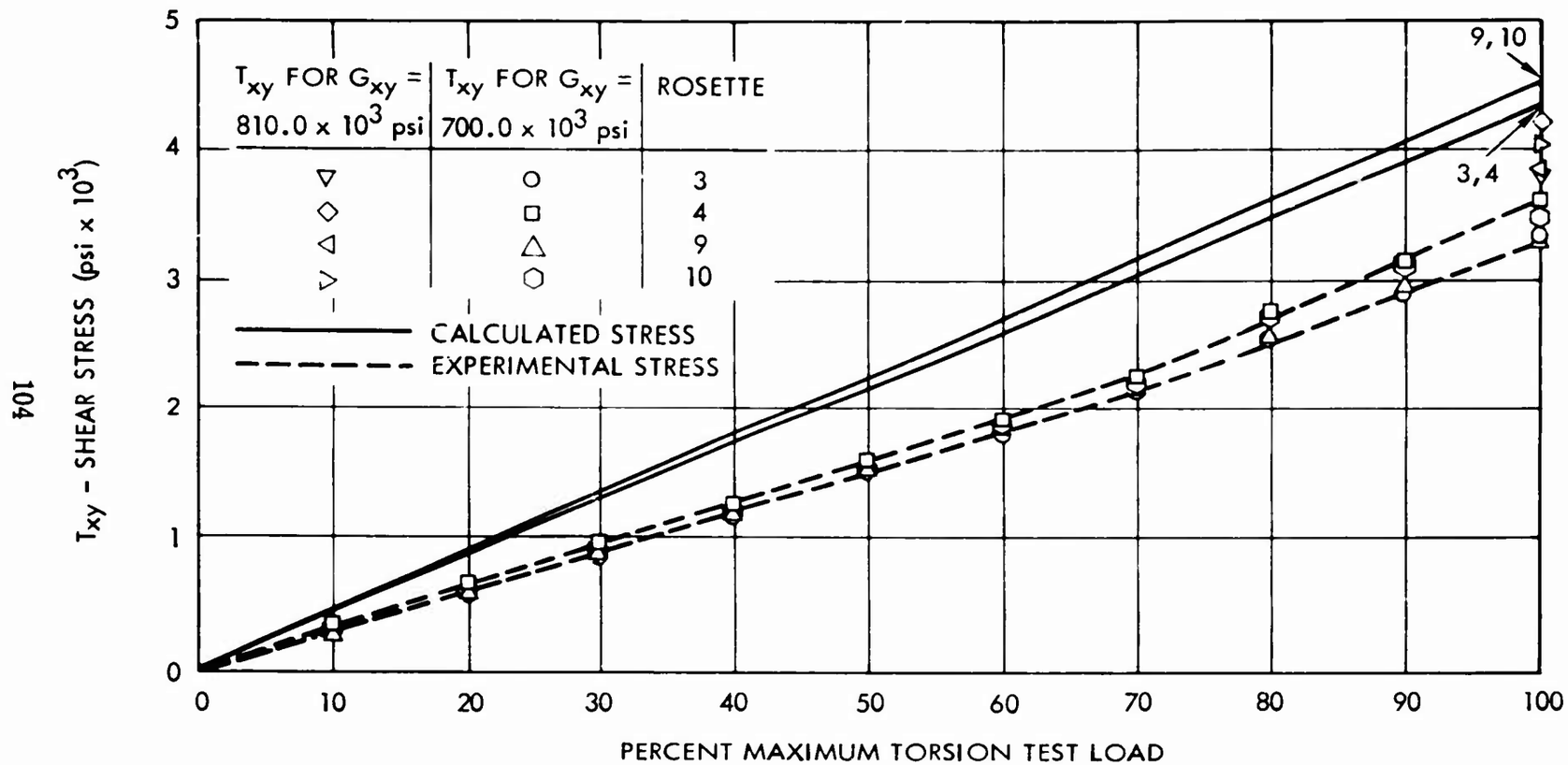

Figure 59. Shear Stresses at the Root Section for the Pure Torque Test.

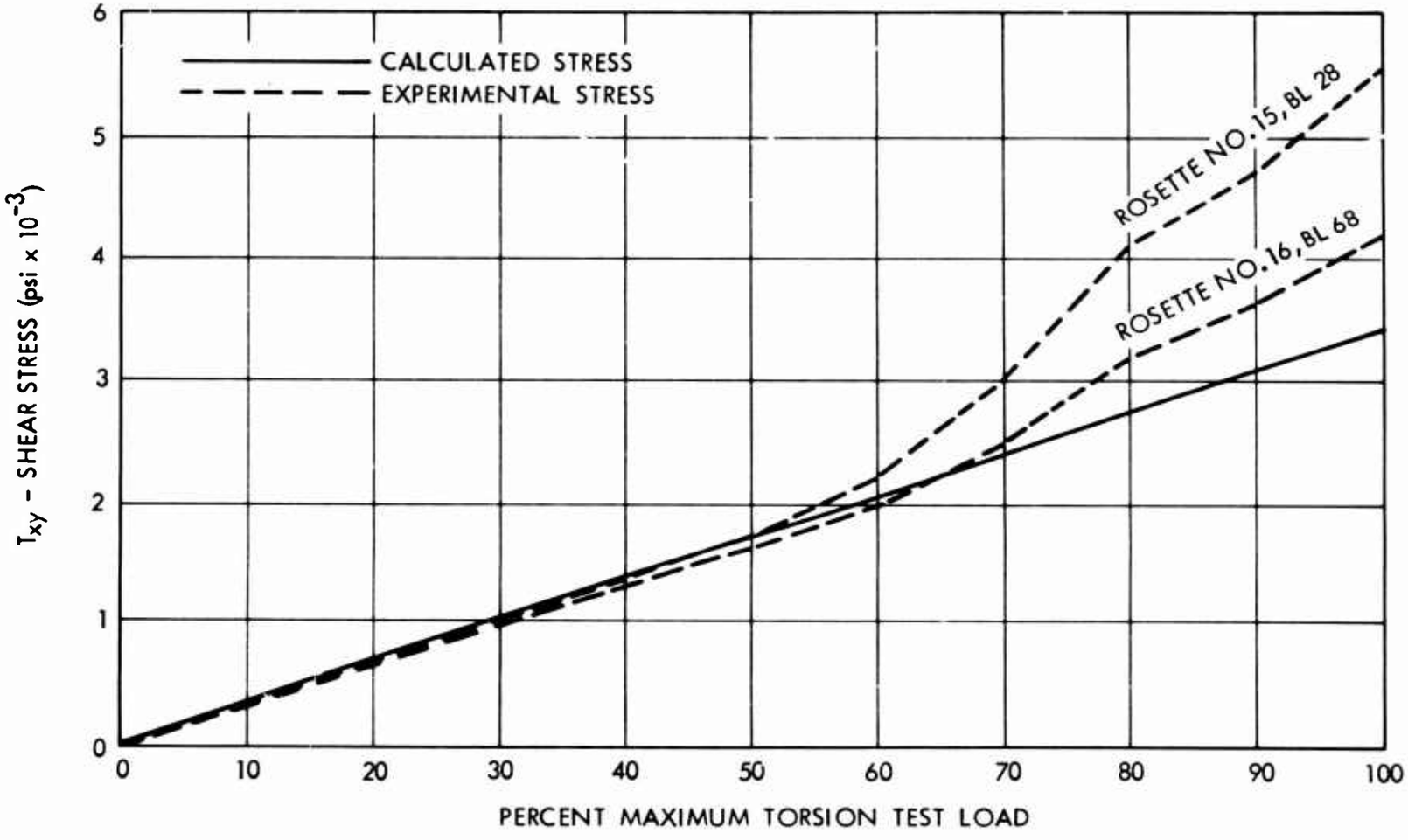

Figure 60. Shear Stresses at the Aft Spar for the Pure Torque Test.

measured and the calculated shear stresses is more pronounced (see Figure 59). Inspection of the longitudinal stress measurements corresponding to the shear stress measurements shows that the measured longitudinal stresses, although negligible at the tip section, were significant at the root section. At 100 percent load, they were approximately equal to the shear stresses, which were in the 3000- to 3500-psi range. This indicates a deviation from pure torsional shear stresses at the root section.

The aft spar, torsional shear curves plotted in Figure 60 show a good correlation between measured and calculated stresses at the lower stress levels at both BL 28 and BL 68. However, at the higher stress levels, the measured stresses become larger than the calculated stresses. As for the skin panels, this is considered to be a characteristic of the variation in G values at different stress levels.

It has been concluded that the major discrepancy between calculated and measured torsional shear stresses is caused by the fact that the slope of the shear stress-strain curve varies with the stress level. Thus, the shear modulus value used in converting strain gage measurements to stresses should be variable and dependent on the stress level. Since G is programmed into the computer analysis as a constant, the measured stresses are computed larger than actual at higher strain levels, where the modulus decreases.

There is some evidence that pure torsional shear is not obtained at BL 68. These gages are located within 1 inch of the end built-up area, which may affect the stress distribution in the area. The gages at BL 28 and BL 51 are located well away from end built-up areas and appear to give better strain measurements. For the second wing test, it has been recommended that a strain rosette be placed on the aft spar centerline at BL 51 to obtain complete data at this BL.

Two phases have been included in the analysis of the bending deflections. The first phase includes a comparison of the calculated deflections and the measured test deflections, and the second is a study of the deflections as a function of load intensity.

The bending deflection calculations have been included in the GAG Development Support section of this report. A number of simplifications were used in these calculations. Actually, the 84-inch wing test section has a 62-inch instrumented test section, exclusive of root and tip reinforcement areas. These reinforced areas were required for mounting the wing at the root and applying loads at the tip. The entire length of the test area section was used in the deflection analysis. This is considered to be conservative. Full fixity was assumed at the root. This is not conservative. Core

and foam areas were not included in the section properties. This is conservative. Thus, actual test deflections can be expected to be slightly less than calculated.

The material properties also affect the deflection calculations. A modulus of elasticity value of 3,500,000 psi and a modulus of rigidity value of 810,000 psi were used. Calculated tip deflection was 4.93 inches at 70 percent DUL.

Test deflections were obtained from potentiometer recordings. The potentiometers were located along the leading and trailing edges of the wing at a number of butt lines (see Figure 33). Test deflections at 70 percent DUL for the No. 1 bending and the No. 4 bending failure tests are plotted on Figure 61, along with the calculated deflection curve.

Inspection of Figure 61 shows that good correlation between calculated and actual test deflections was obtained for the No. 1 test. As was expected, test deflections were approximately 10 percent less than calculated. Good correlation was also obtained between leading-edge and trailing-edge deflections. This indicates that the load was correctly applied at the shear center.

Test No. 4 deflection measurements are more erratic than those for test No. 1. Apparently the intermediate tests had some effect on the wing. The measured deflections were slightly lower than for the first test. However, the more noticeable change is in the difference in deflection between the leading and trailing edges. This indicates that a variable torsional deflection was occurring.

The study of the deflections as a function of the load intensity shows that an increase in the deflection rate occurred at about 45 percent DUL for the No. 1 test. Data for this study are plotted on Figure 62 for test No. 1 and on Figure 63 for test No. 4. Leading- and trailing-edge deflections at BL 6 and BL 20 are plotted as a function of percent of test load.

As was the case in the spanwise deflection plots of Figure 61, good correlation was obtained between the leading-edge and the trailing-edge deflections. However, this was not the case in test No. 4, where torsional deflection is indicated (see Figure 63). This tendency was more pronounced at BL 6 than at BL 20.

The change in the deflection rate shown in Figure 62 may be caused by either initiation of instability at 45 percent of loading or by a reduction in material modulus at this load level. The change in the slope of the No. 4

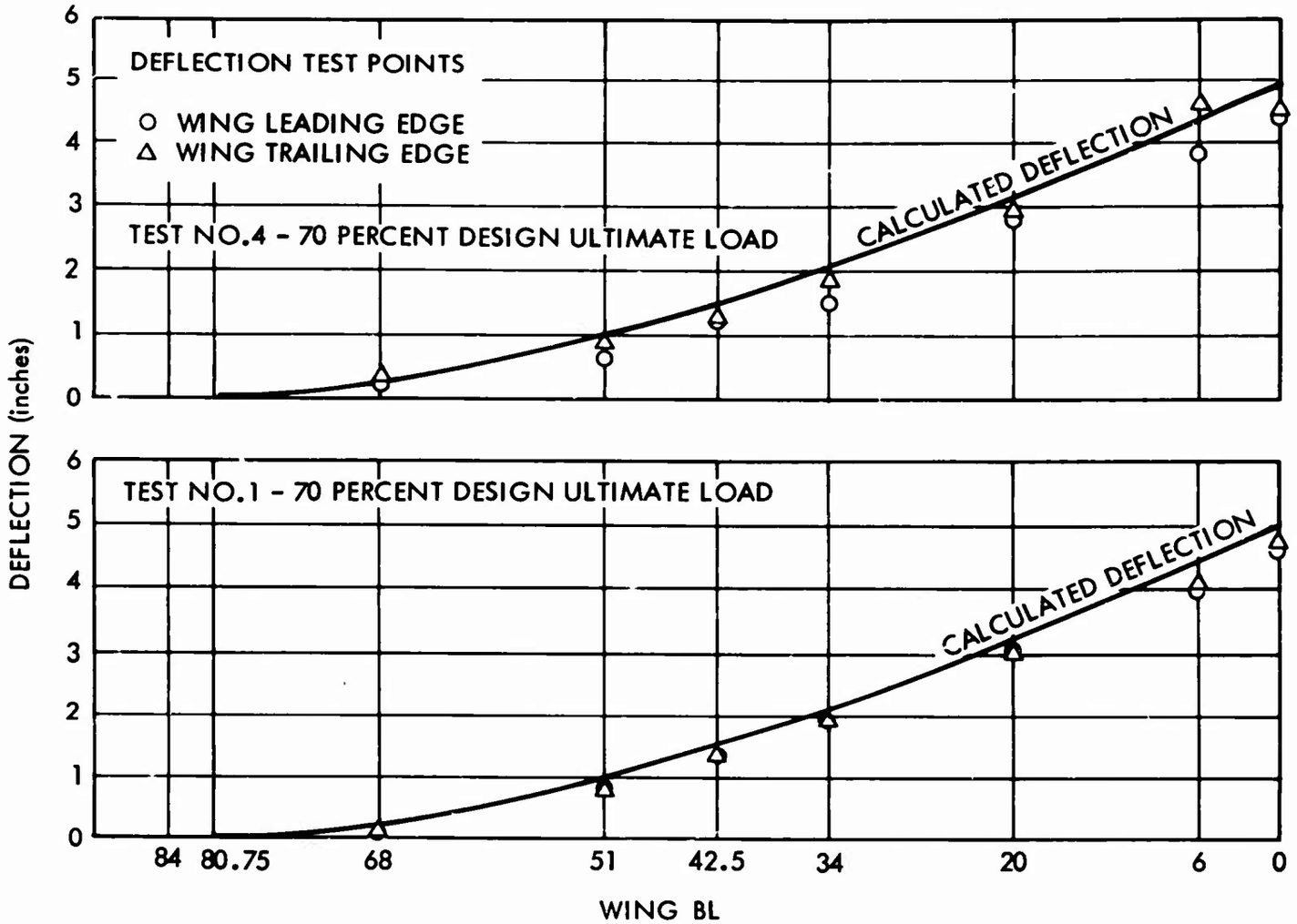

Figure 61. Spanwise Wing Deflection During Bending Tests.

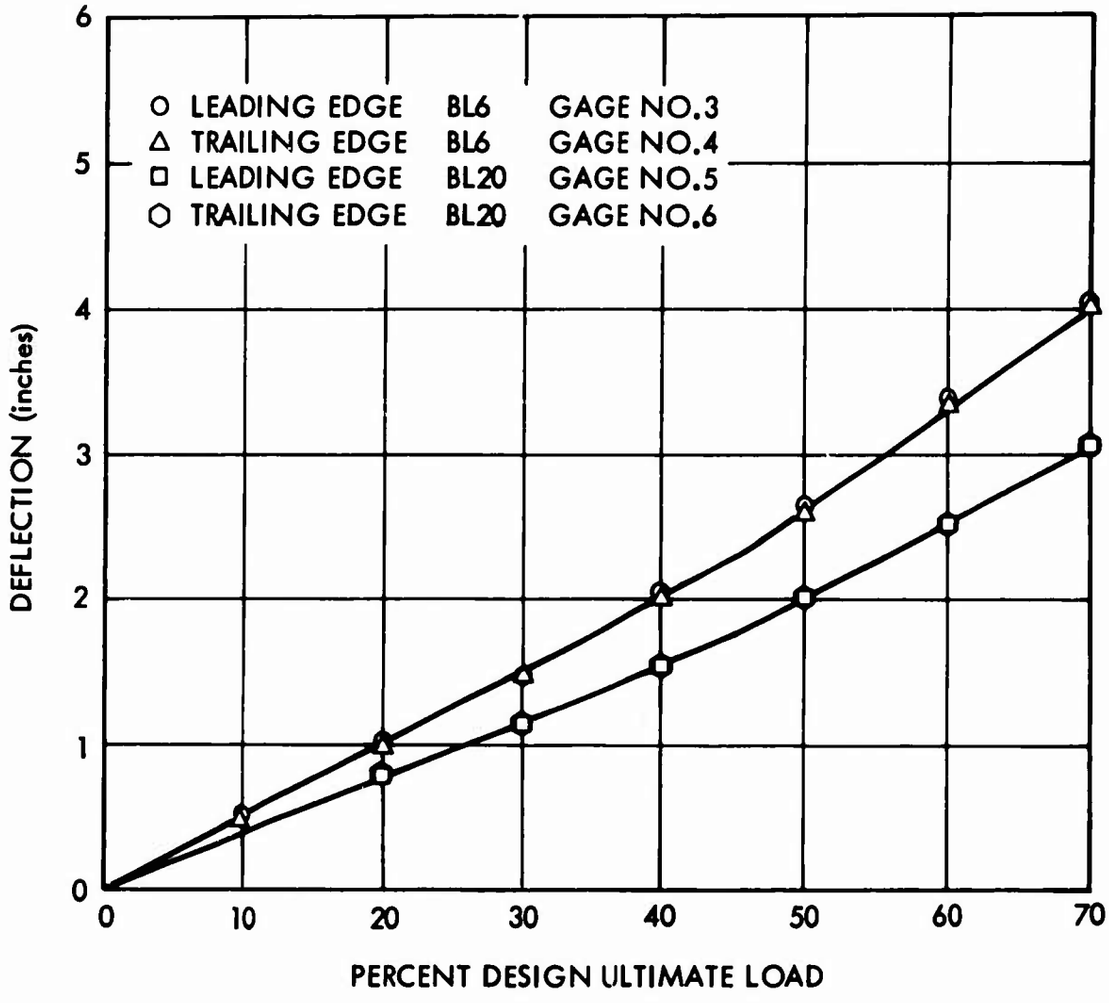

Figure 62. Tip Bending Deflection for Test No. 1 at 70 Percent Bending.

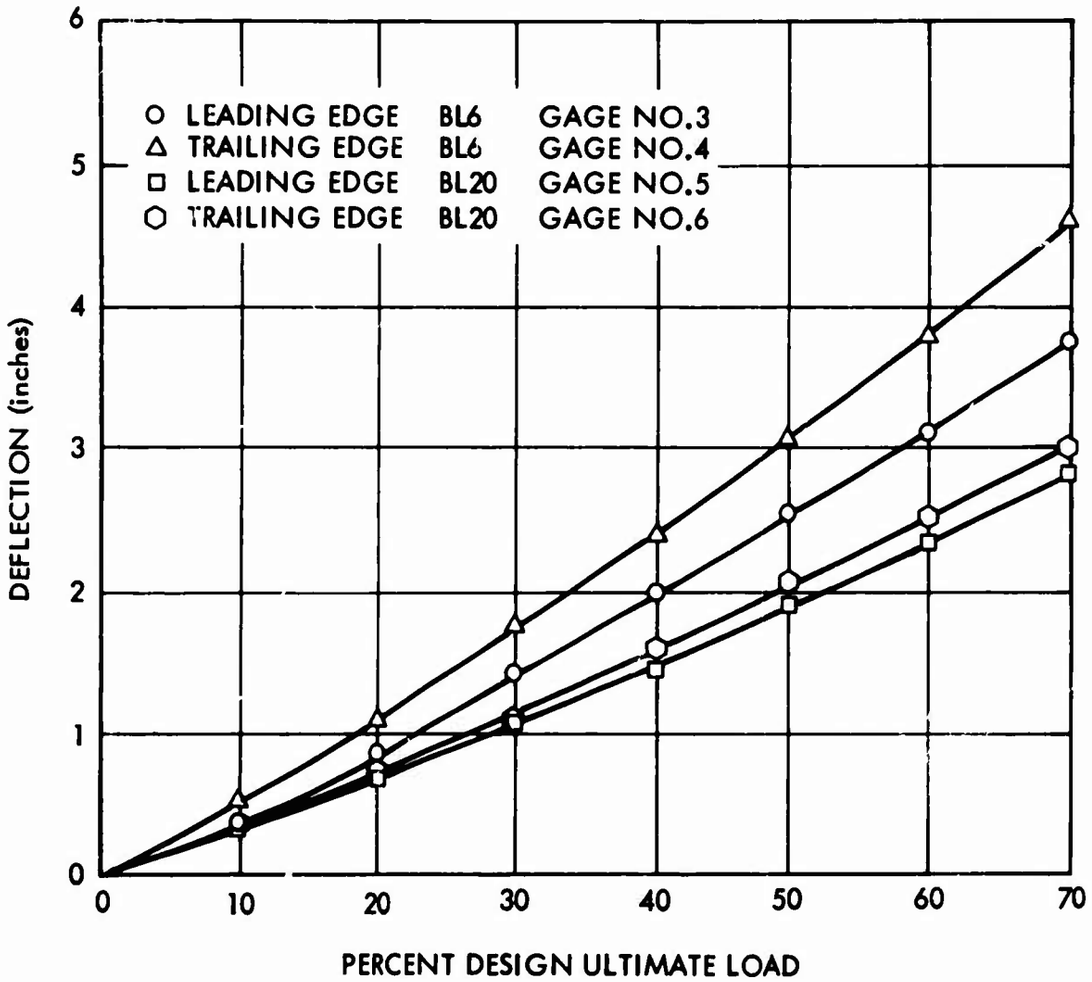

Figure 63. Tip Bending Deflection for Test No. 4 During the Bending Failure Test.

test curves was probably due to some material property changes caused by intermediate tests. The torsion indications are not readily explainable.

The torsional deflections were measured by a series of potentiometers located along the wing leading edge and along the rear spar. The wing section was first loaded to 50 percent of the arbitrarily chosen 186,000 in.-lb test load. The load was then reduced to zero and subsequently returned to 100 percent.

The recorded deflection readings were programmed into a computer at NADC to obtain twist angles at the various potentiometer BL locations. To obtain the proper deflection readings, the wing span from BL 6 to BL 68 was used, since this represented the test section. Deflections over the 62-inch test section are plotted as a function of percent load in Figure 64.

The deflection originally calculated in the GAC Development Support section of this report is also plotted in Figure 64. The calculated deflections correspond to a 62-inch torque box with a torque of 186,000 in.-lb applied. It should be noted that the calculated deflections are based upon a constant shear modulus value of 810,000 psi.

The comparison of calculated and measured deflections is quite good. Measured deflections at the lower loadings are somewhat less than calculated. At 100 percent load, the measured deflection becomes somewhat larger than calculated. This again, as in the torsional stress comparison, reflects the reduction in shear modulus as the stress level is increased. Thus G is probably somewhat larger than 810,000 psi at lower stress levels and less than 810,000 psi at higher stress levels.

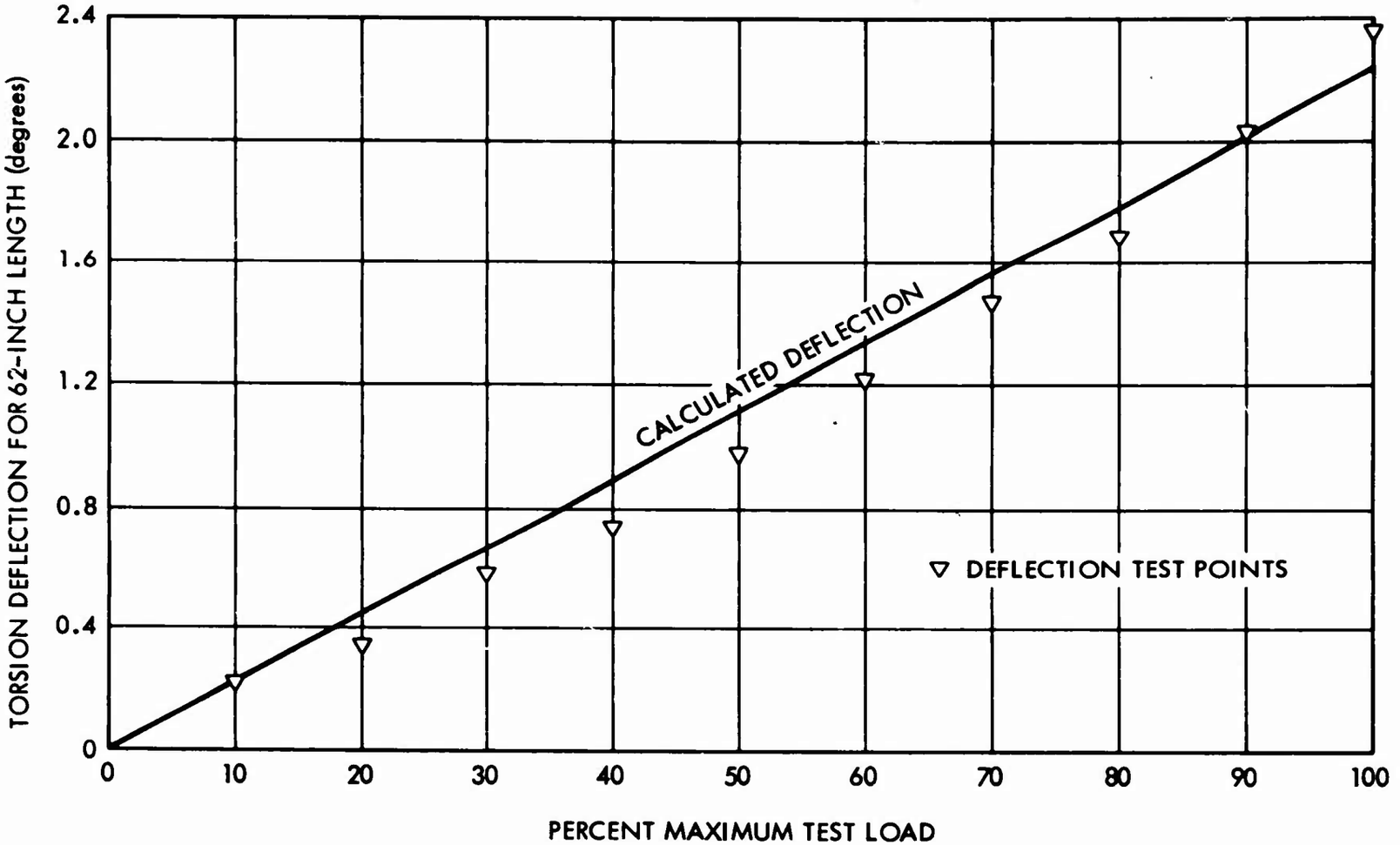

Figure 64. Torsional Deflection of the 62-Inch Section.

STRUCTURAL ANALYSIS AND DESIGN MODIFICATIONS FOR THE NO. 2 WING

GENERAL

Static tests of the first wing section resulted in specimen failure at less than the anticipated ultimate loading. Therefore, the objective of the second task was to redesign the configuration to achieve ultimate design loading with a minimum increase in wing section weight.

Design modification was limited to those changes which would not cause major tool rework. Since all honeycomb core material for this contract was purchased prior to the fabrication of the No. 1 test section, no changes in core thickness or density were made for the No. 2 unit.

Failure of the first wing test section was apparently precipitated by the instability of the aft box compression skin panel. This panel was first observed to buckle at about 40 percent DUL. As loading increased, the buckle deepened and the aft cell resisted less of the total loading than was calculated. Hence, the more stable forward cell carried higher than calculated loads. Center spar shear web failure was also evident on the tested wing. Failure of attaching screws in the top forward spar cap area was also noted. Screw failure is considered to be a possible secondary effect of the buckled skin panel. It is uncertain whether the shear failure was primary or secondary, because measured strains in the spar web indicated stresses which were very close to the shear strength of the material. Inspection of the structural analysis of the wing, presented in the GAC Development Support section of this report, shows that the wing was originally designed using optimistic criteria. This was desirable in order to determine the critical areas during the first test. The stability analysis assumed clamped edges for the skin panel and allowed a higher buckling stress because of panel curvature. Test results showed that simply supported edges and flat panel criteria are more realistic. The spar web shear strength criteria were based on MIL-HDBK-17[2] data for a solid laminate material. A lower allowable shear strength for the sandwich skins is now recommended.

Based on the original structural analysis and the static test results, a logical structural redesign was performed.

DESIGN MODIFICATIONS

The following recommendations were made for the redesign of the structure:

1. Increase the compression side skin thickness to reduce the stress level in the compression skin. Simultaneously reduce the spar cap areas to reduce wing section weight increases. This achieves a more efficient balance between compression and tension strength.

2. Add transverse stiffeners in each box on the compression side. This breaks up the panel size and increases the stress level at which buckling occurs. The objective is to make the panel stable up to a compression stress equivalent to the DUL.

3. Increase the spar web shear strength.

4. Increase the size of the countersunk screws holding the sections together from 3/16-inch to 1/4-inch diameter.

The original bending section analysis resulted in a maximum compression bending stress of 40,000 psi and a maximum tension bending stress of 36,000 psi at DUL. Corresponding strengths were 40,000 psi for compression and 50,000 psi for tension. A shift in material to decrease compression stress and to increase tensile stress produced a more efficient bending section.

The only areas where material transfers to the compression skin could be made were in the spar cap and the thick leading edge. Therefore, the spar cap areas were reduced as much as was practical for bolt bearing and ply continuity criteria. The largest transfer resulted from the reduction of the leading-edge thickness. Since these areas are located near the neutral axis, the materials are ineffective for bending. Compression skin plies were increased from three to five plies on each side of the sandwich, while the three-ply tension side skins remained the same.

Comparison of the old and the new wing section is presented in Table XIV.

TABLE XIV. COMPARISON OF WING SECTIONS

Area of Comparison	No. 1 Wing	No. 2 Wing
Bending Section	11.71 $in.^2$	11.43 $in.^2$
Highest Compression Stress	40,000 psi	32,900 psi
Highest Tension Stress	36,000 psi	39,600 psi

Transfer of materials resulted in a slight reduction in the calculated weight and a 16 percent increase in the calculated failure load. However, the above criterion requires that the compression skin remain stable at stresses up to 32, 900 psi. Transverse stiffeners were added to insure stability, but this addition increased the overall wing weight. Figure 65 is a photograph of the modified test structure.

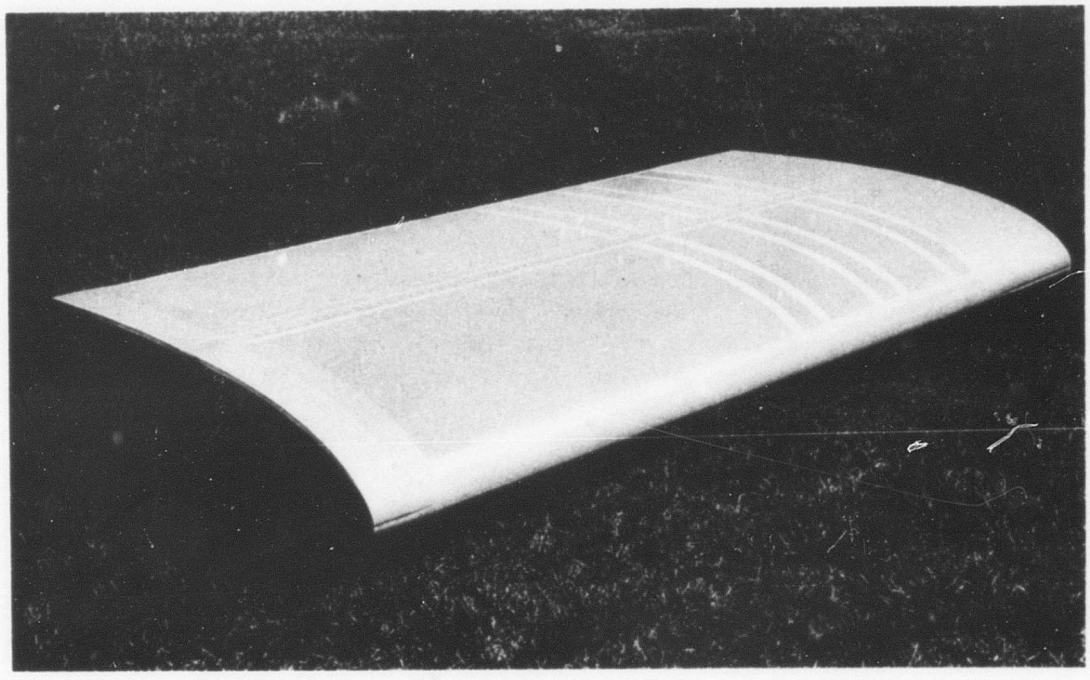

Figure 65. No. 2 Wing Test Section.

NO. 2 WING PROPERTIES

New section properties and design ultimate stresses were calculated for the new wing section. Figure 66 shows the section on which the calculations were based. The elements are blocked in and numbered, and the new neutral axes, centroid, shear center location, and shears used in the shear distribution are shown. These calculations are presented in the remaining paragraphs and tables of this subsection.

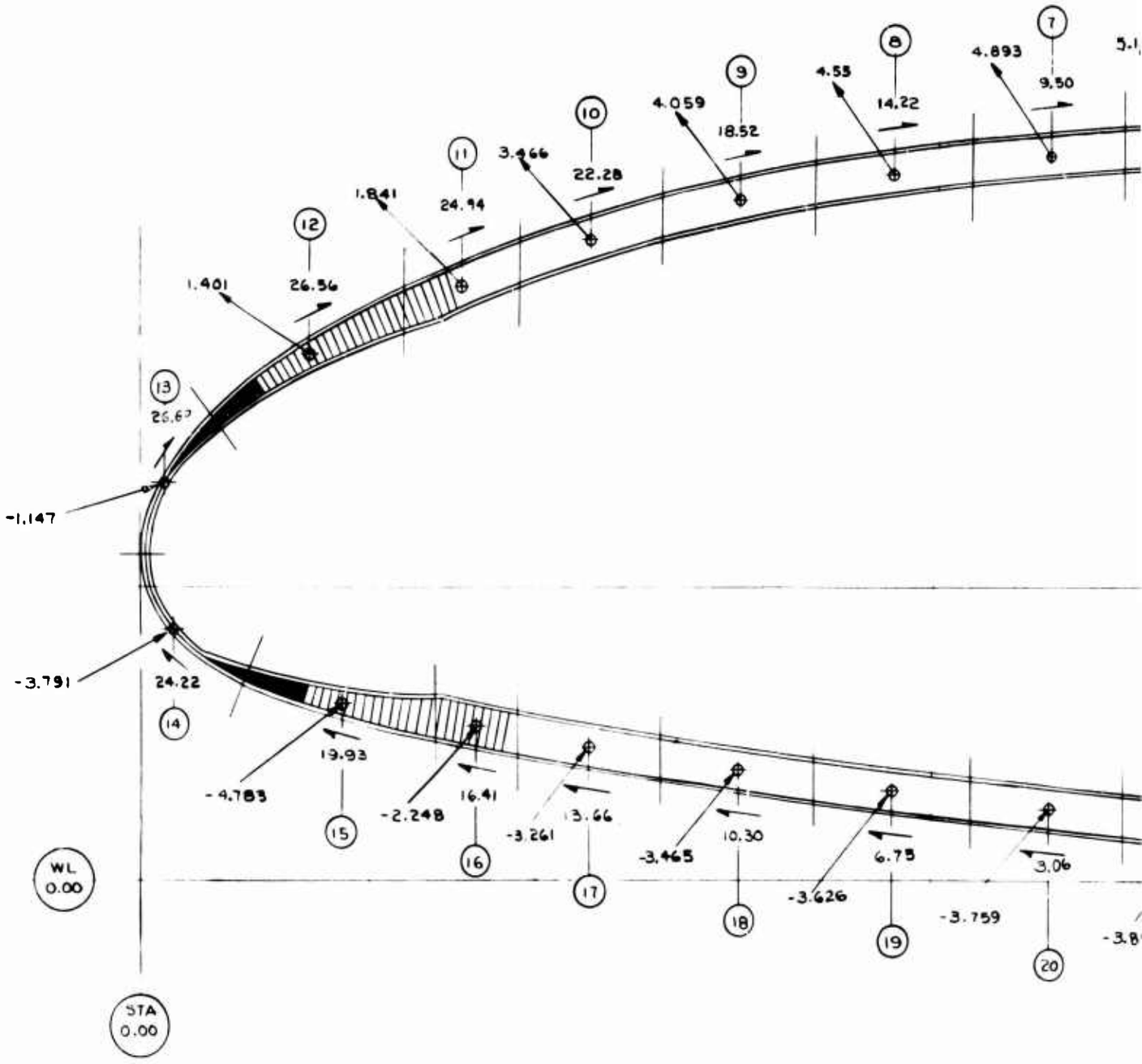

Figure 66. Test Section Layout for the Stress Analysis of the No. 2 Wing.

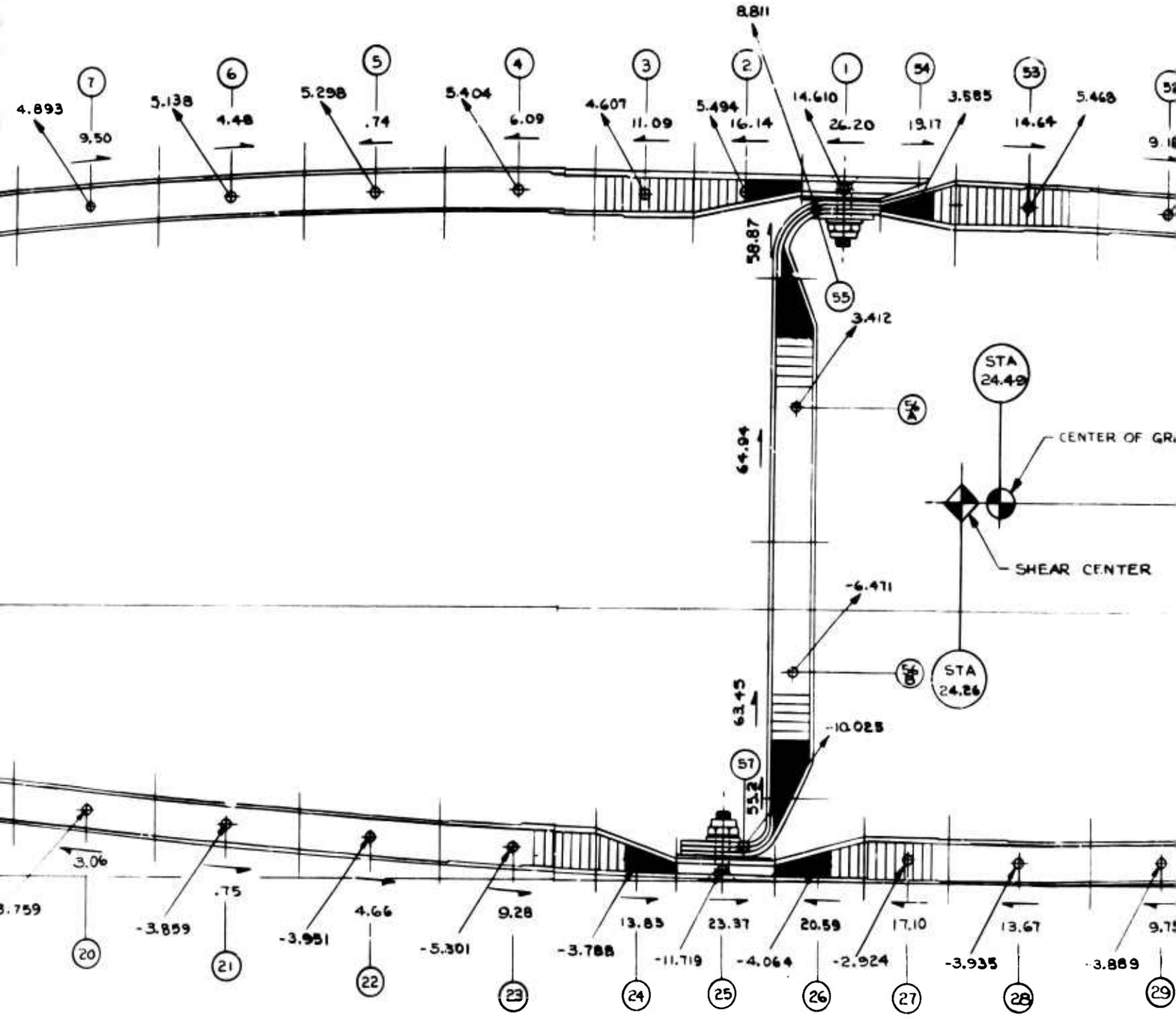
8.811
4.893
9.50
5.138
4.48
5.298
.74
5.404
6.09
4.607
11.09
5.494
16.14
14.610
26.20
19.17
3.585
14.64
5.468
58.87
3.412
64.94
STA 24.42
CENTER OF GR
SHEAR CENTER
-6.471
STA 24.26
63.45
-10.025
3.06
.75
4.66
9.28
13.85
23.37
20.59
17.10
13.67
-3.759
-3.859
-3.951
-5.301
-3.788
-11.719
-4.064
-2.924
-3.935
-3.889
20
21
22
23
24
25
26
27
28
29

b

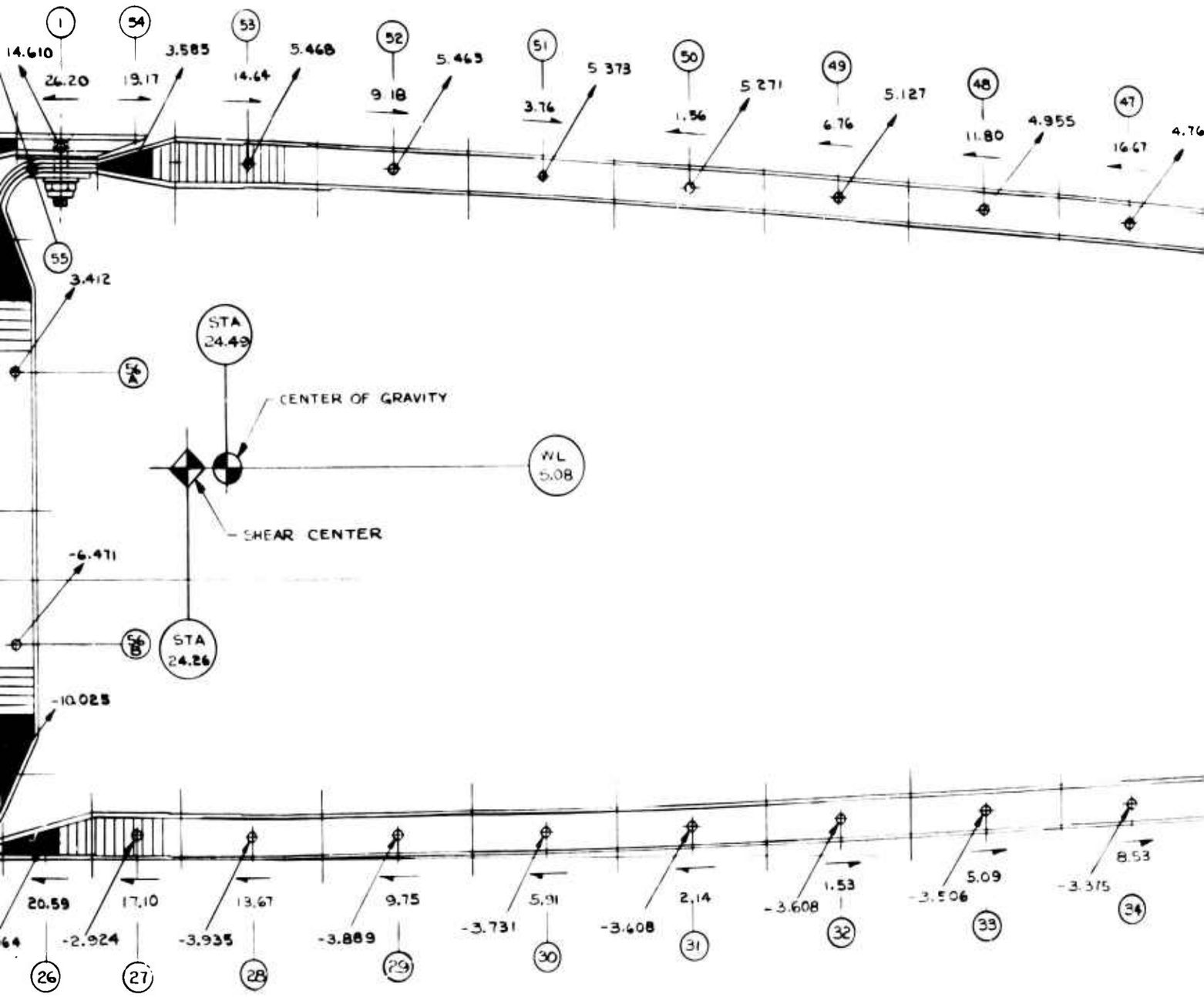
1
14.610
24.20
54
19.17
3.585
53
14.64
5.468
52
9.18
5.463
51
3.76
5 373
50
1.56
5 271
49
6.76
5.127
48
11.80
4.955
47
16.67
4.76
55
3.412
STA 24.49
CENTER OF GRAVITY
WL 5.08
SHEAR CENTER
-6.471
STA 24.26
-10.025
20.59
17.10
13.67
9.75
5.91
2.14
1.53
5.09
8.53
-2.924
-3.935
-3.889
-3.731
-3.408
-3.608
-3.506
-3.375
26
27
28
29
30
31
32
33
34

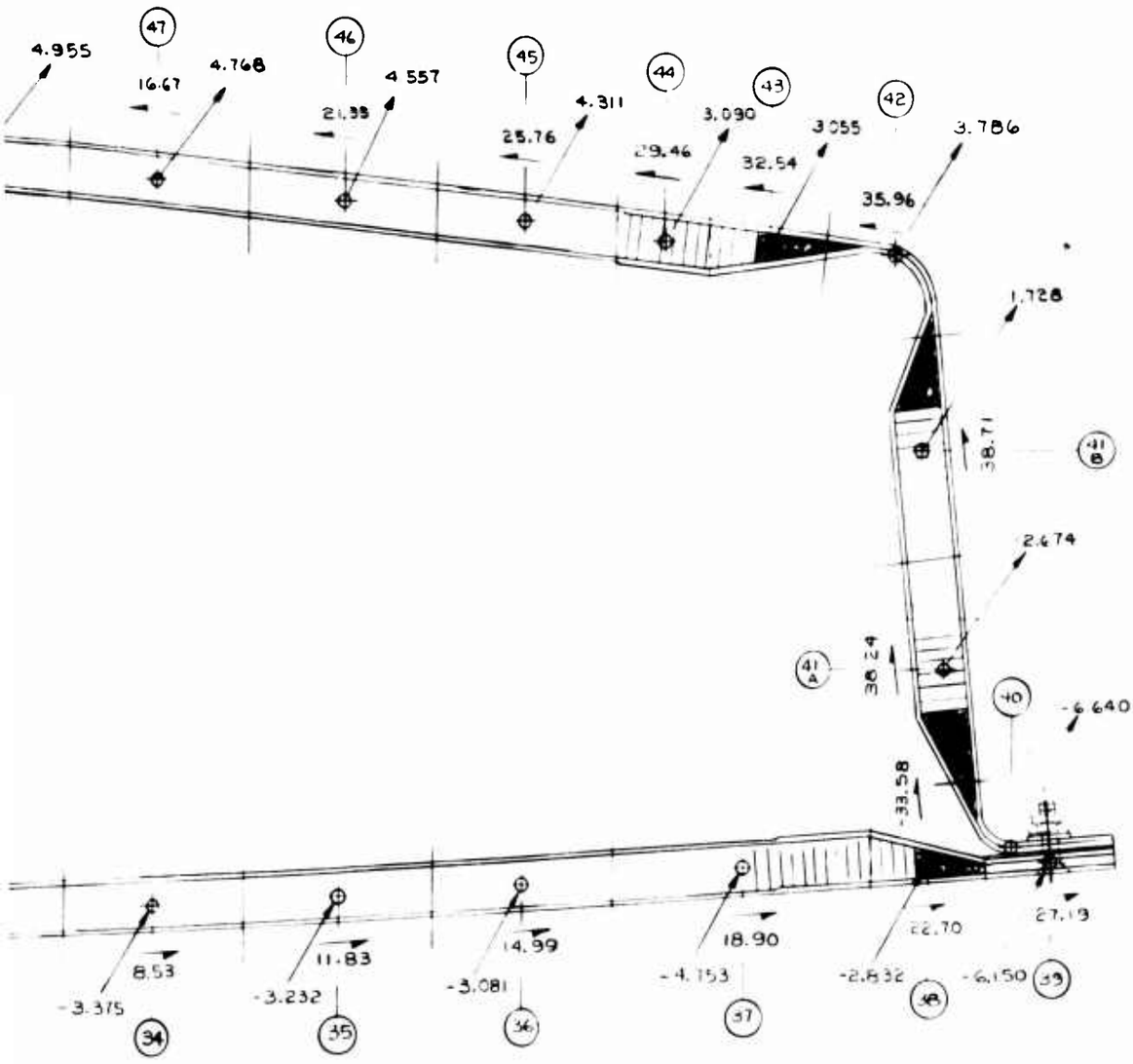

NOTES:

1. SHEAR FLOW q IS IN LBS/INCH
2. VQ/I FORCES ARE IN LBS/INCH OF SPAN FOR EACH ELEMENT
3. ALL LOADS ARE FOR A UNIT SHEAR LOAD OF 1000 POUNDS APPLIED AT THE SHEAR CENTER
4. POSITIVE LOAD DIRECTION IS UP

BLANK PAGE

Section Properties

Table XV establishes the section properties of the modified wing section. The same 57 elements are used as in the No. 1 wing; however, in numerous cases their length, thickness, and area are changed because of the redistribution of section material. Elements 41 and 56 were subdivided into elements 41a, 41b, 56a, and 56b to achieve a better shear distribution on the spars. The colums x_1 and y_1 represent the element distances to the X and Y neutral axes calculated in the stress analysis for wing No. 1. These arms were then multiplied by the element area, and a new set of neutral axes was calculated. The resultant shift in the X axis was 0.82 inch; in the Y axis, 0.53 inch. A new set of element distances was then calculated. The total section area was 11.43 square inches.

TABLE XV. SECTION PROPERTIES

① Element	② Length (in.)	③ Thickness (in.)	④ Area ($in.^2$) ② x ③	⑤ x_1	⑥ y_1	⑦ Ax_1 ④ x ⑤	⑧ Ay_1 ④ x ⑥	⑨ x ⑤ - 0.82	⑩ y ⑥ - 0.53
1	-	-	0.510	-1.40	4.72	-0.714	2.407	-2.22	4.19
2	1.40	0.140	0.196	-2.70	4.67	-0.529	0.915	-3.52	4.14
3	1.40	0.120	0.168	-4.08	4.62	-0.685	0.776	-4.90	4.09
4	2.00	0.100	0.200	-5.80	4.61	-1.160	0.922	-6.62	4.08
5	2.00	0.100	0.200	-7.83	4.59	-1.566	0.918	-8.65	4.06
6	2.00	0.100	0.200	-9.78	4.53	-1.956	0.906	-10.60	4.00
7	2.00	0.100	0.200	-11.80	4.41	-2.360	0.882	-12.62	3.88
8	2.00	0.100	0.200	-13.82	4.22	-2.764	0.844	-14.64	3.69
9	2.03	0.100	0.203	-15.80	3.88	-3.207	0.788	-16.62	3.35
10	2.13	0.100	0.213	-17.80	3.40	-3.791	0.724	-18.62	2.87
11	1.60	0.100	0.160	-19.54	2.76	-3.126	0.442	-20.36	2.23
12	2.80	0.100	0.280	-21.50	1.88	-6.020	0.526	-22.32	1.35
13	-	0.100	0.200	-23.21	0.38	-4.642	0.076	-24.03	-0.15
14	-	0.100	0.214	-23.12	-1.35	-4.948	-0.289	-23.94	-1.88
15	2.50	0.080	0.200	-21.06	-2.30	-4.212	-0.460	-21.88	-2.83
16	1.10	0.080	0.088	-19.30	-2.58	-1.698	-0.227	-20.12	-3.11
17	2.00	0.060	0.120	-17.77	-2.86	-2.132	-0.343	-18.59	-3.39
18	2.00	0.060	0.120	-15.80	-3.16	-1.896	-0.379	-16.62	-3.69
19	2.00	0.060	0.120	-13.82	-3.41	-1.658	-0.409	-14.64	-3.94
20	2.00	0.060	0.120	-11.80	-3.63	-1.416	-0.436	-12.62	-4.16
21	2.00	0.060	0.120	-9.82	-3.80	-1.178	-0.456	-10.64	-4.33
22	2.00	0.060	0.120	-7.82	-3.97	-0.938	-0.476	-8.64	-4.50
23	2.00	0.080	0.160	-5.80	-4.06	-0.928	-0.650	-6.62	-4.59

TABLE XV - Continued

① Element	② Length (in.)	③ Thickness (in.)	④ Area (in.²) ② x ③	⑤ x_1	⑥ y_1	⑦ Ax_1 ④ x ⑤	⑧ Ay_1 ⑤ x ⑥	⑨ x ⑤ - 0.82	⑩ y ⑥ - 0.53
24	1.12	0.100	0.112	-4.22	-4.20	-0.473	-0.470	-5.04	-4.73
25	1.36	0.250	0.340	-3.00	-4.33	-1.020	-1.472	-3.82	-4.86
26	1.20	0.100	0.120	-1.71	-4.28	-0.205	-0.514	-2.53	-4.81
27	1.10	0.080	0.088	-0.50	-4.22	-0.044	-0.371	-1.32	-4.75
28	2.00	0.060	0.120	1.14	-4.20	0.137	-0.504	0.32	-4.73
29	2.00	0.060	0.120	3.07	-4.20	0.368	-0.504	2.25	-4.73
30	2.00	0.060	0.120	5.15	-4.16	0.618	-0.499	4.33	-4.69
31	2.00	0.060	0.120	7.15	-4.13	0.858	-0.496	6.33	-4.66
32	2.00	0.060	0.120	9.15	-4.04	1.098	-0.485	8.33	-4.57
33	2.00	0.060	0.120	11.15	-3.97	1.338	-0.476	10.33	-4.50
34	2.00	0.060	0.120	13.12	-3.87	1.574	-0.464	12.30	-4.40
35	2.00	0.060	0.120	15.12	-3.75	1.814	-0.450	14.30	-4.28
36	2.00	0.060	0.120	17.12	-3.63	2.054	-0.436	16.30	-4.16
37	2.80	0.070	0.196	19.50	-3.49	3.822	-0.684	18.68	-4.02
38	1.25	0.100	0.125	21.54	-3.32	2.692	-0.415	20.72	-3.85
39	1.33	0.200	0.266	22.82	-3.42	6.070	-0.910	22.00	-3.95
40	-	-	0.321	22.42	-3.06	7.197	-0.982	21.60	-3.59
41a	2.31	0.120	0.277	21.68	-1.45	6.005	-0.402	20.86	-1.98
41b	2.31	0.120	0.277	21.44	.85	5.939	0.236	20.62	0.32
42	-	-	0.199	21.08	2.70	4.195	0.537	20.26	2.17
43	1.25	0.120	0.150	19.78	2.93	2.967	0.440	18.96	2.40
44	1.25	0.120	0.150	18.62	3.00	2.793	0.450	17.80	2.47
45	2.00	0.100	0.200	17.00	3.18	3.400	0.636	16.18	2.65
46	2.00	0.100	0.200	15.11	3.41	3.022	0.682	14.29	2.88
47	2.00	0.100	0.200	13.08	3.62	2.616	0.724	12.26	3.09
48	2.00	0.100	0.200	11.11	3.81	2.222	0.762	10.29	3.28
49	2.00	0.100	0.200	9.11	3.99	1.822	0.798	8.29	3.46
50	2.00	0.100	0.200	7.12	4.15	1.424	0.830	6.30	3.62
51	2.00	0.100	0.200	5.12	4.28	1.024	0.856	4.30	3.75
52	2.00	0.100	0.200	3.16	4.40	0.632	0.880	2.34	3.87
53	2.00	0.100	0.200	1.16	4.46	0.232	0.892	0.34	3.93
54	1.10	0.120	0.132	-0.37	4.48	-0.049	0.591	-1.19	3.95
55	-	-	0.348	-1.78	4.25	-0.619	1.479	-2.60	3.72
56a	3.45	0.120	0.414	-2.13	1.80	-0.882	0.745	-2.95	1.27
56b	3.45	0.120	0.414	-2.13	-1.64	-0.882	-0.679	-2.95	-2.17
57	-	-	0.312	-2.75	-4.00	-0.858	-1.248	-3.57	-4.53
Σ	-	-	11.433	0.82	0.53	9.377	6.078	-	-

Moments of Inertia

Table XVI arrives at the new X and Y axes moments of inertia ΣAx^2 and ΣAy^2. The resultant moment of inertia was 2103 inches^4 about the Y axis and 146 inches^4 about the X axis.

TABLE XVI. MOMENTS OF INERTIA

① Element	② Area ④ Table XV	③ x ⑨ Table XV	④ y ⑩ Table XV	⑤ Ax ② x ③	⑥ Ay ② x ④	⑦ Axy ② x ③ x ④	⑧ Ax^2 ③ x ⑤	⑨ Ay^2 ④ x ⑥
1	0.510	-2.22	4.19	-1.132	2.137	-4.743	2.513	8.954
2	0.196	-3.52	4.14	-0.690	0.811	-2.857	2.429	3.358
3	0.168	-4.90	4.09	-0.823	0.687	-3.366	4.033	2.810
4	0.200	-6.62	4.08	-1.324	0.816	-5.402	8.765	3.329
5	0.200	-8.65	4.06	-1.730	0.812	-7.024	14.965	3.297
6	0.200	-10.60	4.00	-2.120	0.800	-8.480	22.472	3.200
7	0.200	-12.62	3.88	-2.524	0.776	-9.793	31.853	3.011
8	0.200	-14.64	3.69	-2.928	0.738	-10.804	42.866	2.723
9	0.203	-16.62	3.35	-3.374	0.680	-11.303	56.076	2.278
10	0.213	-18.62	2.87	-3.966	0.611	-11.382	73.847	1.754
11	0.160	-20.36	2.23	-3.258	0.357	-7.265	66.333	0.796
12	0.280	-22.32	1.35	-6.250	0.378	-8.438	139.500	0.510
13	0.200	-24.03	-0.15	-4.806	-0.030	0.721	115.488	0.005
14	0.214	-23.94	-1.88	-5.123	-0.402	9.631	122.645	0.756
15	0.200	-21.88	-2.83	-4.376	-0.566	12.384	95.747	1.602
16	0.088	-20.12	-3.11	-1.771	-0.274	5.508	35.633	0.852
17	0.120	-18.59	-3.39	-2.231	-0.407	7.563	41.474	1.380
18	0.120	-16.62	-3.69	-1.994	-0.443	7.358	33.140	1.635
19	0.120	-14.64	-3.94	-1.757	-0.473	6.923	25.722	1.864
20	0.120	-12.62	-4.16	-1.514	-0.499	6.298	19.107	2.076
21	0.120	-10.64	-4.33	-1.277	-0.520	5.529	13.587	2.252
22	0.120	-8.64	-4.50	-1.037	-0.540	4.666	8.960	2.430
23	0.160	-6.62	-4.59	-1.059	-0.734	4.861	7.011	3.369
24	0.112	-5.04	-4.73	-0.564	-0.530	2.668	2.843	2.507

TABLE XVI.- Continued

① Element	② Area ④ Table XV	③ x ⑨ Table XV	④ y ⑩ Table XV	⑤ Ax ② x ③	⑥ Ay ② x ④	⑦ Axy ② x ③ x ④	⑧ Ax^2 ③ x ⑤	⑨ Ay^2 ⑤ x ⑥
25	0.340	-3.82	-4.86	-1.299	-1.652	6.313	4.962	8.029
26	0.120	-2.53	-4.81	-0.304	-0.577	1.462	0.769	2.775
27	0.088	-1.32	-4.75	-0.116	-0.418	0.551	0.153	1.985
28	0.120	0.32	-4.73	0.038	-0.568	-0.180	0.012	2.687
29	0.120	2.25	-4.73	0.270	-0.568	-1.277	0.608	2.687
30	0.120	4.33	-4.69	0.520	-0.563	-2.439	2.252	2.640
31	0.120	6.33	-4.66	0.760	-0.559	-3.542	4.811	2.605
32	0.120	8.33	-4.57	1.000	-0.548	-4.570	8.330	2.504
33	0.120	10.33	-4.50	1.240	-0.540	-5.580	12.809	2.430
34	0.120	12.30	-4.40	1.476	-0.528	-6.494	18.155	2.323
35	0.120	14.30	-4.28	1.716	-0.514	-7.344	24.539	2.200
36	0.120	16.30	-4.16	1.956	-0.499	-8.137	31.883	2.076
37	0.196	18.68	-4.02	3.661	-0.788	-14.717	68.387	3.168
38	0.125	20.72	-3.85	2.590	-0.481	-9.971	53.665	1.852
39	0.266	22.00	-3.95	5.852	-1.051	-23.115	128.744	4.151
40	0.321	21.60	-3.59	6.934	-1.152	-24.893	149.774	4.136
41a	0.277	20.86	-1.98	5.778	-0.548	-11.440	120.529	1.085
41b	0.277	20.62	0.32	5.712	0.088	1.828	117.781	0.028
42	0.199	20.26	2.17	4.032	0.432	8.749	81.688	0.937
43	0.150	18.96	2.40	2.844	0.360	6.826	53.922	0.864
44	0.150	17.80	2.47	2.670	0.370	6.595	47.526	0.914
45	0.200	16.18	2.65	3.236	0.530	8.575	52.358	1.405
46	0.200	14.29	2.88	2.858	0.576	8.231	40.841	1.659
47	0.200	12.26	3.09	2.452	0.618	7.577	30.062	1.910
48	0.200	10.29	3.28	2.058	0.656	6.750	21.177	2.152
49	0.200	8.29	3.46	1.658	0.692	5.737	13.745	2.394
50	0.200	6.30	3.62	1.260	0.724	4.561	7.938	2.621
51	0.200	4.30	3.75	0.860	0.750	3.225	3.698	2.813
52	0.200	2.34	3.87	0.468	0.774	1.811	1.095	2.995
53	0.200	0.34	3.93	0.068	0.786	0.267	0.023	3.089
54	0.132	-1.19	3.95	-0.157	0.521	-0.620	0.187	2.058
55	0.348	-2.60	3.72	-0.905	1.295	-3.367	2.353	4.817
56a	0.414	-2.95	1.27	-1.221	0.526	-1.551	3.602	0.668
56b	0.414	-2.95	-2.17	-1.221	-0.898	2.650	3.602	1.949
57	0.312	-3.57	-4.53	-1.114	-1.413	5.046	3.977	6.401
Σ	11.433	-	-	+0.002	+0.018	-59.230	2102.966	145.755

Bending Stresses

The calculations for bending stresses f_b in the nonsymmetrical beam section, where the X and Y axes are not the principal axes, were performed by standard methods which eliminate the necessity of transferring to the principal axes. The constants required for this operation are calculated in Equations 52 through 60. The basic formula for determining the bending stress in a nonsymmetrical beam section is used.

$$f_b = (C_1M_y - C_2M_x)\, y + (C_1M_x - C_3M_y)\, x \qquad (52)$$

To determine the constants in this equation, the following parameters must be known:

$I_y = 2102.966$ $\qquad$ $M_x = 300,000$

$I_x = 145.755$ $\qquad$ $M_y = 0$

$I_{xy} = -59.230$

where

$$\begin{aligned} K &= I_xI_y - I_{xy}^2 \\ &= 145.755 \times 2102.966 - \overline{59.230}^2 \\ &= 306,518 - 3508 \\ &= 303,010 \end{aligned} \qquad (53)$$

Then,

$$C_1 = \frac{I_{xy}}{K} = -\frac{59.230}{303,010}$$

$$= -0.00019547 \qquad (54)$$

$$C_2 = \frac{I_y}{K} = \frac{2102.966}{303,010}$$

$$= 0.0069403 \qquad (55)$$

$$C_3 = \frac{I_x}{K} = \frac{145.755}{303,010}$$

$$= 0.00048102 \qquad (56)$$

$$C_1M_y = -0.00019547 \times 0$$

$$= 0 \qquad (57)$$

$$C_2M_x = 0.0069403 \times 300,000$$

$$= 2082.09 \qquad (58)$$

$$C_1M_x = -0.00019547 \times 300,000$$

$$= -58.641 \qquad (59)$$

$$C_3M_y = 0.00048102 \times 0$$

$$= 0 \qquad (60)$$

The calculations presented in Table XVII determine the bending stresses in each element for the DUL. Data from Tables XV and XVI and from the bending constant calculations were used in these calculations. Element No. 1 is subjected to the highest compression stress, 32,900 psi, and element No. 25 is subjected to the highest tension stress, 39,600 psi.

TABLE XVII. BENDING STRESS

① Element	② x ① (p 119)	③ y ⑩ (p 119)	④ C_1M_y Eq (57)	⑤ $-C_2M_x$ Eq (58)	⑥ C_1M_x Eq (59)	⑦ $-C_3M_y$ Eq (60)	⑧ ④ + ⑤	⑨ ⑥ + ⑦	⑩ ⑧ x ③	⑪ ⑨ x ②	⑫ ⑩ + ⑪	⑬ f_b ⑫ x 3.83
1	-2.22	4.19	0	-2082	-58.64	0	-2082	-58.64	-8,724	130	-8594	-32,915
2	-3.52	4.14	0	-2082	-58.64	0	-2082	-58.64	-8,619	206	-8413	-32,222
3	-4.90	4.09	0	-2082	-58.64	0	-2082	-58.64	-8,515	287	-8228	-31,513
4	-6.62	4.08	0	-2082	-58.64	0	-2082	-58.64	-8,495	388	-8107	-31,050
5	-8.65	4.06	0	-2082	-58.64	0	-2082	-58.64	-8,453	507	-7946	-30,433
6	-10.60	4.00	0	-2082	-58.64	0	-2082	-58.64	-8,328	622	-7706	-29,514
7	-12.62	3.88	0	-2082	-58.64	0	-2082	-58.64	-8,078	740	-7338	-28,105
8	-14.64	3.69	0	-2082	-58.64	0	-2082	-58.64	-7,683	858	-6825	-26,140
9	-16.62	3.35	0	-2082	-58.64	0	-2082	-58.64	-6,975	975	-6000	-22,980
10	-18.62	2.87	0	-2082	-58.64	0	-2082	-58.64	-5,975	1092	-4883	-18,702
11	-20.36	2.23	0	-2082	-58.64	0	-2082	-58.64	-4,643	1194	-3449	-13,210
12	-22.32	1.35	0	-2082	-58.64	0	-2082	-58.64	-2,811	1309	-1502	-5,753
13	-24.03	-0.15	0	-2082	-58.64	0	-2082	-58.64	312	1409	1721	6,591
14	-23.94	-1.88	0	-2082	-58.64	0	-2082	-58.64	3,914	1404	5318	20,368
15	-21.88	-2.83	0	-2082	-58.64	0	-2082	-58.64	5,892	1283	7175	27,480
16	-20.12	-3.11	0	-2082	-58.64	0	-2082	-58.64	6,475	1180	7655	29,319
17	-18.59	-3.39	0	-2082	-58.64	0	-2082	-58.64	7,058	1090	8148	31,207
18	-16.62	-3.69	0	-2082	-58.64	0	-2082	-58.64	7,683	975	8658	33,160
19	-14.64	-3.94	0	-2082	-58.64	0	-2082	-58.64	8,203	858	9061	34,704
20	-12.62	-4.16	0	-2082	-58.64	0	-2082	-58.64	8,661	740	9401	36,006

TABLE XVII - Continued

① Element	② x ⑨ (p 119)	③ y ⑩ (p 119)	④ C_1M_y Eq (57)	⑤ $-C_2M_x$ Eq (58)	⑥ C_1M_x Eq (59)	⑦ $-C_3M_y$ Eq (60)	⑧ ④ + ⑤	⑨ ⑥ + ⑦	⑩ ⑧ x ③	⑪ ⑨ x ②	⑫ ⑩ + ⑪	⑬ f_b ⑫ x 3.83
21	-10.64	-4.33	0	-2082	-58.64	0	-2082	-58.64	9,015	624	9,639	36,917
22	-8.64	-4.50	0	-2082	-58.64	0	-2082	-58.64	9,369	507	9,876	37,825
23	-6.62	-4.59	0	-2082	-58.64	0	-2082	-58.64	9,556	388	9,944	38,086
24	-5.04	-4.73	0	-2082	-58.64	0	-2082	-58.64	9,848	296	10,144	38,852
25	-3.82	-4.86	0	-2082	-58.64	0	-2082	-58.64	10,119	224	10,343	39,614
26	-2.53	-4.81	0	-2082	-58.64	0	-2082	-58.64	10,014	148	10,162	38,920
27	-1.32	-4.75	0	-2082	-58.64	0	-2082	-58.64	9,890	77	9,967	38,174
28	0.32	-4.73	0	-2082	-58.64	0	-2082	-58.64	9,848	-19	9,829	37,645
29	2.25	-4.73	0	-2082	-58.64	0	-2082	-58.64	9,848	-132	9,716	37,212
30	4.33	-4.69	0	-2082	-58.64	0	-2082	-58.64	9,765	-254	9,511	36,427
31	6.33	-4.66	0	-2082	-58.64	0	-2082	-58.64	9,702	-371	9,331	35,738
32	8.33	-4.57	0	-2082	-58.64	0	-2082	58.64	9,515	-488	9,027	34,573
33	10.33	-4.50	0	-2082	-58.64	0	-2082	-58.64	9,369	-606	8,763	33,562
34	12.30	-4.40	0	-2082	-58.64	0	-2082	-58.64	9,161	-721	8,440	32,325
35	14.30	-4.28	0	-2082	-58.64	0	-2082	-58.64	8,911	-839	8,072	30,916
36	16.30	-4.16	0	-2082	-58.64	0	-2082	-58.64	8,661	-956	7,705	29,510
37	18.68	-4.02	0	-2082	-58.64	0	-2082	-58.64	8,370	-1095	7,275	27,863
38	20.72	-3.85	0	-2082	-58.64	0	-2082	-58.64	8,016	-1215	6,801	26,048
39	22.00	-3.95	0	-2082	-58.64	0	-2082	-58.64	8,224	-1290	6,934	26,557
40	21.60	-3.59	0	-2082	-58.64	0	-2082	-58.64	7,474	-1267	6,207	23,773
41a	20.86	-1.98	0	-2082	-58.64	0	-2082	-58.64	4,122	-1223	2,899	11,103
41b	20.62	0.32	0	-2082	-58.64	0	-2082	-58.64	-666	-1209	-1,875	-7,181
42	20.26	2.17	0	-2082	-58.64	0	-2082	-58.64	-4,518	-1188	-5,706	-21,854
43	18.96	2.40	0	-2082	-58.64	0	-2082	-58.64	-4,997	-1112	-6,109	-23,397
44	17.80	2.47	0	-2082	-58.64	0	-2082	-58.64	-5,143	-1044	-6,187	-23,696
45	16.18	2.65	0	-2082	-58.64	0	-2082	-58.64	-5,517	-949	-6,466	-24,765
46	14.29	2.88	0	-2082	-58.64	0	-2082	-58.64	-5,096	-838	-6,834	-26,174
47	12.26	3.09	0	-2082	-58.64	0	-2082	-58.64	-6,433	-719	-7,152	-27,392
48	10.29	3.28	0	-2082	-58.64	0	-2082	-58.64	-6,829	-603	-7,432	-28,465
49	8.29	3.46	0	-2082	-58.64	0	-2082	-58.64	-7,204	-486	-7,690	-29,453
50	6.30	3.62	0	-2082	-58.64	0	-2082	-58.64	-7,537	-369	-7,906	-30,280
51	4.30	3.75	0	-2082	-58.64	0	-2082	-58.64	-7,808	-252	-8,060	-30,870
52	2.34	3.87	0	-2082	-58.64	0	-2082	-58.64	-8,057	-137	-8,194	-31,383
53	0.34	3.93	0	-2082	-58.64	0	-2082	-58.64	-8,182	-20	-8,202	-31,414
54	-1.19	3.95	0	-2082	-58.64	0	-2082	-58.64	-8,224	70	8,154	-31,230
55	-2.60	3.72	0	-2082	-58.64	0	-2082	-58.64	-7,745	152	-7,593	-29,081
56a	-2.95	1.27	0	-2082	-58.64	0	-2082	-58.64	-2,644	173	-2,471	-9,464
56b	-2.95	-2.17	0	-2082	-58.64	0	-2082	-58.64	4,518	173	4,691	17,967
57	-3.57	-4.53	0	-2082	-58.64	0	-2082	-58.64	9,431	209	9,640	36,921

VQ/I Shear Property Calculations

Table XVIII arrives at the VQ/I shear values for each element of the non-symmetrical bending section. These values are calculated using a 1000-pound unit shear load.

Table XVIII. VQ I SHEAR

① Element	② Ay ⑧ Table XVI	③ $-1000C_2$ Eq (55)	④ Ax ⑤ Table XVI	⑤ $1000C_1$ Eq (54)	⑥ ② x ③	⑦ ④ x ⑤	⑧ q ⑥ + ⑦
1	2.137	-6.9403	-1.132	-0.19547	-14.831	0.221	-14.610
2	0.811	-6.9403	-0.690	-0.19547	-5.629	0.135	-5.494
3	0.687	-6.9403	-0.823	-0.19547	-4.768	0.161	-4.607
4	0.816	-6.9403	-1.324	-0.19547	-5.663	0.259	-5.404
5	0.812	-6.9403	-1.730	-0.19547	-5.636	0.338	-5.298
6	0.800	-6.9403	-2.120	-0.19547	-5.552	0.414	-5.138
7	0.776	-6.9403	-2.524	-0.19547	-5.386	0.493	-4.893
8	0.738	-6.9403	-2.928	-0.19547	-5.122	0.572	-4.550
9	0.680	-6.9403	-3.374	-0.19547	-4.719	0.660	-4.059
10	0.613	-6.9403	-3.966	-0.19547	-4.241	0.775	-3.466
11	0.357	-6.9403	-3.258	-0.19547	-2.478	0.637	-1.841
12	0.378	-6.9403	-6.250	-0.19547	-2.623	1.222	-1.401
13	-0.030	-6.9403	-4.806	-0.19547	0.208	0.939	1.147
14	-0.402	-6.9403	-5.123	-0.19547	2.790	1.001	3.791
15	-0.566	-6.9403	-4.376	-0.19547	3.928	0.855	4.783
16	-0.274	-6.9403	-1.771	-0.19547	1.902	0.346	2.248
17	-0.407	-6.9403	-2.231	-0.19547	2.825	0.436	3.261
18	-0.443	-6.9403	-1.994	-0.19547	3.075	0.390	3.465
19	-0.473	-6.9403	-1.757	-0.19547	3.283	0.343	3.626
20	-0.499	-6.9403	-1.514	-0.19547	3.463	0.296	3.759
21	-0.520	-6.9403	-1.277	-0.19547	3.609	0.250	3.859
22	-0.540	-6.9403	-1.037	-0.19547	3.748	0.203	3.951

TABLE XVIII - Continued

① Element	② Ay ⑥ Table XVI	③ $-1000C_2$ Eq (55)	④ Ax ⑤ Table XVI	⑤ $1000C_1$ Eq (54)	⑥ ② x ③	⑦ ④ x ⑤	⑧ q ⑥ + ⑦
23	-0.734	-6.9403	-1.059	-0.19547	5.094	0.207	5.301
24	-0.530	-6.9403	-0.564	-0.19547	3 678	0.110	3.788
25	-1.652	-6.9403	-1.299	-0.19547	11.465	0.254	11.719
26	-0.577	-6.9403	-0.304	-0.19547	4.005	0.059	4.064
27	-0.418	-6.9403	-0.116	-0.19547	2.901	0.023	2.924
28	-0.568	-6.9403	0.038	-0.19547	3.942	-0.007	3.935
29	-0.568	-6.9403	0.270	-0.19547	3.942	-0.053	3.889
30	-0.563	-6.9403	0.520	-0.19547	3.907	-0.102	3.805
31	-0.559	-6.9403	0.760	-0.19547	3.880	-0.149	3.731
32	-0.548	-6.9403	1.000	-0.19547	3.803	-0.195	3.608
33	-0.540	-6.9403	1.240	-0.19547	3.748	-0.242	3.506
34	-0.528	-6.9403	1.476	-0.19547	3.664	-0.289	3.375
35	-0.514	-6.9403	1.716	-0.19547	3.567	-0.335	3.232
36	-0.499	-6.9403	1.956	-0.19547	3.463	-0.382	3.081
37	-0.788	-6.9403	3.661	-0.19547	5.469	-0.716	4.753
38	-0.481	-6.9403	2.590	-0.19547	3.338	-0.506	2.832
39	-1.051	-6.9403	5.852	-0.19547	7.294	-1.144	6.150
40	-1.152	-6.9403	6.934	-0.19547	7.995	-1.355	6.640
41a	-0.548	-6.9403	5.778	-0.19547	3.803	-1.129	2.674
41b	0.088	-6 9403	5.712	-0.19547	-0.611	-1.117	-1.728
42	0.432	-6.9403	4.032	-0.19547	-2.998	-0.788	-3.786
43	0.360	-6.9403	2.844	-0.19547	-2.499	-0.556	-3.055
44	0.370	-6.9403	2.670	-0.19547	-2.568	-0.522	-3.090
45	0.530	-6.9403	3.236	-0.19547	-3.678	-0.633	-4.311
46	0.576	-6.9403	2.858	-0.19547	-3.998	-0.559	-4.557
47	0.618	-6.9403	2.452	-0.19547	-4.289	-0.479	-4.768
48	0.656	-6.9403	2.058	-0.19547	-4.553	-0.402	-4.955
49	0.692	-6.9403	1.658	-0.19547	-4.803	-0.324	-5.127
50	0.724	-6.9403	1.260	-0.19547	-5.025	-0.246	-5.271
51	0.750	-6.9403	0.860	-0.19547	-5.205	-0.168	-5.373
52	0.774	-6.9403	0.468	-0.19547	-5.372	-0.091	-5.463
53	0.786	-6.9403	0.068	-0.19547	-5.455	-0.013	-5.468
54	0.521	-6.9403	-0.157	-0.19547	-3.616	0.031	-3.585
55	1.295	-6.9403	-0.905	-0.19547	-8.988	0.177	-8.811
56a	0.526	-6.9403	-1.221	-0.19547	-3.651	0.239	-3.412
56b	-0.898	-6.9403	-1.221	-0.19547	6.232	0.239	6.471
57	-1.413	-6.9403	-1.114	-0.19547	9.807	0.218	10.025

Forward and Aft Box Shear

The forward box was cut between elements 24 and 25, and the aft box was cut between elements 54 and 55. The shear was assumed to be zero at these points. Shear deflections of the two cut boxes were then equated, and the shears were found for the cuts.

Table XIX presents the shear distribution on each element due to VQ/I shear for the forward box; Table XX presents this information for the aft box. Column 12 of each table presents the design ultimate shear flow in pounds per inch, and column 13 presents the design shear stress psi. For this calculation, elements 41 and 56 were subdivided to obtain better shear data for the highly loaded spar area. A positive q denotes a clockwise shear flow. The values for elements 25, 55, 56a, 56b, and 57 are the same for both tables.

The following schematic can be referenced for the shear values q_a^o and q_b^o at the cuts.

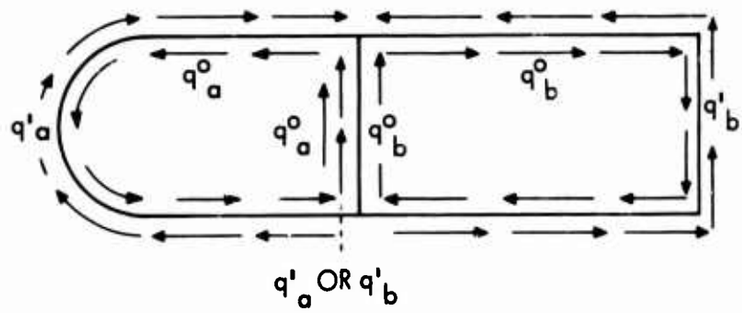

The shear at elements 24 and 25 is assumed to be zero. Then,

$$q'_a \left(\frac{\Delta s}{t}\right)_a - q^o_a \left(\frac{\Delta s}{t}\right)_a - q^o_b \left(\frac{\Delta s}{t}\right)_{ab} = 0 \qquad (61)$$

The shear at elements 54 and 55 is assumed to be zero. Then,

$$q'_b \left(\frac{\Delta s}{t}\right)_b - q^o_b \left(\frac{\Delta s}{t}\right)_b - q^o_a \left(\frac{\Delta s}{t}\right)_{ab} = 0 \qquad (62)$$

TABLE XIX. SHEAR - FORWARD BOX

① Element	② q'_a ⑧ Table XVIII	③ $\Sigma q'_a$	④ $\Sigma q'_{a(avg)}$	⑤ Δs ② Table XV	⑥ t ③ Table XV	⑦ $\Delta s/t$ ⑤ ⑥	⑧ $q'_a \Delta s/t$ ④ x ⑦	⑨ q^o_a	⑩ q_a ④ + ⑨
24	3.788	3.788	1.89	1.12	0.100	11.20	21.17	-15.72	-13.83
23	5.301	9.089	6.44	2.00	0.080	25.00	161.00	-15.72	-9.28
22	3.951	13.040	11.06	2.00	0.060	33.33	368.63	-15.72	-4.66
21	3.859	16.899	14.97	2.00	0.060	33.33	498.95	-15.72	-0.75
20	3.759	20.658	18.78	2.00	0.060	33.33	625.94	-15.72	3.06
19	3.626	24.284	22.47	2.00	0.060	33.33	748.93	-15.72	6.75
18	3.465	27.749	26.02	2.00	0.060	33.33	867.25	-15.72	10.30
17	3.261	31.010	29.38	2.00	0.060	33.33	979.24	-15.72	13.66
16	2.248	33.258	32.13	1.10	0.080	13.75	441.79	-15.72	16.41
15	4.783	38.041	35.65	2.50	0.080	31.25	1114.06	-15.72	19.93
14	3.791	41.832	39.94	2.14	0.100	21.40	854.72	-15.72	24.22
13	1.147	42.979	42.41	2.00	0.100	20.00	848.20	-15.72	26.69
12	-1.401	41.578	42.28	2.80	0.100	28.00	1183.84	-15.72	26.56
11	-1.841	39.737	40.66	1.60	0.100	16.00	650.56	-15.72	24.94
10	-3.466	36.271	38.00	2.13	0.100	21.30	809.40	-15.72	22.28
9	-4.059	32.212	34.24	2.03	0.100	20.30	695.07	-15.72	18.52
8	-4.550	27.662	29.94	2.00	0.100	20.00	598.80	-15.72	14.22
7	-4.893	22.769	25.22	2.00	0.100	20.00	504.40	-15.72	9.50
6	-5.138	17.631	20.20	2.00	0.100	20.00	404.00	-15.72	4.48
5	-5.298	12.333	14.98	2.00	0.100	20.00	299.60	-15.72	-0.74
4	-5.404	6.929	9.63	2.00	0.100	20.00	192.60	-15.72	-6.09
3	-4.607	2.322	4.63	1.40	0.120	11.66	53.99	-15.72	-11.09
2	-5.494	-3.172	-0.42	1.40	0.140	10.00	-4.20	-15.72	-16.14
1	-14.610	-17.782	-10.48	-	-	-	-	-15.72	-26.20
55	-8.810	-26.592	-22.19	1.00	0.150	6.67	-148.01	-36.68	-58.87
56a	-3.412	-30.004	-28.30	3.45	0.120	28.75	-813.62	-36.68	-64.94
56b	6.471	-23.533	-26.77	3.45	0.120	28.75	-769.64	-36.68	-63.45
57	10.025	-13.508	-18.52	0.82	0.120	6.83	-126.49	-36.68	-55.20
25	11.719	-1.789	-7.65	1.36	0.250	5.44	-41.62	-15.72	-23.37
Σ	-	-	-	-	-	606.28	11,018.56	-	-

TABLE XIX. SHEAR - FORWARD BOX

⑤ Δs ② Table XV	⑥ t ③ Table XV	⑦ $\Delta s/t$ ⑤ ⑥	⑧ $q'_a \Delta s/t$ ④ x ⑦	⑨ q^o_a	⑩ q_a ④ + ⑨	⑪ 4.420 x ⑩	⑫ 3.83 x ⑪	⑬ f_s ⑫ / ⑥
1.12	0.100	11.20	21.17	-15.72	-13.83	-61.13	-234.13	-2341
2.00	0.080	25.00	161.00	-15.72	-9.28	-41.02	-157.10	-1965
2.00	0.060	33.33	368.63	-15.72	-4.66	-20.60	-78.89	-1315
2.00	0.060	33.33	498.95	-15.72	-0.75	-3.31	-12.70	-212
2.00	0.060	33.33	625.94	-15.72	3.06	13.53	51.80	863
2.00	0.060	33.33	748.93	-15.72	6.75	29.84	114.27	1905
2.00	0.060	33.33	867.25	-15.72	10.30	45.53	174.37	2906
2.00	0.060	33.33	979.24	-15.72	13.66	60.38	231.25	3854
1.10	0.080	13.75	441.79	-15.72	16.41	72.53	277.80	3472
2.50	0.080	31.25	1114.06	-15.72	19.93	88.09	337.39	4217
2.14	0.100	21.40	854.72	-15.72	24.22	107.05	410.02	4100
2.00	0.100	20.00	848.20	-15.72	26.69	117.97	451.84	4518
2.80	0.100	28.00	1183.84	-15.72	26.56	117.40	449.63	4496
1.60	0.100	16.00	650.56	-15.72	24.94	110.23	422.21	4222
2.13	0.100	21.30	809.40	-15.72	22.28	98.48	377.18	3772
2.03	0.100	20.30	695.07	-15.72	18.52	81.86	313.53	3135
2.00	0.100	20.00	598.80	-15.72	14.22	62.85	240.73	2407
2.00	0.100	20.00	504.40	-15.72	9.50	41.99	160.83	1608
2.00	0.100	20.00	404.00	-15.72	4.48	19.80	75.84	758
2.00	0.100	20.00	299.60	-15.72	-0.74	-3.27	-12.53	-125
2.00	0.100	20.00	192.60	-15.72	-6.09	-26.92	-103.10	-269
1.40	0.120	11.66	53.99	-15.72	-11.09	-49.02	-187.74	-1564
1.40	0.140	10.00	-4.20	-15.72	-16.14	-71.34	-273.23	-1952
-	-	-	-	-15.72	-26.20	-115.80	-443.54	-
1.00	0.150	6.67	-148.01	-36.68	-58.87	-260.21	-996.61	-
3.45	0.120	28.75	-813.62	-36.68	-64.94	-287.03	-1099.37	-9161
3.45	0.120	28.75	-769.64	-36.68	-63.45	-280.45	-1074.15	-8951
0.82	0.120	6.83	-126.49	-36.68	-55.20	-243.98	-934.48	-
1.36	0.250	5.44	-41.62	-15.72	-23.37	-103.30	-395.63	-1582
-	-	606.28	11,018.56	-	-	-	-	-

TABLE XX. SHEAR - AFT BOX

① Element	② q' ⑧ Table XVIII	③ $\Sigma q'$	④ $\Sigma q'_{avg}$	⑤ Δs ② Table XV	⑥ t ③ Table XV	⑦ $\Delta s/t$ ⑤/⑥	⑧ $q' \Delta s/t$ ④ x ⑦	⑨ q_{sa}	⑩ $q' + q_{sa}$ ④ + ⑨	⑪ 4.420 x ⑩	⑫ 3.83 x
54	-3.584	-3.585	-1.79	1.10	0.120	9.17	-16.41	20.96	19.17	84.73	324
53	-5.468	-9.053	-6.32	2.00	0.100	20.00	-126.40	20.96	14.64	64.71	247
52	-5.463	-14.516	-11.78	2.00	0.100	20.00	-235.60	20.96	9.18	40.58	155
51	-5.373	-19.889	-17.20	2.00	0.100	20.00	-344.00	20.96	3.76	16.62	63
50	-5.271	-25.160	-22.52	2.00	0.100	20.00	-450.40	20.96	-1.56	-6.90	-26
49	-5.127	-30.287	-27.72	2.00	0.100	20.00	-554.40	20.96	-6.76	-29.88	-114
48	-4.955	-35.242	-32.76	2.00	0.100	20.00	-655.20	20.96	-11.80	-52.16	-199
47	-4.768	-40.010	-37.63	2.00	0.100	20.00	-752.60	20.96	-16.67	-73.68	-282.
46	-4.557	-44.567	-42.29	2.00	0.100	20.00	-845.80	20.96	-21.33	-94.28	-361.
45	-4.311	-48.878	-46.72	2.00	0.100	20.00	-934.40	20.96	-25.76	-113.86	-436.
44	-3.090	-51.968	-50.42	1.25	0.120	10.42	-525.38	20.96	-29.46	-130.21	-498.
43	-3.055	-55.023	-53.50	1.25	0.120	10.42	-557.47	20.96	-32.54	-143.83	-550.
42	-3.786	-58.809	-56.92	1.66	0.120	13.83	-787.20	20.96	-35.96	-158.94	-608.
41b	-1.728	-60.537	-59.67	2.31	0.120	19.25	-1148.65	20.96	-38.71	-171.10	-655.
41a	2.674	-57.863	-59.20	2.31	0.120	19.25	-1139.60	20.96	-38.24	-169.02	-647.
40	6.640	-51.223	-54.54	0.80	0.120	6.66	-363.24	20.96	-33.58	-148.42	-568.
39	6.150	-45.073	-48.15	-	-	-	-	20.96	-27.19	-120.18	-460.
38	2.832	-42.241	-43.66	1.25	0.100	12.50	-545.75	20.96	-22.70	-100.33	-384.
37	4.753	-37.488	-39.86	2.80	0.070	40.00	-1594.40	20.96	-18.90	-83.54	-319.
36	3.081	-34.407	-35.95	2.00	0.060	33.33	-1198.21	20.96	-14.99	-66.26	-253.
35	3.232	-31,175	-32.79	2.00	0.060	33.33	-1092.89	20.96	-11.83	-52.29	-200.
34	3.375	-27,800	-29.49	2.00	0.060	33.33	-982.90	20.96	-8.53	-37.70	-144.
33	3.506	-24,294	-26.05	2.00	0.060	33.33	-868.25	20.96	-5.09	-22.50	-86.
32	3.608	-20,686	-22.49	2.00	0.060	33.33	-749.59	20.96	-1.53	-6.76	-25.
31	3.731	-16.955	-18.82	2.00	0.060	33.33	-627.27	20.96	2.14	9.46	36.
30	3.805	-13,150	-15.05	2.00	0.060	33.33	-501.62	20.96	5.91	26.12	100.
29	3.889	-9.261	-11.21	2.00	0.060	33.33	-373.63	20.96	9.75	43.10	165.
28	3.935	-5.326	-7.29	2.00	0.060	33.33	-242.98	20.96	13.67	60.42	231.
27	2.924	-2.402	-3.86	1.10	0.080	13.75	-53.08	20.96	17.10	75.58	289.
26	4.064	1.662	-0.37	1.20	0.100	12.00	-4.44	20.96	20.59	91.01	348.
25	11.719	13.381	7.52	-	-	-	-	20.96	28.48	-	-
57	10.025	23.406	18.39	0.82	0.120	6.83	125.60	36.68	55.07	-	-
56b	6.471	29.877	26.64	3.45	0.120	28.75	765.90	36.68	63.32	-	-
56a	-3.412	26.465	28.17	3.45	0.120	28.75	809.89	36.68	64.85	-	-
55	-8.811	17.654	22.06	1.00	0.150	6.67	147.14	36.68	58.74	-	-
	-	-	-	1.10	0.150	7.33	129.40	-	-	-	-
Σ	+17.654	-	-	-	-	725.55	-16,293.83	-	-	-	-

A

TABLE XX. SHEAR - AFT BOX

③ $\Sigma q'$	④ $\Sigma q'_{avg}$	⑤ Δs ②Table XV	⑥ t ③Table XV	⑦ $\Delta s/t$ ⑤/⑥	⑧ $q' \Delta s/t$ ④ x ⑦	⑨ q_{sa}	⑩ $q' + q_{sa}$ ④ + ⑨	⑪ 4.420 x ⑩	⑫ 3.83 x ⑪	⑬ f_s ⑫ /⑥
3.585	-1.79	1.10	0.120	9.17	-16.41	20.96	19.17	84.73	324.53	2704
9.053	-6.32	2.00	0.100	20.00	-126.40	20.96	14.64	64.71	247.84	2478
14.516	-11.78	2.00	0.100	20.00	-235.60	20.96	9.18	40.58	155.41	1554
19.889	-17.20	2.00	0.100	20.00	-344.00	20.96	3.76	16.62	63.65	636
25.160	-22.52	2.00	0.100	20.00	-450.40	20.96	-1.56	-6.90	-26.41	-264
30.287	-27.72	2.00	0.100	20.00	-554.40	20.96	-6.76	-29.88	-114.44	-1144
35.242	-32.76	2.00	0.100	20.00	-655.20	20.96	-11.80	-52.16	-199.76	-1998
40.010	-37.63	2.00	0.100	20.00	-752.60	20.96	-16.67	-73.68	-282.21	-2822
44.567	-42.29	2.00	0.100	20.00	-845.80	20.96	-21.33	-94.28	-361.10	-3611
48.878	-46.72	2.00	0.100	20.00	-934.40	20.96	-25.76	-113.86	-436.09	-4361
51.968	-50.42	1.25	0.120	10.42	-525.38	20.96	-29.46	-130.21	-498.73	-4156
55.023	-53.50	1.25	0.120	10.42	-557.47	20.96	-32.54	-143.83	-550.87	-4591
58.809	-56.92	1.66	0.120	13.83	-787.20	20.96	-35.96	-158.94	-608.77	-5073
60.537	-59.67	2.31	0.120	19.25	-1148.65	20.96	-38.71	-171.10	-655.32	-5461
57.863	-59.20	2.31	0.120	19.25	-1139.60	20.96	-38.24	-169.02	-647.36	-5396
51.223	-54.54	0.80	0.120	6.66	-363.24	20.96	-33.58	-148.42	-568.48	-4737
45.073	-48.15	-	-	-	-	20.96	-27.19	-120.18	-460.30	-
42.241	-43.66	1.25	0.100	12.50	-545.75	20.96	-22.70	-100.33	-384.29	-3843
37.488	-39.86	2.80	0.070	40.00	-1594.40	20.96	-18.90	-83.54	-319.96	-4571
34.407	-35.95	2.00	0.060	33.33	-1198.21	20.96	-14.99	-66.26	-253.77	-4230
31,175	-32.79	2.00	0.060	33.33	-1092.89	20.96	-11.83	-52.29	-200.27	-3338
27,800	-29.49	2.00	0.060	33.33	-982.90	20.96	-8.53	-37.70	-144.40	-2407
24,294	-26.05	2.00	0.060	33.33	-868.25	20.96	-5.09	-22.50	-86.17	-1436
20,686	-22.49	2.00	0.060	33.33	-749.59	20.96	-1.53	-6.76	-25.90	-432
16.955	-18.82	2.00	0.060	33.33	-627.27	20.96	2.14	9.46	36.23	604
13,150	-15.05	2.00	0.060	33.33	-501.62	20.96	5.91	26.12	100.05	1668
9.261	-11.21	2.00	0.060	33.33	-373.63	20.96	9.75	43.10	165.06	2751
5.326	-7.29	2.00	0.060	33.33	-242.98	20.96	13.67	60.42	231.42	3857
2.402	-3.86	1.10	0.080	13.75	-53.08	20.96	17.10	75.58	289.49	3618
1.662	-0.37	1.20	0.100	12.00	-4.44	20.96	20.59	91.01	348.57	3486
13.381	7.52	-	-	-	-	20.96	28.48	-	-	-
13.406	18.39	0.82	0.120	6.83	125.60	36.68	55.07	-	-	-
19.877	26.64	3.45	0.120	28.75	765.90	36.68	63.32	-	-	-
23.465	28.17	3.45	0.120	28.75	809.89	36.68	64.85	-	-	-
17.654	22.06	1.00	0.150	6.67	147.14	36.68	58.74	-	-	-
-	-	1.10	0.150	7.33	129.40	-	-	-	-	-
-	-	-	-	725.55	-16,293.83	-	-	-	-	-

By substituting previously calculated values for the unknowns in Equations (61) and (62), we can solve for q^o by solving Equations (63) and (64) simultaneously.

$$11,019 - 606.3\, q^o_a - 71.00\, q^o_b = 0 \qquad (63)$$

$$16,294 - 725.5\, q^o_b - 71.00\, q^o_a = 0 \qquad (64)$$

$$q^o_a = 15.72$$

$$q^o_b = 20.96$$

Shear Center

The detail calculations required to determine the shear center are presented in Table XXI. These calculations involve summing the moments of the shear flows about the cg of the wing section.

TABLE XXI. SHEAR CENTER

① Element	② q	③ q_{vert}	④ q_{horiz}	⑤ Δs ②Table XV	⑥ V_{vert} ③ x ⑤	⑦ V_{horiz} ④ x ⑤	⑧ x ⑨Table XV	⑨ y ⑩Table XV	⑩ M_x ⑥ x ⑧	⑪ M_y ⑦x ⑨
1	-26.20	0	-26.20	1.50	0	-39.3	-2.22	4.19	0	-165
2	-16.14	0	-16.14	1.40	0	-22.6	-3.52	4.14	0	-94
3	-11.09	0	-11.09	1.40	0	-15.5	-4.90	4.09	0	-63
4	-6.09	0	-6.09	2.00	0	-12.2	-6.62	4.08	0	-50
5	-0.74	0	-0.74	2.00	0	- 1.5	-8.65	4.06	0	-6
6	4.48	0	4.48	2.00	0	9.0	-10.60	4.00	0	36
7	9.50	0.80	9.50	2.00	1.6	19.0	-12.62	3.88	-20	73
8	14.22	2.00	14.00	2.00	4.0	28.0	-14.64	3.69	-59	103
9	18.52	4.20	18.20	2.03	8.4	36.4	-16.62	3.35	-140	122
10	22.28	6.60	21.40	2.13	14.1	45.6	-18.62	2.87	-263	131
11	24.94	9.10	23.30	1.60	14.6	37.3	-20.36	2.23	-297	83
12	26.56	13.00	22.90	2.80	36.4	64.1	-22.32	1.35	-812	87
13	26.69	23.00	13.20	2.00	46.0	26.4	-24.03	-0.15	-1105	-4
14	24.22	18.30	-15.60	2.14	39.2	-33.4	-23.94	-1.88	-938	63
15	19.93	5.70	-19.20	2.50	14.2	-48.0	-21.88	-2.83	-311	136
16	16.41	3.10	-16.00	1.10	3.4	-17.6	-20.12	-3.11	-68	55
17	13.66	2.20	-13.40	2.00	4.4	-26.8	-18.59	-3.39	-82	91
18	10.30	1.50	-10.20	2.00	3.0	-20.4	-16.62	-3.69	-50	75
19	6.75	0.80	-6.65	2.00	1.6	-13.3	-14.64	-3.94	-23	52
20	3.06	0.30	-3.02	2.00	0.6	-6.0	-12.62	-4.16	-8	25

TABLE XXI - Continued

① Element	② q	③ q_{vert}	④ q_{horiz}	⑤ Δs ② Table XV	⑥ V_{vert} ③ x ⑤	⑦ V_{horiz} ④ x ⑤	⑧ x ⑨ Table XV	⑨ y ⑩ Table XV	⑩ M_x ⑥ x ⑧	⑪ M_y ⑦ x ⑨
21	-0.75	-0.10	0.75	2.00	-0.2	1.5	-10.64	-4.33	2	-6
22	-4.66	-0.30	4.60	2.00	-0.6	9.2	-8.64	-4.50	5	-41
23	-9.28	-0.40	9.25	2.00	-0.8	18.5	-6.62	-4.59	5	-85
24	-13.83	0	13.80	1.12	0	15.5	5.04	-4.73	0	-73
25	-23.37	0	23.35	1.36	0	31.8	-3.82	-4.86	0	-155
26	-20.59	0	-20.59	1.20	0	-24.7	-2.53	-4.81	0	119
27	17.10	0	-17.10	1.10	0	-18.8	-1.32	-4.75	0	89
28	13.67	0	-13.67	2.00	0	-27.3	0.32	-4.73	0	129
29	9.75	-0.10	-9.75	2.00	-0.2	-19.5	2.25	-4.73	-1	92
30	5.91	-0.10	-5.90	2.00	-0.2	-11.8	4.33	-4.69	-1	55
31	2.14	-0.10	-2.14	2.00	-0.2	-4.3	6.33	-4.66	-1	20
32	-1.53	0.10	1.50	2.00	0.2	3.0	8.33	-4.57	2	-14
33	-5.09	0.20	5.05	2.00	0.4	10.1	10.33	-4.50	5	-45
34	-8.53	0.40	8.50	2.00	0.8	17.0	12.30	-4.40	10	-75
35	-11.83	0.30	11.80	2.00	1.6	23.6	14.30	-4.28	23	-101
36	-14.99	0.90	14.95	2.00	1.8	29.9	16.30	-4.16	29	-124
37	-18.90	1.20	18.80	2.80	3.4	52.6	18.68	-4.02	64	-211
38	-22.70	0	22.60	1.25	0	28.2	20.72	-3.85	0	-109
39	-27.19	0	27.10	1.33	0	36.0	22.00	-3.95	0	-142
40	-33.56	-	-	-	26.9	46.0	21.60	-3.59	581	165
41a	-38.24	38.00	-3.50	2.31	87.8	-8.1	20.86	-1.98	1832	16
41b	-38.71	38.50	-3.50	2.31	88.9	-8.1	20.62	0.32	1831	-3
42	-35.96	-	-	-	30.6	-28.0	20.26	2.17	620	-62
43	-32.54	0	-32.54	1.25	0	-40.6	18.96	2.40	0	-97
44	-29.46	4.00	-29.40	1.25	5.0	-36.7	17.80	2.47	87	-91
45	-25.76	3.00	-25.70	2.00	6.0	-51.4	16.18	2.65	97	-136
46	-21.33	2.50	-21.30	2.00	5.0	-42.6	14.29	2.88	71	-123
47	-16.67	1.70	-16.65	2.00	3.4	-33.3	12.26	3.09	42	-103
48	-11.80	1.00	-11.80	2.00	2.0	-23.6	10.29	3.28	21	-77
49	-6.76	.60	-6.75	2.00	1.2	-13.5	8.29	3.46	10	-47
50	-1.56	.10	-1.55	2.00	0.2	-3.1	6.30	3.62	1	-11
51	3.76	-0.20	3.75	2.00	-0.4	7.5	4.30	3.75	-2	28
52	9.18	-0.50	9.15	2.00	-1.0	18.3	2.34	3.87	-2	71
53	14.64	-0.10	14.60	2.00	-0.2	29.2	0.34	3.93	0	115
54	19.17	0	19.17	1.10	0	21.1	-1.19	3.95	0	83
55	-58.87	-	-	-	58.9	39.6	-2.60	3.72	-153	147
56a	-64.94	64.94	0	3.45	224.0	0	-2.95	1.27	-661	0
56b	-63.45	63.45	0	3.45	218.9	0	-2.95	-2.17	-646	0
57	-55.20	-	-	-	45.3	39.6	-3.57	-4.53	-162	-179
Σ	-	-	-	-	+1000.0	0.0	-	-	-465	-231

Next, the shear center distance from the wing section cg is determined by adding the M_X and M_Y values in columns 10 and 11 of Table XXI and dividing by the 1000-pound shear load.

The bending moment M is calculated as follows:

$$M = -M_X + M_Y$$

$$= 465 - 231$$

$$= 234 \text{ in.-lb} \curvearrowleft \quad (65)$$

The shear center is calculated to be a distance Δx from the cg as follows:

$$\Delta x = \frac{234}{1000}$$

$$= 0.234 \text{ in. left or forward of cg}$$

Torque Distribution

The torsional shear distribution between the forward and aft cells is calculated below. Note that these calculations show that the torsional shear flow q, in pounds per inch, is about equal in both cells.

The schematic in this section represents a cross section of test wing No. 2. The shear flow q, in pounds per inch, for the specimen is indicated by the arrows, and the cell sections are labeled α and β. The parameters needed for the torque distribution calculations are given in Equations (66) through (70), and the calculations follow.

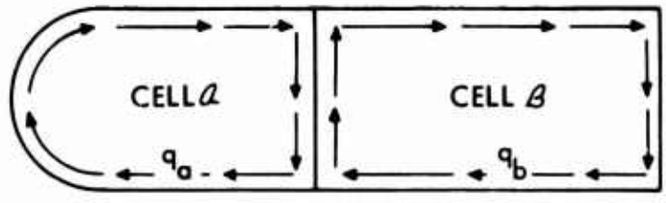

$$A_a = 157 \text{ in.}^2 \quad (66)$$

$$\left(\frac{\Delta s}{t}\right)_a = 606 \quad (67)$$

$$A_b = 193 \text{ in.}^2 \tag{68}$$

$$\left(\frac{\Delta s}{t}\right)_b = 726 \tag{69}$$

$$\left(\frac{\Delta s}{t}\right)_{ab} = 71 \tag{70}$$

For the torque distribution calculations, the angle of deflection ϕ_a for cell $\mathcal{A}$ is equal to the angle of deflection ϕ_b for cell $\mathcal{B}$. Then,

$$\frac{q_a\left(\frac{\Delta s}{t}\right)_a - q_b\left(\frac{\Delta s}{t}\right)_{ab}}{2A_a} = \frac{q_b\left(\frac{\Delta s}{t}\right)_b - q_a\left(\frac{\Delta s}{t}\right)_{ab}}{2A_b} \tag{71}$$

By substituting the appropriate parameters in Equations (66) through (70) into Equation (71), Equation (72) results.

$$\frac{606q_a - 71q_b}{314} = \frac{726q_b - 71q_a}{386} \tag{72}$$

By solving Equation (72) for q_a in terms of q_b, we find that

$$1.930q_a - 0.226q_b = 1.881q_b - 0.184q_a \tag{73}$$

Then,

$$1.704q_a = 1.697q_b$$

and

$$q_a = 0.996q_b \tag{74}$$

To solve for q_a or q_b when T = 1000 in.-lb,

$$2A_aq_a + 2A_bq_b = 1000 \tag{75}$$

By substituting Equations (66) and (68) into Equation (75), Equation (76) is derived.

$$314q_a + 386q_b = 1000 \tag{76}$$

By substituting Equation (74) into Equation (76), we solve for q_b.

$$314 \times 0.996q_b + 386q_b = 1000$$

$$699q_b = 1000$$

$$q_b = 1.43 \qquad (77)$$

We solve for q_a using the equality in Equation (74).

$$q_a = 0.996 \times 1.43$$

$$q_a = 1.43 \qquad (78)$$

Since $\phi_a = \phi_b$, we can use either side of Equation (71) to solve for the angle of deflection by substituting the appropriate unknown from Equation (71) or (78) into Equation (71).

$$\phi_a = \phi_b = \frac{606 \times 1.43 - 71 \times 1.43}{314} \times \frac{L}{G}$$

$$= 2.44\ L/G \text{ (radians per 1000 in.-lb torque)}$$

where L = length between reinforcement, inches

G = shear modulus, psi

Summary of Bending and Shear Stresses

The bending and shear stresses on each element for the various test loading conditions are summarized in Table XXII.

TABLE XXII. SUMMARY OF BENDING AND SHEAR STRESSES

① Element	② f_b ⑪ Table XVII	③ q V = 16,925	④ q T = 38,500	⑤ q ③ + ④	⑥ q T = 186,000	⑦ t ③ Table XV	⑧ f_s ③ ⑦	⑨ f_s ⑤ ⑦	⑩ f_s ⑥ ⑦
1	-32,915	-443.54	55.06	-388.48	265.94	-	-	-	-
2	-32,222	-273.23	55.06	-218.17	265.94	0.140	-1952	-1558	1900
3	-31,513	-187.74	55.06	-132.68	265.94	0.120	-1564	-1106	2216
4	-31,050	-103.10	55.06	-48.04	265.94	0.100	-269	-480	2659
5	-30,433	-12.53	55.06	-42.53	265.94	0.100	-125	-425	2659
6	-29,514	75.84	55.06	130.90	265.94	0.100	758	1309	2659
7	-28,105	160.83	55.06	215.89	265.94	0.100	1608	2159	2659
8	-26,140	240.73	55.06	295.79	265.94	0.100	2407	2958	2659
9	-22,980	313.53	55.06	368.59	265.94	0.100	3135	3686	2659
10	-18,702	377.18	55.06	432.24	265.94	0.100	3772	4322	2659
11	-13,210	422.21	55.06	477.27	265.94	0.100	4222	4773	2659
12	-5,753	449.63	55.06	504.69	265.94	0.100	4496	5047	2659
13	6,591	451.84	55.06	506.90	265.94	0.100	4518	5069	2659
14	20,368	410.02	55.06	465.08	265.94	0.100	4100	4651	2659
15	27,480	337.39	55.06	392.45	265.94	0.080	4217	4906	3324
16	29,319	277.80	55.06	332.86	265.94	0.080	3472	4161	3324
17	31,207	231.25	55.06	286.31	265.94	0.060	3854	4772	4432
18	33,160	174.37	55.06	229.43	265.94	0.060	2906	3824	4432
19	34,704	114.27	55.06	169.33	265.94	0.060	1905	2822	4432
20	36,006	51.80	55.06	106.86	265.94	0.060	863	1781	4432
21	36,917	-12.70	55.06	42.36	265.94	0.060	-212	706	4432
22	37,825	-78.89	55.06	-23.83	265.94	0.060	-1315	-397	4432
23	38,086	-157.10	55.06	-102.04	265.94	0.080	-1965	-1275	3324
24	38,852	-234.13	55.06	-179.07	265.94	0.100	-2341	-1791	2659
25	39,614	-395.63	55.06	-340.57	265.94	0.250	-1582	-1362	1064
26	38,920	348.57	55.06	403 63	265.94	0.100	3486	4036	2659
27	38,174	289.49	55.06	344.55	265.94	0.080	3618	4307	3324
28	37,645	231.42	55.06	286.48	265.94	0.060	3857	4775	4432
29	37,212	165.06	55.06	220.12	265.94	0.060	2751	3669	4432
30	36,427	100.05	55.06	155.11	265.94	0.060	1668	2585	4432
31	35,738	36.23	55.06	91.29	265.94	0.060	604	1521	4432
32	34,573	-25.90	55.06	29.16	265.94	0.060	-432	486	4432
33	33,562	-86.17	55.06	-31.11	265.94	0.060	-1436	-518	4432
34	32,325	-144.40	55.06	-89.34	265.94	0.060	-2407	-1489	4432
35	30,916	-200.27	55.06	-145.21	265.94	0.060	-3338	-2420	4432
36	29,510	-253.77	55.06	-198.71	265.94	0.060	-4230	-3312	4432
37	27,863	-319.96	55.06	-264.90	265.94	0.070	-4571	-4415	3799
38	26,048	-384.29	55.06	-329.23	265.94	0.100	-3843	-3292	2659
39	26,557	-460.30	55.06	-405.24	265.94	-	-	-	-
40	23,773	-568.48	55.06	-513.42	265.94	0.120	-4737	-4278	2216
41a	11,103	-647.36	55.06	-592.30	265.94	0.120	-5396	-4936	2216
41b	-7,181	-655.32	55.06	-600.26	265.94	0.120	-5461	-5002	2216
42	-21,854	-608.77	55.06	-553.71	265.94	0.120	-5073	-4614	2216
43	-23,397	-550.87	55.06	-495.81	265.94	0.120	-4591	-4132	2216

TABLE XXII - Continued

① Element	② f_b ⑬ Table XVII	③ q V = 16,925	④ q T = 38,500	⑤ q ③ + ④	⑥ q T = 186,00	⑦ t ③ Table XV	⑧ f_s ③ ⑦	⑨ f_s ⑤ ⑦	⑩ f_s ⑥ ⑦
44	-23,696	-498.73	55.06	-443.67	265.94	0.120	-4156	-3697	2216
45	-24,765	-436.09	55.06	-381.03	265.94	0.100	-4361	-3810	2659
46	-26,174	-361.10	55.06	-306.04	265.94	0.100	-3611	-3060	2659
47	-27,392	-282.21	55.06	-227.15	265.94	0.100	-2822	-2272	2659
48	-28,465	-199.76	55.06	-144.70	265.94	0.100	-1998	-1447	2659
49	-29,453	-114.44	55.06	-59.38	265.94	0.100	-1144	-594	2659
50	-30,280	-26.41	55.06	28.65	265.94	0.100	-264	286	2659
51	-30,870	63.65	55.06	118.71	265.94	0.100	636	1187	2659
52	-31,383	155.41	55.06	210.47	265.94	0.100	1554	2105	2659
53	-31,414	247.84	55.06	302.90	265.94	0.100	2478	3029	2659
54	-31,230	324.53	55.06	379.59	265.94	0.120	2704	2216	2216
55	-29,081	-996.61	0	-996.61	0	-	-	-	-
56a	-9,464	-1099.37	0	-1099.37	0	0.120	-9161	-9161	0
56b	17,967	-1074.15	0	-1074.15	0	0.120	-8951	-8951	0
57	36,921	-934.48	0	-934.48	0	-	-	-	-

STRESS ANALYSIS

Stiffener design, shear web design, bearing stress calculations, and torsion bending deflection calculations for the No. 2 wing test section are presented in this subsection.

Transverse Stiffeners

Assume simple support along the spar edges. This assumption is conservative, but based on the first wing test results it appears realistic.

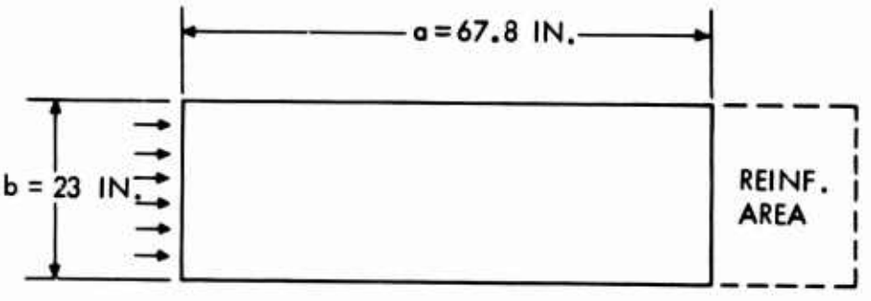

The basic stability formula is used, where

$$\sigma_{cr} = K \frac{Et^2}{b^2} \quad \text{or} \quad \sigma_{cr} = K_1 \frac{\pi^2 E}{12(1-\mu^2)} \frac{t^2}{b^2} \tag{79}$$

where $K_1 = 4.0$

$K = 3.64$

The value of K is adjusted for the value of $\pi^2/12(1-\mu^2)$.

$$K = 0.91\ K_1$$

Then consider the first wing:

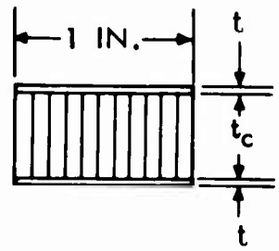

First relate the sandwich EI to an equivalent solid plate:

$$EI = 2Et\left(\frac{t_c + t}{2}\right)^2 = \frac{E' t'^3}{12} \tag{80}$$

and

$$EA = 2Et = E't' \tag{81}$$

From Equation (81), we see that

$$E' = \frac{2Et}{t'} \tag{82}$$

By substituting Equation (82) into Equation (80), we derive Equation (83).

$$\frac{Et\,(t_c + t)^2}{2} = \frac{2Et}{t'} \times \frac{t'^3}{12} \tag{83}$$

Then solving for t' and E',

$$t' = \sqrt{3}\,(t_c + t) \tag{84}$$

and

$$E' = \frac{2Et}{\sqrt{3}\,(t_c + t)} \tag{85}$$

When t = 0.03 (both faces), the values for Equation (84) and (85) are as follows:

$$t' = 1.73\ (0.500 + 0.030)$$

$$= 0.917 \tag{86}$$

and

$$E' = \frac{2 \times 3,000,000 \times 0.030}{0.917} \tag{87}$$

$$= 196,000$$

Substitute the values from Equations (86) and (87) into Equation (79) and solve.

$$\sigma_{cr} = \frac{3.64 \times 196,000 \times \overline{0.917}^2}{\overline{23}^2} \tag{88}$$

$$= 1130 \text{ (based on } t')$$

or

$$= 1130 \times 0.917/0.060 \text{ (based on } t)$$

$$= 17,300 \text{ psi}$$

By relating the test results where buckling was noticeable at 40 percent DUL, we can solve for the test value of σ_{cr}.

$$0.40 \times 40,000 = 16,000 \text{ psi}$$

We see that this corresponds closely to the calculated value in Equation (88), where a value of 17,300 psi was determined.

By comparing Equations (86) through (88) with Equations (89) through (91), it becomes evident that increasing skin t does not appreciably increase the critical buckling stress.

Solve Equations (84), (85), and (79), when t = 0.05:

$$t' = 1.73\ (0.500 + 0.050) \tag{89}$$

$$= 0.950$$

$$E' = 2 \times 0.050 \times \frac{3,000,000}{0.950} \tag{90}$$

$$= 316,000$$

$$\sigma_{cr} = \frac{3.64 \times 316,000 \times \overline{0.95}^2}{\overline{23}^2} \tag{91}$$

$$= 1950 \text{ (based on } t')$$

$$= 1950 \times 0.95/0.10 \text{ (based on t)}$$

$$= 18,500 \text{ psi}$$

Thus, it is desirable to add stiffeners to the panel to reduce the size of the buckle pattern until the panel does not buckle up to compression ultimate stress, which is calculated to be 32,900 psi.

Both longitudinal and transverse stiffeners were considered. The longitudinal stiffeners would pick up a portion of the bending load as well as stiffen the skin. The transverse stiffeners only provide stiffening. Transverse stiffeners were selected for incorporation into the design of the No. 2 wing test section.

The basic parameter in stiffener design involves skin and stiffener bending and torsion ratios. It is desirable that the stiffener provide a simple support for bending and no rotation for torsion. As this is rather impractical, an in-between support condition will be used.

The basic curves for this analysis are found in NACA TN 3782.[7] Assuming a/b ratio of 0.5 where

a = stiffener spacing

b = panel width = 23 inches

the important parameters are

$$\frac{EI}{bD} \text{ and } \frac{GJ}{EI}$$

where EI = stiffener bending stiffness

bD = skin bending stiffness

GJ = stiffener torsional stiffness

Stiffener Properties

The following sketch is a schematic representation of the stiffener.

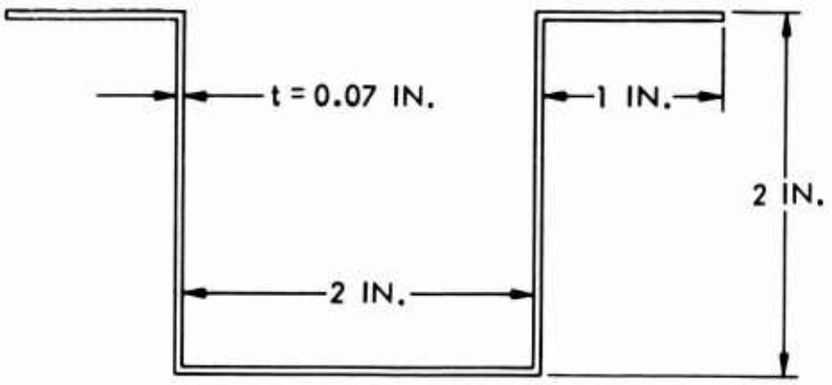

The moment of inertia I for the stiffener is calculated as follows:

$$I = 2\left(0.14 \times \bar{1}^2 + \frac{0.07 \times \bar{2}^3}{12}\right)$$

$$= 0.327 \text{ in.}^4 \tag{92}$$

The cross-sectional area A of the stiffener is

$$A = 8 \times 0.07$$

$$= 0.56 \text{ in.}^2 \tag{93}$$

The polar moment of inertia J is calculated as follows:

$$J = 2I = 2 \times 0.327$$

$$= 0.654 \text{ in.}^4 \tag{94}$$

Skin Properties

The skin bending stiffness per inch D is

$$D = \frac{E' t'^3}{12}$$

$$= \frac{316,000 \times \overline{0.950}^3}{12}$$

$$= 22,500 \qquad (95)$$

Combined Properties

The ratio of the stiffener bending stiffness to the skin bending stiffness is

$$\frac{EI}{bD} = \frac{3,000,000 \times 0.327}{23.0 \times 22,500}$$

$$= 1.90 \qquad (96)$$

The ratio of the stiffener torsional stiffness to the stiffener bending stiffness is

$$\frac{GJ}{EI} = \frac{800,000 \times 0.654}{3,000,000 \times 0.327} \qquad (97)$$

$$= 0.533$$

By applying the calculated values for EI/bD and GJ/EI to the graph given in Figure 13 of NACA TN 3782,[7] we arrive at a value of 7.8 for K. The stiffeners will therefore increase the buckling stress calculated on page 142 by a ratio of K equal to 7.8/4.0, or 1.95.

The resulting calculated buckling stress will then be

$$\sigma_{cr} = 18,500 \times 1.95$$

$$= 36,000 \text{ psi} \qquad (98)$$

The maximum compression stress in the upper skin at DUL is 32,900 psi. Then the margin of safety is

$$MS = \frac{36,000}{32,900} - 1 = 0.09 \tag{99}$$

Short Panel Buckling

As a check of the buckling criteria, the skin between stiffeners will be checked as a column. This is conservative, as edge support is neglected. Then the following are true:

$$E' = 316,000 \tag{100}$$

$$t' = 0.95 \tag{101}$$

$$I = \overline{0.95}^3/12 = 0.0714 \tag{102}$$

$$A = 0.95 \tag{103}$$

$$\rho = \sqrt{I/A} = \sqrt{\frac{0.0714}{0.95}} = 0.274 \tag{104}$$

$$L/\rho = \frac{11.5}{0.274} = 42 \tag{105}$$

In considering pinned ends, we find the following:

$$\sigma_{cr} = \frac{\pi^2 E}{(L/\rho)^2} \tag{106}$$

Substitute and solve for σ_{cr}.

$$\sigma_{cr} = \frac{\pi^2 \times 316,000}{\overline{42}^2}$$

$$\sigma_{cr} = 1780 \text{ (based on } t')$$

$$= 1780 \times 0.95/0.10 \text{ (based on t)}$$

$$= 16,900 \text{ psi}$$

The stiffener, if torsionally rigid, would provide fixed ends with a factor of 4 over pinned ends. An in-between condition for end fixity of 2.0 is assumed.

Then σ_{cr} becomes

$$\sigma_{cr} = 16,900 \times 2.0$$

$$= 34,000 \text{ psi}$$

Spar Web Shear Analysis

The spar web is of sandwich construction with a 0.50-inch core and 0.060-inch skins for each face. The 0.060-inch skin thickness makes use of two plies of 481 cloth at ±45-degree orientation and four plies of 0- to 90-degree orientation.

For these two orientations, shear moduli G and shear strengths F_s are approximately as follows:

$$0 - 90^{o} \ldots\ldots G = 0.7 \times 10^{6} \text{ psi} \qquad F_s = 12,000 \text{ psi} \tag{107}$$

$$\pm 45^{o} \ldots\ldots G = 1.4 \times 10^{6} \text{ psi} \qquad F_s = 22,000 \text{ psi} \tag{108}$$

Then for the composite:

$$\Sigma Gt = (2 \times 1.4 + 4 \times 0.7)\, 0.01 \times 10^{6} = 5.6 \times 0.01 \times 10^{6} \tag{109}$$

The maximum shear flow q in the spar is 1099 pounds per inch. Therefore, the shear flow in each of the orientations is as follows:

$$(0 - 90^{o})\ q = (1099/5.6) \times 2.8 = 550 \text{ lb/in.} \tag{110}$$

$$(\pm 45^{o})\ q = (1099/5.6) \times 2.8 = 550 \text{ lb/in.} \tag{111}$$

The shear stresses are

$$(0 - 90^{o})\ f_S = 550/(4 \times 0.01 \times 2) = 6870 \text{ psi} \quad (112)$$

$$(\pm 45^{o})\ f_S = 550/(2 \times 0.01 \times 2) = 13,740 \text{ psi} \quad (113)$$

Assuming a constant relationship to failure between G's in the two orientations, the margins of safety are

$$(0 - 90^{o})\ MS = \frac{12,000}{6870} - 1 = +0.74 \quad (114)$$

$$(\pm 45^{o})\ MS = \frac{22,000}{13,740} - 1 = +0.60 \quad (115)$$

Bolt Bearing Design

The basic criteria determining the bearing thicknesses required at the center and rear spar bolted connections are summarized as follows:

1. Spar shear for the center spar is 934 lb/in.
2. Spar shear for the aft spar is 406 lb/in.
3. The 3/16-in. screws have a 0.080-in. countersink depth, and the 1/4-in. screws in the center spar caps have a countersink depth of 0.106 in. These areas will not be considered as bearing areas.
4. The bearing allowable is set at 40,000 psi. A t/d ratio of one is generally required to achieve this value[2]

Bearing Stress Calculations

The bearing stress f_{br} calculation for the center spar lower flange is based on a shear flow of 934 lb/in. and skin thickness t of 0.180 in. The f_{br} is then calculated to be

$$f_{br} = \frac{934}{(0.18 \times 0.187)} = 27,700 \text{ psi} \quad (116)$$

Then the margin of safety MS is

$$MS = \frac{40,000}{27,700} - 1 = +0.44 \quad (117)$$

The f_{br} calculation for the center spar lower skin is based on a q of 934 lb/in. and skin thicknesses of

$$t = 0.25 - 0.08 = 0.17\text{-in. for the 3/16-in. bolt} \tag{118}$$

and

$$t = 0.25 - 0.106 = 0.144\text{-in. for the 1/4-in. bolt} \tag{119}$$

The maximum f_{br} then becomes

$$\text{Max } f_{br} = \frac{934}{(0.17 \times 0.187)} = 29,400 \text{ psi} \tag{120}$$

Then the MS is

$$MS = \frac{40,000}{29,400} - 1 = +0.36 \tag{121}$$

The f_{br} for the center spar upper flange and the center spar upper skin are not calculated, since an analysis of the data for these two areas will quickly show that the MS for these areas will be much higher than for the lower areas.

For the center spar upper flange, q = 265.9 lb/in. and t = 0.180 in.

For the center spar upper skin, q = 265.9 lb/in. and

$$t = 0.290 - 0.08 = 0.21 \text{ in. for the 3/16-in. bolt} \tag{122}$$

$$t = 0.290 - 0.106 = 0.184 \text{ in. for the 1/4-in. bolt} \tag{123}$$

The f_{br} calculation for the aft spar lower flange is based on a q of 406 lb/in. and a t of 0.120 in. The f_{br} is then calculated.

$$f_{br} = \frac{406}{(0.120 \times 0.187)} = 18,120 \text{ psi} \tag{124}$$

Then the MS is

$$MS = \frac{40,000}{18,120} - 1 = +1.20 \tag{125}$$

The f_{br} calculation for the aft spar lower skin is based on a q of 406 lb/in. and a t of 0.120 in. The f_{br} is then calculated.

$$f_{br} = \frac{406}{(0.120 \times 0.187)} = 18,120 \text{ psi} \quad (126)$$

Then the MS is

$$MS = \frac{40,000}{18,120} - 1 = +1.20 \quad (127)$$

Bending Deflection Estimates for the No. 2 Wing

The bending deflection estimates for the No. 2 wing are presented in Table XXIII. The actual test deflections that will be encountered by the No. 2 wing are expected to be approximately 10 percent less than the calculated deflections presented in this table.

TABLE XXIII. SECOND WING BENDING DEFLECTION ESTIMATE

Wing BL	Wing No. 1 Calculated Deflection* (in.)	Wing No. 1 Calculated Deflection** (in.)	Wing No. 2 Calculated Deflection*** (in.)
0	4.83	6.90	6.71
6	4.31	6.16	5.99
20	3.14	4.49	4.36
34	2.06	2.94	2.86
42.5	1.48	2.11	2.05
51	0.97	1.39	1.35
68	0.25	0.36	0.35
80.75	0.01	0.02	0.02
84	0.00	0.00	0.00

*Bending deflection based on 70 percent DUL and I = 138.59 in.^{4}

**Adjusted to 100 percent DUL

***Adjusted to new I = 142.557 in.^{4} and 100 percent DUL

Torsional Deflection Estimate for the No. 2 Wing

The basic torsional stiffness criterion is calculated in the property calculations section (page 137) where the torsion distribution is calculated. The basic equation is $\phi_a = \phi_b = 2.44\ L/G$ per 1000 in.-lb torque,

where ϕ_a = deflection of the forward cell, radians

ϕ_b = deflection of the aft cell, radians

L = length of test section, in.

G = shear modulus, psi

The test section is considered to extend from BL 6 to BL 68, which is a length of 62 inches. G is a variable depending on the stress level.

CONCLUSIONS AND RECOMMENDATIONS

WING TEST SPECIMEN FABRICATION

The design and fabrication concepts followed in this program were to integrally mold sandwich skin, honeycomb core, spar caps, and shear webs to produce a typical airplane wing assembly utilizing the fewest individual parts. Only two moldings were required to produce the wing test assembly. This is in contrast to typical designs wherein skins, spar caps, and spar webs are fabricated separately, resulting in the assembly of a large number of detail parts.

The design and fabrication concept proved to be quite practical. The wing test section quality was excellent, the attachment of the two moldings was satisfactory, and the wing test section was accepted for static testing. Following the test of the first wing test section, a second wing test section was produced, using the same design and fabrication concepts. Again, an excellent-quality test section was produced. Thus, repeatability of the fabrication procedure was established.

The layup of the complex parts required several days and several layup procedures. However, the material handling procedures were carefully programmed to avoid deterioration of the material during this period. This programming was required because the basic materials must be stored under refrigeration, since their shelf life is short at room temperature. It was shown that material handling can be quite satisfactorily accomplished through careful fabrication processing.

Dimensionally, the finished parts matched the design tolerances very well, except that springback from the mold occurred in the cured material. The tools used in the fabrication were not designed to allow for springback. It is recommended that future tooling designs take this into consideration.

TEST DATA AND DESIGN CORRELATION

The primary objective of this program was to determine the practicality of designing a wing structure using available material strength and strain data. To accomplish this objective, a conventional wing stress and deflection analysis was performed for a wing test section, and static tests were performed. The analysis of the calculated structural performance of the wing was then compared with the static test strain and deflection data. This comparison revealed that the structural analysis of the wing test section satisfactorily matched the test results. It was therefore

concluded that the use of available strength and strain data can be practical for analysis and design. The degree of practicality is, however, a function of the structural designer's knowledge of the material properties. The basic difference between conventional metal design and fiber glass reinforced plastic design involves the nonlinear stress-strain properties of the fiber glass reinforced plastic materials. It is concluded that the accuracy of the analysis can be improved as more complete material stress-strain properties are obtained. This is particularly applicable to shear properties.

The structural design approach for the wing test section employed the use of optimistic values and assumptions. By so doing, critical areas could be better determined in the static tests, and design modifications could be accomplished for the second test wing. The results of the static test for the first wing showed that certain assumptions were overly optimistic, since the wing failed at approximately 80 percent DUL.

It was concluded that the failure mode of the first wing was a buckling failure of the aft box compression skin. The stress calculation for the buckling stress of this panel was based on the assumption of fixed edge supports. Test data indicated that buckling was initiated at 40 percent DUL, and failure occurred at 80 percent. An analysis using simply supported edge criteria shows much closer correlation with test data. In designing the second wing, several transverse stiffeners were added to the critical area of the compression skins. These stiffeners were added to keep the skins stable up to a compression stress of 40,000 psi.

Comparison shows that the calculated stresses and the stresses computed from test strain measurements correspond quite closely. In the bending tests, the variance increased as the stress level increased, and buckling of the skin panel became more pronounced. This is logical since instability causes a change in the stress distribution of the overall section. The calculated and measured shear stresses also compare quite closely in the tension tests. The only exceptions to good correlation were found in the spar cap bending stresses. Measured test stresses were considerably less than were the calculated stresses. This may be attributed to erratic strain readings of the spar cap gages. It is recommended that this area be further evaluated during the second wing test to pinpoint the cause.

The plotted comparisons of calculated and measured test deflections also show a good correlation. This was true for both bending and torsional load conditions. The torsional deflection data for the torque box tests and the wing test section tests demonstrated the importance of obtaining accurate shear stress-strain data for design purposes. The nonlinear

behavior of FRP material in shear at relatively low stress levels prohibits the use of conventional methods of analysis derived from purely elastic stress-strain relationships. Thus, in general, shear deflections are a function of the stress level.

It is concluded that the wing test data confirm that, in general, the use of small specimen test data and conventional methods of analysis is practical for airframe structure design. However, it is recommended that future efforts be expended to obtain more complete stress-strain data, particularly for shear loadings.

The spar cap and sandwich skin materials utilized in this wing fabrication were oriented at 0^{o} and 90^{o} to the wing axis. These were not necessarily the optimum orientations. However, optimization of materials and orientation was not part of the work program. It is recommended that in future development, material and orientation optimization be incorporated even though the complexity of the structural analysis will be increased.

REFERENCES CITED

1. TEST PLAN REPORT FOR STATIC TESTS AND VIBRATION SURVEYS FOR GLASS-REINFORCED PLASTIC WING SECTION DESIGNED AND FABRICATED BY GOODYEAR AEROSPACE CORPORATION, Aero Structures Department Report No. P14, Naval Air Development Center, Johnsville, Warminster, Pennsylvania, 1 December 1966.

2. PLASTICS FOR FLIGHT VEHICLES, PART I, REINFORCED PLASTICS, MIL-H-DBK-17, Armed Forces Supply Support Center, Washington, D.C., 5 November 1959.

3. Peery, D.J., AIRCRAFT STRUCTURES, New York, McGraw-Hill Book Co., Inc., 1949.

4. SUMMARY REPORT ON STATIC TESTS OF GAC JOINT SPECIMEN V - BOX BEAMS, Naval Air Development Center, Aero Structures Department, Johnsville, Warminster, Pennsylvania.

5. SUMMARY REPORT ON STATIC TESTS AND VIBRATION SURVEYS OF GAC WING SECTION 1, Naval Air Development Center, Aero Structures Department, Johnsville, Warminster, Pennsylvania.

6. PROCESS SPECIFICATION MANUFACTURE OF POSITIVE PRESSURE MOLDED PREIMPREGNATED EPOXY GLASS CLOTH FACED METAL HONEYCOMB CORE STRUCTURAL SANDWICH, Goodyear Aerospace Corporation, GER-12920, Akron, Ohio, 11 November 1966.

7. Becker, Hubert, HANDBOOK OF STRUCTURAL STABILITY, PART II, BUCKLING OF COMPOSITE ELEMENTS, NACA TN 3782, New York, New York University, July 1957.

APPENDIX I
EVALUATION OF THE EFFECTS OF VARIATIONS IN MATERIAL PROPERTIES ON CONFIGURATION WEIGHT

DESIGN STUDY

At the request of the U.S. Army Aviation Materiel Laboratories (USAAVLABS), a study was made to evaluate the effects on weight of changes in the material properties and the applied loading outlined below. The study is defined by four phases which make use of the original specimen geometry. These phases are as follows:

PHASE I - Using the present loading conditions and material strengths, determine change in specimen weight which results from modulus variations in 5×10^6 psi increments from 5×10^6 psi to 20×10^6 psi.

PHASE II - With existing loads, assume material strengths of 140,000 psi for a unidirectional layup with 90,000-psi cross-ply strength and determine the weight changes resulting from the same modulus changes as in Phase I.

PHASE III - Assume twice the existing specimen loading, the same strengths as in Phase II, and determine weight changes due to the same modulus variations as in Phase I.

PHASE IV - With twice the existing loading and present material strengths, vary the modulus as in Phase I and determine the effect on weight.

The details of the investigation are developed in the following sections.

ANALYSIS

The design ultimate load for the No. 1 test article is derived in the GAC Development Support section of this report and is repeated here for convenience.

The calculated ultimate bending moment of 1,149,000 in.-lb at the root section was based on a compression strength of 40,000 psi for the material and sufficient edge fixity to prevent instability. The buckling stress σ_{cr} of a flat sandwich panel subjected to uniform compression loading on two opposite edges is

$$\sigma_{cr} = \frac{\pi^2}{4} K \frac{h^2}{b} \frac{E}{1 - \mu^2} \tag{128}$$

where h = panel thickness in inches

b = loaded side of panel in inches

The constant K in this equation is a function of the panel aspect ratio, the degree of edge restraint, and the transverse shear stiffness of the core.

For the original specimen, the panel aspect ratio (length to width) is approximately 84/23 = 3.66 if the reinforced areas at the ends are included in the length dimension. The parameter involving the core shear stiffness V is given by

$$V' = \frac{\pi^2 t t_c E}{2(1 - \mu) b^2 G_c} \tag{129}$$

and for the specimen geometry is calculated as

$$V' = \frac{\pi^2 (0.030)(0.500)\ 3 \times 10^6}{2\ (1 - 0.122)(23)^2\ 32,000} = 0.0133 \tag{130}$$

The effects of core shear stiffness are considered to be negligible for this low value of V'. Then from Equation (128), assuming the same edge restraint and panel aspect ratio for all phases of the study, the buckling stress is dependent only on the modulus E.

The section modulus of the specimen cross section is represented in the generalized form in Equation (131).

$$I/c = k_1 A_1 + k_2 A_2 = A_1 [k_1 + k_2 (A_2/A_1)] \tag{131}$$

where A_1 = skin area

A_2 = spar cap area

Then the maximum stress in bending f_b is given by Equation (132).

$$f_b = \frac{M_c}{I} = \frac{M}{A_1 [k_1 + k_2 (A_2/A_1)]} \tag{132}$$

If the spar cap area to skin area ratio is held constant for all phases of the study,

$$f_b = \frac{M}{A_1} H \tag{133}$$

where $$H = \frac{1}{k_1 + k_2 (A_2/A_1)} \tag{134}$$

The weight of the structure per unit length is

$$W = (A_1 + A_2)\rho_F + W_c + W_m \tag{135}$$

where ρ_F = the density of the reinforced plastic material

W_c = the core weight per unit length

W_m = the weight of the foam, bolts, nuts, bond, etc., per unit length of the specimen

By holding A_2/A_1 constant as before,

$$W = A_1 (1 + A_2/A_1) \rho_F + W_c + W_m \tag{136}$$

From Equation (133),

$$A_1 = \frac{MH}{f_b} \tag{137}$$

and when this is substituted into Equation (136),

$$W = \frac{MH}{f_b} \left(1 + A_2/A_1\right) \rho_F + W_c + W_m \tag{138}$$

To compare the weight of a new configuration with the original configuration,

$$\frac{(W)_N}{(W)_O} = \frac{H\,(M/f_b)_N\,(1 + A_2/A_1)\rho_F + W_c + W_m}{H(M/f_b)_O\,(1 + A_2/A_1)\rho_F + W_c + W_m}$$

$$= \frac{(M/f_b)_N + R}{(M/f_b)_O + R}$$

$$= \frac{(M/f_b)_N}{(M/f_b)_O + R} + S \tag{139}$$

where N = a subscript identifying the new configuration

O = a subscript identifying the original configuration

$$S = \frac{(W_c + W_m)/H(1 + A_2/A_1)\rho_F}{\left(\frac{M}{f_b}\right)_O + \frac{(W_c + W_m)}{H\,(1 + A_2/A_1)\rho_F}} \tag{140}$$

$$R = \frac{W_c + W_m}{H\,(1 + A_2/A_1)\rho_F} \tag{141}$$

When the data from the GAC Development Support section of this report are used, the constants defined in this appendix have the following numerical values:

$$A_2/A_1 = 5.256/5.284 = 0.995 \tag{142}$$

$$H = 1/[12.106 + 14.20(0.995)] = 1/26.22 \tag{143}$$

$$W_c + W_m = 0.340 \tag{144}$$

$$R = \frac{0.340\,(26.22)}{1.995\,(0.070)} = \frac{8.9148}{0.13965} = 63.84 \tag{145}$$

$$S = \frac{63.84}{287.254 + 63.84} = 0.1818 \qquad (146)$$

By substituting the values for the constants into Equation (139), we derive Equation (147):

$$\frac{(W)_N}{(W)_O} = \frac{(M/f_b)_N/(M/f_b)_O}{1 + 0.2222} + 0.1818$$

$$= 0.8182\,(M/f_b)_N/(M/f_b)_O + 0.1818 \qquad (147)$$

RESULTS

To obtain the results from the analysis that are called for in the four-phase study, the following information should be given relative to the calculations for the phases:

1. The present weight $(W)_O$ is assumed to develop the face sheet strength at 40,000 psi

2. The modulus of the present configuration (E_O) is taken as 3.0×10^6 psi.

3. Increases in Young's modulus are assumed to be accompanied by a corresponding change in face sheet compression strength sufficient to develop the higher buckling stress.

For Phases I and II, $M_N = M_O$ and

$$(f_b)_N = \left(\frac{E_N}{E_O}\right)(f_b)_O \qquad (148)$$

Equation (147) then becomes

$$\frac{(W)_N}{(W)_O} = 0.8182\,\frac{E_O}{E_N} + 0.1818 \qquad (149)$$

From this equation, we can then determine the following tabulated values as required by Phases I and II:

$E_N \times 10^{-6}$ (psi).....	5	10	15	20
E_O/E_N	0.6	0.3	0.2	0.15
0.8182 (E_O/E_N)	0.4909	0.2455	0.1636	0.1227
$(W)_N/(W)_O$	0.6727	0.4273	0.3454	0.3045
f_b (in.-lb)	66,700	133,500	200,000	265,000

For Phases III and IV, $M_N = 2M_O$ and

$$(f_b)_N = \left(\frac{E_N}{E_O}\right)(f_b)_O \tag{150}$$

Equation (147) then becomes

$$\frac{(W)_N}{(W)_O} = 1.6364 \frac{E_O}{E_N} + 0.1818 \tag{151}$$

From this equation, we can then determine the following values as required for Phases III and IV:

$E_N \times 10^{-6}$ (psi)	5	10	15	20
$(W)_N/(W)_O$ 1.1636		0.6728	0.5090	0.4272
f_b (in.-lb).....66,700		133,500	200,000	265,000

The results are plotted in Figure 67.

With reference to Figure 67, the curve identified by R_I indicates the weight ratio R_W as affected by compression modulus. The dashed line, F_c, defines the compression strength required to coincide with buckling. The curves labeled t_{st} and A_2 represent the total skin thickness and spar cap area required.

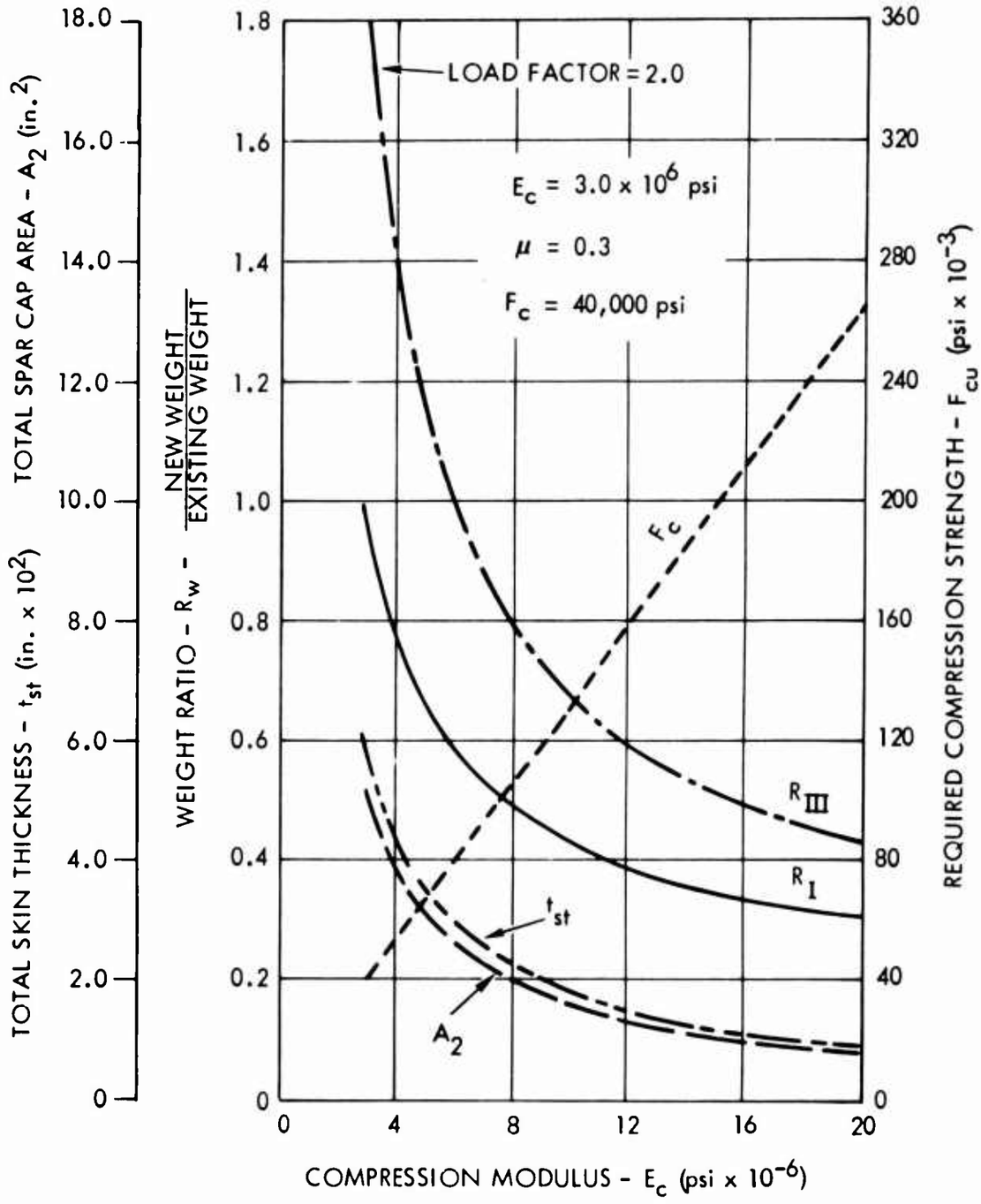

Figure 67. Effects of Compression Modulus on Specimen Weight.

For example, if E is increased to 9×10^6, the total weight is 46 percent of the present weight, but the skin material must have a compression strength of 120,000 psi. Further, the skin thickness reduces to 0.020 inch (0.010 inch per face) and the spar cap area reduces to 1.75 $in.^2$.

It will also be seen from the curves that if the compression strength is increased to 140,000 psi, the modulus must increase to 10.6×10^6 psi. Total skin thickness and spar cap area in this case are reduced to 0.016 inch (0.008 inch per skin) and 1.5 $in.^2$ respectively. The weight is reduced to 41 percent of the present weight.

The curve identified as R_{III} indicates the weight ratio for the original configuration with a loading factor of 2.0. For example, with a compressive strength of 140,000 psi, the weight is 65 percent of the original weight, but as before, a modulus of 10.6×10^6 psi is required to take advantage of the higher strength.

APPENDIX II
TEST PROGRAM*

The tests to be performed in this program are listed below in order of performance. Each wing section will be weighed and examined for workmanship before performing any tests.

Static tests of joint specimens.

Joint specimens I through IV.

Joint specimen V-A (box beam A - - bolted).

Joint specimen V-B (box beam B - - bonded).

Tests of wing sections.

Test No. 1. Evaluation of shear center calculations.

Test No. 2. Dynamic evaluation.

A) Damping evaluation by logarithmic decrement.

B) Dynamic response to forced vibration.

Test No. 3. Static Loading.

A) Bending (cantilever).

B) Pure torque.

C) Bending plus torque.

Test No. 4. Failure loading.

---

*The test plan in this appendix is presented in the same format as the Naval Air Development Center, Aerostructures Department Report No. P14.[1]

SECTION A - STATIC TESTS OF JOINT SPECIMENS

Test Objective

To develop a system of joint construction that will effectively transmit the applied stress and not result in unacceptable changes in the rate of curvature of the deflection curve.

Joints I through IV

Test Setup

The specimens will be placed in self-aligning type grips of a testing machine.

Instrumentation

No instrumentation is required for these tests.

Test Procedure

The joint specimens will be loaded using a constant rate of crosshead movement of 0.05 in./min. The maximum load carried by each specimen will be recorded. During all tests, the specimens will be observed closely for signs of failure.

Joint V--Box Beams

Loads

The box beam will be loaded in torsion only. The maximum torque expected is 324,000 in.-lb; this value will be designated the design ultimate load (DUL). The test loads for positive torsion moment are shown in Figure 68 at the design ultimate load.

Test Setup

The box beam will be simply supported in bending at both ends. The left-hand support will have two load points to resist the torque; the right-hand support will be designed so that this end of the box beam is free to twist about the section centroid and free to move spanwise.

Test loads will be applied by means of hand pumps and hydraulic jacks attached directly to load points at the right-hand loading plate.

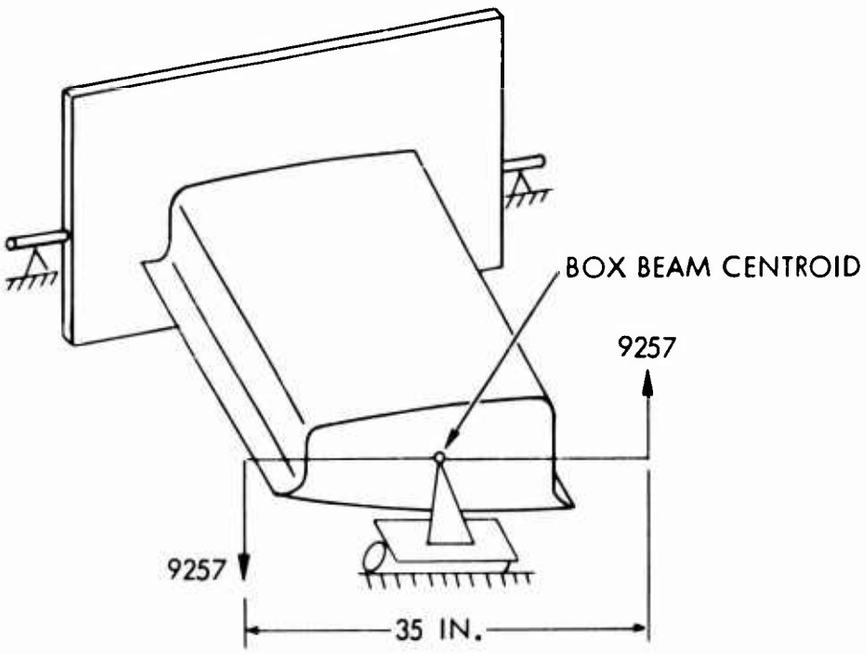

Figure 68. Test Loads for Positive Torsion Moments.

Instrumentation

Dial indicators will be positioned at the two reference planes at the forward and rear spars as shown in Figure 69.

Test Procedure

1. The beam will be loaded to produce positive torsion moment in the following increments of design ultimate load: 2%, 4%, 6%, 8%, 10%, 15%, 20% --- up to 70%. Deflection data will be recorded at each increment.

2. The loads will be decreased in 20% increments down to zero load, and deflection data will be taken at each increment.

3. The beam will be loaded to produce negative torsion moment, and steps 1 and 2 will be repeated.

4. The beam will again be loaded to produce positive torsion moment in 10% increments of design ultimate load up to failing load. Deflection data will be recorded at each increment.

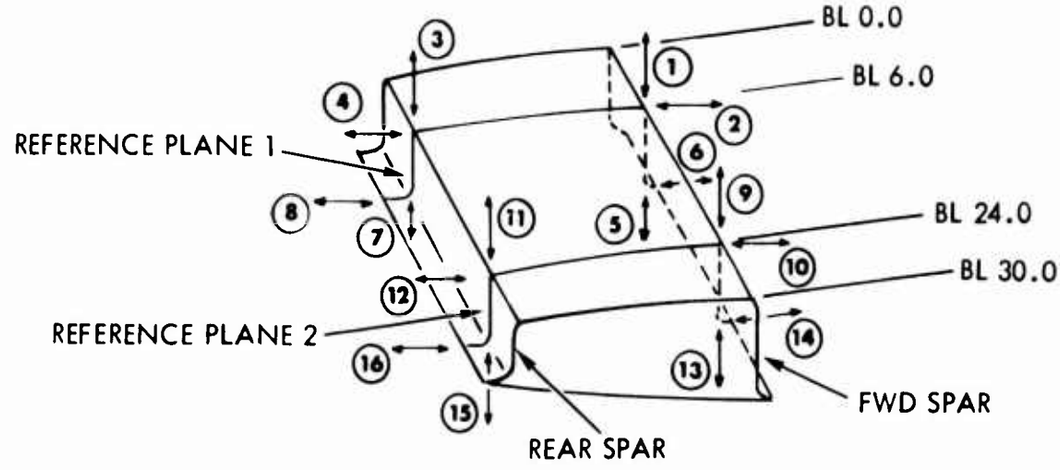

Figure 69. Dial Indicator Positions on the Two Reference Planes.

SECTION B - WING SECTION TESTS

Test No. 1 - Evaluation of Shear Center Calculations

Test Object.

To determine the shear center of the cross section for comparison with the calculated value and to establish the point of load application for subsequent testing.

Test Setup

The specimen is considered to be a right-hand wing section and will be cantilevered to the strongback test fixture and subjected to loadings at the end plate. The end plate will identify the location of the calculated shear center and the section centroid and will also locate the horizontal axis through these points. Two loading points will be provided on this axis. Point 1 will be 8 inches forward of the indicated shear center, and point 2 will be 18 inches forward of the indicated shear center. These points will be capable of taking a 1000-lb vertical load. The setup is shown in Figure 70.

Instrumentation

Two dial gages are necessary: one near the forward edge of the end plate and the other near the aft edge of the end plate. Auxiliary dial gages 1, 2, 3, and 4 will be used as shown in Figure 70 to obtain a reasonable

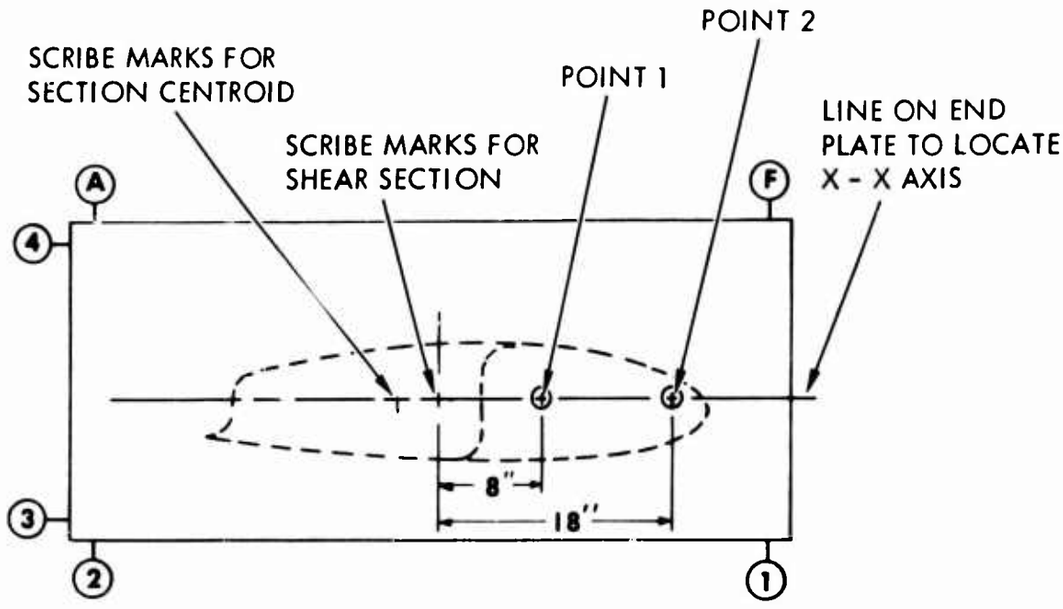

Figure 70. End Plate Load Points.

check on the primary readings. Strain data will be recorded as a preliminary check of stress calculations based on the applied loads.

Test Procedure

The following procedure will be followed:

1. Zero readings on all dial gages will be obtained.

2. Loads of 200 lb, 400 lb, 600 lb, 800 lb, and 1000 lb will be applied.

3. The loads will be removed and all gages read; a load of 200 lb will be applied and deflection data recorded.

4. Steps 1, 2, and 3 will be repeated.

5. Steps 1, 2, 3, and 4 will be repeated for point 2.

Test No. 2 - Vibration Survey

Test Objectives

To determine the dynamic characteristics of the wing section and to compare the results with published data related to FRP materials.

Testing is defined for two conditions: (A) the free vibration and (B) the forced vibration.

Test No. 2A

This test is to determine (1) the fundamental and/or least damped bending and torsional natural frequencies and (2) the logarithmic decrement for evaluation of damping properties.

Test Setup

The wing section will be cantilevered to the strongback, and vertical loading will be applied at the end plate through the shear center.

A torsion moment will be applied to the end plate as a separate loading condition. If a pure torque is not easily applied, a shear load will be applied near the leading edge.

As a second part of the test, a bungee cord will be attached to the end plate and preloaded to approximately 300 lb.

Instrumentation

All axial strain gages will be active, with outputs recorded on an oscillograph. Simultaneously, the output of three accelerometers attached to the wing end plate at the leading edge, center spar, and trailing edge will be recorded on a high-speed oscillograph so that a logarithmic decay curve can be recorded.

Test Procedure

Loads will be applied as necessary to obtain 2000 psi, 6000 psi, and 12,000 psi at the root section on the gage reading the highest strain. With all gages active and accelerometers placed as described above, the following will be performed:

1. The wing section will be loaded at the end plate to produce a stress of 2000 psi at the root section.

2. The wing section will be suddenly released, and the free vibration of the specimen will be allowed to damp to zero.

3. Steps 1 and 2 will be repeated for the 6000- and 12,000-psi levels.

4. A bungee cord will be attached to the end plate and loaded upward to approximately 300 lb in the cord, and steps 1 through 3 will be repeated.

5. With the bungee cord attached, a pure torque of 18,000 in.-lb will be applied at the free end.

6. The wing section will be suddenly released, and the specimen will be allowed to oscillate until motion stops.

7. Steps 5 and 6 will be repeated without the bungee cord.

Note: If a pure torque is not feasible, a vertical (up) load of 1000 lb at point 2 will be applied as described under Test No. 1 for steps 5 through 7.

Strain gages and accelerometers will be continuously recording during these tests.

Test No. 2B

The purpose of this test is to determine natural frequencies, mode shapes, and damping characteristics by forced vibration.

Test Setup

A portable shaker and a voice coil exciter will be used to apply vibration inputs at (1) the free end through the shear center and (2) the free end near the leading edge.

Instrumentation

All strain gages active in the preceding test will also be active and recording during this test. The three free end accelerometers used in Test No. 2A will also be used here. In addition, single accelerometers will be placed on the lower panel at the centers of the forward and aft panels to determine if flat panel vibration modes are excited during the test. Sufficient accelerometers will be spaced along the wing span over the forward and rear spars to define the mode shapes. The number used depends on availability and the number of channels permitted (see Figure 71).

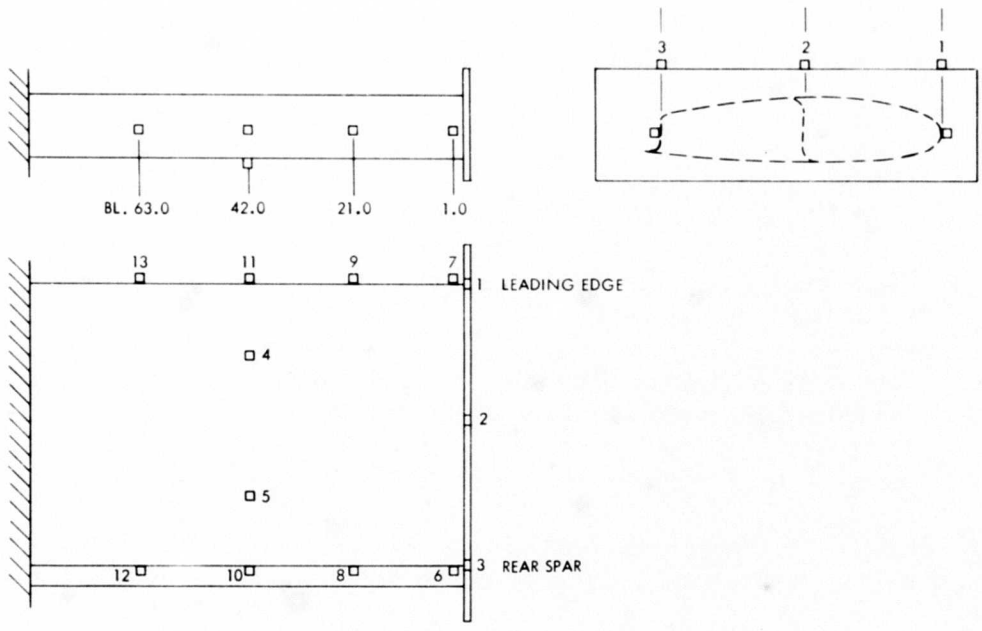

Figure 71. Wing Span Accelerometer Locations.

The portable shaker will be attached to the free end at the shear center and, with the accelerometers output displayed on a low speed oscillograph, a vibration scan to 500 cps will be performed to locate the natural frequencies. Once the peaks have been identified, oscillograph records with a high paper speed will be run at each natural frequency in order to display phase relationships between pickups.

The same procedure will then be repeated with the portable shaker attached near the loading edge at the free end.

The same procedures will then be repeated with the voice coil exciter.

Test No. 4 - Static Loading

Test Objective

To compare actual deflections and stress distributions with calculated values based on conventional design and analytical methods.

Definition of Test Conditions

The loads that will be used for tests are based on those at wing station 85.0 of the GA-22A aircraft. The low-angle-of-attack condition appears to be the most critical structurally. Although the stress level that results from these loads is quite low (because of practical minimum gage thicknesses available), the loads are of representative proportions. The loads were ratioed up to estimate the maximum load-carrying capacity of an actual wing section. The design ultimate loads at the test section (BL 68.0) for the three loading conditions are as follows:

Bending Condition
1,151,200 in.-lb

Torsion Condition
38,500 in.-lb

Combined Condition
Bending: 1,151,200 in.-lb
Torsion: 38,500 in.-lb

The maximum test limit loads (70% DUL) that will be applied at the end plate are shown in Figure 72.

Test Setup

The wing section will be cantilevered from the strongback and subjected to the loads at the end plate as shown in Figure 72.

Instrumentation

Strain gages and rosettes will be located as shown in Figure 73; deflection gages will be positioned as shown in Figure 74.

Test Procedure

Three tests will be performed as indicated above. The procedure will be the same for each test and is as follows:

1. Zero readings will be taken on all strain and deflection gages.

2. Loads will be applied in 10% increments of the DUL with readings taken at each increment up to 30% DUL.

3. The loads will be decreased and readings taken at each 10% increment down to zero load.

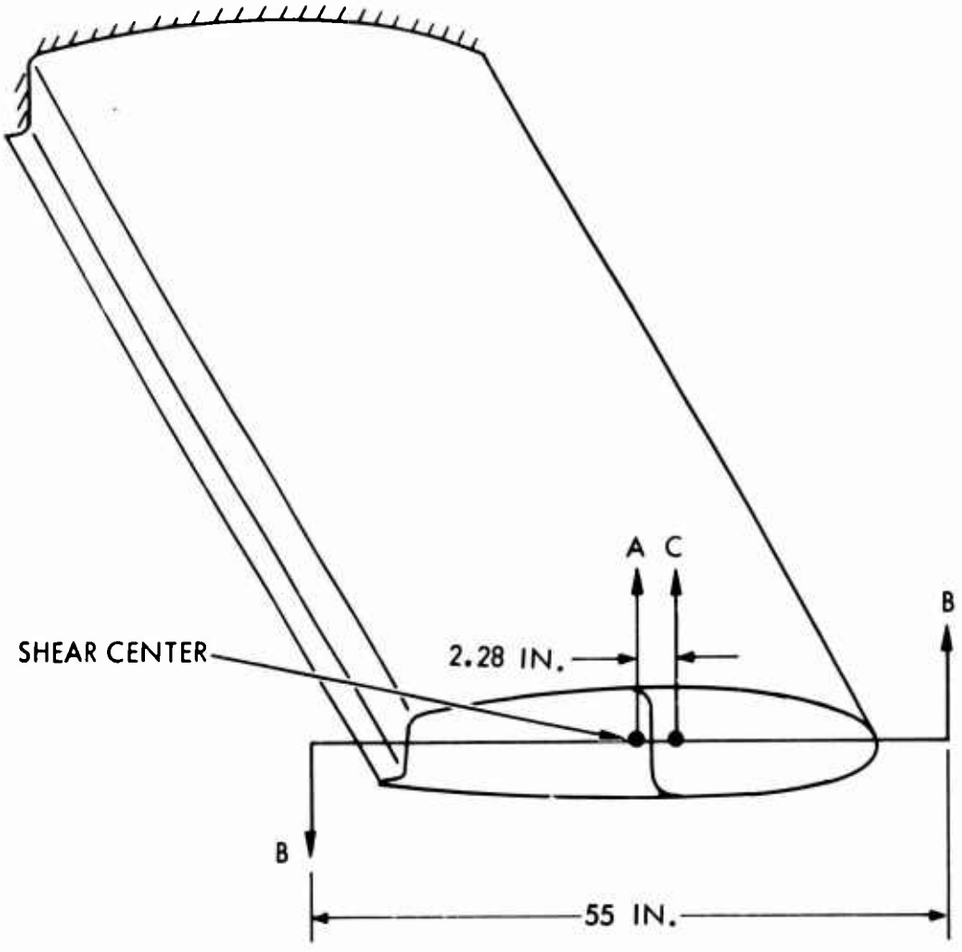

BENDING CONDITION FOR LOAD A = 11,850 LB
TORSION CONDITION FOR LOAD B = 491 LB
COMBINED CONDITION FOR LOAD C = 11,850 LB

Figure 72. Design Limits and Test Conditions for the Wing Section.

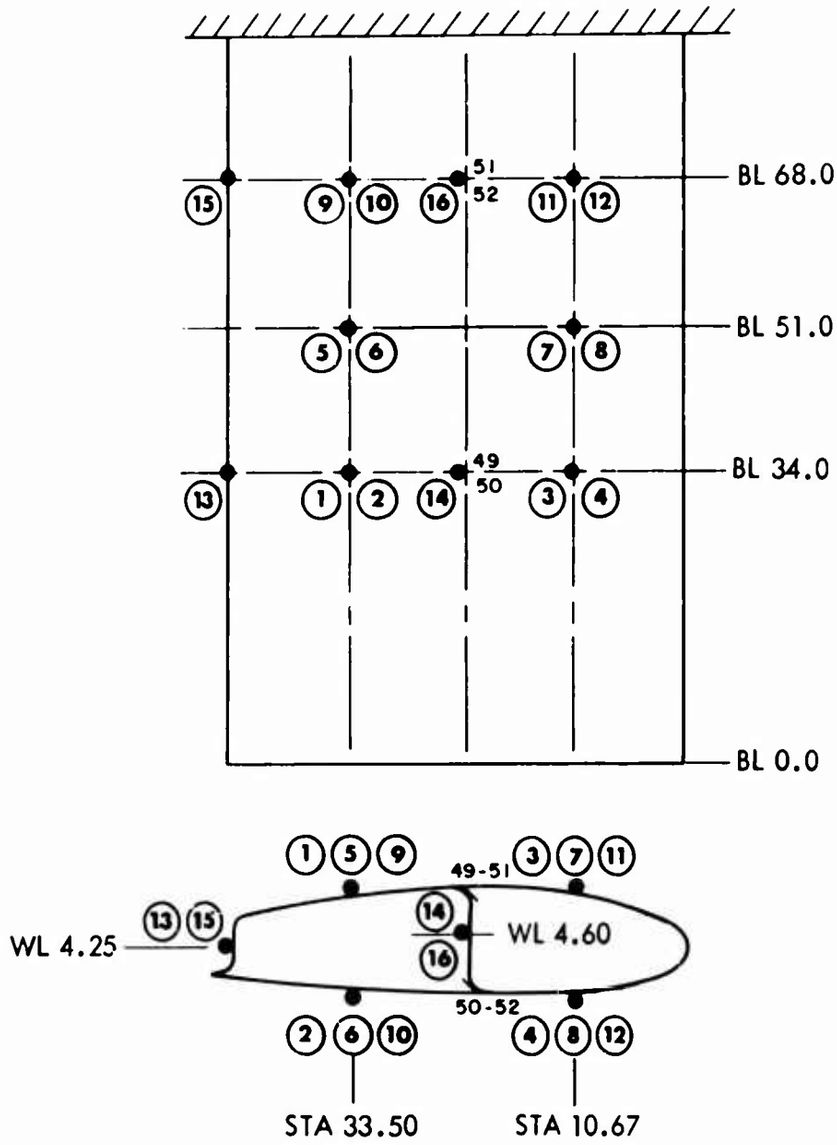

NOTE: CIRCLED NUMBERS REPRESENT ROSETTE NUMBERS; SINGLE GAGES 49-52 LOCATED AT SOLID INSERTS OF CENTER SPAR.

Figure 73. Rosette and Strain Gage Locations for the Wing Section.

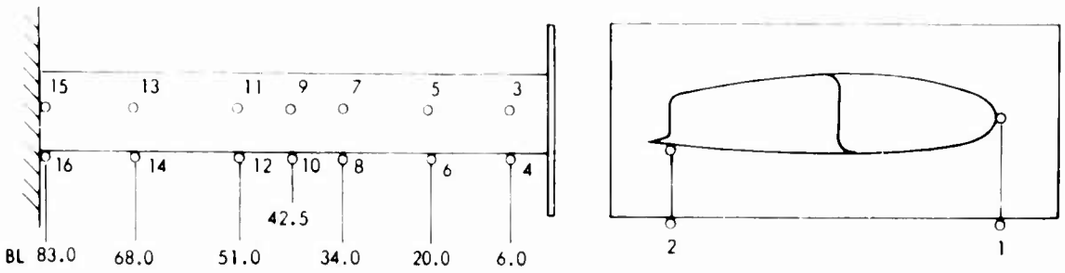

Figure 74. Deflection Gage Positions for the Wing Section.

4. Loads will be applied in 10% increments up to 70% DUL with readings taken at each increment.

5. The loads will be decreased and readings taken at each 20% increment down to zero load.

Test No. 5 - Static Test to Failing Load

Test Objective

To verify failure calculations and to determine the failure mode.

Test Condition

The wing section will be loaded to failing load for the bending condition. The calculated failing bending moment (DUL) is 1,151,200 in.-lb at BL 68.0.

Test Setup

The specimen will be mounted as for Test No. 4.

Instrumentation

Instrumentation is the same as for Test No. 4.

Test Procedure

A vertical load will be applied at the end plate through the shear center in increments of 10% DUL until failure occurs. Strain and deflection data will be recorded up to failure.

APPENDIX III
PROCESS SPECIFICATION FOR THE MANUFACTURE OF POSITIVE PRESSURE MOLDED PREIMPREGNATED EPOXY CLOTH FACED METAL HONEYCOMB CORE STRUCTURAL SANDWICH*

TABLE OF CONTENTS

*The process specification in this appendix is presented in the same format as in the GAC specification.[6]

1. SCOPE

1.1 This specification establishes the materials and processing for structural parts fabricated by a multistage sandwich process.

2. REFERENCE DOCUMENTS

2.1 Military

MIL-A-5090	Adhesive, Airframe Structural, Metal to Metal
MIL-C-7438	Core Material; Aluminum Honeycomb
MIL-P-25421	Plastic Materials, Glass Fiber Base - Epoxy Resin, Low-Pressure Laminated
MIL-R-9300	Resin Epoxy, Low-Pressure Laminating
MIL-STD-401	Sandwich Construction and Core Materials; General Test Method

2.2 Goodyear Aerospace Corporation (GAC)

CL1	Cleaning

3. GENERAL REQUIREMENTS

3.1 Materials

3.1.1 The materials listed below are incorporated into the part during fabrication and shall be certified to meet the requirements stated herein.

	Materials	Sources
3.1.1.1	Epoxy Prepreg E293-481-550 Resin Content - Dry - 36 ±2% Gel Time 1/2 - 1-1/2 min at 325°F Volatiles 2 - 4% at 325°F Flow 13 - 18% at 325°F & 60 psi	Cordo Div. of Ferro Corp. Norwalk, Conn.

	Materials	Sources
3.1.1.2	Epoxy Prepreg E293-1582-550 Resin Content - Dry 34 ±2% Gel Time 1/2 - 1-1/2 min at 325°F Volatiles 2 - 4% at 325°F Flow 10 - 16% at 325°F & 60 psi	Cordo Div. of Ferro Corp. Norwalk, Conn.
3.1.1.3	Liquid Epoxy Resin DER 332	Dow Chemical Co. Midland, Mich.
3.1.1.4	Curing Agent A	Shell Chemical Co. Pittsburg, Calif.
3.1.1.5	Adhesive, Bondmaster M602-1, M602-2	Pittsburgh Plate Glass Co. Adhesive Products Div. Pittsburgh, Pa.
3.1.1.6	Glass Microballoon Spheres IG101	Sohio Chemical Co. Microballoons Spheres Div. Midland Bldg. Cleveland, Ohio
3.1.1.7	Aluminum Honeycomb 1/8-0.001-5052H39	Hexcell Products, Inc. Havre de Grace, Md.
3.1.1.8	Diethanolamine	Union Carbide Corp. New York, N.Y.
3.1.1.9	Cab-O-Sil	Cabot Corp. Boston, Mass.
3.1.1.10	Glacial Acetic Acid	E.I. DuPont de Nemours & Co. Wilmington, Del.

3.1.2 The materials listed below are not incorporated into the product. Certification of these materials is not required.

	Materials	Sources
3.1.2.1	Vacuum Bag Material PVA (Polyvinyl Alcohol) Film	Reynolds Company Grottoes, Virginia
3.1.2.2	Parting Agents	
	Teflon FEP Fluorocarbon Film	E.I. DuPont de Nemours Co. Film Dept. Wilmington, Del.
	Release Agent Ramm 225 Release Agent Ramm 334	Dacco Inc. Cleveland, Ohio
3.1.2.3	Surface Bleeder - Glass Cloth 128	Open
3.1.2.4	Edge Bleeder - Glass Cloth TG30	Open
3.1.2.5	Peel Ply - Dacron Fabric 15,004	Stern & Stern Textiles Inc. Hornell, N.Y.
3.1.2.6	Sealing Compound, Presstite 587	Interchemical Co. Presstite Div. St. Louis, Mo.
3.1.2.7	MEK (Methylethyl ketone)	Open
3.1.2.8	Acetone	Open
3.1.2.9	Naphtha	Open
3.1.2.10	Gloves, white, lightweight, knitted	Open
3.1.2.11	Thermocouple Wire, Iron-Constantan 12432P 30 gauge or finer	Open

3.2 Storage and Handling of Materials

3.2.1 The preimpregnated (prepreg) material is fully catalyzed and ready for use. It shall be packaged with an interlayer

of polyethylene film or equivalent, and the roll shall be wrapped in a cover of laminated Kraft paper, polyethylene, and aluminum foil. The prepreg shall be suspended horizontally by its core. After removal from refrigeration, the material shall be brought to room temperature before its protective wrapping is removed.

3.2.2 Honeycomb shall be stored in clean, dry areas and shall not be contaminated by moisture, dirt, or other substances. After vapor degreasing and prior to priming, it shall be handled only by persons wearing white gloves.

3.3 Facilities Control

3.3.1 Autoclave - A heated air, circulating autoclave shall be used to provide the temperature and pressures required by Section 5.4.1 of this specification.

3.3.2 Oven - An air circulating oven shall be used to provide the temperature required by Sections 4.1.3.4, 4.1.3.5, 4.1.4.5 and 5.1.24 of this specification.

3.3.3 Layup Area - All prepreg layups shall be accomplished in a temperature- and humidity-controlled room.

Limits - Temperature $75^{o} \pm 5^{o}F$
Relative Humidity 55% (Max)

3.4 Tools

3.4.1 The parts shall be fabricated so that the aerodynamic skin is adjacent to the mold surface.

3.4.2 The mold surface shall be nonporous and shall be free of cracks, pits, and any other irregularities which would affect the quality of the part.

3.4.3 Plastic molds are suitable for fabrication of parts to this specification. The material on the mold surface should be completely nonreactive with the resin used in the part. The mold should be unaffected by the conditions of the cure.

3.4.4 In-Process Control Forms - A GAC process control form outlining the fabrication steps and materials used must be prepared for each item produced to this specification.

4. PREPARATION OF MATERIALS

4.1 Honeycomb Materials

4.1.1 In cases where core forming is required, this forming shall be accomplished prior to the core priming operation.

4.1.2 Prior to priming, all honeycomb core material shall be vapor-degreased. The core shall receive its first primer coat within 24 hours after it has been vapor-degreased.

4.1.3 Core Priming

4.1.3.1 Mix Resin M602

Part I 100 pbv
Part II 80 pbv

(Continue to stir batch while using to assure good mixture)

4.1.3.2 Roller coat each piece 3 times, each side. Each coat is to be applied with roller strokes at approximately 120° to previous stroke (allow approximately 30 minutes between coats).

4.1.3.3 After last coat - air dry

1 hr (min)
72 hr (max)

4.1.3.4 Oven dry 1 hr at 200° - 225°F.

4.1.3.5 Cure 45 - 50 minutes at 325° ±50° F.

4.1.3.6 Cover each cured piece with a protective film and store in a clean, dry area.

4.1.4 Core Stabilization

4.1.4.1 Trim primed honeycomb to drawing dimensions.

4.1.4.2 Mix resin

Epoxy Resin DER 332	64.6 pbw
Glass Microballoons IG101	27.6 pbw
Cab-o-sil	3.0 pbw
Glacial Acetic Acid	0.44 pbw
Diethanolamine	0.76 pbw
Curing Agent A	4.5 pbw

4.1.4.3 Fill honeycomb edges to drawing dimensions with above resin mix.

4.1.4.4 Cure 8 hours minimum at room temperature.

4.1.4.5 Oven cure 2 hours at 250° ±10°F.

4.1.4.6 Cool to below 125°F, remove flash, and clean up part.

4.1.4.7 Cover each stabilized piece with a protective film and store in a clean, dry area.

4.2 Preparation of Mold

4.2.1 Parting agents (mold release) per Section 3.1.2.2 shall be applied to the tool surface and allowed to dry.

5. FABRICATION PROCEDURE

5.1 Layup Procedure (warp direction for all plies shall be specified on the part drawing).

5.1.1 The prepreg material per Section 3.1.1.1 (E293-481) shall be carefully positioned in the mold.

5.1.2 Position the necessary number of E293-481 plies to obtain a doubler thickness consistent with drawing requirements. There must be no cutting of doubler plies directly over other plies of the layup. Any evidence of this practice shall be cause for immediate rejection of the part.

5.1.3 Cover the entire layup with FEP film.

5.1.4 Apply surface bleeder in accordance with Section 5.2.1.

5.1.5 Apply edge bleeder in accordance with Section 5.2.2.

5.1.6 Bag layup, 3-mil PVA, and apply vacuum pressure.

5.1.7 Allow layup to remain under vacuum pressure at room temperature for 12 hours (min).

5.1.8 Remove vacuum, bag, bleeder, and FEP film.

5.1.9 Locate honeycomb core material on skin and doubler layups.

5.1.10 Cover exposed honeycomb surfaces with FEP film.

5.1.11 Trim prepreg material per Section 3.1.1.2 (E293-1582) to drawing dimensions for layup in cap strip and edge band areas.

5.1.12 Carefully position the necessary number of plies of E293-1582 material to obtain the required cap strip and edge band thickness for this operation.

5.1.13 Cover all exposed prepreg with a peel ply of Dacron cloth.

5.1.14 Cover peel ply with FEP film.

5.1.15 Apply surface bleeder in accordance with Section 5.2.1.

5.1.16 Apply edge bleeder in accordance with Section 5.2.2.

5.1.17 Install thermocouple wire into edge of part outside of part-net-trim line.

5.1.18 Bag part (6-mil PVA), and apply pressure per Section 5.3.1.

5.1.19 Cure part per Section 5.4.1.

5.1.20 Remove bag, bleeder, FEP film, and peel plies.

5.1.21 Mix Resin

Epoxy Resin DER 332	64.6 pbw
Microballoons IG101	27.6 pbw
Cab-o-sil	3.0 pbw
DETA	4.5 pbw

5.1.22 Fill and flush, with above resin mix, those edge band areas designated by the drawing to receive filler.

5.1.23 Cure 8 hours at room temperature.

5.1.24 Oven cure 2 hours at 250° ±10°F.

5.1.25 Sand filled areas smooth.

5.1.26 Locate vent positions per process card, and drill 3/32-in.-dia holes through the honeycomb stabilizing syntactic foam into honeycomb panel to facilitate venting.

5.1.27 Trim prepreg material per Section 3.1.12 (E293-1582) to drawing dimensions for layup in cap strip and edge band areas.

5.1.28 Carefully position the necessary number of plies of E293-1582 material to bring the cap strips and edge bands to final thickness.

5.1.29 Lay up inner skin plies of prepreg material per Section 3.1.1.1 (E293-481) over honeycomb, cap strips, and edge band areas.

5.1.30 Position the necessary number of E293-481 plies to obtain doubler thicknesses consistent with drawing requirements.

5.1.31 Position the necessary number of E293-1582 plies to obtain edge reinforcement thicknesses consistent with drawing requirements.

5.1.32 Cover entire assembly with perforated FEP film.

5.1.33 Apply surface bleeder in accordance with Section 5.2.1.

5.1.34 Apply edge bleeder in accordance with Section 5.2.2.

5.1.35 Install thermocouple wire into edge of part outside of part-net-trim line.

5.1.36 Bag part (6-mil PVA), and apply pressure per Section 5.3.1.

5.1.37 Cure part per Section 5.4.1.

5.1.38 Remove bag, bleeder, and FEP film.

5.1.39 Remove part from mold.

5.1.40 Abrade mold surface of part which is to receive secondary edge reinforcement layup.

5.1.41 Mask areas of part which do not receive above layups to protect against excess resin flow.

5.1.42 Position the necessary number of E293-1582 plies to obtain an edge reinforcement thickness consistent with drawing requirements.

5.1.43 Cover layup with FEP film.

5.1.44 Apply surface bleeder in accordance with Section 5.2.1.

5.1.45 Apply edge bleeder in accordance with Section 5.2.2.

5.1.46 Install thermocouple wire into edge of part outside of part-net-trim line.

5.1.47 Bag part (6-mil PVA), and apply pressure per Section 5.3.1.

5.1.48 Cure part per Section 5.4.1.

5.1.49 Remove bag, bleeder, and FEP film, and clean up part.

5.2 Application of Bleeders

5.2.1 Surface Bleeder

5.2.1.1 Place 128 glass cloth bleeder as required over FEP film. The bleeder shall be tailored as required to make intimate contact with the layup. No bridging is to be tolerated, and the glass bleeder should extend sufficiently beyond the edge of the part to contact the edge bleeder, which serves as the direct connection to the vacuum line.

5.2.2 Edge Bleeder

5.2.2.1 Edge bleeder may be made from rolled strips of TG30 glass fabric.

5.2.2.2 Place edge bleeder around the edge of the layup. Edge bleeders shall not be in direct contact with the layup; rather, they shall be separated by a layer of FEP film.

5.3 Application of Pressure

5.3.1 Vacuum Pressure

5.3.1.1 Vacuum pressure is applied to the part by the use of a bag or diaphragm made using polyvinyl alcohol.

5.3.1.2 A sealing compound per Section 3.1.2.C shall be used to effect a seal between the prepared form and the diaphragm.

5.3.1.3 Slowly apply full plant vacuum (22 inches of mercury, minimum) to the interior of the vacuum bag. As the air is evacuated, make the bag conform to the shape of the part and keep wrinkles to a minimum. Wrinkling of the surface bleeder under the bag shall not be allowed.

5.3.1.4 There shall be no bridging of the fabric of the part, the bleeder cloth, or the bag material. Elimination of bridging can best be accomplished by performing a squeegee operation employing a Teflon paddle having generously radiused edges. If any holes develop in the bag, they must be sealed immediately with cellulose tape.

5.4 Cure

5.4.1 Autoclave Cure

5.4.1.1 All temperatures referred to are part temperatures as taken by a thermocouple imbedded in the part.

5.4.1.2 Place the assembly, while under vacuum pressure, in the autoclave and apply 50 ±5 psi positive pressure into the autoclave cavity. When the autoclave pressure reaches 15 ±5 psi, vent the vacuum to atmosphere.

5.4.1.3 Heat the part to 160^{o} ±10^{o}F at the rate of 2^{o} - 4^{o}F per minute and hold for 30 minutes ±5 minutes.

5.4.1.4 Heat from 160° to 250° ±10°F at a rate not to exceed 2° per minute and hold for a minimum of 30 minutes.

5.4.1.5 Heat from 250° to 290° ±10°F at a rate not to exceed 1° per minute, and cure for a minimum of 2 hours.

5.4.1.6 Apply full plant vacuum and depressurize autoclave.

5.4.1.7 Remove part from autoclave.

5.4.1.8 Cool under vacuum until part is 125°F or less.

5.5 Finishing

5.5.1 Trimming shall be accomplished in such a manner that delamination and scorching of the part edges do not occur.

5.5.2 Drilling and countersinking shall be accomplished with carbide-tipped drills, or equivalent, and the material shall be properly clamped to minimize delamination around drilled holes.

6. QUALITY CONTROL

6.1 The prepreg shall be tested for compliance with MIL-P-25421. The resin shall be approved under MIL-R-9300, and the honeycomb shall be purchased to MIL-C-7438.

6.2 Temperature checks shall be run on curing ovens periodically to establish and maintain satisfactory operation. The autoclave shall also be checked for proper operating conditions.

6.3 A quality control check shall be run biweekly on all prepreg skin material. This shall be in the form of a gel time check. Gel time must not exceed 1 minute 30 seconds when run at 60 psi and at 325°F. Skin layup date, roll number and batch number, gel time, and gel time check date shall be entered on the process control card for each skin layup of each part.

6.4 Autoclave temperature and pressure shall be recorded for each autoclave cure. Part temperatures shall be recorded for each autoclave cure to verify compliance with Section 5.4.1.

6.5 A running recording shall be kept of the temperature and relative humidity of the part layup room. The record must confirm that the conditions as set forth in Section 3.3.3 are met.

Unclassified

Security Classification

DOCUMENT CONTROL DATA - R & D

(Security classification of title, body of abstract and indexing annotation must be entered when the overall report is classified)

1. ORIGINATING ACTIVITY (Corporate author) Goodyear Aerospace Corporation Akron, Ohio	2a. REPORT SECURITY CLASSIFICATION Unclassified 2b. GROUP

3. REPORT TITLE

FABRICATION AND TESTING OF THE COMPOSITE MATERIALS AIRCRAFT WING SECTION

4. DESCRIPTIVE NOTES (Type of report and inclusive dates)
Final Technical Report

5. AUTHOR(S) (First name, middle initial, last name)

Fred E. Bauch, Robert W. Nordlie, and Robert C. Lair

6. REPORT DATE September 1968	7a. TOTAL NO. OF PAGES 207	7b. NO. OF REFS 7
8a. CONTRACT OR GRANT NO. DA44-177-AMC-407 (T) b. PROJECT NO. Task 1F162204A17003 c. d.	9a. ORIGINATOR'S REPORT NUMBER(S) USAAVLABS Technical Report 68-66 9b. OTHER REPORT NO(S) (Any other numbers that may be assigned this report) GER 13857	

10. DISTRIBUTION STATEMENT

This document has been approved for public release and sale; its distribution is unlimited.

11. SUPPLEMENTARY NOTES	12. SPONSORING MILITARY ACTIVITY U.S. Army Aviation Materiel Laboratories Fort Eustis, Virginia

13. ABSTRACT

A 7-foot-long aircraft wing test section was fabricated with fiber glass reinforced plastic materials and subjected to static and dynamic tests. Good correlation between predicted and actual test values was obtained. The structure failed in compression buckling of the aft cell, top panel. A design modification was incorporated in the fabrication of a second test structure.

DD FORM 1 NOV 68 1473 REPLACES DD FORM 1473, 1 JAN 64, WHICH IS OBSOLETE FOR ARMY USE.

Unclassified

Security Classification